Culvert Blockage Caused by Boulders in the Western Cape and the Development of Mitigation Measures: Physical Model Study

Johannes Andreas Brooks

Thesis presented in partial fulfilment of the requirements for the degree of Master of Engineering (Research) in the Faculty of Civil Engineering at Stellenbosch University

Supervisor: Mrs A Bosman

Department of Civil Engineering

March 2020

Declaration

By submitting this thesis electronically, I declare that the entirety of the work contained therein is my own, original work, that I am the sole author thereof (save to the extent explicitly otherwise stated), that reproduction and publication thereof by Stellenbosch University will not infringe any third party rights and that I have not previously in its entirety or in part submitted it for obtaining any qualification.

J.A. Brooks

Date: March 2020

Abstract

Culverts are widely used as drainage structures to allow streams to traverse a roadway in a controlled manner. Due to the reduced flow area of a culvert, culverts can be seen as a constriction in a stream. Interference with the normal flow conditions caused by a culvert in a stream can lead to boulder deposition at the culverts. Mountainous areas have been identified as locations where the potential for boulder blockages are higher due to the hydraulically steep bed slope. Limiting the study to the Western Cape specified the boulder type that was tested, thus, naturally rounded boulders were considered.

The occurrence of blockages caused by boulder accumulation at culvert sites motivated the study. Boulders will settle at the culvert entrance which reduces the available flow area through the culvert. A reduced flow area increases the risk of flooding, and in extreme cases, the roadway could be washed away. The objective of the study was therefore to investigate boulder blockages at culverts and to develop a modified culvert inlet design to mitigate boulder deposition at a culvert. Achieving the objective comprised of field research and a physical hydraulic model in the Hydraulics Laboratory of Stellenbosch University.

The required slope for the incipient motion of 1 m diameter boulders was determined to be 1:25 in the laboratory setting at a prototype discharge of 28.53 m^3/s. The laboratory flume had a width of 12 m (prototype). A rectangular 5 m × 2 m (B × D) culvert was selected for the experimental tests and model development. Experimental tests were conducted at a scale of 1:16 using Froude scale similitude.

The inlet of the culvert was identified as the location where boulders would generally settle. A modified inlet was proposed to streamline the flow through the culvert barrel and to prevent boulder deposition in the barrel of the culvert. Three culvert inlet layouts were developed as a desktop study, of which two of the inlet layouts were tested as physical models, namely the tapered and compound tapered inlet.

The tapered inlet model featured an inlet with a side-wall contraction and slope depression, with a 1:10 (V × H) slope, to increase the flow velocity through the culvert. The tapered inlet produced unstable flow conditions with a shock wave forming in the inlet just upstream of the barrel inlet. A compound tapered model was developed, featuring a side wall taper of 1:4 and a bed slope taper of 1:9.6 (V × H) to increase the flow velocity. A control point was created by the taper upstream, effectively moving the control of the barrel upstream. Experimental results indicated that the flow depth through the culvert is reduced, increasing the flow velocity. The self-scouring velocity prevented boulders from settling near the inlet of the compound tapered culvert. Boulders that settled upstream of the culvert inlet, settled out upstream of the new control section. Therefore, the compound tapered culvert inlet layout can effectively mitigate boulder deposition near the inlet and inside the culvert barrel.

A two- and three-cell compound tapered model was tested. The two-cell model performed in a comparable manner to that of the single-cell model. The three-cell model caused boulders to deposit at the inlet since the upstream control point was not designed as a flow control point. The contraction between the upstream flow and the inlet lip was not sufficient to control the flow. In conclusion, the compound tapered models proved to mitigate boulder deposition at culvert entrances, if designed correctly.

Design guidelines were developed in designing culvert inlets to mitigate boulder deposition.

Opsomming

Padduikers dien as belangrike strukture om dreinering te bied vir strome onder deur die pad oppervlak. Die nadeel van kasduikers is dat die strukuur ‘n obstruksie in die vloei van die water is. As gevolg van die obstruksie, neem die vloei snelheid af wanneer die vloei die duiker nader. Die opdamming en stadige vloei veroorsaak dat klippe uitsak en die kasduiker toe spoel. Bergagtigegebiede bied die benodige hidroulliese styl helling om klip beweging in die rivier aan te moedig. Die studie het gefokus rondom die berggebiede van die Wes-kaap, die gevolg hiervan is dat natuurlike geronde klip vir die eksperimentele toetse gebruik is.

Die motivering vir die studie was dus gegrond op die toespoel van kasduikers as gevolg van klippe wat stroomaf spoel. Vloeiarea van die kasduiker word verminder deur die klippe wat die inlaat versper, wat tot ‘n hoër risiko van oorstroming kan lei, en in sekere gevalle kan die vloei die pad ook weg spoel. Die doelstelling van die studie was dus om klip blokasies by kasduikers te ondersoek en te bepaal hoe die klip by die kasduiker uitsak. ‘n Metode moes ontwikkel word om die blokkasies deur klippe by kasduikers te verhoed. Om die doelstelling van die studie te bereik was gebruik gemaak van veldwerk om die probleem te ondersoek en ‘n fisiese model in die Hidrouliese Laboratorium van Stellenbosch Universiteit.

Tydens die eksperimentele toetse is daar bepaal dat vir ‘n prototipe ontwerpdeurstroming van 28.53 m³/s, ‘n 1 m diameter klip teen ‘n helling van 1:25 weggespoel kan word. Die wydte van die opstelling was 12 m wyd (prototipe). ‘n 5 × 2 m (B × D) kasduiker is gekies vir die experimentele toetse teen ‘n model skaal van 1:16, deur ‘n Froude skaal te gebruik.

Tydens die toetse is daar bepaal dat die klippe by die inlaat van die kasduiker uitsak. Daar is dus gemotiveer om ‘n inlaat te ontwikkel wat die vloei van die water belyn met die inlaat van die duiker om sodoende die vloei te versnel en klip uitsakking te verminder. Drie kasduiker inlaat uitlegte is ontwikkel, waarvan twee getoets is in die laboratorium as fisiese modelle, naamlik ’n vernouing model en saamgestelde vernouing model.

‘n Vernouing model met ‘n vernouing aan die kant mure in die rigting van die inlaat, asook ‘n vloer wat na onder sak om die vloei te versnel is getoets. Die vernouing inlaat het onstabiele vloei stroomop van die kasduiker inlaat veroorsaak in die vorm van ‘n skokgolf. Die tweede model, die saamgestelde vernouing model, het soortegelyke vernoude kant-mure gehad, maar teen ‘n verhouding van 1:4, die vloer het ook ’n styl helling van 1:9.6 (V × H) om die vloei te versnel. Addisioneel het die tweede model ‘n gedefinieerde kontrole punt sroomop van die inlaat gehad, met die idee dat geen klip stroomaf van die kontrole punt, mag uitsak nie. Die resultate het aangedui dat die vloeidiepte deur die saamgestelde vernouing model verlaag, wat dus die vloei versnel het. Die self-uitskuur vermoë van die vinnige vloei

het verhoed dat klippe in die duiker uitsak. Klippe wat wel uitgesak het, het uitgesak stroomop of by die nuwe kontrole punt. Dit was dus bepaal dat die saamgestelde vernouinging inlaat uitleg verhoed dat die uitsak van klippe naby die inlaat en binne die kasduiker plaasvind.

‘n Twee-opening en drie opening saamgestlede vernouingduiker was ook getoets. Die twee-opening model het op die selfde wyse as die enkel duiker model gefunksioneer. Die drie-inlaat kasduider het getoon dat die kontrole punt goed gedefinieer moet word om die uitsak van klippe in die inlaat te verhoed. Daar was dus bevind dat die saamgestelde vernouingmodel goed werk om klip deponeering te verhoed by die inlaat van ’n kasduiker, mits die kontrole punt deeglik ontwerp word.

Ontwerpriglyne was ontwikkel vir die ontwerp van kasduiker inlate om klip deponeering te verhoed.

Acknowledgements

I would like to express my deepest appreciation towards the following individuals and institutions for their contributions, continuous support and guidance throughout the journey of my studies and helping me to succeed:

- Mrs Adèle Bosman, my supervisor, for your guidance, support and motivation to persevere throughout the course of my studies.
- Prof. Gerrit Basson, for his assistance and providing valuable advice on my thesis.
- The South African National Road Agency SOC Ltd. (SANRAL) and Stellenbosch University for providing me with the financial support to allow me to complete my post-graduate studies.
- Mr Johann Nieuwoudt and Mr Iliyaaz Williams for their hard work in the Hydraulic laboratory. For building all the experimental models that I tested and their friendliness when assisting me in the laboratory.
- Mr Hans King for providing me with photographs and sharing his practical knowledge and experiences relating to my studies.
- Mr Frikkie Mostert and Mr Henry Horn their friendly assistance during my fieldwork and for taking time out of their schedule to show me around the sites.
- Mr Anton Kunneke for providing me with the Trimble GNSS unit for the fieldwork and assisting me with the post-processing of the data.
- Charmaine, for all your patience, love and support throughout my post-graduate studies.
- My mother, family and friends for encouraging me and continuously supporting me during my studies.

Finally, I would like to dedicate my thesis in memory of my late father who sparked my interest and passion for civil engineering at a very young age.

Table of Contents

List of Figures

List of Tables

Nomenclature

Symbol	Description	Unit
A	Cross-sectional area	m^2
a,b,c	Triaxial particle dimensions, a is the longest and c the shortest	m
B	Culvert barrel width	m
B_{lip}	Arc length of inlet lip	m
B_T	Taper face width	m
C	Chézy coefficient $C = 18Log(12R/k_s)$	$m^{0,5}/s$
C_B	Inlet coefficient for rectangular culverts with $0 \leq H_1/D \leq 1.2$	dimensionless
C_D	Drag coefficient	dimensionless
C_H	Inlet coefficient for rectangular culverts with $H_1/D > 1.2$	dimensionless
D	Culvert barrel height	m
d	particle size	m
d_{50}	Median particle size	m
d_r	Reference particle size	m
E	Specific energy ($E = y + v^2/(2g)$	m
E_u	Euler number	dimensionless
Fr	Froude number	dimensionless
g	Gravitational acceleration ($g = 9,81\ m/s^2$)	m/s^2
H	Energy head	m
h_1	upstream flow depth	m
H_e	Entrance energy head loss	m
H_f	Friction head loss	m
H_L	Total energy head loss	m
H_o	Outlet energy head loss	m
HW	Headwater	m
HW_B	Flow depth of barrel for tapered section	m
HW_C	Flow depth upstream of inlet depression	m
HW_T	Flow depth inside inlet depression	m
HW_u	Flow depth upstream of the culvert	m
k	Absolute roughness	m
K_e	Secondary inlet loss coefficients	dimensionless
K_o	Secondary outlet loss coefficients	dimensionless
k_s	Roughness coefficient	m
L	Culvert barrel length	m
L_a	Apron length	m

Symbol	Description	Unit
L_{lip}	Length from transition to inlet lip apex	m
L_T	Taper length	m
MN	Movability number	dimensionless
n	Manning's roughness coefficient	$m/s^{1/3}$
P	Wetted perimeter	m
Q	Discharge rate (flow rate)	m^3/s
q_c	Critical unit discharge	m^2/s
q_{ci}	Critical unit discharge for particle size i	m^2/s
Q_d	Design discharge rate	m^3/s
Q_T	Return period discharge	m^3/s
R	Hydraulic radius (R = A/P)	m
Re	Reynolds number	dimensionless
Re*	Particle Reynolds number	dimensionless
S_0	Bed slope	m/m
S_c	Critical bed slope	m/m
SF	Shape factor	dimensionless
S_f	Friction slope	m/m
T	Elevation change of taper	m
TW	Tailwater depth	m
V	Velocity	m/s
$\bar{V}$	Average velocity	m/s
V*	Shear velocity	m/s
V_{*c}	Critical shear velocity	m/s
V_{SS}	Particle settling velocity	m/s
V_d	Velocity downstream of culvert outlet	m/s
$\bar{v}_e$	Culvert entrance velocity	m/s
$\bar{v}_o$	Culvert outlet velocity inside the barrel	m/s
v_u	Upstream fow velocity	m/s
W	Weber number	dimensionless
y	Flow depth	m
y_c	Critical flow depth	m
z	Elevation	m
α	Wing-wall angle	°
ΔP	Pressure change	kN/m^2
θ	Shields shear parameter	dimensionless

Symbol	Description	Unit
λ	Subcriticality factor ($\lambda = y/y_c$)	dimensionless
ν	Kinematic viscosity ($\nu = 1{,}14 \times 10^{-6}$)	m^2/s
ρ_s	Rock density	kg/m^3
ρ_w	Density of water ($\rho_w = 998\ kg/m^3$)	kg/m^3
σ	Surface tension	N/m
τ	Shear stress	N/m^2
τ_{*ci}	Average critical Shields parameter	dimensionless
ϕ	Inlet fan angle	°

Abbreviations and Acronyms

AOP – Aquatic Organism Passage

CFD – Computational Fluid Dynamics

CIRIA – Construction Industry Research and Information Association

CPAA – Concrete Pipe Association of Australasia

CT – Compound Tapered

EGL – Energy Grade Line

FHWA – Federal Highway Administration

GNSS – Global Navigation Satellite System

GPS - Global Positioning System

HDS-5 – Hydraulic Design Series No. 5

HEC – Hydraulic Engineering Circular

HGL – Hydraulic Grade Line

MEL – Minimum Energy Loss

MN – Movability Number

NBIS – National Bridge Inspection Standard

NC – No Culvert

NGL – Natural Ground Level

SANRAL – South African National Road Agency SOC Ltd.

SF Shape Factor

TEL – Total Energy Line

TW – Tailwater

USBR – United States Bureau of Reclamation

WL – Water Level

1. Introduction

1.1 Background

Culverts, as defined by (Rooseboom and Van Vuuren (2013b), are structures that are used primarily to convey water from one side of the road to the other. These structures are placed in the flow path of smaller streams and rivers to provide drainage to the surface water. A culvert should be designed in such a way to reduce the disturbance to the natural watercourse, which in turn is in a constant quasi-equilibrium state between flow and erosion processes.

Culverts should not only be designed in accordance with the hydraulic requirements set-out during the design process but also adhere to an environmental requirement in terms of the existing natural processes in the watercourse, such as debris transport of organic material and fluvial processes. Blockages caused by boulders are of a concern where the watercourse slope is hydraulically steep since the incipient motion of the boulders would occur at lower flow rates compared to a mild slope. Steep slopes provide the required shear velocity (Armitage, 2002) or shear stress (Shields, 1936) resulting in the movement of boulders. Mitigation measures are generally put in place to prevent blockages in cases where a watercourse supplies high amounts of boulders. These mitigation measures are, however, high maintenance structures and require periodic cleaning for them to operate effectively (Mizuyama, 2008).

1.2 Problem Statement

The study was motivated by the flooding of roadways caused by boulder blockages as depicted in **Figure 1.1**. Boulder blockages at culverts reduce the discharge capacity of a culvert and increase the potential for other debris and smaller particles to settle, further reducing the discharge capacity.

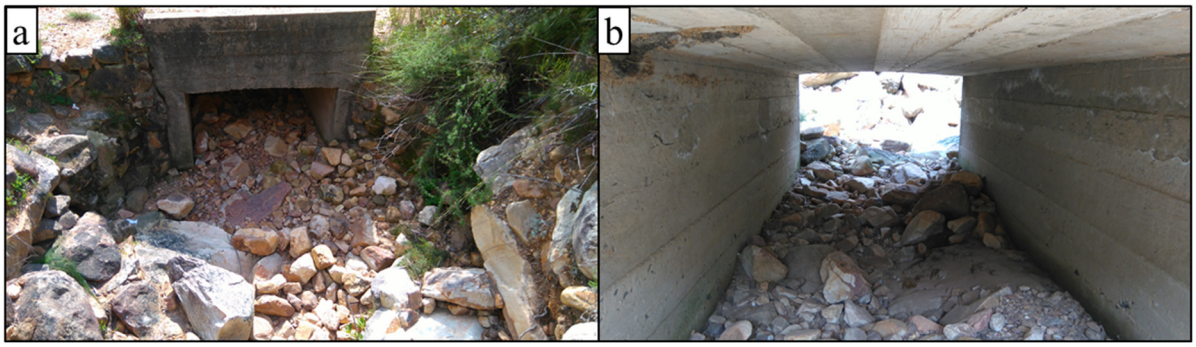

Figure 1.1: Boulders and sediment reduce culvert discharge capacity.

Figure 1.1(a) illustrates a poorly placed culvert entrance, the inlet acts as a drop structure, resulting in sediment and boulder deposition in the barrel **Figure 1.1(b)**. Due to the inlet geometry, the entire barrel

length is influenced by the deposition of boulders and sediment. Optimising the inlet to promote self-cleaning velocities in the barrel will reduce the potential for boulder deposition in the barrel.

Mitigation methods for boulders that are typically used require periodic maintenance and can in some cases be very costly to construct. Placing the existing mitigation methods at culverts with boulder transport problems would be unfeasible.

1.3 Objective of the Study

The primary objective of the research was to provide a culvert design guideline to mitigate the blockage of culverts caused by boulders in hydraulically steep mountain rivers. Ideally, the boulders would be able to pass through the culvert undisturbed and settle out naturally as prior to the installation of the culvert. The research is limited to the Western Cape mountain rivers to limit the type of boulder associated with the watercourse.

The objective of the research was achieved by ensuring that the following criteria were satisfied:

- The boulders need to be able to pass through the culvert without causing a significant increase in water depth, i.e. it should not cause flooding of the roadway or a significant increase in backwater.
- Design guidelines that are developed should be easily adaptable to any site where boulder blockages or the potential for blockages have been identified.
- The culvert has to be low maintenance or, ideally, maintenance-free to reduce the risk of blockages caused by the lack thereof.
- Provision should be made for the reduction in the risk of floating debris accumulation at the piers in the case of a multi-cell culvert.
- Taking cost and complexity into consideration, the structure should be designed to be as short and simple as possible to reduce these factors.
- The design should allow for boulders sized between 0.4 m and 1 m to pass through.

The objective was met by a proposed field study to understand and achieve a better perspective on the identified problem. Two sites were identified, and the data accumulated at the two sites provided useful insight into the culvert blockages. Based on the literature gathered and the site visits, a desktop study was carried out to design three prototype inlets, of these inlets, two were selected and tested as physical models. From the results of the physical models, proposed guidelines were set out for future design purposes.

The boulder size distribution was selected to represent the largest 15% of particles of a riverbed. A sample from the Berg river shows that the d_{85} particle size was slightly larger than 0.4 m and the largest

boulders were recorded between 0.9 m and 1 m (Gazendam, 2005). Boulder size would vary on the stream for each site, the sizes used for this study was selected as representative of a typical Western Cape river.

1.4 Significance of the Study

The findings from this research aim to provide a viable solution to a problem experienced at culverts not previously studied. Findings from this research could be used towards better understanding the problem of boulders blocking culverts. The findings would also encourage engineers to consider each stream crossing separately with its own natural characteristics that need to be accounted for to prevent problems arising from the modification for the natural watercourse. A set of guidelines, developed by means of the results obtained from this research, to provide assistance for cases where a risk of boulder blockages has been identified.

1.5 Thesis Overview

The thesis overview provides a short summary of the main theme for each of the chapters and the contribution each of the chapters provides to the thesis:

- The background, problem statement and objectives of the study are presented in **Chapter 1**.
- **Chapter 2** comprises the literature review in order to attain a better understanding of the problem at hand and to provide the resources to develop a suitable solution from the available research in the field of study.
- A detailed account for the fieldwork performed at the two sites that have been identified as problem areas is presented in **Chapter 3**.
- The general layout for the experimental tests and the apparatus used are discussed in **Chapter 4**. The experimental test limitations identified and their effect on the results are discussed.
- Preliminary tests were conducted in **Chapter 5** to establish an experimental model setup that was required for the design of the proposed experimental models. This preliminary model served as a reference to all the other models tested. The results of the preliminary model are also discussed in this chapter.
- **Chapter 6** deals with the proposed model development and testing procedure followed. Three inlet culvert designs were produced by conducting a desktop study based on the preliminary model results.
- Two of the three models were selected based on cost, design simplicity and practicality in terms of construction. Two models were then constructed and tested in the physical model setup. The results of the two models are analysed and the best performing culvert was identified.

- A multi-barrel setup was designed in **Chapter 7** to test the effect of multiple dividing walls on the proposed structure.
- Final conclusions are drawn in **Chapter 8**.
- The proposed guidelines that have been developed with the results and findings from the thesis are presented in **Chapter 9**.
- **Chapter 10** presents recommendations for further studies to address the boulder blockage problem.

2. Literature Review

2.1 Introduction

This chapter is a review of the contributions made, available research and design manuals that are of interest to this research. The literature review contains all the relevant information used to aid in the development of a prototype model and to gain a better understanding of the problem as identified in the Problem Statement. There is limited to no research available regarding boulder deposition at culverts, therefore culverts and boulder transport were viewed separately. The culvert hydraulics and operation are the focus of the study, boulder transport in rivers were reviewed to gain a better understanding and to supplement the design considerations.

Sections that were focussed on in this section are as follows: current culvert design guidelines, boulder transport, erosion control and scale effects. An overview of current culvert design guidelines has been investigated. Conditions at which boulders would be transported was of interest in order to identify the boulder size that needs to be considered for a given flow rate. One of the significant reasons for culvert failure is downstream erosion. Thus, existing erosion control measures have been investigated, and the methods that would be applicable to boulder transport have been identified. In order to understand and correctly design and interpret the physical model results, it is important to identify the scale-effects that would affect the accuracy of the model and to consider it as part of the design.

2.2 Open Channel Definitions and Equations

Open channel flow, or free surface flow, is defined as flow that always experiences a free surface open to the atmosphere (water surface) (Chadwick *et al.*, 2013). This section summarises some of the general hydraulic equations used and referred to throughout this thesis. The following equations form a fundamental part of open channel hydraulics.

Energy Equation

The energy equation for determining the flow conditions between two points (point 1 and 2) can be determined by considering Bernoulli's equation together with continuity ($Q_1 = Q_2$). Since the flow rate (Q) at point 1 must be equal to point 2 and considering the conservation of energy, then it must hold true that the energy at point 1 (E_1) must be equal to the energy at point 2 (E_2). $E_1 = E_2$ describes the energy equation given by the following equation (Chadwick *et al.*, 2013):

$$z_1 + y_1 + \frac{V_1^2}{2g} = z_2 + y_2 + \frac{V_2^2}{2g} \qquad \textbf{2-1}$$

Where:

Q = Discharge (m^3/s)

z = Bed elevation (m)

y = Water depth (m)

V = Velocity (m/s)

The energy equation (**Equation 2-1**) is suited to smooth channel conditions with no friction or transition losses. These limitations make the Bernoulli equation applicable to short and smooth transitions, the energy losses are negligible producing sufficiently accurate results. In other situations where transition losses, friction losses or any other losses are present, they must be accounted for in the Bernoulli equation (Chanson, 2004).

Froude Number

The Froude number is a dimensionless parameter defined as a ratio between the acceleration of a fluid particle due to a force acting on it and the acceleration due to the force of gravity (Munson *et al.*, 2009). Therefore, the Froude number is proportional to the square root of the inertial force over the fluid weight (Chanson, 2004). For a rectangular channel, the Froude number is given by the following equation:

$$Fr = \frac{V}{\sqrt{gy}} \qquad \textbf{2-2}$$

Where:

V = Velocity (m/s)

g = Gravitational acceleration (m/s^2)

y = Water depth (m)

Flow regimes are typically described by the Froude number, for a Fr = 1 the flow is said to be critical, at this point the discharge is a maximum at the lowest energy (Chanson, 2004). A Fr < 1 produces subcritical flow, the water velocity is lower than the wave velocity, which causes disturbances in the flow move upstream and downstream. Flow depth is influenced by downstream controls for subcritical flow. A Fr > 1 produces supercritical flow, water velocity is greater than wave velocity, disturbances only move downstream, therefore upstream water levels are not affected by downstream controls (Chadwick *et al.*, 2013).

Hydraulic Jump

Conservation of momentum is applied where the conservation of energy cannot accurately describe the flow, typically this would be in the case of a hydraulic jump where energy is lost in the flow by means

of turbulence. A hydraulic jump forms when flow transitions from supercritical to subcritical flow, the conjugate flow depth (y_2) can be calculated by the following equation (Chanson, 2004):

$$y_2 = \frac{y_1}{2}\left(\sqrt{1 + 8Fr_1^2} - 1\right) \qquad \textbf{2-3}$$

The flow depth upstream of the hydraulic jump (y_1) and the conjugate flow depth (y_2) can be used interchangeably in **Equation 2-3**, with its corresponding Froude number.

Uniform Flow Formulae

If the flow in a channel is uniform, it is considered that the frictional forces and gravitational forces are in equilibrium. The flow in the channel can then be described by either the Manning or Chézy Equation for turbulent flow conditions. Each equation has a friction factor to describe the roughness in a channel, Manning (**Equation 2-4**) uses a Manning's n roughness coefficient (Chadwick *et al.*, 2013) and Chézy (**Equation 2-5**) uses a roughness coefficient (k_s) to describe the roughness of a given channel (Rooseboom and Van Vuuren, 2013a).

$$Q = \frac{A^{5/3}\sqrt{S_0}}{n\,P^{2/3}} \qquad \textbf{2-4}$$

$$Q = A18\mathrm{Log}\left(\frac{12R}{k_s}\right)\sqrt{RS_0} \qquad \textbf{2-5}$$

Where:

- Q = Discharge (m^3/s)
- A = Flow area (m^2)
- S_0 = Channel bed slope (m/m)
- n = Manning's roughness coefficient ($s/m^{1/3}$)
- P = Wetted perimeter (m)
- R = Hydraulic radius, A/P (m)
- k_s = Roughness coefficient (m)

2.3 Overview of Culverts

Culverts are defined as hydraulically short structures typically used to allow flow to traverse a road (Chow, 1959; Henderson, 1966). A culvert is comprised of three sections, namely the inlet, barrel and outlet, **Figure 2.1** shows a simple rectangular culvert with wing-walls at the inlet and outlet (Chanson, 2004).

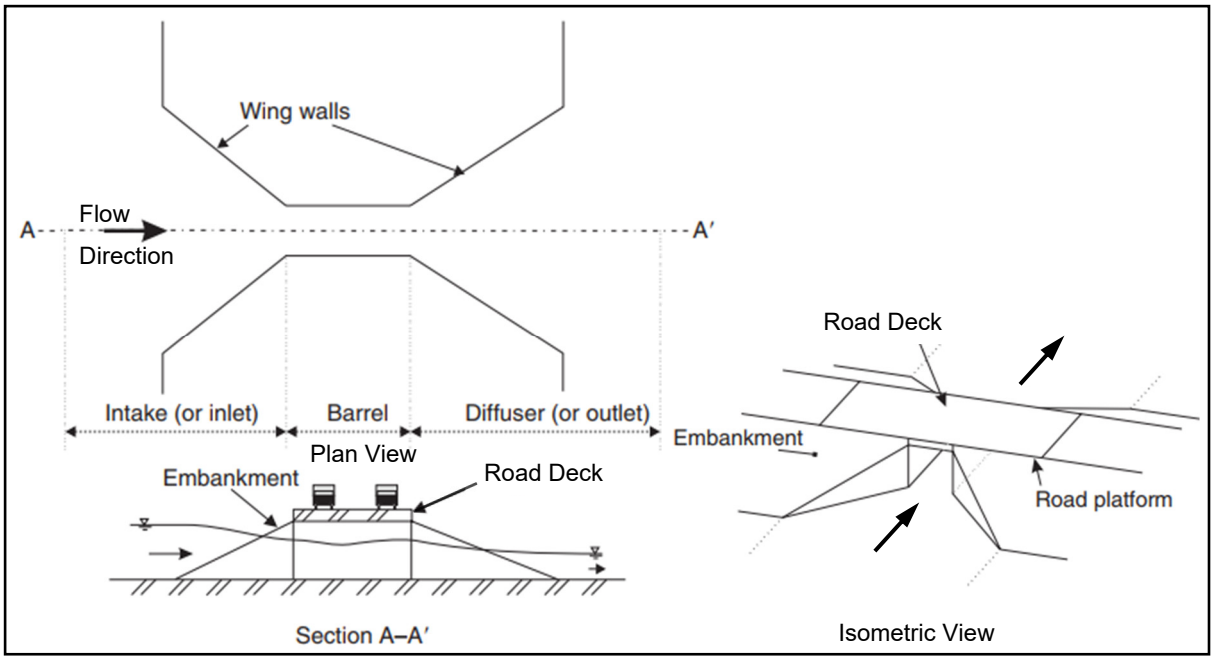

Figure 2.1: Schematic layout of rectangular culverts and all its components (Chanson, 2002).

Different culvert shapes exist and are actively used, some less common culvert shapes are arches, mostly used in open-bottom culverts, and elliptical shapes (Schall *et al.*, 2012). Circular and rectangular cross-section culverts are most commonly used. The focus of this research was on the use of rectangular culverts, and any further reference made to the design or layout of the culvert will relate to a rectangular culvert unless otherwise stated.

The hydraulic design of culverts has been thoroughly investigated which resulted in detailed design guidelines. The culvert design guidelines provide the basis on which most culverts are designed while reducing the risk associated designing a water crossing out of fundamental principles (Balkham *et al.*, 2010; CPAA, 2012). The hydraulic performance of a culvert is influenced by various factors, such as the upstream and downstream flow depths, inlet geometry, and barrel shape and size (Schall *et al.*, 2012). Generally, different geographic areas or countries have different hydraulic design guidelines for culverts, however, these guidelines are very similar. Currently, the main culvert design guidelines are the HDS-5, 2012 (U.S.A); CIRIA, 2010 (U.K.); CPAA, 2012 (Australia) and the SANRAL Road Drainage Manual, 2013 (South Africa).

Culverts are used in cases where the management of stormwater runoff and watercourses are required to traverse roadways, where bridges are not required or uneconomical as opposed to culverts (Schall *et al.*, 2012). The FHWA, 2012, cites the National Bridge Inspection Standard (NBIS) that defines a culvert as a structure shorter than 6.1 m (span length) while Jansen van Vuuren *et al.* (2013) sets out a further distinction between bridges, major culverts and lesser culverts. It is noted however, that neither

the CPAA (2012), FHWA (2012) or Henderson (1966) made this further classification between culverts and bridges.

According to Jansen van Vuuren *et al.* (2013), a structure is classified as a bridge if it meets one of the following criteria:

- A single horizontal span greater than 6 m.
- The overall length across the watercourse being greater than 20 m, and multiple openings greater than 1.5 m.
- If the opening height between the soffit and bed level is greater than 6 m.
- A total cross-sectional area greater than 36 m².

Jansen van Vuuren *et al.* (2013) classified structures as major culverts if the structure is smaller than a bridge, but has a total span greater than 2.1 m, or if the culvert has a cross-sectional area greater than 5 m². A lesser culvert is if the structure is smaller than a major culvert.

The typical failure mode associated with culverts according to Rooseboom and Van Vuuren (2013b) are as follows:

- Inadequate erosion protection and energy dissipation that causes scouring downstream of a culvert.
- Failure caused by approaching supercritical flow conditions that cause a hydraulic jump to form at the entrance of the culvert. The hydraulic jump causes the roadway to be overtopped, leading to scour downstream of the culvert.
- Blockage at the culvert entrance by debris could cause overtopping and scouring of the embankment and surface layers.
- Wide flood plains cause flow alongside the road towards the culvert causing scour around the inlets.
- Piping, caused by the backfill material becoming saturated, causing a flow path to develop between the culvert and the backfill.
- Hydraulically small culverts at large embankments causing failure due to debris blocking the entrance of the culvert, which can cause overtopping or the road substructure to become saturated.

2.4 Culvert Flow Control

A culvert typically has one of two controls that control the flow through the culvert, namely inlet control and outlet control. The control condition classification is based on the location of the control point at the culvert. The capacity of the culvert may be limited by either inlet or outlet control, depending on various factors (Schall *et al.*, 2012). Both controls need to be considered in a hydraulic design.

2.4.1. Inlet Control

Inlet control is experienced when the culvert barrel is capable of conveying more water than what the inlet is able to accept. The control section for inlet control is located just inside the entrance of the culvert. Critical flow would occur at or near the inlet of the culvert, where flow passes from subcritical to supercritical flow as seen in **Figure 2.2**. During inlet control the downstream surface disturbances are not propagated upstream, therefore only the discharge intensity and the geometry of the inlet affects the headwater (Schall *et al.*, 2012). Contraction effects and energy losses at the culvert entrance must be allowed for. **Table 2.1** illustrates the factors that influence the discharge of an inlet-controlled culvert. The channel slope is usually steep ($S_0 > S_c$) and the barrel of the culvert is normally steep for inlet control to govern the design (Metzler and Rouse, 1959; CPAA, 2012).

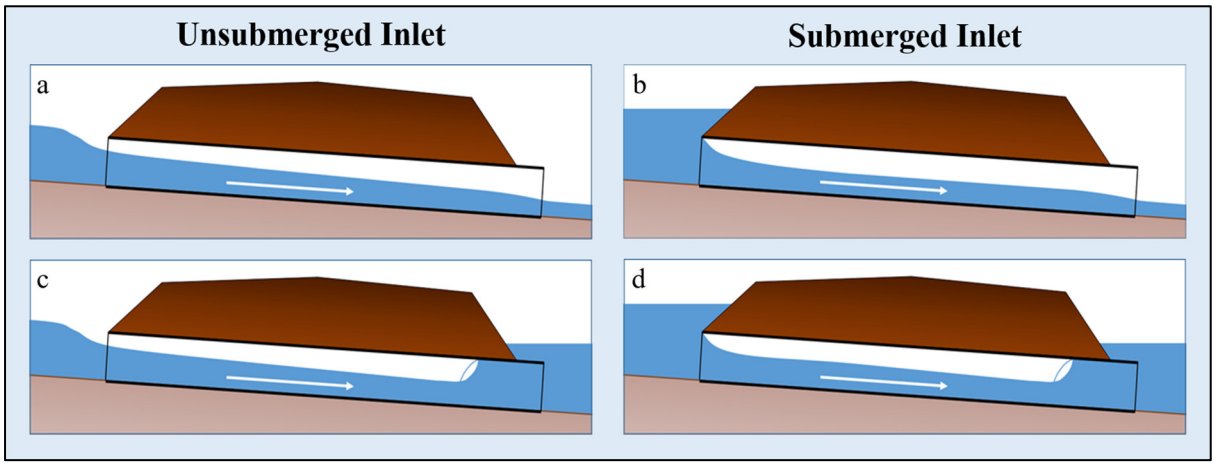

Figure 2.2: Inlet control conditions typically experienced at culverts (recreated from FHWA, 2012).

(a) & (b) illustrates flow passing through critical flow at the culvert inlet, resulting in supercritical flow inside the barrel with a high flow velocity. This is considered as the desirable case for the flow in the barrel considering boulder movement since sediment deposition would not occur inside the barrel.

(c) & (d) illustrates flow passing through critical flow at the culvert inlet, however a hydraulic jump forms inside the barrel. This is an undesirable scenario since sediment and cobbles would be deposited just downstream of the hydraulic jump inside the barrel (Carling, 1995). Wellman *et al.* (2000) observed

gravel bars in rectangular culverts extending downstream after flood events. He concluded that the break in the grade of the culvert caused the deposition inside the culvert. The deposition potential inside the barrel is therefore increased due to the backwater effects caused by the lower downstream bed.

Tsidrintzis (1995), cited by Wellman *et al.* (2000), observed that flood events carried large volumes of sediment downstream, deposition took place in the inlet and just upstream of the culvert. Sedimentation caused additional head losses upstream leading to further deposition. (Wargo and Weisman, 2007) concluded that the contraction of a culvert, due to the wider river cross-section, and subsequent upstream damming causes sediment to settle out upstream of the inlet.

Table 2.1: Factors influencing flow conditions for inlet control and outlet control (recreated from FHWA, 2012).

Factor	Inlet Control	Outlet Control
Headwater	✓	✓
Area	✓	✓
Shape	✓	✓
Inlet Configuration	✓	✓
Barrel Roughness	×	✓
Barrel Length	×	✓
Barrel Slope	✓	✓
Tailwater	×	✓

Note: For inlet control, the area and shape refer to the inlet and for outlet control they refer to the barrel of the culvert.

2.4.2. Outlet Control

Outlet control is experienced at the culvert when the culvert barrel is not able to covey the amount of water accepted by the inlet of the culvert, or the tailwater level submerges the culvert exit. The control section is situated at the barrel exit or further downstream. Pressure flow or subcritical flow conditions are present during outlet control, and the barrel can typically run full over the length or at least for part of the length (CPAA, 2012), **Table 2.1** illustrates the factors influencing the capacity of the culvert for outlet control (Schall *et al.*, 2012). **Figure 2.3(a-d)** shows the typical flow profiles experienced with outlet control. For outlet control, all the geometric and hydraulic properties of the culvert play a role to determine the flow capacity,

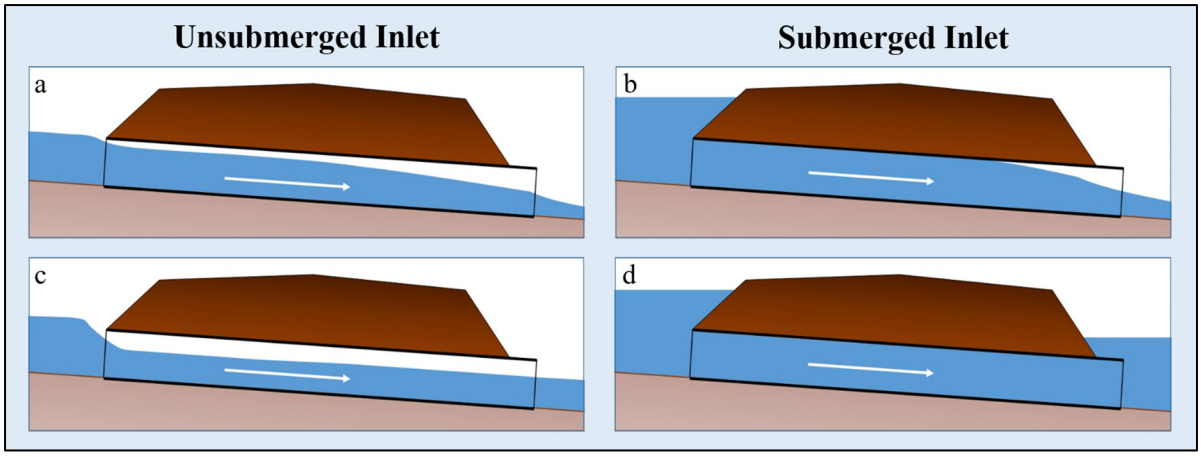

Figure 2.3: Outlet control conditions typically experienced at culverts (recreated from FHWA, 2012).

2.5 Increasing Inlet Efficiency

One of the factors that has an influence on flow capacity for an inlet-controlled culvert is the inlet. A modified inlet that has been properly designed has the potential to increase the discharge with up to 100% in certain cases (Metzler and Rouse, 1959; Schall *et al.*, 2012). Possible modifications include the rounding of the vertical edges, increasing the inlet in terms of an inlet taper, an inlet depression, or a combination of both. Modifications that are made to inlets provide a more efficient design since it becomes possible to reduce the size of the barrel if inlet control governs the design (Schall *et al.*, 2012).

2.5.1. Rounding Inlet Edges

Rounding of the inlets at a culvert reduce the contraction effects and energy entry losses at the inlet. Henderson (1966) suggested a rounding with a radius of 0.1B, where B is the width of the culvert to eliminate contraction effects. Jones *et al.* (2006) found that rounding the edges of wing walls has no appreciable effect on the inlet efficiency and that contraction effects are only eliminated when rounding the culvert entrance.

If the inlet is submerged, it is beneficial to provide a fillet on the soffit of the inlet, this greatly increases the inlet efficiency. A radius of approximately 200 mm provides an inlet with no contraction loss experienced at the inlet of a submerged inlet. The higher the headwater, the more pronounced the efficiency of the rounded inlet becomes (Jones *et al.*, 2006).

2.5.2. Inlet Taper

Inlet tapers, also referred to as side-tapered inlets, are defined as an enlarged face section (B_T) upstream of the culvert barrel. A transition section between the larger inlet and barrel is utilised to reduce the head loss associated with contractions (Schall *et al.*, 2012). Shown in **Figure 2.4** is a side-tapered inlet, with the taper section constructed with a closed soffit in this case.

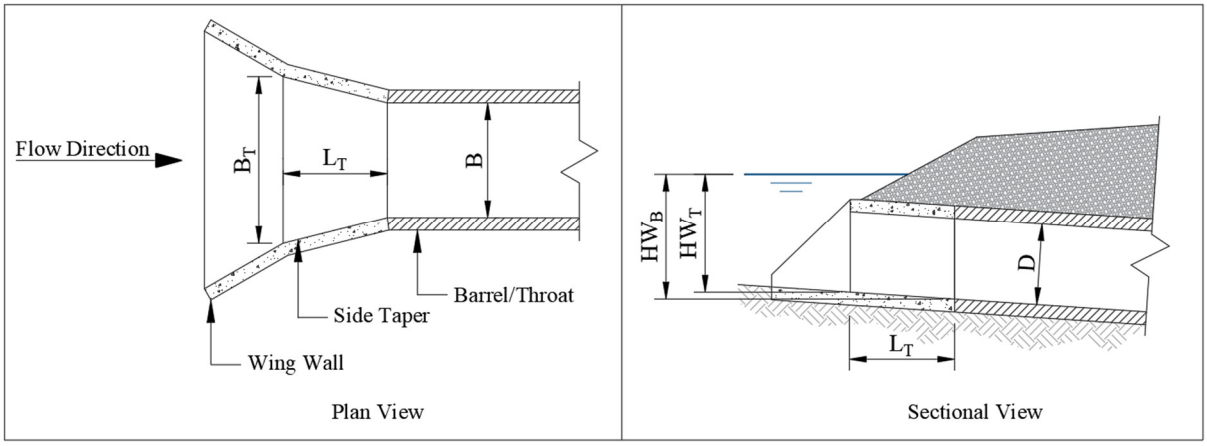

Figure 2.4: Schematic layout of a side-tapered inlet (recreated from FHWA, 2012).

The function of a tapered inlet is to reduce the flow contraction at an inlet resulting in a more hydraulically efficient culvert design. A tapered inlet is an effective solution to increase the flow of an existing culvert if the need for an increase in flow capacity is required. Tapered inlets can be retrofitted to existing culverts without the need to rebuild the existing structure.

Additional control sections exist for the tapered inlet and need to be checked together with inlet- outlet control as any of the control sections may control the flow through the culvert. For the tapered inlet depicted in **Figure 2.4** the flow can be controlled at the outlet, at the culvert barrel (HW_B) or at the start of the inlet taper (HW_T) (Schall *et al.*, 2012). It has been argued by Metzler and Rouse (1959) that the control could exist at any intermediate point between the inlet face (HW_T) and the barrel (HW_B).

FHWA (2012) recommends that the sides should taper between 1:4 and 1:6, assuming that Fr does not exceed two. The United States Bureau of Reclamation (USBR) recommends a 1:3Fr taper as discussed in more detail in **Section 2.7,** which is in agreement with FHWA's (2012) taper ratios. The 1:4 recommendation seems to be a balance between the USBR (1987) recommendation and economical considerations. Considering that the flow would most likely be critical at the face section, provided it is the control section, a taper of 1:4 would still be conservative to minimise contraction effects and losses.

2.5.3. Inlet Depression

Where the natural streambed allows it, it is possible to construct the barrel of the culvert below the bed elevation at a flatter hydraulic slope than that of the streambed, provided the culvert slope is sufficiently steep to avoid sediment deposition. At the inlet, a depression is created that acts as a transition between the streambed and barrel. The advantage of such a modification is the additional upstream head available which increases the flow rate through the culvert (Schall *et al.*, 2012). **Figure 2.5** illustrates a culvert with an inlet depression. The inlet can either include wing-walls (**Figure 2.5(a)**), allowing water

to only flow the approaching direction or have a sump upstream of the inlet (**Figure 2.5(b)**). The recommended minimum dimensions for an inlet depression are illustrated in **Figure 2.5**.

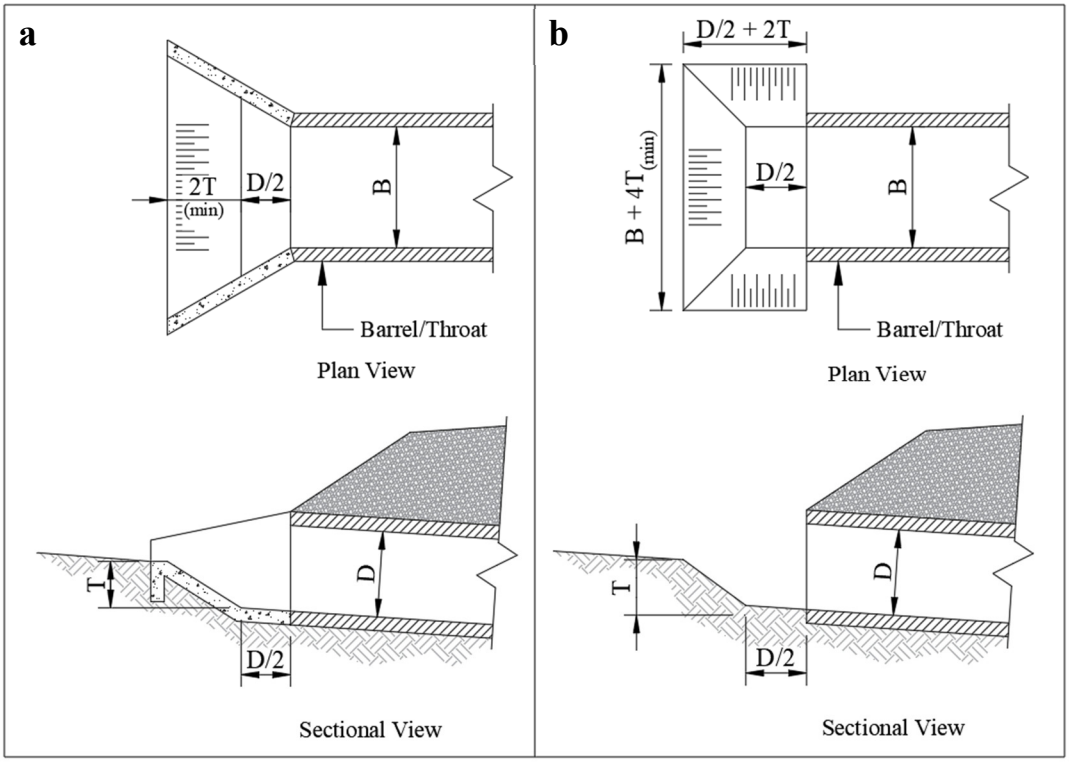

Figure 2.5: Inlet depression configuration. **A** - Inlet depression with wing walls, **B** - Inlet depression with sump upstream of the barrel (recreated from FHWA, 2012).

It is worth noting that both the side-taper and inlet depression is only effective for a culvert operating under inlet control. The efficiency increase for the tapered inlets is about the same as for rounded inlet, with a much greater cost penalty (Schall *et al.*, 2012). It is not advised to place the entire barrel of the culvert under the natural ground level, since sedimentation problems may occur (Thompson and Kilgore, 2006).

2.5.4. Combination Inlets

The tapered and depressed inlets can be combined to further increase the efficiency and capacity of the culvert, it does come with an economical penalty and construction complexity. Hydraulic performance and the need for a reduced barrel size needs to justify the associated cost and complexity (Schall *et al.*, 2012).

There are two configurations of slope-tapered inlets, an inlet depression just upstream of the taper (**Figure 2.6(a)**) and the inlet depression forming part of the tapering sides (**Figure 2.6(b)**). A type I, slope-tapered inlet (**Figure 2.6(a)**) has the advantage of additional headwater on the inlet face resulting in the need for a smaller inlet face and barrel. A minimum distance of 0.5D should be allowed between

the depression and the face section of the taper, which should be on the same slope as that of the taper. Three possible control points should be investigated to determine which is controlling the flow: the crest of the depression, the face section of the taper and the barrel section of the culvert (Schall *et al.*, 2012). Each of these control sections has been indicated in **(Figure 2.6a)**.

The Type II slope-tapered inlet (**Figure 2.6(b)**) requires a larger face section than that of the Type I inlet since the depression in the taper produces additional head that increases the flow through the barrel. As with the Type I inlet, the Type II inlet has three possible control sections: the face section, the bend section and the barrel section. However, the length between the barrel and bend section should be chosen conservatively to prevent the bend from controlling the flow (Schall *et al.*, 2012). **Figure 2.6(b)** illustrates the possible control sections.

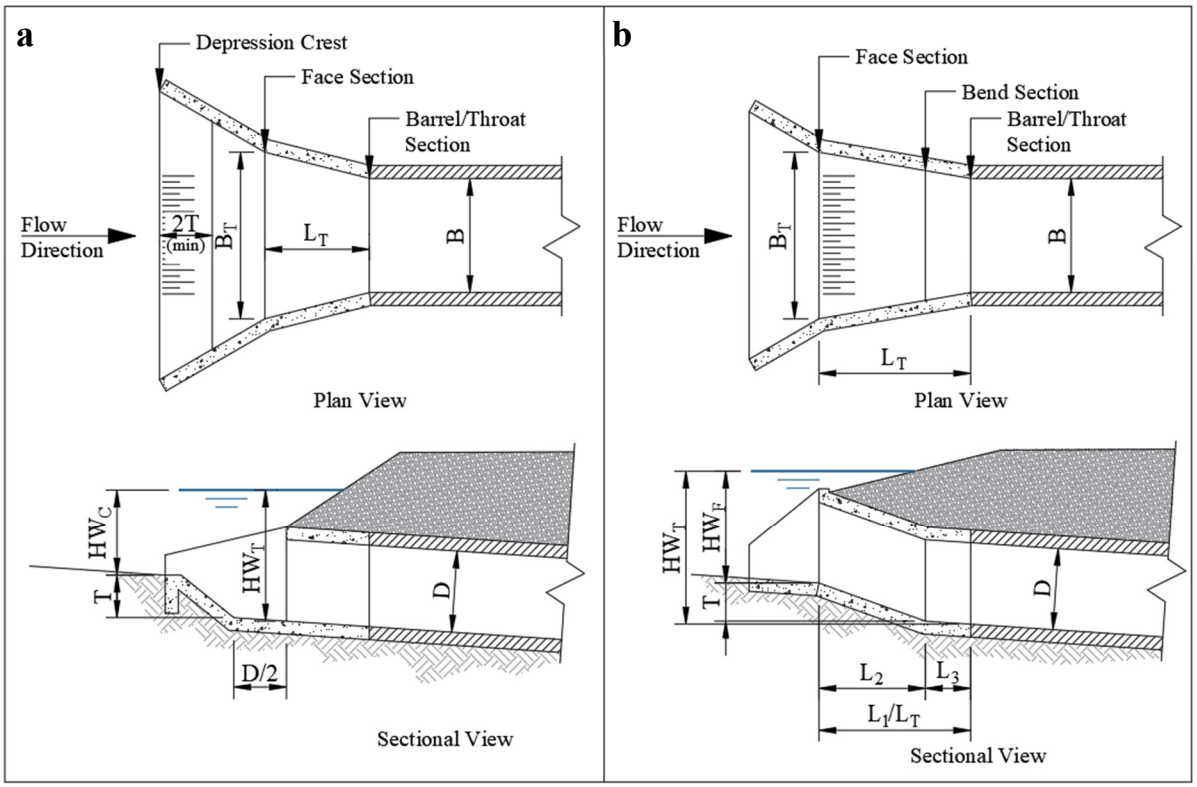

Figure 2.6: Slope-Tapered inlets, **a** - Type I inlet: Tapered inlet with depression upstream; **b** - Type II - Tapered inlet with depression in the tapering section (recreated from FHWA, 2012).

2.6 Hydraulic Design of Culverts

The hydraulic design of box (rectangular) culverts are reviewed in this section. Pipe (circular) culverts were not considered for this research since pipes are typically used for lower discharges that do not transport boulders. The guidelines as set out by Rooseboom and Van Vuuren (2013b) was mainly used for the hydraulic design of the culverts. Both inlet (upstream) and outlet (downstream) control should be tested for since it is unknown which forms the control. If the design discharge is known, the highest

upstream damming head (H_1) is putative as the representing control flow level (Rooseboom and Van Vuuren, 2013b).

2.6.1. Inlet Control

For an inlet-controlled culvert, Henderson (1966) defined an H/D limit for inlets as 1.2 as the optimum hydraulic section. For an H/D = 1.2 limit, the clearance between the free-surface level and the soffit of the culvert would be about 20%, and the discharge through the inlet would provide the maximum discharge for a given head (Rooseboom and Van Vuuren, 2013b). Hee (1969) and the USBR (1987) determined that the H/D limit should not be greater than 1.2, whereas Chow (1959) provided the limit as a range between 1.2 and 1.5. Generally, it is accepted that the H/D limit be set to 1.2.

If the discharge is known and the resulting upstream head needs to be determined (H_1), the H/D ratio would be unknown. The upstream damming head H_1 should be determined for two conditions, free-surface flow (H/D ≤ 1.2) using **Equation 2-6**, and submerge inlet conditions (H/D > 1.2) using **Equation 2-7**. The submerged and unsubmerged inlet-control flow types are shown in **Figure 2.7**. For unsubmerged flow, there is a slight improvement in discharge efficiency if rounded inlets are used as opposed to square inlets if the radius of the rounding is greater than 0.1B. (Henderson, 1966).

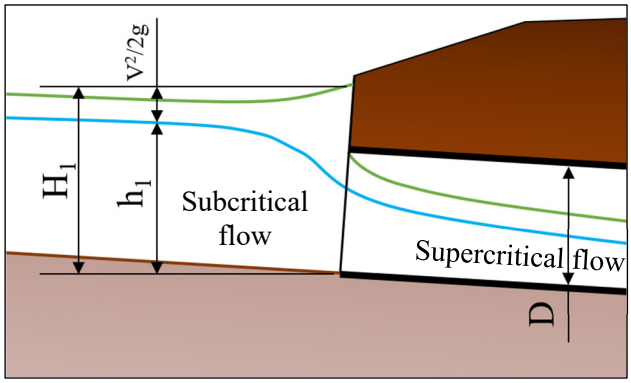

Figure 2.7: Submerged (green) and unsubmerged (blue) flow through an inlet-controlled culvert.

For $0 < H_1/D \leq 1.2$:

$$Q = \frac{2}{3} C_B B H_1 \sqrt{\frac{2}{3} g H_1} \qquad \textbf{2-6}$$

Where: $C_B = 0.9$ for square inlets

$C_B = 1$ for rounded inlets

For $H_1/D > 1.2$:

$$Q = C_h B D \sqrt{2g(H_1 - C_h D)} \quad \textbf{2-7}$$

Where: $C_h = 0.6$ for square inlets

$C_h = 0.8$ for rounded inlets

2.6.2. Outlet Control

To Determine the required head for a given discharge for outlet control, it is assumed that the culvert would flow full over at least part of the culvert. The energy and continuity equations are used to determine the flow conditions under outlet control (Rooseboom and Van Vuuren, 2013b). **Figure 2.8** illustrates the parameters used for outlet control calculation. The notation used by The SANRAL Drainage Manual (2013) is unclear as to when a parameter refers to being in the channel (upstream or downstream) or in the culvert (inlet or outlet), the notation adopted by the FHWA in HDS-5 is instead used to describe the procedure. The hydraulic design guidelines for outlet control presented by both Rooseboom and Van Vuuren (2013b) and HDS-5 (FHWA, 2012) utilise continuity and conservation of energy.

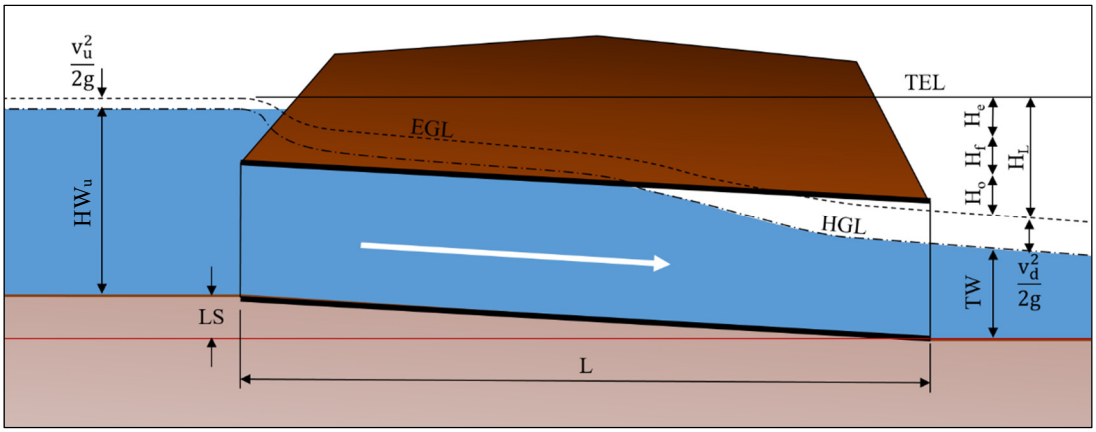

Figure 2.8: Energy components influencing the hydraulic performance of a culvert under outlet control (recreated from FHWA, 2012)

The total energy and friction losses (H_L) experienced by the culvert can be described by the following equation:

$$H_L = H_e + H_f + H_o \quad \textbf{2-8}$$

Where:

H_e = Entrance loss (m)

H_f = Friction loss in the barrel (m)

H_o = Outlet loss (m)

Losses for bends, grates and junctions are not included in this design, their losses are therefore not described here. All of the aforementioned components would not be applicable when considering boulder transport. The three components are restrictive in some way which would cause the boulder to either settle in the bend or junction or deposit against the grate.

The friction loss can be calculated by either the Manning or Chézy equation. Normally, a Manning's n value of 0.016 $s/m^{1/3}$ is considered for a rectangular concrete barrel. Manning's and Chézy's equations for friction loss are given by **Equation 2-9** and **2-10** respectively (Rooseboom and Van Vuuren, 2013a):

$$H_f = \frac{\bar{V}^2 n^2 L}{R^{4/3}} \qquad \textbf{2-9}$$

Where:

$\bar{V}$ = Average velocity inside the barrel (m/s)

n = Manning's roughness coefficient ($s/m^{1/3}$)

L = Length of barrel (m)

R = Hydraulic radius for barrel flowing full (m)

$$H_f = \frac{\bar{V}^2 L}{C^2 R} \qquad \textbf{2-10}$$

Where:

$C = 18\text{Log}(12R/k_s)$ [$m^{0.5}/s$]

To determine the entrance and exit losses of a culvert, it is necessary to first determine the loss coefficient (K) that is associated with the type of transition. Square, or blunt, inlets have a K-value of 0.5, well-rounded inlet K = 0.2, and a wing wall inlet K = 0.25. The outlet transition can be described as being sudden, therefore a K-value of 1 is recommended (Rooseboom and Van Vuuren, 2013a). The entrance and outlet losses are given by **Equations 2-11** and **2-12** respectively (Rooseboom and Van Vuuren, 2013b):

$$H_e = \frac{K_e \bar{v}_e^2}{2g} \qquad \textbf{2-11}$$

Where:

v_e = Entrance velocity in the culvert barrel (m/s)

K_e = entrance loss coefficient

$$H_o = \frac{K_o \bar{v}_o^2}{2g} \qquad \textbf{2-12}$$

Where:

v_o = Outlet velocity in the culvert barrel (m/s)

K_o = Outlet loss coefficient

The energy equation for a culvert operating under outlet control can be calculated using **Equation 2-8**:

$$HW_u + \frac{v_u^2}{2g} + LS_0 = TW + \frac{v_d^2}{2g} + H_L \qquad \textbf{2-13}$$

Where:

HW_u = Water depth upstream of the culvert (m)

v_u = Upstream velocity in the watercourse (m/s)

LS_0 = Difference in elevation between the inlet and outlet (length × slope) (m)

TW = Tailwater depth at the outlet (m)

v_d = Velocity downstream of the culvert outlet in the watercourse (m/s)

H_L = Total head loss defined in **Equation 2-8** (m)

Generally, the upstream flow velocity is low due to the damming effect, therefore the upstream velocity head $\left(\frac{v_u^2}{2g}\right)$ may be ignored. The upstream velocity head may be considered as part of the design when it is considered to have a greater effect on the available energy upstream. (Schall *et al.*, 2012).

2.7 Contraction and Expansion Effects

Sidewall convergence of a channel in supercritical flow could produce unfavourable conditions if the convergence angle is too great. Issues that might occur include cross-waves, an uneven distribution of flow in the channel and wave run-up on the side walls (USBR, 1987). If the constriction in a supercritical channel is great enough to cause damming past critical depth, a hydraulic jump would form upstream of the constriction. For a hydraulically steep watercourse, the water profile would follow that of an S1-curve with a hydraulic jump at the upstream end of the damming, with the damming only extending a short distance upstream (Chow, 1959).

The USBR (1987) has experimentally concluded that the contraction of the sidewalls of a discharge channel should be limited to 1:3Fr. This contraction angle produces acceptable results for both contractions and expansions. The contraction angle recommendation seems to align with the limit of inlet tapers (**Section 2.5.2**), set out by Schall *et al.* (2012), which is between 1:4 and 1:6; translating to a Froude number between 1.33 and 2.

The expansion angle of an outlet is also recommended to be 1:3Fr according to Thompson and Kilgore (2006). An expansion angle greater than the recommended 1:3Fr would result in unused space where the water cannot expand fast enough. Keeping in mind that the unused sections downstream of the culvert would probably cause boulder depositions, therefore, elimination of the unused space would be beneficial to prevent boulder deposition downstream.

2.8 Pier Considerations for Multi-Cell Culverts

Piers act as an obstruction for oncoming flow and care must be taken to assess the effect piers have on the upstream and downstream flow patterns. Piers increase the risk of blockages by floating debris and in certain cases even that of boulders. **Figure 2.9** shows a large boulder (approximately 1.2 m × 2 m) that came to rest against a pier of a low water bridge. The flow is constricted for two of the spans, while the boulder increases the risk of further sediment and debris accumulation.

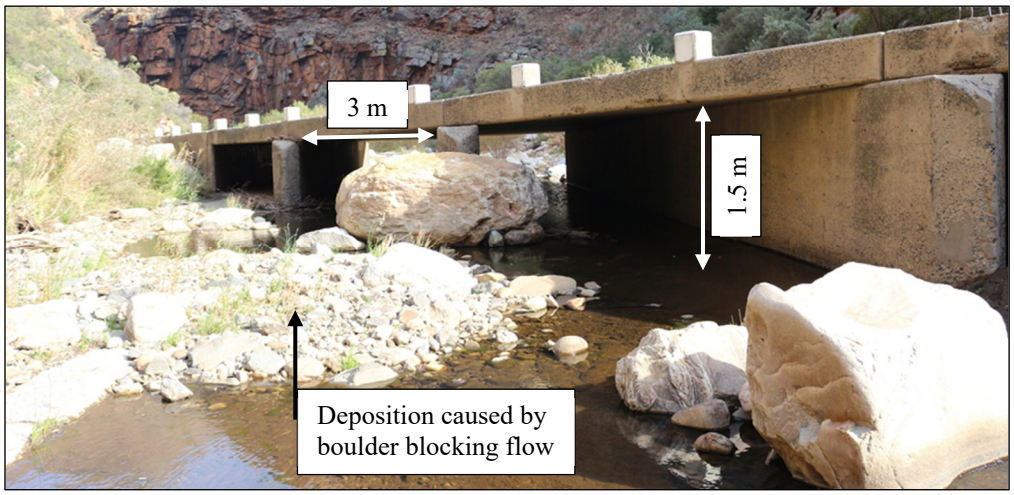

Figure 2.9: Large boulder partially blocking the inlet to a multi-cell culvert.

2.8.1. Debris Fin

There is no hydraulic effect when extending the inner walls onto the apron. They may, however, be included for the management of floating debris or aesthetics (Thompson and Kilgore, 2006). Debris fins, also called debris noses, could be placed as extensions of the pier on the upstream face of a bridge. Debris fins are normally used if a high amount of floating debris is expected in the stream. A wedge-shaped fin, as depicted in **Figure 2.10**, is shaped in such a way to either break the debris up or cause it to float up with the water level to reduce the flow capacity loss experienced by blockages (Stockstill, 2006).

A study conducted at the hydraulics laboratory of Stellenbosch University concluded that for the optimum pier width for mitigating floating debris is 900 mm with a 30° debris fin. The wider pier produces a local increase in flow velocity around the pier which reduces the potential for debris accumulation. It is necessary to keep in mind that a wider pier would result in greater upstream energy losses and an increase in upstream flow depth (Stockstill, 2006).

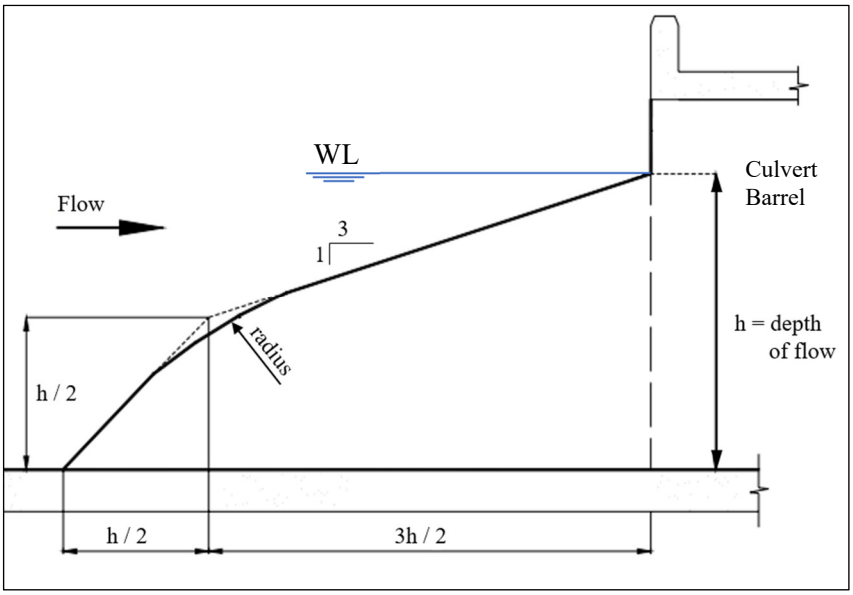

Figure 2.10: Proposed layout of debris fin by USACE (adapted from Stockstill, 2006).

2.8.2. Pier Extensions

The piers can be extended upstream if the capacity of the culvert needs to be increased. It is an innovative and simple solution to increase the efficiency of the flow through the structure. The design is based on the principle that if the piers are controlling the flow, the piers can be extended upstream to force the flow into supercritical flow further upstream resulting in lower water levels through the structure. Pier extensions have been successfully implemented at the Rio Hondo River where problems with run-up and water splash on the road deck were eliminated. The physical model results of the Rio Hondo River shown in **Figure 2.11** illustrates the effectiveness of the pier extensions, increasing the flow capacity.

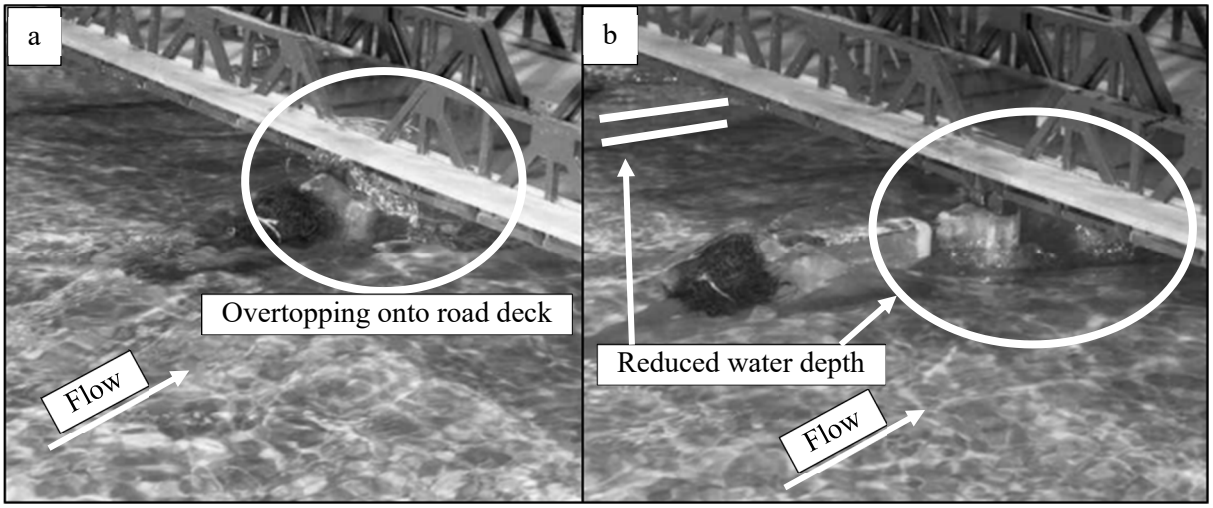

Figure 2.11: Pier extension effectiveness of the Rio Hondo River. **a** - without pier extension; **b** - with pier extension (Stockstill, 2006).

2.8.3. Debris Walls

In an effort to mitigate blockages caused by urban debris, a solution was sought to remove the debris from the flow whilst allowing the safe operation of the culvert. A solution to build debris walls upstream of the culvert proved to ensure that the inlet remains unblocked during flood events. Debris walls just upstream of a multi-barrel culvert are shown in **Figure 2.12(a)**. The design ensures that even if the debris wall becomes clogged up, the water can still flow into the culvert by means of weir flow over the blockage (Tooley, 2017) as shown in **Figure 2.12(b)**.

Figure 2.12: Debris walls constructed upstream of a multi-cell culvert (Tooley, 2017).

Designing the debris walls consists of constructing them the distance D upstream of the inlet at a height of 2/3D, with D the culvert height (D). The lower height of the debris wall compared to the culvert height ensures that the water would still be able to pass underneath the road through the culverts when the debris wall is completely blocked. For the scenarios where the debris wall is completely blocked, the increase in backwater level is equal to a culvert blockage of approximately 30%. Debris wall requires maintenance with regular cleaning after flood events (Tooley, 2017).

2.9 Culverts on Steep Slopes

The main area of concern for the case of boulders blocking culverts is in mountainous areas. Therefore, it is assumed that the slopes would tend to be defined as hydraulically steep. Chanson (2002) confirms that the flow would typically be supercritical in mountain areas. A bed slope greater than 1.5% (1:66.67) will under most circumstances operate as an inlet-controlled culvert. Hydraulically steep slopes are defined as a slope which would produce a flow with a Froude number greater than one (i.e. supercritical flow) under uniform flow conditions. **Equation 2-14** and **2-15** can be used to determine whether a slope is hydraulically steep or mild for a wide rectangular channel, provided uniform conditions exist in the stream. If $S_c > S_0$ for uniform flow, the slope is defined as steep (Chadwick *et al.*, 2013).

$$y_c = \left(\frac{q^2}{2g}\right)^{1/3} \quad \textbf{2-14}$$

$$S_c = \frac{gn^2}{y_c^{1/3}} \quad \textbf{2-15}$$

Where:

y_c = Critical flow depth (m)

q = Unit discharge ($m^3/s/m$)

S_c = Critical bed slope (m/m)

n = Manning roughness coefficient ($s/m^{1/3}$)

A hydraulically steep gradient would generally always produce an inlet-controlled culvert, with the flow inside the barrel being supercritical, given that both the inlet and outlet remain unsubmerged. However, both inlet and outlet control should be tested for the culvert. The control would only change to an outlet controlled culvert in the event that the tailwater level is raised sufficiently (Metzler and Rouse, 1959).

2.10 Freeboard and Overtopping

Freeboard and overtopping considerations are required as safety measures against possible failure of the structure. Inadequate allowance for freeboard has the potential to lead to unwanted overtopping of the structure and road. Overtopping could lead to failure of the structure if the effects of overtopping are not dealt with in the design and construction of the structure.

2.10.1. Minimum Required Freeboard

Freeboard acts as a buffer between the overtopping of the structure and the design water depth to account for the effects of wave action and debris build-up (Schall *et al.*, 2012). Supercritical flow is usually associated with standing waves in locations where three is a sudden change in the cross-section of the flow area, or when there is a large change roughness (Stockstill, 2006).

For scenarios where severe debris build-up is expected at a culvert, a minimum freeboard of 300 mm is recommended for discharges up to 100 m^3/s. For discharges higher than 100 m^3/s, the minimum required freeboard, in meters, is given by the following equation (Jansen van Vuuren *et al.*, 2013):

$$F = 0.78\log(Q_T) - 1.26 \quad \textbf{2-16}$$

It is essential to survey the surrounding area to determine if debris build-up can be expected at the culvert. Regular maintenance is required to remove the accumulated debris from the piers to prevent further blockages (Jansen van Vuuren *et al.*, 2013).

2.10.2. Overtopping of the Roadway

Roads classed between 1 and 3 may not be overtopped with a design flood of twice the return period (Q_{2T}), meaning if a road is designed with a 1:20 year return period the road may not be overtopped for a flood with a 1:40 year return period. Q_{2T} must be considered when determining the embankment height above the culvert. The required freeboard is added only to the design flow, Q_T, and is not included when calculating the embankment height using Q_{2T} (Jansen van Vuuren *et al.*, 2013).

In the case of an overtopping, the buoyancy forces exerted on the structure should be considered and allowances should be made to ensure that the structure remains stable during overtopping. Attention should be paid to the effects of scour on the embankment, especially downstream where the flow returns to the channel (Rooseboom and Van Vuuren, 2013b). Overtopping would be concentrated on the lowest section in the road geometry, where erosion protection measures should be included downstream of the embankment if the location does not correspond with the stream crossing (Schall *et al.*, 2012).

2.11 Scour and Abrasion

A culvert is constructed as a constriction in the natural channel which causes the water to accelerate as it enters the culvert. Vortices are formed due to the acceleration in the flow that may scour away the embankment slopes or the bed of the natural channel where the flow enters the culvert. It is therefore important to provide embankment and channel bed protection against scour at the inlet (Schall *et al.*, 2012).

Scour at piers is of great concern if the piers are not built in a section with a concrete floor, this is especially true for cases where the flow around the piers are supercritical (Stockstill, 2006). It is not only the main flow that causes erosion, the secondary currents, identified by rollers and eddies can cause appreciable scour to the inlet, piers or outlet of the culvert (Metzler and Rouse, 1959). A culvert is constructed as a constriction in the natural channel which causes the water to accelerate as it enters the culvert, this acceleration of flow causes vortices that may scour away the embankment slopes or the bed of the natural channel where the flow enters the culvert. It is therefore important to provide embankment and channel bed protection against scour at the inlet (Schall *et al.*, 2012).

2.11.1. Self-Cleansing Culvert Barrels

Scour can also be used to benefit the design of a structure, for instance, scour is used to prevent the pump intakes of run of river abstraction works from filling with sediment. Scour is also used to periodically clean the gravel-, boulder, and sand-traps at abstraction works (Basson, 2005). Basson (2005) recommends a self-cleaning scour velocity between 2-4 m/s and a bed slope not less than 1:50 (0.02).

Culverts have a similar recommendation to prevent sediment accumulation in the barrel of a culvert. Rooseboom and Van Vuuren (2013) recommend a self-cleaning velocity of 1 m/s and a minimum bed slope of 0.001 (1:100).

2.11.2. Open-Bottom Culverts

Culverts with an open-bottom, or embedded bottom, provide a natural invert to the culvert. A natural invert is beneficial for crossings where Aquatic Organism Passage (AOP) is required. Embedded or natural inverts are also preferable in channels with high sediment transport. Abrasion that is caused by the movement of coarse sediment such as gravel and cobbles may benefit from the use of natural inverts. The advantage that an embedded culvert offers is the invert provides grade control as well as protection against extreme scour than compared to an open-bottom culvert (Schall *et al.*, 2012).

Scour along the foundation can become a problem in open-bottom culverts. Therefore it is important to take the effects of scour into consideration during the design (Schall *et al.*, 2012). The US Army Corps of Engineers (2006) also cautions against using open-bottom culverts in steep slopes regions due to the scour processes experienced on the piers under supercritical flow conditions.

2.11.3. Outlet Scour Protection

Outlet scour protection is required to release the water back to the stream in the same direction and at the same velocity prior to the installation of a culvert (Rooseboom and Van Vuuren, 2013b). Energy dissipation could be achieved by different means to decrease the scour potential of the water. Flow transitions could provide sufficient protection by means of a stilling basin (Thompson and Kilgore, 2006). **Table 2.2** lists energy dissipation methods downstream of a culvert suitable for boulder transportation. These energy dissipation methods coincidentally all allow for high transportation rates of sediment and floating debris. This section briefly described each dissipation method, the full design guidelines are available in the FHWA Hec-14 (2006) documentation.

Table 2.2: Type of energy dissipators suitable for boulter transport (Thompson and Kilgore, 2006).

Dissipator Type	Froude Number (Fr)	Tailwater (TW)
Flow transitions	N/A	Desirable
Scour hole	N/A	Desirable
Hydraulic jump	>1	Required
Riprap basin	< 3	Not needed
Riprap apron	N/A	Not needed

Flow Transitions

If properly designed, flow transitions may be the only required erosion protection needed downstream of a culvert to the original state. Flow separation and turbulence should be avoided at outlet transitions. This method provides an appropriate method for the case of steep streams, where both the culvert and channel flow are at the supercritical state. A smooth transition out of the culvert might prove to be beneficial for boulder movement.

Scour hole

Natural scour holes are permitted in cases where the local scour hole that forms do hold a risk of undermining the culvert or embankment, or if the scour hole does not pose a threat to property (Gross *et al.*, 2019). It is therefore of extreme importance to accurately estimate the size of the scour hole that can form for the worst possible case scenario. Scour depth estimation must be used in conjunction with field observations and previous maintenance data to ensure an accurate estimation can be made (Thompson and Kilgore, 2006). It is unknown what the effect of boulders would have on the energy dissipating potential of a scour hole should it fill the hole with boulders.

Hydraulic Jump

A hydraulic jump would form where the flow passes from supercritical to subcritical flow, it is accompanied by large energy losses, turbulence and an increase in water depth (Thompson and Kilgore, 2006). This increase in water depth results in a decrease in flow velocity and is thought to be the cause of boulders settling out downstream (MacDonald, 2012).

For a hydraulic jump to form the flow needs to pass through critical flow to subcritical flow. Generally, a stilling basin downstream of the culvert exit is used to produce a sufficiently high tailwater level to create subcritical flow conditions.

Riprap Basin and Apron

A Riprap apron could be used to protect the natural ground from the erosive potential of supercritical flow downstream of the culvert.

2.12 MEL Culverts

"Minimum energy loss" (MEL), "minimum energy" or "constant energy", further referred to as MEL structures are terms typically used to describe the type of culverts and waterways described in this section. A MEL structure is defined as a structure that passes the flow through at near-critical conditions with minimal upstream afflux and at near maximum unit discharge. The MEL culvert is identified by its distinctly shaped inlet fan and outlet fan to reduce transition energy losses (Chanson, 2003).

The MEL culvert consists of three sections: The inlet fan, barrel and outlet fan, as shown in **Figure 2.13**. Minimising the energy losses due to contractions and expansions is achieved by means of streamlining the flow through the structure with a curved inlet and outlet fan (Chanson, 2004). The contours indicated should, in theory, form a flow net with the streamlined flow, illustrating that inlet and outlet contractions are minimised (Apelt, 1983).

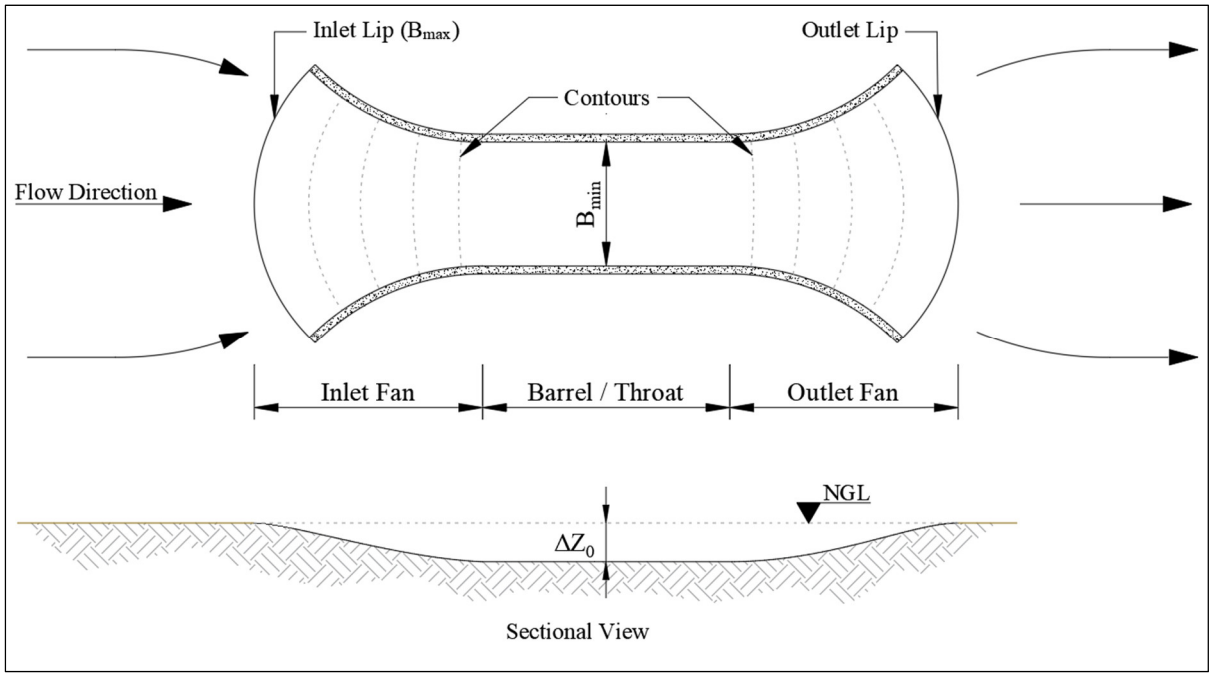

Figure 2.13: Schematic layout of a MEL Structure (Recreated from Chanson, 2002).

2.12.1. Brief History of MEL Structures

Initially designed and developed by G.R. McKay in 1971 (Apelt, 1983), the MEL structure was developed to allow water to pass through a contraction by means of a streamlined inlet and outlet while achieving relatively small energy losses (Apelt, 1983; Chanson, 2004). MEL culverts were developed for low lying areas with hydraulically mild slopes, the result of that was to develop culverts that flow at below critical flow ($Fr \leq 1$) (Chanson, 2004). There are a few applications to MEL structures namely bridge waterways, weir structures and culverts. MEL weirs have been incorporated to act as spillways

for small dams (Chanson, 2004). **Figure 2.14** shows a MEL culvert constructed as a stormwater drainage channel, during times of no flow the culvert is used as part of a bike path and recreational park.

MEL structures, varying in size from small to large structures, have been designed to operate with little to no head losses (zero afflux). Smaller structures usually operate with some allowable head loss and most of the larger structures with zero afflux. The Australian developed MEL structure has been built in a few locations, mainly in Queensland Australia, according to Chanson (2003), more than 200 MEL culverts, as well as MEL weirs, have been built. Eight of the culvert prototypes built between 1959 and 1975 are still in operation to date. The largest MEL culvert has been built between 1960 and 1970, with a design discharge of 800 m^3/s. The hydraulic calculations of the design were developed so that the complex flow of the structures could easily be designed by a set of simple equations, within the provided design constraints (Apelt, 1983).

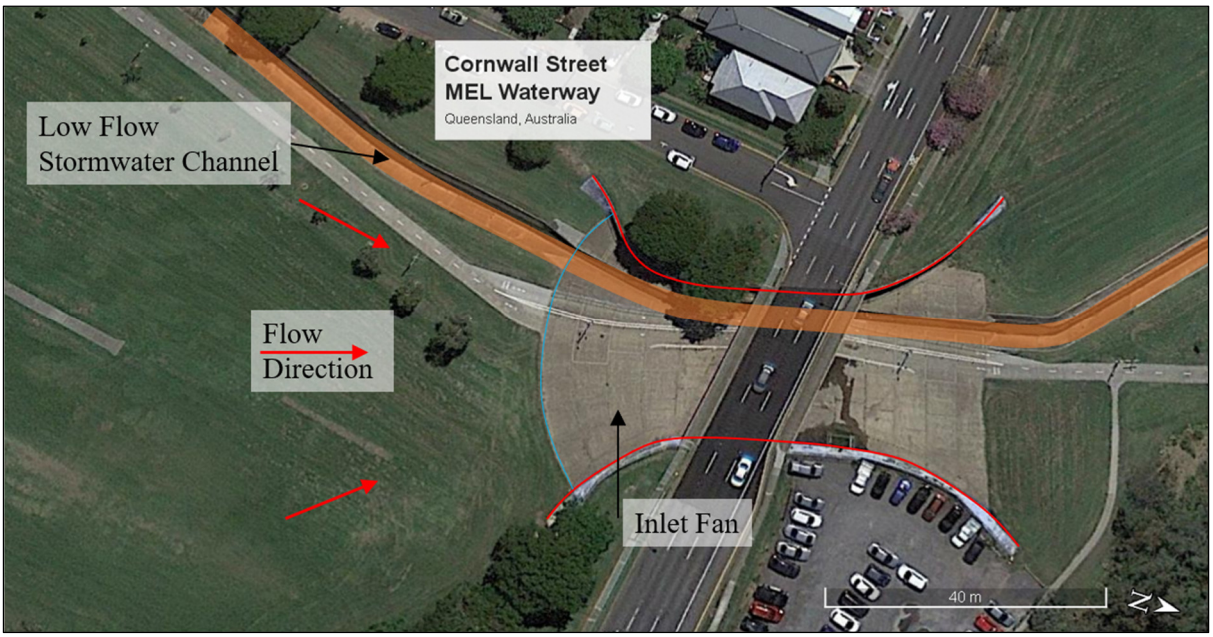

Figure 2.14: Google Earth image of a MEL structure constructed in Queensland, Australia (Google Earth, 2019).

2.12.2. Advantages to MEL Structures

A reduction in energy loss relates to an increase in discharge capacity or the reduction in the width of the barrel. An increase in the discharge capacity makes it a good option in the case where the discharge capacity of a bridge is not adequate, the inlet and outlet fans can be retrofitted without alterations of the existing structure required. Reducing the barrel width is beneficial if the available space is limited or if the span of the bridge needs to be reduced. Additionally, the invert of the barrel can be lowered to further increase the discharge capacity while keeping the energy losses to a minimum (Chanson, 2004).

2.12.3. Disadvantages of MEL Structures

The NBIS as cited in the FHWA (2012), guideline confirms that while there is a slight improvement in the use of curved inlet walls and inverts, it does not outweigh the construction difficulties associated with curved or rounded surfaces. The design and construction may be complex and there is limited expert knowledge on the subject which could cause further problems during design and construction (Chanson, 2003)

No mention of sedimentation or sediment cleaning properties is made by Apelt (1983) or Chanson (2002). Chanson (2003) does make mention to the need for drainage to prevent ponding of the recessed section of the culvert, he specifically mentions the need for a drainage channel as pipes are prone to clogging. Drainage underneath the inlet and outlet slabs is also required which further complicates the design of the structure.

2.12.4. Hydraulic Design of Inlet Fan

Apelt (1983) described a simplified method to design a MEL culvert, he describes the flow through the structure as complex, but the design as simple due to the assumption that the velocity is uniform across the width of the flow. The design assumes that the flow will be critical throughout the structure, which makes it possible to make use of critical depth and discharge equations. Free-surface undulations and other flow instabilities are associated with critical flows, the MEL culvert is, therefore, best designed with a Froude number between 0.6 and 0.8 (Chanson, 2004). Energy equations will then be used if the flow is not critical as described by the simplified method, the design remains the same, the calculations become more cumbersome.

Simplified Method

The simplified method is described for critical flow and assuming the inlet. Apelt (1983) described it for critical flow conditions but mentions that energy equations can be used for non-critical cases. Continuity and energy equations for critical flow are used throughout between the different sections.

Determine the design discharge (Q_{des}) and the corresponding water depth upstream of the structure, it is then assumed that the conditions at the inlet will be the total energy head through the structure. For the first part, energy losses are ignored, the following steps then follow:

1. With Fr = 1, determine the minimum barrel width (B_{min}) and the elevation (z_{barrel}) of the barrel invert. **Equations 2-17** and **2-18** is used for critical depth (y_c) calculations.
2. The inlet lip width (B_{max}) is then determined, the inlet lip is a smooth line that is assumed to run normal to the oncoming flow (**Figure 2.13**).
3. Select the shapes of the wing wall fans or select the desired bed profile

4. Determine the geometry of the fans or the bed profile, whichever was not selected in (3), to satisfy critical flow at every point in the fan. The width is assumed to be a smooth line normal to the oncoming flow (similar to flow nets).
5. Steps 3 and 4 are used to determine the longitudinal profile and distance.

Now including friction and form losses (energy losses):

6. Calculate the energy loss throughout the structure and adjust the bed profile to retain critical flow through the structure, the slope of long barrels are set equal to the critical slope (S_c).

The following equations are used in the simplified method, y_c for a rectangular section:

$$y_c = \sqrt[3]{\frac{q^2}{g}} \qquad \textbf{2-17}$$

The specific energy for critical flow conditions:

$$y_c = \frac{2}{3}E \qquad \textbf{2-18}$$

The critical slope for long barrels, uniform flow conditions is assumed:

$$S_c = \frac{gn^2}{y_c^{1/3}} \qquad \textbf{2-19}$$

Where:

y_c = Critical depth (m)
q = Unit discharge ($m^3/s/m$)
E = Specific energy (m)
S_c = Critical bed slope (m/m)
n = Manning's roughness coefficient ($m/s^{1/3}$)

The design of MEL culverts needs to adhere to several boundaries to operate as designed, these boundaries are described in detail by Chanson (2002).

2.13 Physical Characteristics of Boulders

Armitage (2002) pointed out that to define incipient motion, one must consider particle size as one of the most important parameters. This section covers the most important physical characteristics of boulders in order to define incipient motion accurately. Characteristics considered are the size, shape, settling velocity

Particle size is an important factor to consider in incipient motion, the Wentworth scale was typically used to classify sediment according to size. **Table 2.3** displays the Wentworth scale classification, apart from being a classification system (Chadwick *et al.*, 2013), it is not of any importance to measure incipient motion on its own. The shape and settling velocity are the main influential factors, both, however, consider the size.

Table 2.3: Wentworth scale for sediment classification (Chadwick et al., 2013).

Sediment Class	Size (mm)
Boulders	> 256
Cobbles	64 – 256
Gravel	2 – 64
Very Coarse Sand	1 – 2
Coarse Sand	0,5 – 1,0
Medium Sand	0,25 – 0,5
Fine Sand	0,125 – 0,25
Very Fine Sand	0,062 – 0,125
Silt	0,004 – 0,062
Clay	0,00024 – 0,004
Colloids	< 0,00024

Research published by Armitage (2002) refers to a shape factor defined as the Corey shape factor, **Equation 2-20**. A Corey shape factor of 1 would indicate a perfect sphere, care should be exercised however, as a cube also has a shape factor of 1. Other methods have been developed to overcome the problem, but the study focusses on the Western Cape rivers, which assumes reasonably rounded boulders. Quartz particles that have been naturally worn have an estimate Corey shape factor of 0.7 (Simons and Senturk, 1992).

$$SF = \frac{c}{\sqrt{ab}} \qquad \textbf{2-20}$$

Where:

SF = Shape factor

a, b, c = triaxial dimensions of the particle, where ‘a’ is the longest dimension and ‘c’ the shortest dimension (m).

The settling velocity of a particle is defined as the terminal velocity that a particle can reach in a body of water, without other forces acting on the particle, apart from water resistance and gravity (Simons

and Senturk, 1992) The settling velocity, or V_{SS}, is given by **Equation 2-21**, the equation calls for a drag coefficient which is a function of the particle shape and particle fall Reynolds number (Re), given by **Equation 2-22**. For low Re values, the C_D coefficient is typically high and for a high Re value, C_D is typically low (Simons and Senturk, 1992; Armitage, 2002).

$$V_{SS} = \sqrt{\frac{4}{3}\frac{\rho_s - \rho}{\rho}\frac{gd}{C_D}} \qquad \textbf{2-21}$$

Where:

V_{SS} = Particle Settling Velocity (m/s)

ρ_s = Density of reference material (kg/m³)

ρ = Density of fluid (kg/m³)

C_D = Particle drag coefficient

$$Re = \frac{V_{ss}d}{\nu} \qquad \textbf{2-22}$$

The density of quarts and felspathic minerals is about 2650 kg/m³, these are the typical sediments found in rivers so it would be a safe assumption if the density of the sediment is unknown. Care should be taken when the density of sediments is used to determine the correct density if it is not of quarts and felspathic minerals (Simons and Senturk, 1992).

Determining the settling velocity of a particle by using **Equation 2-21** requires a drag coefficient (C_D), which varies for different boulder shapes and sizes. Carling *et al.* (2002) mention that various research has determined that a C_D Coefficient between 0.71 and 1.2 can be used of boulders that are irregular in shape. Concha (2009) compiled and presented a graph (**Figure 2.15**) representing the drag coefficient vs. the Reynolds number for different isometric particles, it shows that for flow in the turbulent region (Re > 2000) the C_D of particles separates to values between 2 for tetrahedrons and 0.4 for spheres. Concha (2009) provides an explanation for the variation in results, he observed that the particles start to oscillate and vibrate at the higher Reynolds numbers.

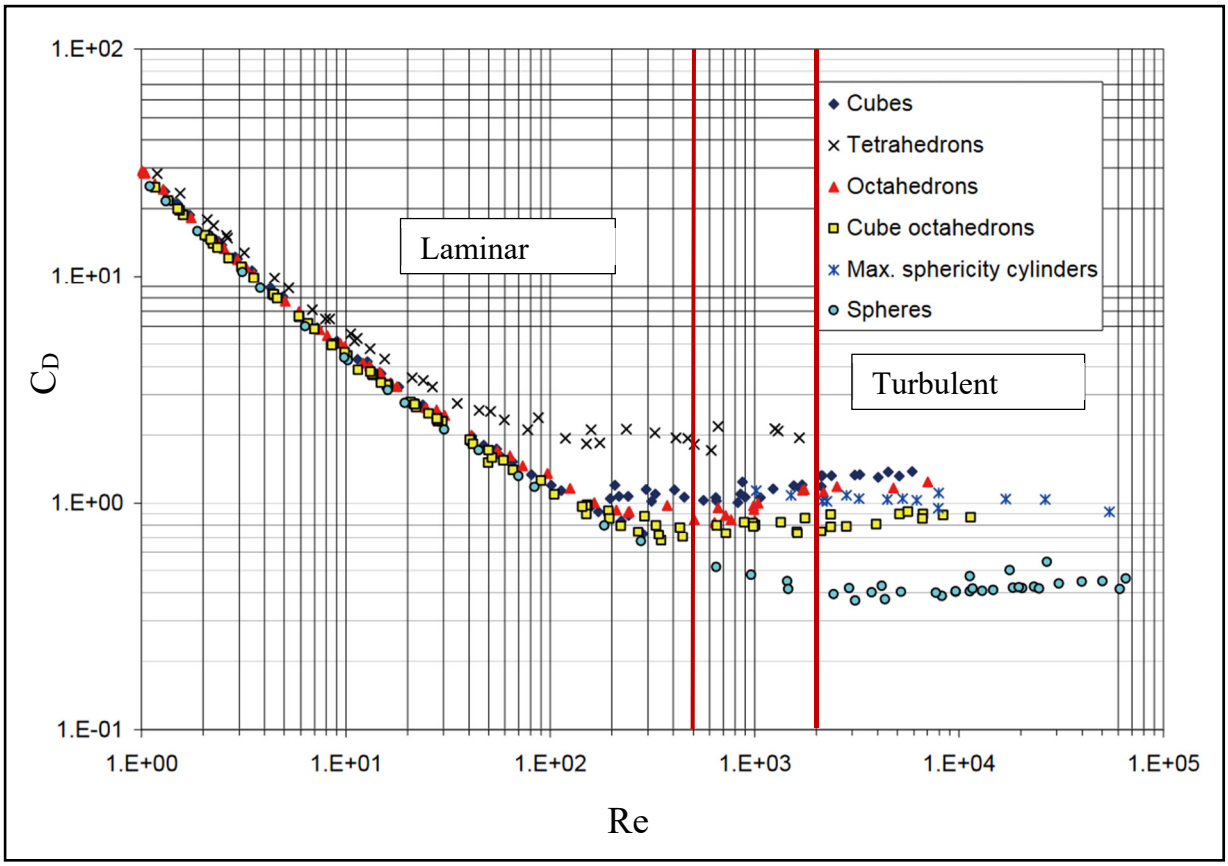

Figure 2.15: Drag Coefficient vs. Reynolds Number graph for the settling of isometric particles (Concha, 2009).

2.14 Incipient Motion

Generally accepted as the point at which a given stationary particle (sediment, riprap, boulders) is transferred to a state of initial, or incipient, motion. The initiation of the particles is normally through the increase in hydrodynamic forces that act on the particles (Simões, 2014). Once the hydraulic conditions exceed some critical condition, particle movement will occur (Stoffberg, 2005), however, there is no clear point at which incipient motion would occur (Chanson, 2004; Stoffberg, 2005; Simões, 2014). Different approaches by researchers have been considered to determine the critical condition for sediment movement. The focus of this study was not to determine the incipient motion of boulders, this Section merely serves as a background to gain a better understanding of boulder movement.

Considered as the most popular and most studied parameters to quantify incipient motion is shear stress, most notably the Shields shear parameter. The Shields parameter has been questioned by some for the use in steep slopes and for non-uniform particle distributions (Bathurst, 1987; Bunte *et al.*, 2013). Bunte *et al.* (2013) proposed the use of a new critical Shields value as a criterion for incipient motion in steep, coarse-bedded streams. Lui (1957) approached incipient motion theory by considering a critical shear

velocity, also known as stream power, as a measure for sediment movement (Langmaak, 2013). Bathurst (1987), proposed a new method, by using unit-discharge as a measure of particle movement.

2.14.1. Shear Stress

The Shields (1936) shear stress model is one of the most widely used and accepted models of sediment transport (Stoffberg, 2005; Simões, 2014). Shields first introduced the stability parameter (τ_* or θ), also referred to as the Shields parameter, in 1936, as a dimensionless parameter (Chanson, 2004).The initiation of movement for particles is defined as a relationship between the shear stress, θ, and the particle Reynolds number, Re^*. **Equations 2-23** and **2-24** respectively, defines the Shields Parameter and the particle Reynolds number, which is based on the shear velocity (Simões, 2014).

Shields Parameter:

$$\theta = \frac{\tau}{(\rho_s - \rho)gd} \qquad \textbf{2-23}$$

Where:

τ = bottom shear stress (Pa)

ρ = water density (kg/m³)

ρ_s = Sediment density (kg/m³)

d = sediment diameter (m)

g = gravitational acceleration (9.81 m/s²)

Reynolds number around a particle:

$$Re^* = \frac{V^* d}{\nu} \qquad \textbf{2-24}$$

Where:

V^* = Shear Velocity ($V^* = \sqrt{gDS_f}$) (m/s)

ν = Kinematic Viscosity (m²/s)

Considering the case for fully rough turbulent flow (75-100 < Re_*), the critical Shields parameter has a value between 0.04 and 0.06, meaning particles with a Shields value above this threshold would become mobile. It is noted that the Shields parameter becomes nearly constant in the fully rough turbulent flow regime (Chanson, 2004), this observation can be visually seen from the Shields curve in **Figure 2.16**. The Shields curve is a graph showing the relationship between the critical Shields stress and the particle Reynolds number, the limits as defined by Chanson (2002) have been included in **Figure 2.16**.

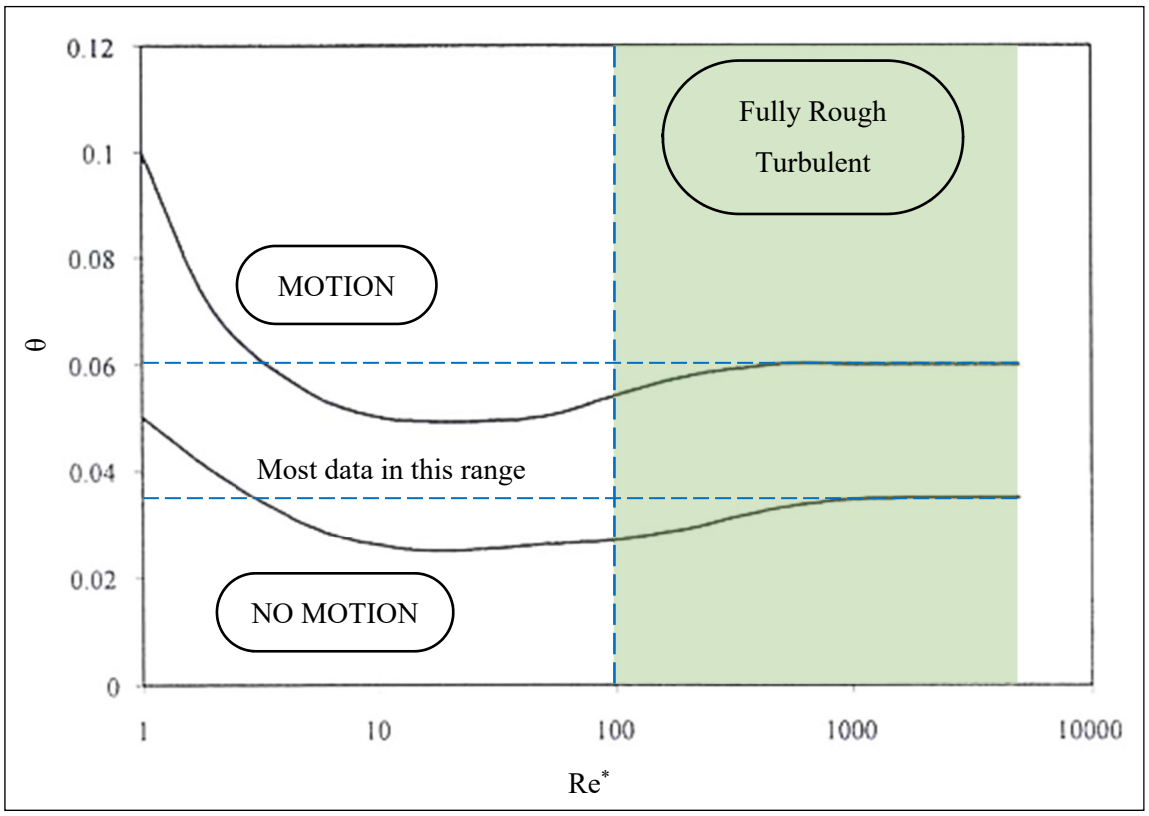

Figure 2.16: Shields curve indicating incipient motion (after, Raudkivi, 1986).

There have been a few reported cases where the Shields parameter has been questioned for the use in steep streams with a wide particle size distribution. It has been noted by some that the Shields parameter may not accurately predict sediment motion in these cases as it may overestimate (Baker and Ritter, 1975; Bathurst, 1987; Chanson, 2004; Bunte *et al.*, 2013), or even underestimate (Chanson, 2004) the critical shear stress required to move a particle.

Considering overestimation: It has been argued by Bunte et al (2013) that for unstable beds with a slope of about 0.1, θ is closer to 0.03 for the large fraction of particles, furthermore lower θ values are obtained for the d_{84} than for the d_{50} particle size, and similar for d_{50} and d_{16}. This is attributed to exposure to the streamflow. Chanson (2002) has referred to the works by van Rijn (1993) that the steep slope may aid in destabilizing the sediment, causing motion at lower shear stresses than expected. The case for the underestimation stems from the idea that some of the smaller particles are shielded by the large particles and that once the small particles have washed away the large particles would form a layer called an armour layer, also referred to as bed armouring (Blom *et al.*, 2003; Chanson, 2004).

2.14.2. Applied Stream Power

For alluvial streams, Rooseboom recommended that the settling velocity should be considered as a measure for incipient motion (Jansen van Vuuren *et al.*, 2013). When incipient motion is considered in terms of stream power of cohesionless material, a relationship between the ratio of shear velocity and

settling velocity and the shear Reynolds number can be seen. This relationship led to the development of the Modified Lui Diagram, **Figure 2.17** (Jansen van Vuuren *et al.*, 2013). The Modified Lui Diagram represents the boundary between no sediment movement and sediment movement.

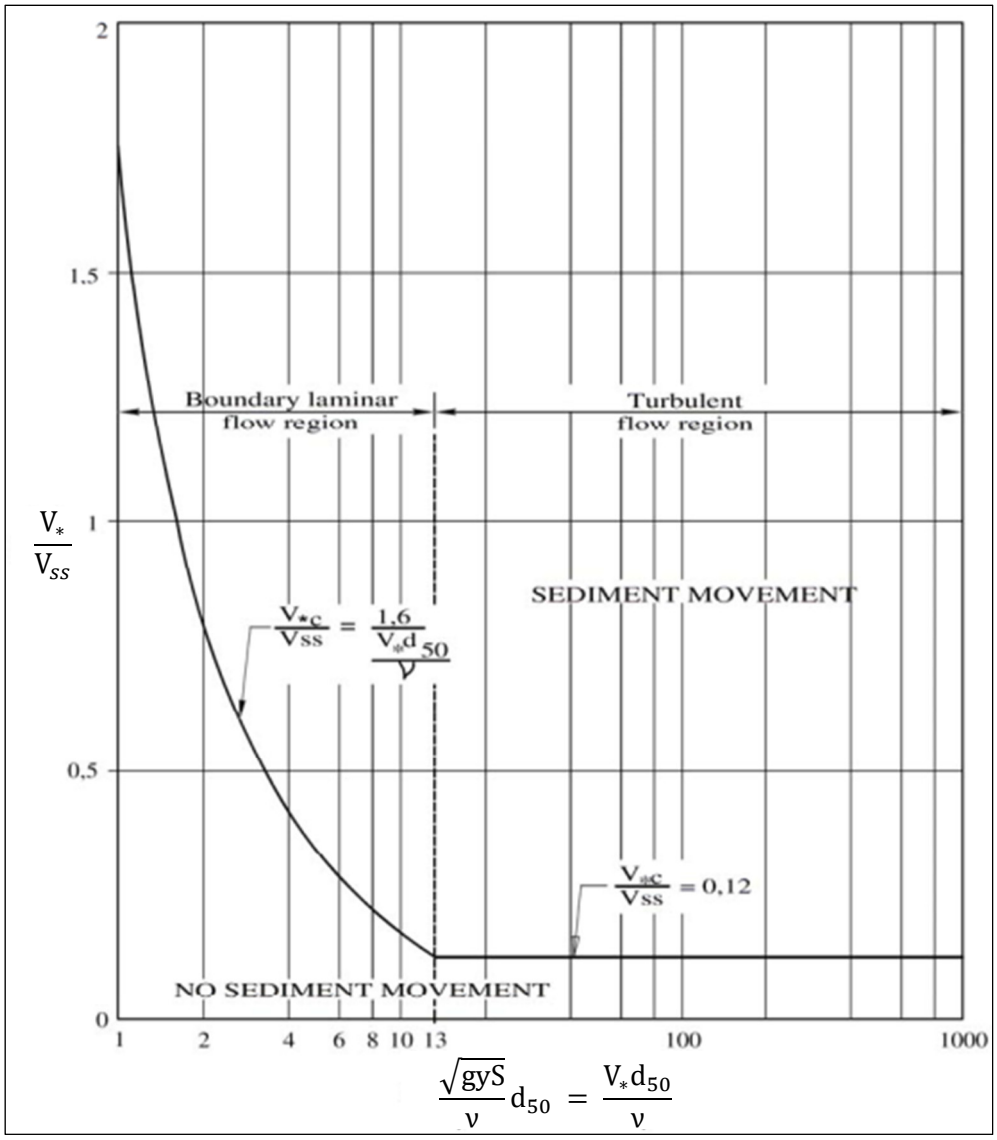

Figure 2.17: Modified Lui Diagram for determining the incipient motion threshold based on settling velocity (from Jansen van Vuuren *et al*., 2013).

For the turbulent flow region, the boundary for the ratio between the critical shear velocity and settling velocity, also referred to as the Movability number (MN), (**Equation 2-25**) has been determined to be 0.12. A higher MN would cause sediment to be moved by the stream, while a lower MN would produce no sediment movement. Only the turbulent section is of interest as the flow will be in the fully turbulent regime. **Equation 2-25** is a representation of the ratio between the applied stream power and the power required to transport particles of uniform size. To account for a non-uniform bed, **Equation 2-25** was adjusted to include differentiation between particle size and absolute roughness (k). The absolute roughness has been defined as being approximately equal to the d_{84} particle size in the grading if the

flow depth was lower than the d_{84} particle size, the maximum water depth was is used (Cullis *et al.*, 2008). The Movability Number equation to account for non-uniform gradings are described by **Equation 2-27**.

$$\frac{V_{*c}}{V_{SS}} = 0.12 \qquad \textbf{2-25}$$

The shear velocity (V_*) is expressed by the following equation:

$$V_* = \sqrt{gyS} \qquad \textbf{2-26}$$

$$MN = \frac{\sqrt{gyS}}{V_{ss}} \cdot \left(\frac{d}{k}\right)^{1/3} \qquad \textbf{2-27}$$

Representing the x-axis on the modified Lui diagram (**Figure 2.17)** is the Reynolds number for flow around a particle, defined by **Equation 2-28.**

$$Re_* = \frac{\sqrt{gyS}}{\nu} d_{50} \qquad \textbf{2-28}$$

Where:

V_* = Shear velocity (m/s)
V_{*C} = Critical shear velocity (m/s)
y = Flow depth (m)
S = Energy Slope (m/m)
V_{SS} = Particle settling velocity (m/s)
ν = Kinematic Viscosity (m^2/s)
d = Particle size (m)
k = Absolute Roughness (m)

The settling velocity of a particle needs to be determined to use the Modified Lui Diagram. It has been shown in **Section 2.13** that the settling velocity of a particle (V_{SS}) is typically determined by an experimental means as there is no definitive method to determine the drag coefficient.

2.14.3. Critical Unit Discharge

Bathurst (1987) proposed the use of discharge as a criterion for incipient motion in steep, boulder-bed rivers with non-uniform size distributions. The argument for the use of discharge is based on the premise that, instead of a singular flow condition bringing uniform particles into motion, that different flow conditions, or discharges, would entrain different sized particles. Bathurst (1987) refers to studies by Egiazaroff (1965) and White & Day (1982) that the non-uniform particles' movement threshold would

vary, depending on the position within the non-uniform grading, the same observations as made by Chanson (2002) and Bunte *et al.* (2013). The aim of Bathurst's (1987) research was to combine the equations developed by Schoklitsch (1962) and an adjusted equation of Andrews (1983).

Schoklitsch (1962) developed an empirical relationship for the prediction of a critical discharge that would cause particles to move. **Equation 2-29** was developed, but the equation was derived for slopes between 0.25 and 20% and for particle sizes ranging from 3 mm to 44 mm. Whereas Andrews (1983) developed **Equation 2-30** to measure the effect of critical shear stress by means of field data. His equation was valid for a dimensionless parameter (d_i / d_{50}) between 0.3 and 4.2 (Bathurst, 1987).

$$q_c = 0.15 g^{0.5} \boldsymbol{d}^{1.5} S^{-1.12} \quad \textbf{2-29}$$

Where:

q_c = Critical discharge per unit width ($m^3/s/m$)

d = Particle size (m)

S = Slope (m/m)

$$\tau_{*ci} = 0.0834 \, (d_i/d_{50})^{-0.872} \quad \textbf{2-30}$$

Where:

τ_{*ci} = Average critical Shields parameter (Pa)

Bathurst (1987) sought to combine these two equations to form a single equation that would be able to predict incipient motion in terms of a unit discharge. He went on to develop **Equation 2-31**, with the observation that as q_{ci} increases, d_i would also increase, **Equation 2-32** was proposed. Factors a and b were constants that were developed for a site-specific area. **Table 2.4** shows the results from the fitted equations to the data he considered for his tests.

$$q_{ci} = q_{cr} \left(\frac{d_i}{d_r} \right)^b \quad \textbf{2-31}$$

$$q_{ci} = a d_i^b \quad \textbf{2-32}$$

Where:

q_{ci} = Critical unit discharge for particle D_i ($m^3/s/m$)

d_r = Reference particle size assumed to be D_{50} (m)

b = Constant

a = Constant

Table 2.4: Fitted equation data for Equation 2-32, results from the study carried out by Bathurst, 1987 (Recreated from Bathurst, 1987).

Period of Validity	Equation Parameters		Equation	Reference Particle Size
	a	**b**	**(%)**	**(mm)**
Ypsilon Lake Trail Bridge				
1984 & 1985	0.0933	0.392	61.1	93
Fall river road Bridge				
1984	0.103	0.220	49.9	68
18/05-27/05/1985	0.0955	0.239	91	76
27/05-06/06/1985	0.168	0.201	75.5	94

In order to develop a set of equations, Bathurst derived **Equation 2-33** empirically which would produce a set of equations that could be used to predict the unit discharge for any particle given the reference sized particle. For **Equation 2-33** he assumed that b would be equal to 1.5 if a uniform particle distribution is used, i.e. $d_{16}/d_{84} = 1$.

$$b = 1.5(d_{84}/d_{16})^{-1} \quad \textbf{2-33}$$

Based on the results produced by Bathurst (1987), **Equations 2-29**, **2-31** and **2-33**, could successfully be used together to predict the incipient motion of a given sized particle. The slope of the stream, D_{16}, D_{50} and D_{84} characteristics is required to determine the incipient motion. While the results from using this method are within 10% of the measured data, Bathurst cautions the reader that the data that the research was based on is very limited and should be verified and further studied before it can be implemented.

It is therefore not a viable option to use unit discharge as a measure for incipient motion reliably, the claims made by Bathurst regarding the accuracy of the Shields parameter in steep, coarse-bedded streams remains valid. It can be clearly seen from his analysis of the results that for larger particles, the required discharge to move the particles is lower than if the size were uniform, and for smaller particles, higher discharges are required as the larger particles shield the smaller particles from the flow.

2.15 Paleo Flood Estimation

Since the research considers the largest boulders in the stream which can be transported by the water, the use of paleo flood estimation was considered and whether it might be a good measure or estimation of a boulder being transported, given the size and flood peak. Works by W.C Bradley and A.I. Mears (1980) were mainly cited, they performed a comparative analysis of the most frequently used paleo hydrological methods to determine the best-suited method. Bradley and Mears (1980) concluded that paleo-hydrologic reconstruction was of an imprecise nature but was still applicable and of value to estimate flows that would probably produce boulders.

The study performed by Bradley and Mears (1980) analysed 11 different models of flood estimations capable of moving a 1.88 m boulder. **Table 2.5** lists the results for the eight velocity calculations from their tests based on their study site of Boulder, Colorado. In their tests, they found that the engineering methods underestimated the size of a boulder that would be moved by a flood event. They concluded that the velocity estimations predicted the competence to move a boulder with sufficient accuracy, while the depth estimations were not sufficiently successful.

Table 2.5: Summary of velocity results obtained for each method reviewed (Bradley and Mears, 1980).

Method	Year Published	Velocity
Empirical Estimations		
Engineering Formulas		(m/s)
(A) Mavis & Laushey	(1949)	7,9
(B) Peterka & others	(1956)	9,5
(C) Torpen	(1956)	4,9 - 9,2
Data Compilations: Velocity		
(D) Novak	(1973)	2,4 - 6,7
Data Compilations: Tractive Force		
(E) Church	(1972)	3,4 - 6,7
(F) Baker & Ritter	(1975)	5,2 - 7,9
Theoretical Estimations		
(G) Helley	(1969)	6,7 - 8,8
(H) Mears	(1980)	4,9 - 6,7

Based on the velocity results it was determined that velocities between 4.6 to 6.1 m/s would be able to move a 1.88 m boulder. They supplied two reasons for narrowing the band to the lower velocities:

- Once a particle is entrained it may continue to be transported downstream by a lower velocity, as observed by Hjultrom (1939).

- Sediment concentration would increase fluid densities, that would, in turn, reduce the required flow velocity for particle entrainment. Bradley and Mears (1980) argue that Doerhring and others (1978) and Rosgen (1978) observed that in floods sediment concentrations may easily transport more than 10% suspended solids, for their calculations they assumed 10% sediment concentration.

Based on the conclusions presented by Bradley and Mears (1980), they seem to be in favour of the results on the lower end by Torpen (1956) (C), Church (1972) (E) and the equation proposed by them (H). **Figure 2.18** illustrates the results for all the methods reviewed with the band of velocities capable of moving the boulders.

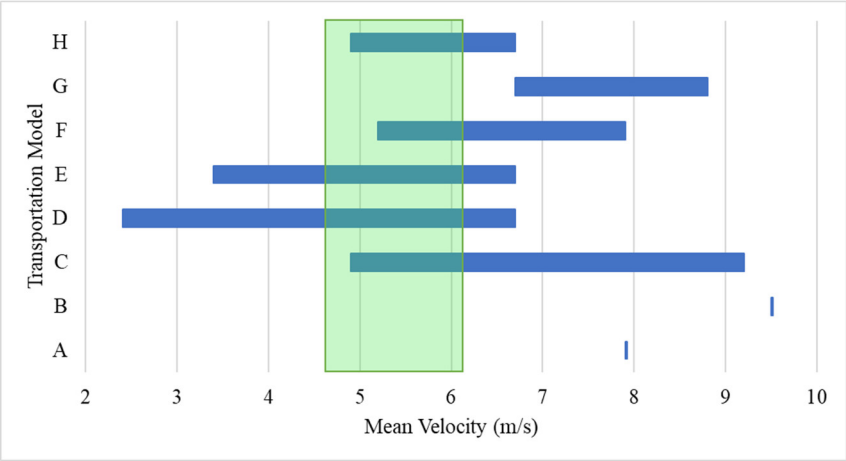

Figure 2.18: Results for velocities capable of transporting boulders at the Justice Center (recreated from Bradley and Mears, 1980).

This study illustrates the challenges when determining boulder movement and the variability in results from one method to another. For paleo flood estimations, the correct magnitude of flow is provided by the equations, but they may not be of use where accuracy is expected or if the design is linked to some form of risk (Bradley and Mears, 1980). If not for the discrepancy in methods tested, paleo flood estimates would otherwise provide a good indication of flows capable of moving boulders.

2.16 Scale Effects

The physical hydraulic model is used to observe a wide range of possible conditions that could be encountered in practice to make recommendations and possibly improve the design (Webber, 1971). These scale models have been used as a cost-effective method of analysing the performance of a structure and to make recommendations on improving the structure, in order for the model to be similar to the prototype they are required to be hydraulically similar. The ratio between the inertial forces and viscous forces (dimensionless Reynolds Number) and the ratio between inertial forces and gravity forces (dimensionless Froude Number) is of interest when analysing hydraulic models (Gill and Pugh, 2009).

The laws of hydraulic similarity govern the relationship between the performance of the model and the prototype. It is impossible to comply with all the laws simultaneously, thus it becomes necessary to extrapolate certain aspects to the full scale. The discrepancy that arises from the extrapolation is known as the scale effect (Webber, 1971). In order to transfer the results from the model to the prototype it is required that the two flow systems are hydraulically similar, meaning similarity in geometry, kinematics and dynamics (Webber, 1971; Gill and Pugh, 2009).

Open channel hydraulic designs are often designed to conform to Froude number scaling as the viscous forces (Reynolds number scaling) can be significantly diminished if the prototype and model are designed to operate in turbulent flow conditions. The performance of the model setup compared to the prototype will be to an acceptable degree of accuracy if the turbulent flow conditions are maintained for the model setup (Gill and Pugh, 2009). For open channel flow, a Reynolds number greater than 2000 is considered to be turbulent flow (Chadwick *et al.*, 2013).

2.16.1. Hydraulic Similitude

Geometric Similarity

Geometric similarity entails the similarity of shape, meaning that the ratio of any two dimensions in the model has to be the same ratio between the two dimensions in the prototype, with subscript m and preferring to the model and prototype, and L referring to linear dimensions, it can be expressed as:

$$\frac{(L_1)_m}{(L_2)_m} = \frac{(L_1)_p}{(L_2)_p} \qquad \textbf{2-34}$$

From Equation 2-34 the following scalar relationships for area and volume can be derived if the linear model scale is 1:x, for the area this becomes $1:x^2$ and for the volume the scalar relationship becomes $1:x^3$. Geometric similarity requires that the surface finish of the model is an exact representation of the prototype, this relationship is, however, difficult to achieve for small-scale models with smooth prototype surfaces such as well-finished concrete (Webber, 1971).

Kinematic Similarity

Kinematic similarity can be described as the similarity of motion, therefore, a vector quantity and time factor are introduced. The time factor is important when considering problems with unsteady flow, such as tidal movement. The model and prototype velocity and acceleration must have the same ratio at a given homologous time and location, finally, the direction of flow must be the same. This can be expressed by **Equation 2-35**, with V = velocity (m/s) and a = acceleration (m/s^2) (Webber, 1971).

$$\frac{(V_1)_m}{(V_2)_m} = \frac{(V_1)_p}{(V_2)_p} \quad \text{and} \quad \frac{(a_1)_m}{(a_2)_m} = \frac{(a_1)_p}{(a)_p} \qquad \textbf{2-35}$$

Dynamic similarity

Dynamic similarity requires forces at homologous points in the model and prototype systems to act in the same direction and have the same ratio to each other. **Equation 2-36** illustrates the relationship between the model and prototype forces.

$$\frac{(F_1)_m}{(F_2)_m} = \frac{(F_1)_p}{(F_2)_p} \qquad \textbf{2-36}$$

Given that the flow patterns are a result of the forces acting on it, it can be assumed that if dynamic similarity exists throughout, geometric and kinematic similarity will exist throughout (Webber, 1971).

2.16.2. Laws of Similarity for Physical Models

Similarity laws are of great importance in the development of a hydrodynamic model, identifying the influence of each of the laws will ensure accurate results are obtained from the model. The four laws considered are the Froude law, Euler law, Reynolds law and the Weber law. Webber (1971) stated that the compressibility property of the prototype fluid can be ignored in model studies as it is rarely of significance.

Euler Law

Euler law relates to the relationship between pressure and velocity. When modelling an enclosed fluid system in which fully developed turbulence is present, the inertial forces are much greater than viscous forces, making them insignificant and Gravity force and surface tension are absent (Webber, 1971). The Euler number, **Equation 2-37**, have been derived from the fundamental force-momentum concept, describing the basic relationship between pressure and velocity (Webber, 1971).

$$E_u = \frac{V}{\sqrt{\frac{2\Delta p}{\rho}}} \qquad \textbf{2-37}$$

Where:

E_u = Dimensionless Euler Number

V = Velocity (m/s)

Δp = Pressure change (kN/m^2)

ρ = Density (kg/m^3)

Froude Law

The Froude law is applicable where the motion of the fluid is predominantly influenced by gravity, therefore where a free surface gradient exists. For a model to conform to the Froude law (**Equation 2-38**), the velocities must be related as indicated in **Equation 2-39** (Webber, 1971), where x relates to the scale factor.

$$Fr = \frac{V}{\sqrt{gL}} \qquad \textbf{2-38}$$

$$\frac{V_p}{V_m} = \frac{(gL_p)^{1/2}}{(gL_m)^{1/2}} = x^{1/2} \qquad \textbf{2-39}$$

Assuming that x is greater than 1, the velocities observed in the model will be less than that of the prototype, this is advantageous as the required pumping capacity of the model test is reduced. **Table 2.6** summarises the scalar relationships based on the Froude law to be used in physical model tests.

Table 2.6: Froude scale similitude for the scalar relationship between prototype and model.

Description	Dimension	Natural Scale (1:x)
Geometric		
Length	L	x
Area	L^2	x^2
Volume	L^3	x^3
Kinematic		
Time	T	$x^{1/2}$
Velocity	L/T	$x^{1/2}$
Acceleration	L/T^2	1
Discharge	L^3/T	$x^{5/2}$
Dynamic		
Pressure	M/LT^2	$\rho_r x$
Force	ML/T^2	$\rho_r x^3$
Energy	ML^2/T^2	$\rho_r x^4$
Power	ML^2/T^3	$\rho_r x^{7/2}$

Where:

L = linear dimension (m)

T = time (sec)

M = mass (kg)

ρ_r = density ratio between prototype and model ($\rho_r = \rho_p / \rho_m$).

Reynolds Law

It is important to take the effects of viscous shear forces acting on a fluid model into consideration as all fluids are viscous to some degree. Water has a relatively low viscosity, this means that the effect of the viscous forces on the prototype is nearly always secondary, but should still be considered in the boundary friction as well as the cause of fluid turbulence (Webber, 1971).

To comply with the Reynolds law (**Equation 2-40**), the velocities must be related as indicated in **Equation 2-41** (Webber, 1971), where x relates to the scale factor.

$$\mathrm{Re} = \frac{\mathrm{VL}}{\nu} \qquad \textbf{2-40}$$

$$\frac{V_p}{V_m} = \frac{\upsilon_p}{\upsilon_m}\frac{L_m}{L_p} = \frac{\upsilon_p}{\upsilon_m}\frac{1}{x} \qquad \textbf{2-41}$$

Following **Equation 2-41** it is seen that if the same fluid is used in the prototype and model, the model velocity would need to be x times the velocity of the prototype, a difficult requirement to achieve in a physical model (Webber, 1971)

Weber Law

Surface curvature tends to be reduced or equalised by surface tension experienced where there is an air-water interface, this is only of significance if the linear dimensions are small. Examples of physical models where surface tension must be considered include very low weir head, spray, splash or air entrainment (Webber, 1971).

To comply with the Weber Law (**Equation 2-42**), the model velocities would be required to be $x^{1/2}$ times that of the prototype if the same fluid was used for the model and prototype. However, in most cases the effect of surface tension on the prototype has little to no influence, it is thus required that the model scale be large enough, or the range of operation limited to ensure that surface tension remains insignificant.

$$W = \frac{V}{\sqrt{\frac{\sigma}{L\rho}}} \qquad \textbf{2-42}$$

Where:

W = Dimensionless Weber number

σ = Surface tension (N/m)

Weber's law may be ignored if the model scale is large enough. A model with A Weber number smaller than 120 is considered to be influenced by the effects of surface tension. In such a case the scale would be increased or the effect of surface tension must be taken into consideration (Peakall and Warburton, 1996).

2.16.3. Scale Model Similarity Laws

Gravitational force has been found to be the main acting force on a section with an upstream control, model studies, therefore, produce accurate results when compared to that of the prototype when scaled in accordance with the Froude Law (gravity dominating) (Metzler and Rouse, 1959). Culverts flow predominantly as open channel structures, and gravity will be the largest force influencing the motion of the fluid.

The culvert may flow full, which is known as pressure flow, but this would mainly apply when the downstream water level is high causing back pressure (Schall *et al.*, 2012). The design of the prototype is based around mountainous areas with steep slopes; thus, it was assumed that pressure-flow would not occur. For the purpose of the model study, Euler's Law and Weber's Law can be ignored as the system would not be a pressure system (Euler) and the model scale would be large enough in order to reduce the effects of surface tension on the model.

2.16.4. Scaling of Sediment

Viscosity

Viscosity plays a major role in the movement of particles if the flow is laminar the viscous forces would have a strong influence on the flow and the movement of particles. As seen from **Figure 2.19**, this would generally not be of any concern in normal open channel scenarios as the flow would generally always be in the turbulent flow regime (Chow, 1959). For physical modelling, it may become a problem if Froude scale is used to define the model parameters, if the flow regime for the model becomes laminar due to the scale of the model, viscous forces would then influence the flow and not produce an accurate result.

Care should be taken to ensure that the flow for both the model and prototype is in the same flow regime, i.e. fully turbulent in the case of a Froude scaled model. There is some variation in the definition of the lower limit for fully-turbulent flow, Robertson and Rouse (1941) and Chadwick, Morfett and Borthwick (2013) define this limit as 2000, Chow, 1959, mentions that this limit may be between 500 and 12 500 if the characteristic length is taken as the hydraulic radius in the Reynolds number equation **(Equation 2-22**, V_{ss} becomes flow velocity V). Chow (1959) and Chadwick, Morfett and Borthwick (2013), does, however, state that there is no defined upper limit for the transitional zone and that these recommendations are based on experimental tests.

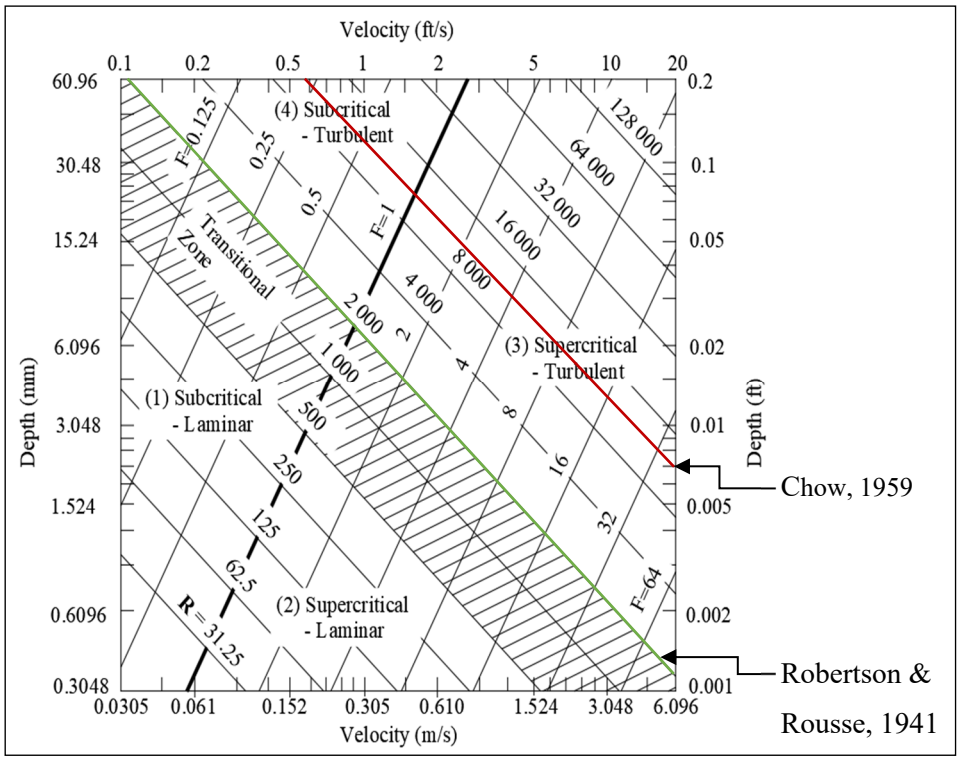

Figure 2.19: Relationship between velocity, water depth, Froude number and Reynolds number; illustrating the four regimes of flow (recreated from Robertson and Rouse, 1941).

Assuming that the prototype would be in the fully turbulent regime, it can be assumed that for viscous forces to not influence the results the Reynolds number should be greater than 12 500, and at the very minimum larger than 2000. If the model is scaled according to Froude Law and if the Reynolds number is below the lower limit for turbulent flow, the scale of the model would need to be increased.

Boundary-Layer Thickness

For a channel with a smooth surface, in the turbulent flow regime, there will always form a very thin layer of low-velocity flow, this film is defined as the laminar sublayer (also called viscous sublayer). The flow in this layer remains laminar due to the low flow velocity and is the thickness between the surface where the velocity is zero and the boundary between laminar flow and transitional flow (Chow, 1959; Munson *et al.*, 2009). This layer can be deemed as problematic in the case of physical models due to the strong viscous forces associated with laminar flow (Breusers, 1974).

Figure 2.20 illustrates the effects of surface roughness on the boundary layer. If the channel is defined as hydraulically smooth, the roughness elements, defined by the effective roughness (k), is so small that the eddies and turbulence caused by the surface of the channel are contained within the viscous sublayer, resulting in the establishment of the sublayer between the turbulent flow and the channel surface. If the surface is sufficiently rough for the effective roughness (k) extends past the laminar sublayer the surface

would be defined as hydraulically rough. In this section the effects of the roughness elements cause turbulence and eddies to form, breaking through this laminar layer of flow, once this is achieved, the effective laminar sublayer becomes very thin, therefore effectively eliminating the viscous effects of the flow at the bottom of the channel (Chow, 1959). **Figure 2.21** graphically illustrates the relationship between the Reynolds number and surface roughness for the determination in the thickness of the viscous sublayer (δ), it can be seen that as the Reynolds number and effective roughness increases the thickness of the viscous sublayer will decrease.

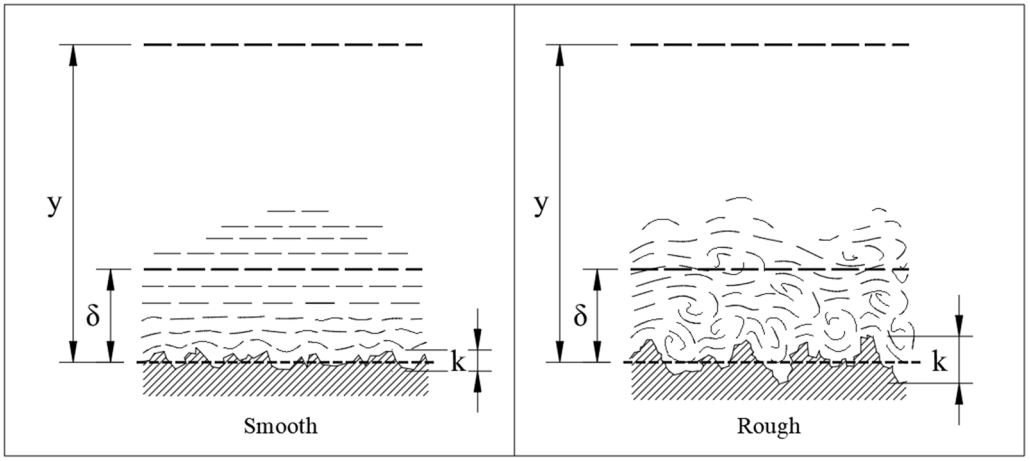

Figure 2.20: Effect of surface roughness on viscous sublayer (adapted from Chow, 1959).

Chow (1959) provides an alternative method to verify viscous forces in the laminar boundary layer

$$\frac{V_* k}{\nu} > 5 \qquad \textbf{2-43}$$

Where:

V_* = Shear velocity $\left(V_* = \sqrt{gRS}\right)$ (m/s)

k = Effective roughness (m)

ν = Kinematic viscosity (m²/s)

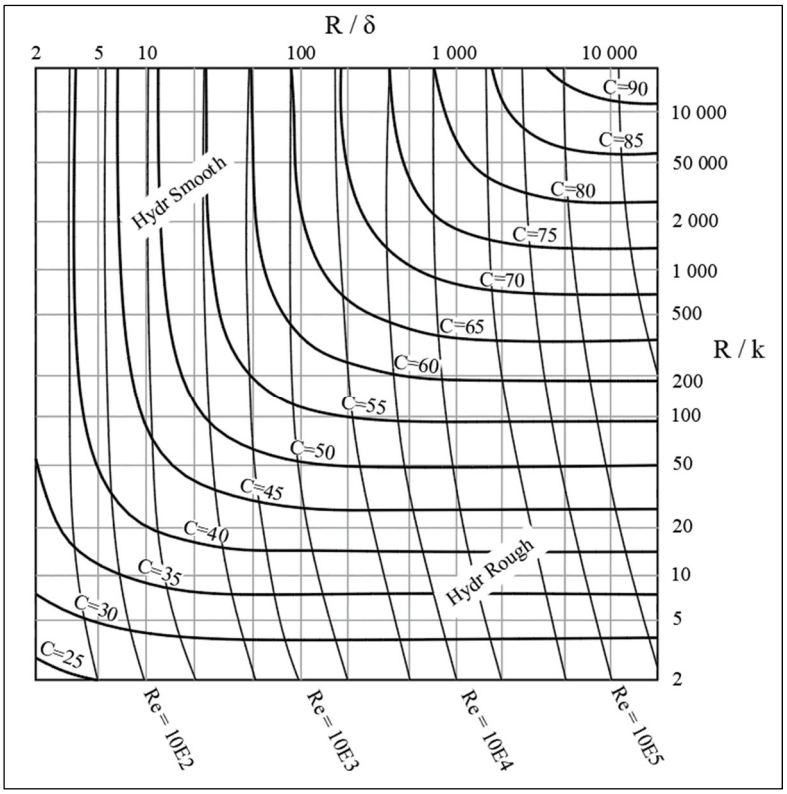

Figure 2.21: Laminar boundary thickness relationship between Reynolds number and hydraulic radius (recreated from Breusers, 1974).

2.17 Conclusion

A review on the available research provided insight into boulder blockages experienced at culverts, considering the limited research available on the phenomenon. Culvert hydraulics and boulder movement were viewed as separate with a small overlapping section regarding sediment movement around culverts used to bring the two study areas together. Lastly, an overview of scale effects for physical hydraulic models was set out.

Culverts and their hydraulic design have been very well studied. The FHWA produced guidelines for debris management, culvert design and energy dissipation. These guidelines provide a comprehensive guide for the design and protection of a culvert and the area surrounding it. The FHWA (2012) and the guidelines set out by Rooseboom and Van Vuuren (2013b) in the SANRAL Drainage Manual (2013) was referred to for the culvert designs.

MEL culverts are a unique approach to reduce energy losses and upstream afflux while increasing the discharge for a similar-sized culvert. Concerns about using MEL culvert designs were mentioned and could be problematic in the case of boulder transport. The barrel invert below the NGL would potentially prevent boulders from exiting the culvert.

The literature identified inlet control with supercritical flow in the barrel to have the potential to produce a feasible solution in the prevention of boulder blockages. Outlet control and subcritical flow in the barrel has the potential to settle out boulders as observed just downstream of hydraulic jumps. Sedimentation at the inlets indicated that the upstream damming results in sediment settling out, for an inlet-controlled culvert, this has the potential to cause blockages.

Rooseboom and Van Vuuren (2013b) recommends a culvert barrel velocity greater than 1 m/s and a barrel slope greater than 1% (1:100) to prevent sediment accumulation in the barrel. Basson (2005) recommended self-cleansing velocities of around 2-4 m/s and a minimum bed slope of 2% (1:50). The recommendation made by Basson (2005) was made toward gravel trap designs in river abstraction works but, could be applicable to culverts transporting coarse bed material.

An investigation into boulder transport proved that conditions for boulder transport are very dependent on-stream characteristics, which could change over time. The Shields parameter is thought to overestimate the required shear stress to move a boulder, this has the potential to result in an under-designed structure. Paleo flood estimations were considered as an alternative, a review of paleo flood estimation methods revealed that while some degree of accuracy is possible, it is considered to be accurate to an order of magnitude. Applied stream power modified to allow for non-uniform particle sizes were selected as a measure of boulder movement.

3. Field Research

3.1 Introduction

Two sites with possible problems concerning boulder movement and blockages have been identified. The site visits were performed in order to gain a better understanding of how boulders block culverts, and where the problem areas exist in a full-size field-constructed culvert. Measurements at the sites included boulder measurements, slopes and cross-sections. The advantages of the two selected sites were the availability of historical aerial photos providing information regarding the impact before and after the culverts were constructed.

Both sites are situated in mountainous areas within the Western Cape, each with differing slopes and stream sizes, including catchment areas. **Figure 3.1** is a satellite image indicating the position of each site and the approximate catchment. Site A is situated North-East of Site B.

Figure 3.1: Satellite image of two selected field study sites (Google Earth, 2019).

3.2 The objective of Field Research

The study proved to be the first documented study of boulder blockages at culverts, it was therefore seen as advantageous to perform two site visits to provide some background to this phenomenon. The objective of performing field research was to furnish the researcher with details regarding the stream characteristics and boulder sizes associated with the stream and to provide details regarding the causes of the boulders settling out at the culverts.

The objective of the field research was to inspect a structure with a known problem, attention was placed on the layout of the structure and observations made upstream and downstream of the culverts. The

field research did not take bed samples for grading as the design assumed that the river can transport the boulders that have been visually moved by a flood event.

3.3 Apparatus Used

3.3.1. Surveying

A GPS device was selected for surveying the cross-sections and slope of each of the streambeds. The Trimble R4 GNSS system was used for the survey which offers reasonable accuracy in a mobile platform. Accuracy is estimated to be around 8 mm in the horizontal plane and 15 mm in the vertical direction after post-processing has been completed (Trimble, 2013). The GNSS unit is mounted onto a 2 m tall pole with a bubble level, the unit is controlled via a handheld unit to measure survey points. **Figure 3.2** shows the R4 GNSS receiver and handheld unit.

Each of the sites where post-processed by using the Worcester base sensor (WORC), which is a Trimble NetR9 type sensor, with coordinates: Lat: S 33°38’41.57997” Lon: E 19°26’42.14827” (National Geospatial Institute, 2019b). The base sensor is about 22.14 km from site A and 12.37 km from site B.

Figure 3.2: Trimble R4 GNSS System; **Left:** GNSS Receiver unit and handheld unit. **Right:** Handheld unit mounted on 2 m measuring pole with bubble level.

3.3.2. Measurements

A 2 m long foldable ruler with 100 mm marked increments were used as a scale ruler for photographs (**Figure 3.3**), it provides a spatial reference to an otherwise photograph with no indication of size. A tape measure was used to measure the triaxial lengths of the largest boulders found in the streambed. The culverts and bridge structures were measured using the tape measure.

Figure 3.3: Folding ruler with 100 mm increments.

3.4 Site Visit

Site A was selected based on observations of flash flooding and high boulder and cobble transport capabilities, unfortunately, the site did not have a culvert at the road crossing. Site B was selected based on the high amounts of boulders at the site and it was observed that two of the three openings were filled almost a third of the way up with boulders. Site B consisted of a three-span bridge. These two sites were two known sites with reported boulder movement. Upon further inspection, both these streams have been trained to maximize the agricultural land, this could have an impact on the boulder movement due to the canalization of the stream.

3.4.1. Site-A

Site A located in a Winelands area where a small catchment (3.24 km^2) in a valley drains into a channel to meet the roadway at a perpendicular angle. The channel out of the valley is very steep (10.78% slope) and the bed comprised mainly cobbles and boulders. The estimated flood peaks have been determined to be 25 m^3/s for a 1:10 year flood and 50 m^3/s for a 1:100 flood event (King, 2007).

Figure 3.4 is a satellite image of the study site with the catchment area shown in red. The straight section of watercourse can be seen where it meets the roadway at a perpendicular angle (arrow A, **Figure 3.4**). Between the catchment on the right and the roadway on the left signs of the previous delta that used to form there can be observed. Historic imagery confirms that the delta used to form where the stream exits the valley and extended to as far as the road, the water has since been canalized to flow downstream (King, 2007).

Figure 3.4: Site A layout and catchment area.

At the road the watercourse runs into a type of retention pond **(Figure 3.5**), it is assumed that is was constructed to allow the water to flow over the sides perpendicular to the road towards the existing culverts, to prevent the water from overtopping the road at this location and to capture any cobbles and boulders that are transported downstream. The gabion structure is approximately 4 m x 4 m wide and 800 mm deep from the invert to the outlet.

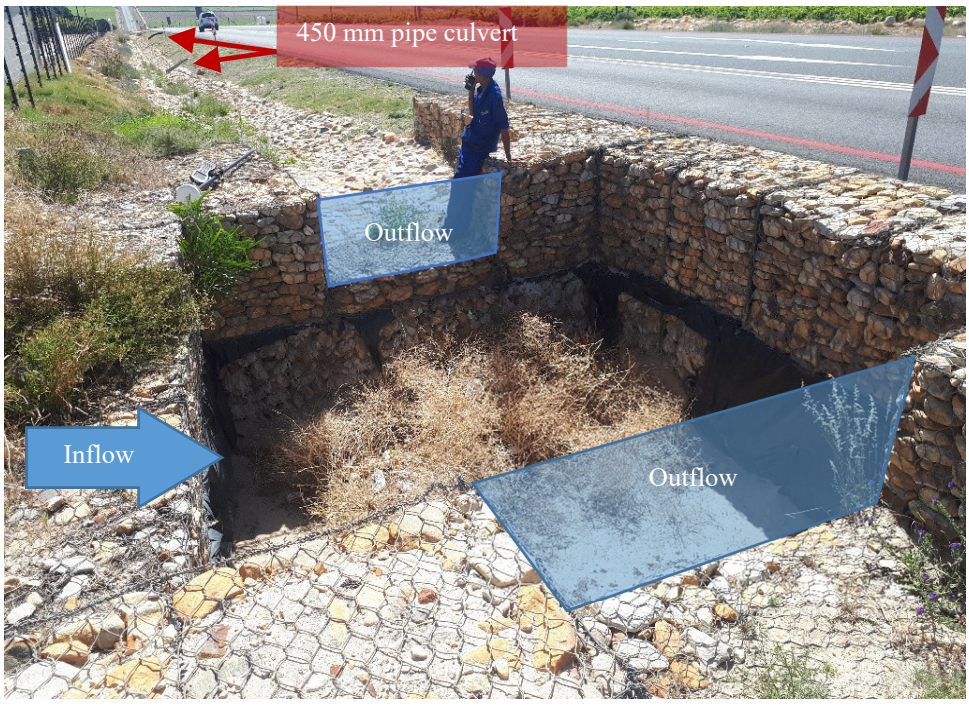

Figure 3.5: Gabion retention structure downstream of the stream to redirect the flow parallel with the road.

Figure 3.6 was from a previous flood event, it is understood that this was taken before the installation of the gabion structure. In the figure the water has to turn 90° at the culvert inlet, deposition of small boulders and cobbles can be seen at the inlet if the deposition continues it has the potential to block the inlet of the culvert, which is only a 450 mm pipe culvert, which is smaller than some boulders identified in the stream.

From the valley the river is almost straight with very little changes in direction, this could contribute to the high bed mobility experienced at the site, there are no signs of any form of natural energy dissipation in the watercourse such as step pools or bends that could promote deposition on the inside bank.

Figure 3.6: Coarse bedload deposition at the inlet of a 450 mm pipe culvert.

Slope Calculation

The slope was calculated over the 1.2 km section of the stream from where the stream exits the valley to the inlet of the gabion structure. A point was recorded approximately every 10 m or where a noticeable change in the stream could be observed. **Figure 3.7** shows an elevation plot of the stream from the valley to the roadway, it is noted that there is no noticeable gradual decline in slope over this distance. The slope calculation was performed over the last 600 m (chainage 636 m to 1242 m) from the road upstream, an estimated average slope of 7.86% (1:12.72) was calculated.

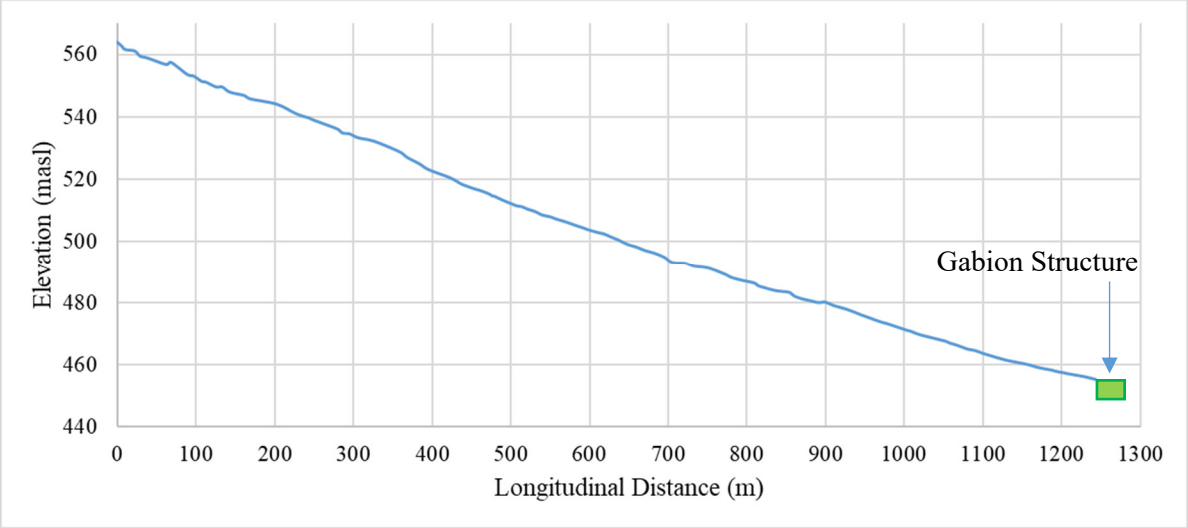

Figure 3.7: Elevation plot of the watercourse at Site A from the roadway 1.2 km upstream.

Bed Composition

The alluvial bed in the stream can be described as a mixture of sandy sediment, gravels, cobbles and boulders, observations have been made that the valley produces high loads of sediment. **Figure 3.8** shows the stream where it exits the valley, the slope here is steep (8.28%) and the high concentration of boulder is clearly visible, in the foreground the finer particles can be clearly seen. At this point in the stream, there is no defined watercourse, it is assumed that the flow depth is very low and fast-flowing due to the high slope. **Figure 3.9** is a downstream view taken from the same location, large boulders in excess of 1 m can be identified as visibly moved by the flowing water, these boulders are not embedded in the alluvium and indicates that they have been transported downstream by the flow.

Figure 3.8: Upstream view of Site A where the stream exits the valley.

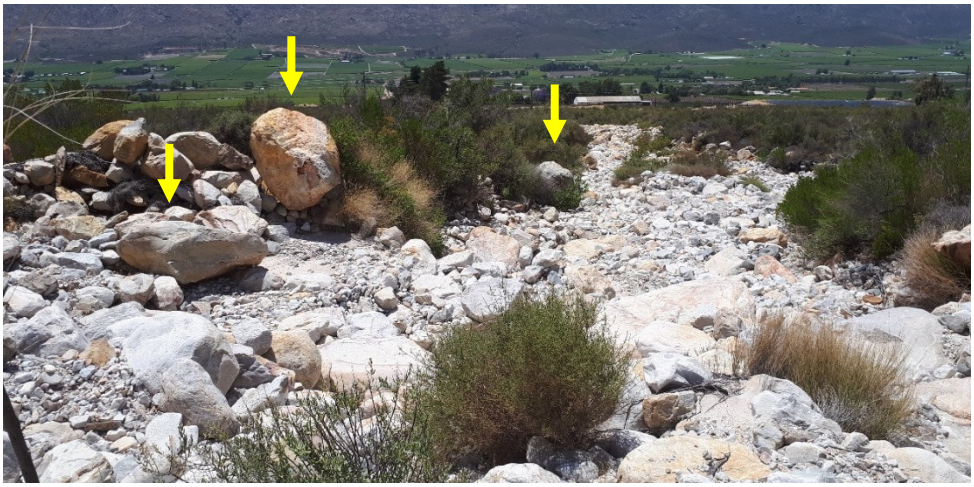

Figure 3.9: Downstream view of Site A where the stream exits the valley, large boulders observed at this location.

Further downstream the larger boulders become less frequent, it was unknown whether the section was cleared of potential blockage material to reduce the possibility of flooding. Smaller boulders were observed in the channel, it was assumed that if the boulder was present in the channel, it was transported downstream by the flow. **Figure 3.10** shows a boulder that has been deposited further downstream closer to the gabion structure, note the alluvium surrounding the boulder is of a much smaller size than the boulder itself. Refer to **Appendix A** for more photographs taken during the site visit.

Figure 3.10: Boulder that settled out on top of the alluvial bed.

Largest Movable Boulders

The largest boulders in the stream bed have been measured and listed in **Table 3.1**, these boulders have been identified to have been moved by water flow, meaning, a boulder was selected if it was in the

stream bed and was not embedded in the bed of the stream. The average Corey shape factor for the measured boulders is 0.721 and the mean boulder size measured on the b-axis is 605 mm. Smaller samples of the same boulders have been taken at the site to measure the density of the boulders, the procedure is explained in **Section 4.2** and the results from the tests are in **Appendix B**. The average density of the sample boulders has been determined to be (2 616 kg/m³).

Table 3.1: Measurements of a selection of the largest boulders observed at Site A.

Number	Triaxial Dimension (mm)			SF	Number	Triaxial Dimension (mm)			SF
	a	b	c			a	b	c	
1	1200	1050	950	0,846	11	700	650	550	0,815
2	1600	1200	800	0,577	12	500	450	300	0,632
3	700	600	450	0,694	13	800	600	500	0,722
4	550	500	500	0,953	14	750	700	650	0,897
5	550	400	350	0,746	15	500	450	250	0,527
6	500	400	300	0,671	16	650	550	450	0,753
7	600	500	300	0,548	17	500	400	200	0,447
8	450	400	300	0,707	18	550	550	300	0,545
9	1100	900	800	0,804	19	650	600	600	0,961
10	550	500	450	0,858	20	850	700	550	0,713

3.4.2. Site-B

Situated 28.66 km South-West of Site A, Site B comprises a boulder bed river with a three-span bridge with the openings aligned with the flow. The catchment area was estimated to be 51 km², considerably larger than that of Site A. From the observations at the site, it was assumed that the boulder transport rate is considerable as well as the floating (organic) debris. The stream upstream and downstream of the bridge can be described as a pool-riffle type of channel, high sediment storage at low flows and transport at near bank full flows are typically associated with pool-riffles (Buffington and Montgomery, 2013).

The Bridge is situated approximately 4 km downstream of the valley and access to the river was limited to the bridge site. **Figure 3.11** shows an aerial photograph of the site with the boulder bed river clearly visible, the focus of this study was on the bridge due to reports indicating that the bridge had some boulder deposits. Approximately 1 km downstream of the site is two additional bridges, spaced 60 m apart, it is unknown if these bridges could contribute to the aggradation experienced at the road bridge upstream, the effects thereof have not been investigated.

Figure 3.11: Aerial photograph of Site B indicating river layout and flow direction (Bing Maps, 2019).

This stream has been trained to prevent flooding of the houses built, as indicated in **Figure 3.11**, in close proximity to the stream banks. Training techniques used was the planting of trees along the banks of the stream (**Figure 3.12 A**) and the use of steel mats packed with rock in the same manner as gabion baskets (**Figure 3.12 B**). Aerial photos indicate that these methods have already been implemented as far back as 1973 (National Geospatial Institute, 2019a).

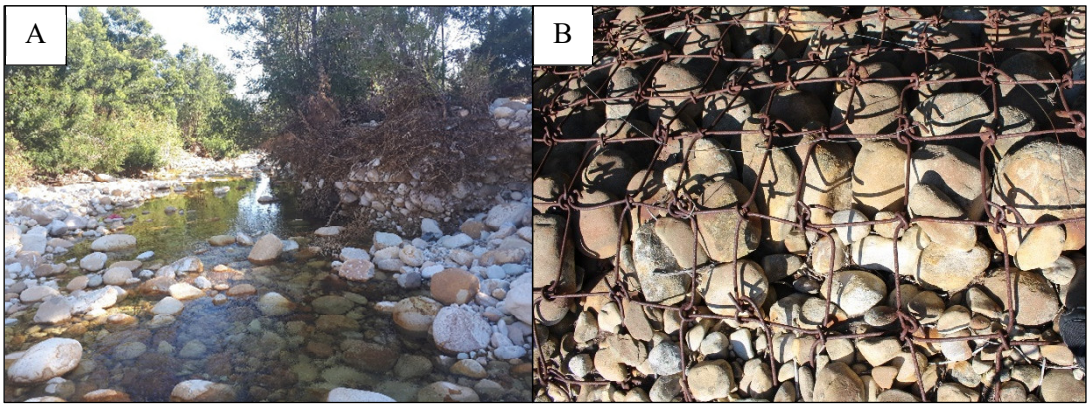

Figure 3.12: A - Erosion on banks where trees are not planted, trees in the background protect banks from erosion; **B** - Steel mat type structure to protect the banks against erosion.

Slope Calculation

Due to the limited access to the site, the slope was determined for a section upstream and downstream of the bridge, approximately 730 m upstream and 100 m downstream to determine if the bridge has an influence on the upstream slope. **Figure 3.13** shows a longitudinal profile of the riverbed, with the bridge location. The average slope over the upstream section has been determined as 1.68% (≈ 1:60) and downstream 1.66% (≈ 1:60), the natural slope has, therefore, remained the same upstream and downstream of the bridge.

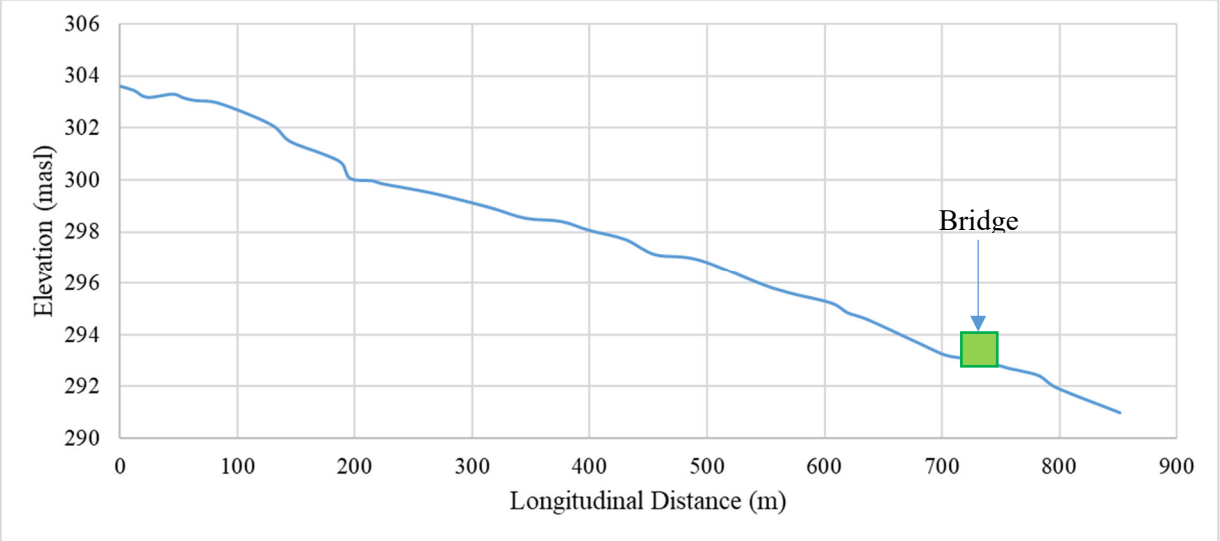

Figure 3.13: Elevation plot of Site A approximately 730 m upstream and 100 m downstream.

Bridge Layout and Sedimentation

The three-span bridge over the stream has attracted large amounts of debris and boulder depositions at the inlet and in two of the spans. **Table 3.2** lists the geometric details of the bridge. It is unknown over which period the aggradation occurred, but maintenance on the bridge was performed approximately four years prior to the site visit, it is therefore assumed that the accumulation of boulders and debris spanned over a maximum four-year period.

A survey of the cross-section just upstream of the bridge aims to quantify the large deposition that has occurred. The blockage caused by the floating debris and boulders is also listed in **Table 3.2**. The survey was performed approximately 3.5 m upstream of the opening, it was the closest straight line that could be surveyed between the wing walls, slope adjustments have been made to represent the blockage at the inlet. **Figure 3.14** shows the surveyed cross-section just upstream of the inlet, the substantial boulder and debris blockage is included in the figure. **Figure 3.15** is a downstream view of the inlet of the bridge. It is assumed that due to the pool-riffle type flow the stream seems to favour the left span whilst depositing boulders in the two other spans. While major deposition took place in the right span of the bridge, the outer wall was scoured almost to the full height of the opening, including the wing walls upstream and downstream. It is assumed that the accelerating flow at the wing walls prevents deposition at this location. This anomaly should be observable in the physical model of a multi-span structure (**Section 7.4**).

Table 3.2: Measured properties of the bridge structure and blocked inlet.

Bridge Properties			Inlet Span Blockage		
Span Width =	9	m	Area Blocked Span 1 =	4,469	m²
Span Height =	3,5	m	Area Blocked Span 2 =	15,191	m²
Span Flow Area =	31,5	m²	Area Blocked Span 3 =	13,201	m²
Number of Spans =	3		Total Blockage =	32,861	m²
Total Flow Area =	94,5	m²	Percentage Blocked	34,77	%
Wing Wall Angle	30	°	Percentage Open	65,23	%
Wing Wall Length =	5,5	m	Percentage Floating Debris =	32,86	%
Soffit to Road Surface =	0,5	m	Percentage Alluvium =	67,14	%
Bridge Length =	13	m			
Pier Thickness =	0,6	m			
Type of Pier =	Round Nose				

It was assumed that the bridge is the cause of the boulder aggregation at the bridge. The pool-riffle type flow and sinusoidal flow pattern are consistent throughout the river, the only accumulation of boulders of this magnitude can be found at the bridge site. This accumulation has not only led to the bridge having an effective opening of two spans, but it has also led to trees and bushes sprouting and growing in the accumulated boulders.

It has been observed that the largest boulders were deposited upstream of the inlet and downstream close to the flow path of the water, inside the spans, the sediment resembled large cobbles and small boulders. Behind the organic debris, sand was observed to have accumulated. It is assumed that the deposition was initiated from upstream where a possible afflux in water depth resulted in the larger boulders settling out, restricting flow to the affected spans. Downstream it is assumed that the boulders settled out as the flow depth decreased as the water exits the bridge and expands to the full stream width. The point bar that forms out of the middle span expands away from the left-most span at an angle of approximately 1:3, assuming that the flow exiting the bridge was flowing near critical, it would correspond with an abrupt expansion (Thompson and Kilgore, 2006) which causes the boulders to settle out.

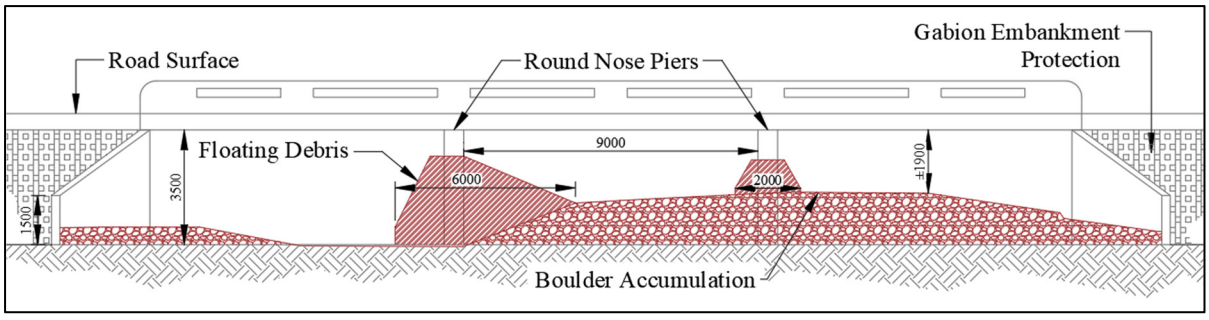

Figure 3.14: Downstream view of surveyed bridge inlet at Site B with debris and boulder aggradation indicated.

Figure 3.15: Downstream view of bridge inlet at Site B.

As shown in **Figure 3.16**, the trees growing upstream (**Figure 3.16 A**) and downstream (**Figure 3.16 B**) is of major concern, this further reduces the flow rate and it essentially stabilizes the soil, in the same manner as bank stabilization has been achieved through the vegetation on the banks. Additional images of the site are listed in **Appendix A**.

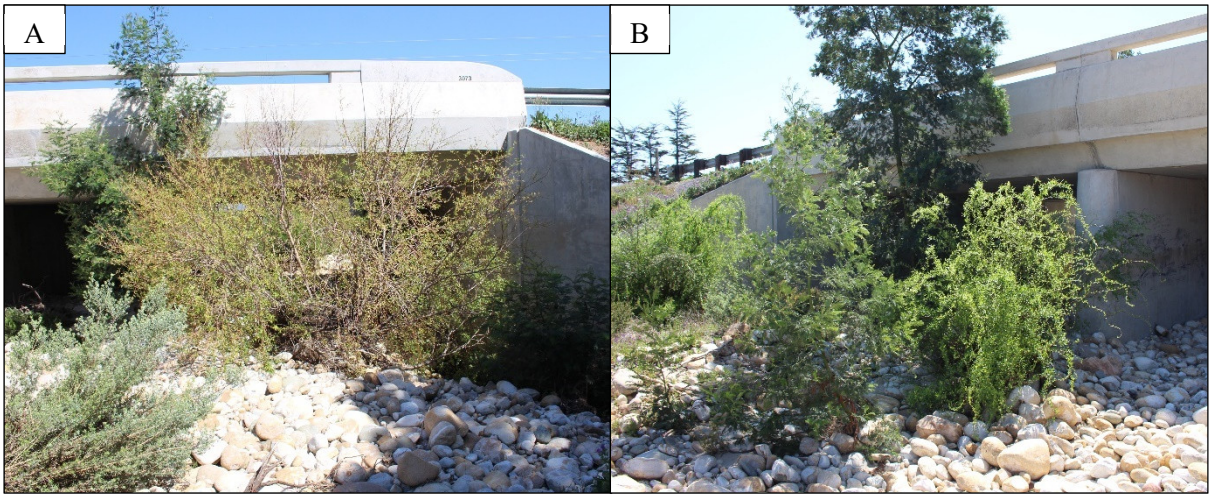

Figure 3.16: Trees growing in near proximity to the bridge at Site B; A - upstream, B- Downstream.

Largest Movable Boulders

The largest boulders that have been transported downstream have been recorded in **Table 3.3**. An average Corey shape factor of 0.678 was calculated for this site, sample boulders for density measurements were not taken at this site. The average boulder size measured based on the b-axis was 571 mm.

Table 3.3: Measurements of a selection of the largest boulders observed at Site B.

Number	Triaxial Dimension (mm)			SF	Number	Triaxial Dimension (mm)			SF
	a	b	c			a	b	c	
1	600	500	500	0,913	11	500	350	300	0,717
2	750	500	400	0,653	12	800	700	600	0,802
3	600	550	300	0,522	13	460	370	280	0,679
4	500	500	450	0,900	14	800	350	330	0,624
5	1200	700	400	0,436	15	900	750	600	0,730
6	600	500	450	0,822	16	740	500	400	0,658
7	650	500	400	0,702	17	820	650	450	0,616
8	1400	1100	800	0,645	18	650	600	400	0,641
9	850	750	400	0,501	19	900	600	550	0,748
10	600	400	350	0,714	20	800	550	350	0,528

3.5 Conclusion

The two sites visited for the field research provided valuable insight into how the boulders deposit at the sites and the slopes at which these boulders tend to travel downstream. The two sites varied greatly in catchment size, stream size, slope and boulder composition. It is believed that an abundance of boulders is available for site B as opposed to site A with the smaller catchment and steeper slope, which results in fewer boulders being deposited in the stream.

The Shape Factor of the measured boulders for site A and B was 0.721 and 0.678 respectively. Both shape factors, while different from each other is quite close to the shape factor for naturally worn quarts at 0.7 (Simons and Senturk, 1992). The mean of the largest boulder sizes between site A and B was measured as 605 mm and 571 mm respectively. The sizes were very similar in that respect. There was a clear difference in the grading of each river based on the observations made during the site visit. It is believed that the lower slope at Site B would deposit boulders easier due to the flatter slope and higher roughness provided by the boulders in the stream.

Research performed at Site A was used to develop the stream setup for the physical model and the data and observations from Site B provided information regarding deposition at multi-span structures.

4. Experimental Model Setup

4.1 Introduction

The objective of the experimental model setup is to study the interaction between the boulders and the prototype that has been developed as well as to determine the accuracy of the hydraulic performance of the design. Conducting hydraulic tests in a laboratory environment allows for repeatable tests to be performed, whilst reducing the risk and cost of the prototype. This Chapter describes the general experimental setup in the laboratory, initial tests that were required as part of the development and provides comments and observations into the use of a fixed bed for experimental testing.

Due to the complex nature of the model setup, the experimental tests were performed in two phases. Phase one comprises the initial setup of the model and the determination of the flume characteristics to be used in the development of the model. After phase I, three different inlet models was developed of which the preferred two were tested in phase II.

Figure 4.1 visually illustrates the sequence followed during the experimental investigation, the general experimental setup is discussed in detail in this chapter. Phase I, including the accompanying experimental tests, is discussed in **Chapter 5**. The development of the proposed prototypes and the experimental tests is presented in **Chapters 6** and **7** respectively.

The dimensions and parameters used, including the results, have been converted to reflect the prototype values for ease of use and practicality unless stated otherwise.

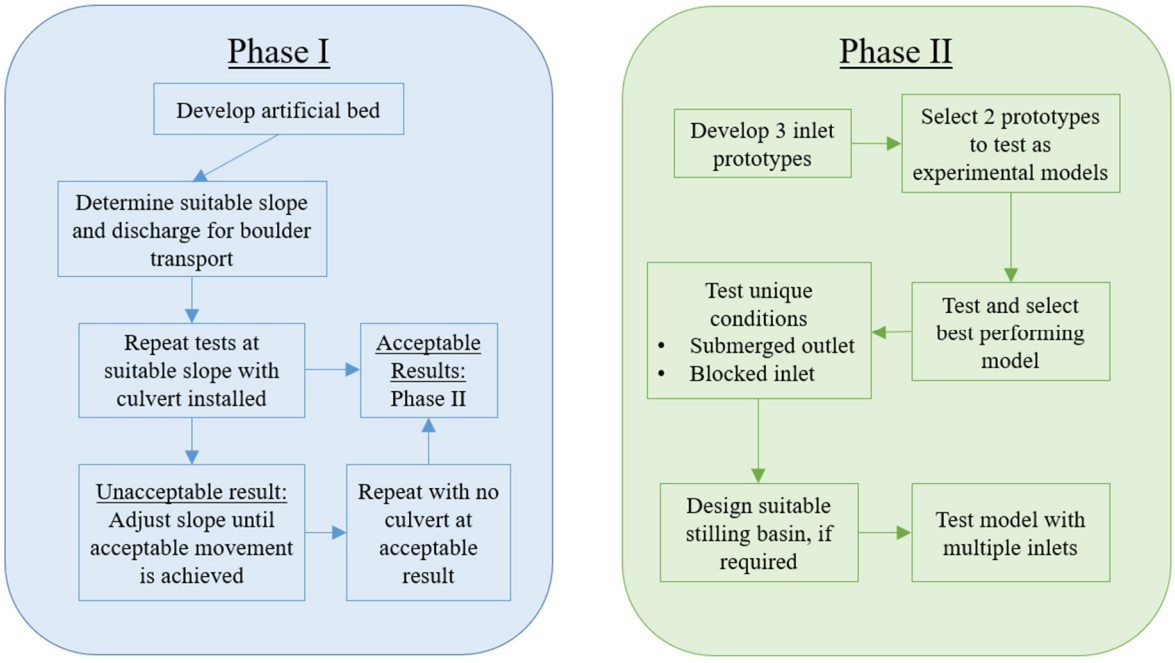

Figure 4.1: Outline of the procedure followed for the experimental tests.

4.2 Experimental Boulder Properties

4.2.1. Rock Density Calculation

For the determination of the drag coefficient (C_D) the density of the rock used in the experimental model was required. The density of the rock was determined by using a scale to determine the weight and a beaker containing water to measure the volume. The rock density was then calculated as follows:

$$\rho_s = \frac{\text{mass}}{\text{volume}} = \frac{m}{V}\ ;\ [kg/m^3] \qquad \textbf{4-1}$$

Each of the rocks was weighed and their weights recorded. The rock was then placed in a measuring beaker with the volume before the rock was placed inside recorded. **Equation 4-1** could then be used to determine the density of a singular rock.

A sample of 30 rocks was selected for the density calculations, due to the small size of some of the rock, some samples comprised two rocks. The results from the calculation yielded an average rock density (ρ_s) of 2640 kg/m³. **Table 4.1** shows the measured model weight and volume for each of the samples taken, the slight discrepancy in some of the results is attributed to the accuracy of the beaker used.

Table 4.1: Rock density determination.

Sample No	Num. Rock in Sample	Weight (g)	Vol 0 (ml)	Vol 1 (ml)	Δ Vol (ml)	Density (kg/m³)	Sample No	Num. Rock in Sample	Weight (g)	Vol 0 (ml)	Vol 1 (ml)	Δ Vol (ml)	Density (kg/m³)
1	2	76	390	419	29	2620,69	16	2	244	488	580	92	2652,17
2	2	170	420	485	65	2615,38	17	1	370	960	1100	140	2642,86
3	1	406	1105	1260	155	2619,35	18	1	270	583	685	102	2647,06
4	2	322	485	608	123	2617,89	19	1	256	685	783	98	2612,24
5	2	604	422	650	228	2649,12	20	1	326	512	635	123	2650,41
6	2	126	523	571	48	2625,00	21	1	120	580	625	45	2666,67
7	1	614	1145	1380	235	2612,77	22	2	98	623	660	37	2648,65
8	1	418	570	725	155	2696,77	23	1	144	658	710	52	2769,23
9	2	180	495	565	70	2571,43	24	1	120	710	755	45	2666,67
10	2	292	565	678	113	2584,07	25	1	238	1090	1180	90	2644,44
11	1	290	1420	1530	110	2636,36	26	2	338	472	600	128	2640,63
12	1	186	678	748	70	2657,14	27	1	302	600	715	115	2626,09
13	2	462	520	690	170	2717,65	28	2	144	715	770	55	2618,18
14	1	304	685	800	115	2643,48	29	1	206	472	550	78	2641,03
15	1	552	1690	1905	215	2567,44	30	2	182	552	620	68	2676,47

4.2.2. Settling Velocity and Drag Coefficient

The drag coefficient for the model rock was determined experimentally, the literature showed that there is no accurate method to calculate the settling velocity of a particle. Settling velocity was required to

compare the results from the tests with that of the Modified Lui diagram (**Figure 2.17**). **Equation 2-21** was used to determine the drag coefficient, which was compared to the works presented by Concha (2009).

$$V_{SS} = \sqrt{\frac{4}{3}\frac{\rho_s - \rho}{\rho}\frac{gd}{C_D}} \qquad \textbf{2-21}$$

30 samples of each model rock size (26.5, 37.5, 50, 63 mm) were selected for the settling tests. The samples were numbered and their triaxial dimensions recorded with a Vernier calliper. The triaxial dimensions were used to determine the SF of each sample. Triaxial measurements and SF calculation results of the samples are listed in **Appendix B**.

Settling Tests

The settling velocity of particles was determined through a settling test (fall test), using a vertical tank, with a water depth of 5.1 m and 1.8 m in diameter. Horizontal braces inside reduced the number of possible successful tests, if a rock contacted a brace the test was withdrawn.

For each sample the following procedure was repeated:

- Place sample just inside the water, deep enough to just cover the top of the sample.
- Release the sample in place with no upward or downward motion of the hand, the stopwatch is started simultaneously.
- The sample makes an audible sound as it hits the bottom of the tank, the stopwatch is then stopped and the time is recorded.

From the recorded settling time and the depth of the tank, the settling velocity (V_{ss}) was obtained through the following Equation:

$$V_{ss} = \frac{\text{Tank Depth (m)}}{\text{Time (s)}} \qquad \textbf{4-2}$$

Results

Appendix B lists the results from the settling tests. The 26.5 mm sample size produced 27 usable results, the 37.5 mm sample produced 24 results, the 50 mm sample 21 results and the 63 mm sample 22 results. In total 94 usable results from 120 tests were produced.

The C_D coefficient was determined for each sample with **Equation 2-21**. shows the results plotted against the shape factor (SF). There is some variability in C_D for a given SF. A trend can be identified where the smaller SF results in a larger C_D coefficient. A maximum C_D of 1.95 and a minimum of 0.731 was calculated. If an SF of 0.7 (Simons and Senturk, 1992) is assumed to represent the boulders a C_D value of 1.086 is obtained.

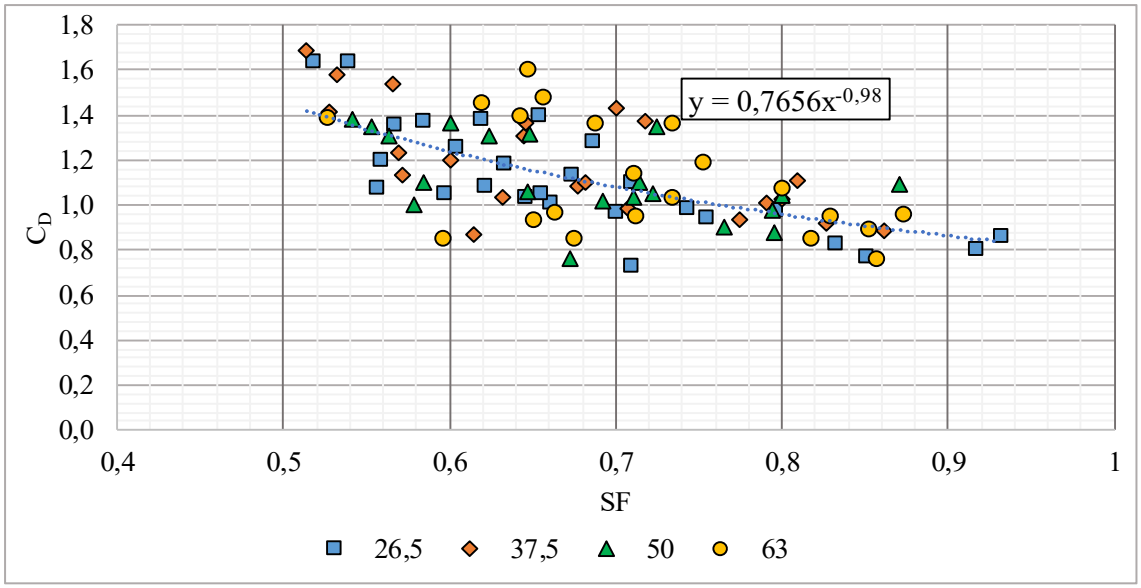

Figure 4.2: Experimental result of the drag coefficient vs the shape factor.

Figure 4.3 shows the C_D coefficient vs the Reynolds Number (Re), included in the graph is the results from the works of Concha (2009). The results show a good comparison of the experimental C_D values determined for the model rock and that of the isometric shapes. The figure shows that a C_D value for spheres underestimates the drag experienced by a natural rock particle.

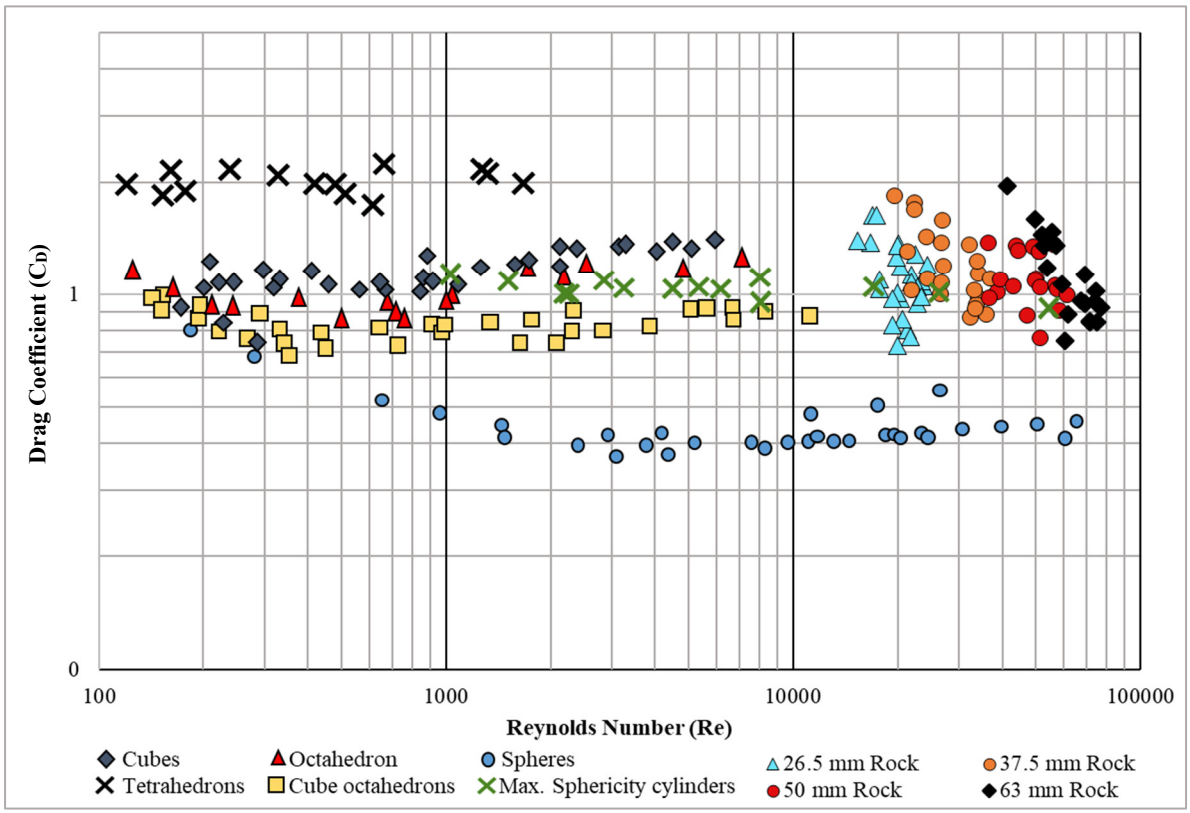

Figure 4.3: Particle Reynolds number vs. experimental drag coefficient; experimental results compared to drag coefficients of isometric particles (after Concha, 2009).

Summary of Results

From the settling tests performed a C_D coefficient of 1.086 have been determined for an SF of 0.7 from . Langmaak (2013) performed similar tests on larger rock, for rock with an SF of 0.58 he obtained a C_D coefficient of 1.66. For an SF of 0.58, a C_D of 1.31 is determined using . Considering the size of the boulders used by Langmaak (2013) and the number of samples used, the results from his test was considered to be comparable with the results obtained in the current study.

The C_D coefficient that has been obtained is in agreement with Carling (2002) who noted that a C_D value for boulders can be between 0.71 and 1.2. He refers to prototype scale boulders in his findings, the C_D coefficient for the model scale can, therefore, be compared to that of the prototype.

4.3 General Experimental Setup

Determining the conditions at which the boulders would initiate movement in the flume required the use of a tilting flume along the longitudinal axis. For the purpose of the study, the tilting flume located at the hydraulic laboratory of Stellenbosch University was used. The slope of the flume could be adjusted between 0 and 1:40 (2.5%). The flume is roughly 12 m long, with a width of 2 m and a height of 0.6 m, the sides are constructed of glass panels. Water is supplied to the flume via two 100 mm steel pipes, each equipped with a magnetic flow meter (*SAFMAG* and *Endress + Hauser* respectively) and controlled via gate valves. Two pipes were required as a singular flow meter could not provide an accurate reading for the higher flows (>21 L/s), the two combined pipes could satisfy the maximum flow rate of 40 L/s.

Figure 4.4 illustrates the closed system in the laboratory which provided the water to the tilting flume. Water was pumped into a large basin which provides a constant head to the flume via a 300 mm steel pipe. From the steel pipe, water is diverted into the two 100 mm pipes with flow meters attached which are controlled by manual gate valves. Water enters the flume upstream into a stilling basin, downstream the water falls through a grid into a drainage canal which returns the water to the storage tanks.

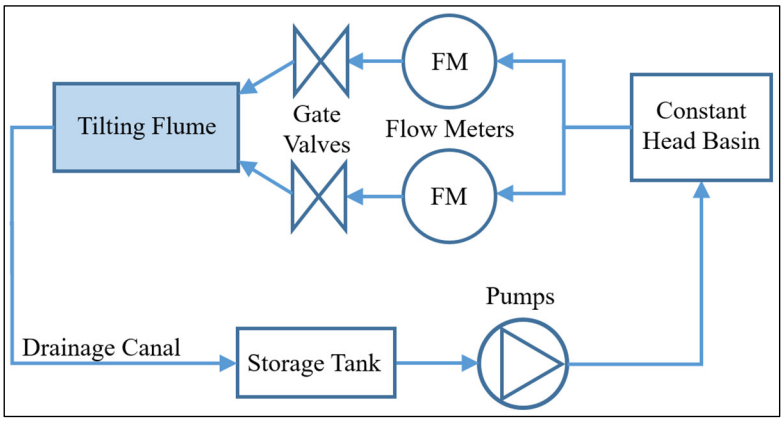

Figure 4.4: Closed water cycle in the Hydraulics Laboratory.

Due to the height and slope limitations of the glass flume, modifications were made in order to retain a large scale that would reduce the scale effects on the model. Height restrictions resulted in reducing the width of the flume to 0.75 m, an artificial slope was added to the flume, this changed the range of the flume from 0 – 0.025 (0 – 1:40) to 0.025 – 0.05 (1:40 – 1:20). Shown in **Figure 4.5** is the glass flume setup as used in the experimental setup.

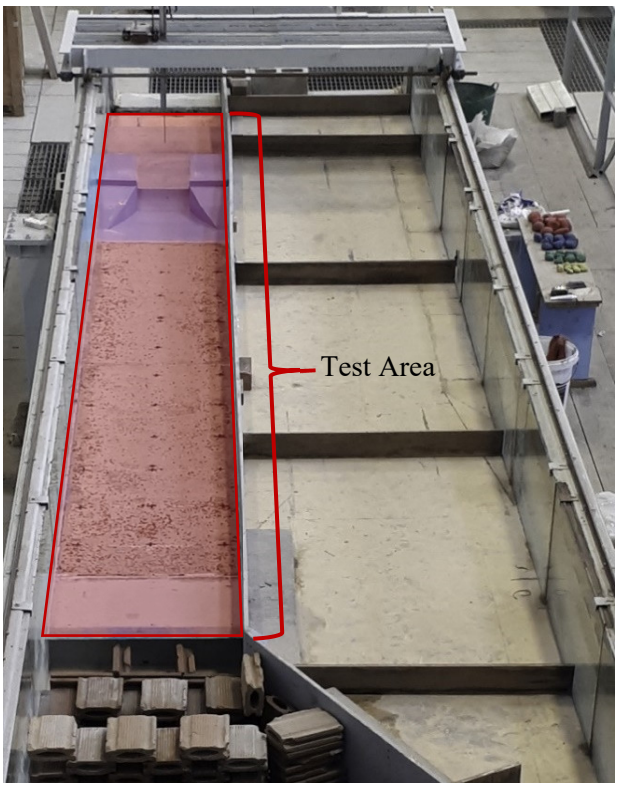

Figure 4.5: Glass flume with the modified test area.

To produce consistent and comparable results, the boulders were placed in the same location for each test. Inconsistent flow patterns and currents caused by the water favouring the lower roughness of the smaller boulders were prevented by alternating the boulders for each successive row of boulders. This was achieved by placing five boulders in a row with the four boulder sizes from largest to smallest. **Figure 4.6** shows a plan view photograph of the artificial bed with the boulders placed at 6.4 m (400 mm model) intervals, this pattern was kept identical for each test of all the models.

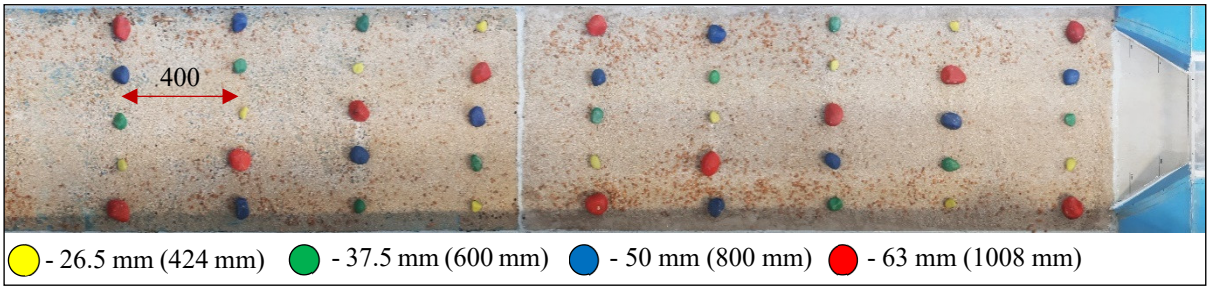

Figure 4.6: Boulder layout on Artificial bed spaced 400 mm (6.4 m) on the x-axis (longitudinal distance), model size, prototype in brackets.

A needlepoint gauge mounted on a carriage was used to measure the water levels during testing. Flow straighteners were used upstream of the test area to mitigate the effect of the contraction and to stabilize the flow over the width of the flume. Tailwater downstream of the culvert was controlled by a tailgate that could be adjusted for different tailwater levels if necessary. A grid placed downstream served as a catchment basin for all the rocks that were used in the tests, the same rocks were used for all tests to ensure repeatability. **Figure 4.7** shows a plan view and sectional view of the laboratory setup with the modified flume to allow for the narrower test area. The artificial bed which made up the experimental area was 70.88 m (4.43 m model) in length and 12 m (750 mm) wide.

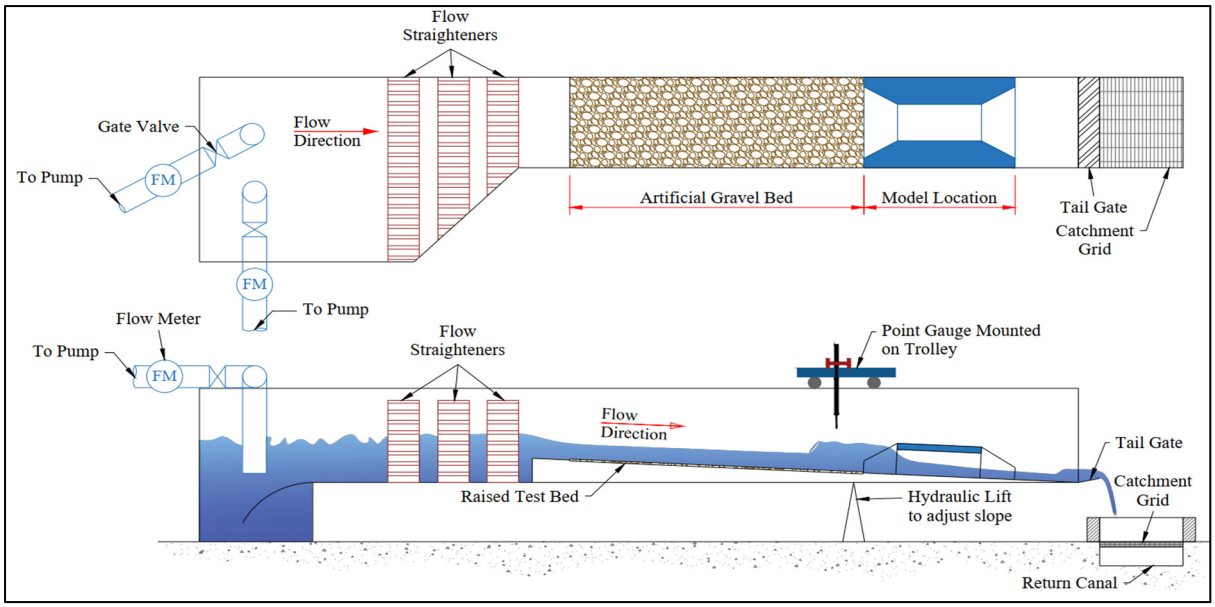

Figure 4.7: Schematic illustration of the model setup and test area (not to scale).

4.3.1. Scale Effects

Each of the models was scaled using Froude scale, with a scale factor of 1:16. (see **Section 2.16)**. Considering a relatively large scale reduces the effects of a scaled model and allowed the use of regular rock to represent the boulders. The main concern was the viscous effect that the fluid could have on the model should the scale become too small, in other words, Reynolds Law. **Table 4.2** illustrates the model Reynolds numbers that were calculated using **Equation 2-22** and the measured results from the preliminary tests. From the measured data, it is shown that the Reynolds Number is large enough to ensure that the model operates in the turbulent regime.

For each of the discharges in the model laminar boundary layer thickness calculation have been determined from **Figure 2.21** and included in **Table 4.2**. This shows that the boundary layer thickness is comparatively small with the size of rock used, thus the effects of viscous forces on the material could be ignored.

Table 4.2: Model Reynolds number and viscous sublayer thickness.

Q (m³/s)	V (m/s)	Re	Hydr Rough >5	δ (mm)
0,01	0,696	11696	742	0,192
0,015	0,840	17544	828	0,198
0,02	0,959	23392	894	0,154
0,025	1,058	29240	952	0,126
0,02786	1,075	32585	997	0,115
0,03	1,103	35088	1021	0,104
0,035	1,149	40936	1081	0,104

4.4 Laboratory Apparatus

4.4.1. Elevation Measurement

Setting the slope of the flume required the use of a dumpy level and a levelling staff. The Elevations of the flume bed and the installed models were measured at three points for each cross-section, as shown in **Figure 4.8**. Three measurements across the flume ensure that the bed is level across the width of the flume. For the longitudinal slope, elevation measurements were taken at known distances along the x-axis. Elevation measurements were recorded on the z-axis. Making use of **Equation 4-3** the slope for a given section is obtained. For a slope in the downstream direction, a negative reading would be obtained from **Equation 4-3**. The calculated value is multiplied by a factor of minus one to keep the sign convention consistent with the flow direction.

$$S_0 = \frac{z_1 - z_2}{x_1 - x_2} \qquad \textbf{4-3}$$

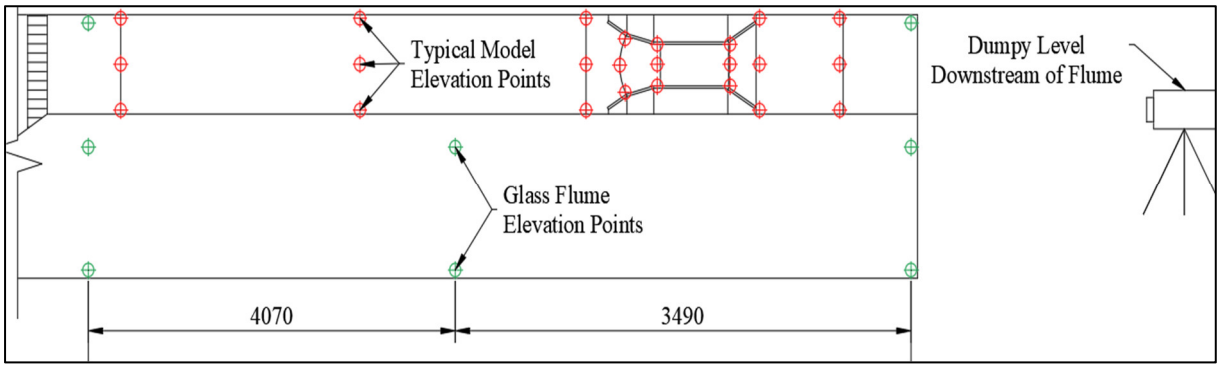

Figure 4.8: Plan view schematic layout of a typical elevation survey.

4.4.2. Water level Measurement

A needlepoint gauge on a carriage (**Figure 4.9**) that can move in the x- and y-directions was used to measure the upstream and downstream water levels. The needle gauge requires a datum, or zero reading, for each measured point in the flume, subtracting the water level measurement from the datum gives the flow depth at a given point.

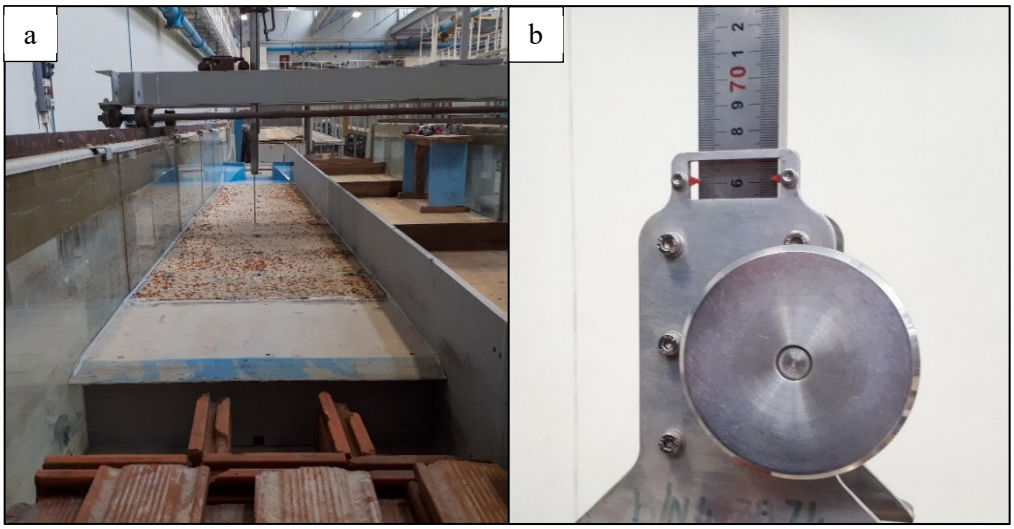

Figure 4.9: (a) - Needlepoint gauge mounted on a carriage **(b) -** Needlepoint gauge ruler and adjustment knob.

4.4.3. Flow Measurement

Two electromagnetic flowmeters (**Figure 4.10**) were used to measure the flow rate in litres per second (L/s). Making use of two smaller flow meters gives a more accurate flow rate and allows the user to make minor changes to the flow rate using the gate valves at the outlet of each of the pipes. Each flow meter is connected to a 100 mm steel pipe that supplies water to the flume. The Endress + Hauser flow meter limits the flow it can supply to 21 L/s and the SAFMAG flow meter can supply flow up to 80 L/s, but the flow rate is limited by the inlet pipe to around 30 L/s. The two combined flow meters satisfy the water supply necessary for the model tests.

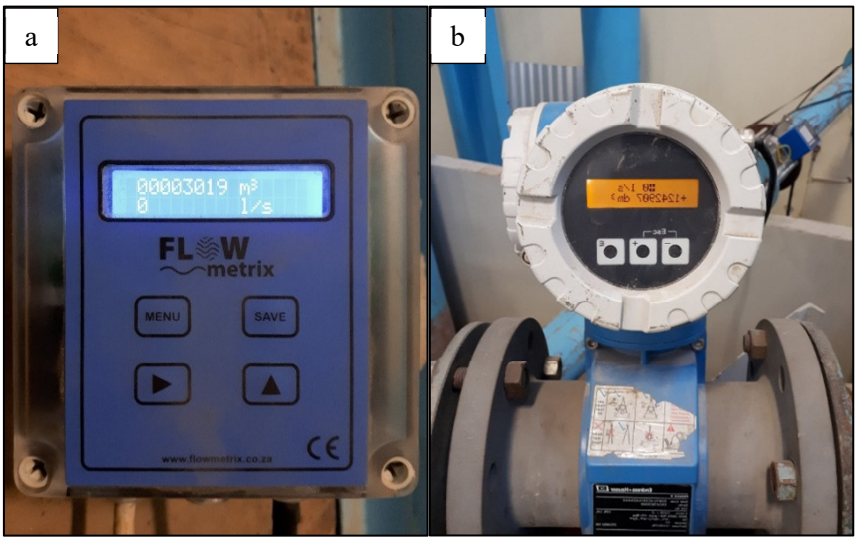

Figure 4.10: Electromagnetic flow meters; **(a) -** SAFMAG **(b) -** Endress + Hauser.

4.5 Artificial Bed Development

During the preliminary tests and model set up, the need for some type of artificial bed became clear as the options were limited in terms of bed material to use in the test area. Initially, it was assumed that the flume bed would not be suitable and that the boulders would slide downstream under the force of the water due to the low friction coefficient between the two materials. A single test with the model boulder which was transported downstream by sliding action under very low flows confirmed the assumption.

Another option was to make use of a uniform bed for each boulder size, the concern was that the boulders would act as rip rap. The slope would, therefore, need to be unnaturally steep or the flow depth would need to be deep according to **Equation 4-4**. Stoffberg (2005) derived the simplified criterion for riprap stability in **Equation 4-4** as derived by from the SANRAL Road Drainage Manual of 1997. Various literature (described in **Section 2.14**) stated that it would not be suitable as the boulders would create a shielding effect effectively trapping the boulders and keeping it in place.

$$d_{50} = 11yS_0 \qquad \textbf{4-4}$$

A single test confirmed that this would be the case, for the test a uniform bed of 63 mm (1.01 m prototype) rock was used for the test area, at a slope of 1:50 (2%). The flow was increased in excess of 120 L/s (122.9 m³/s prototype) with no rock being transported downstream. The model boulders would simply roll over into a stable position and remain in place for the entire duration of the test.

Two options that remained was the use of a mobile bed of smaller diameter material, modelling, for instance, a gravel-bed river in prototype with some boulders. The other option was the use of a fixed bed that represents a model bed similar to a gravel or boulder bed river. With the use of field observations from the site visits discussed in **Chapter 3** a gravel bed model was developed. Two gravel beds were modelled with the latter model being built to provide repeatable and reliable tests in terms of boulder movement and the factors causing the boulders to settle out. **Figure 4.11 (a)** shows the section of the river from the site visit that the artificial bed in **Figure 4.11 (b)** was modelled from. It can be seen that the streambed was made up of mainly gravel and cobbles with some larger boulders and cobbles being spread out along the bed of the river. Creating the artificial bed meant that the focus could be on the movement of the boulders and the same test would be repeated for a different culvert model for exactly the same test area.

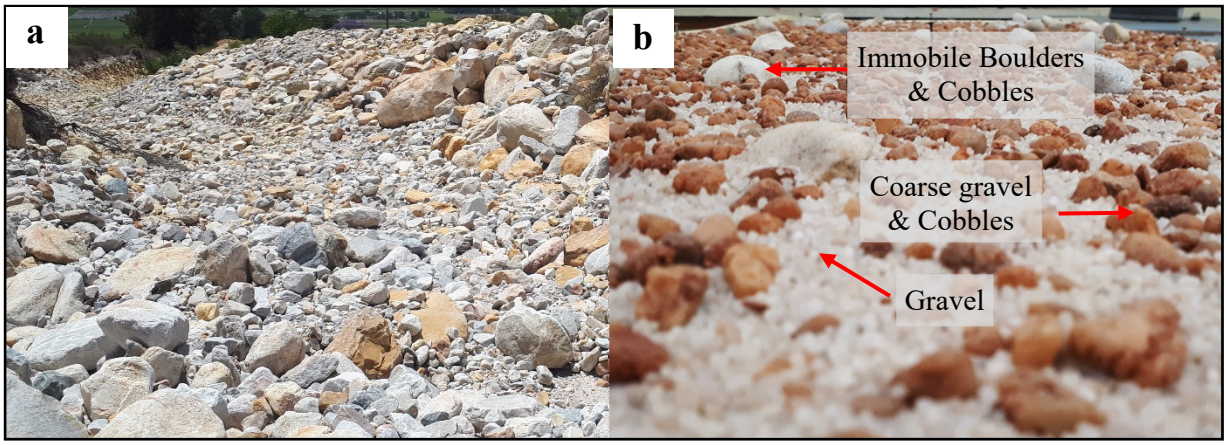

Figure 4.11: (a) - Photo from site visit illustrating the streambed; **(b) -** First iteration of artificial bed modelled from site data.

The second fixed bed was modelled with the larger "cobbles" and protruding "boulders" removed. During the initial tests, these protrusions and obstructions meant that some of the model boulders would become stuck and cause upstream model boulders to pile up against the newly formed obstruction. It was regarded as a factor influencing repeatability, therefore the bigger obstructions were removed leaving a gravel bed (**Figure 4.12**) that provided the roughness in the model for the boulders to initiate movement either by saltation or rotation.

Figure 4.12: **Artificial bed II - sand and gravel glued to the bed of the model.**

4.6 Limitations and Repeatability of Tests

It is very difficult, if not near impossible, to replicate each condition under which boulders would behave in rivers during flood events or under normal circumstances. Therefore, it is required to limit the number of variables in the model in order to obtain test results that are consistent and can be repeated and used for comparisons between different structures. The mentioned limitations will change the conditions under which the boulder would be transported downstream. The operation of the proposed models will not be affected by the limitations. The focus of this study is not to determine the incipient

conditions for boulder transport, but rather the way in which a culvert could be altered to improve on the ability to flush the boulder through without causing additional flooding or a complete blockage of the culvert.

Factors that have been limited to ensure repeatability is as follows: channel cross-sectional shape, channel width, discharge, channel roughness and channel bends. The channel has been kept rectangular, it allows for a greater cross-sectional test area and allows for a higher probability of boulders depositing at the wing-walls. Channel width has been kept constant to reduce the number of models required to be built and the time required to widen the channel for each test. A straight approach channel was used as it simplifies the setup and produces repeatable tests. The tests were done at incremental flow rates up to the overtopping of the model, the valve opening is set manually so replicating a flood hydrograph is difficult to ensure consistency.

The biggest factor that has been kept constant that would initiate boulder movement is the roughness and the sediment transport processes associated with it. **Figure 4.12** shows the artificial bed that was developed for testing. Sufficient roughness was provided by the artificial bed that would prevent sliding of the boulders on the bed. The fixed bed allowed for repeated tests to be performed without the bed being transported downstream.

Ensuring accurate testing and results, as well as determining whether the results can be consistently repeated meant that 10% of all the tests for each model were repeated as individual experiments. Results from the repeat tests could be compared to confirm accuracy with the test results.

4.7 Image Post-Processing

A method to analyse movement patterns of armour units in coastal areas is through comparing imagery taken between different time intervals. By overlaying the images with known base points, the movement of the armour units can be measured (Tulsi and Schoonees, 2016).

By having reference points of known distances on the subject being photographed, the image taken after each test can be post-processed to deliver an image with no perspective distortion. The post-processed image is in the two-dimensional plane and measurements can be taken. **Figure 4.13(a)** is an example of the post-processing performed for a simple grid with known distances. The image is taken at an exaggerated angle to show the effectiveness of the post-processing (**Figure 4.13(b)**). After post-processing (**Figure 4.13(c)**) the accuracy is estimated to be 99%, the precision is attributed to the precise lines of the original image.

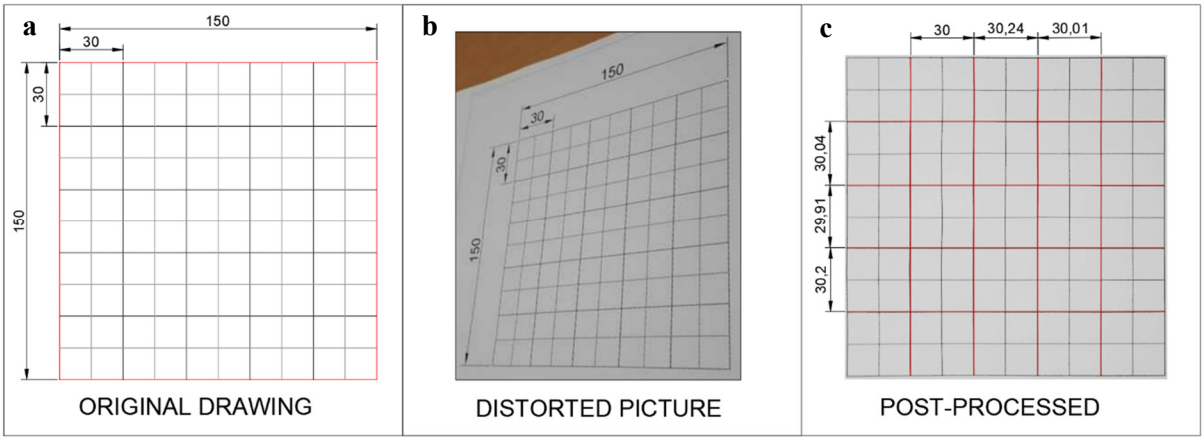

Figure 4.13: Example of post-processing accuracy of a photograph.

Figure 4.14(a) is a photograph of one of the experimental tests that have been performed on the modified inlet in **Chapter 6**, the photograph has been taken after the test has been completed. **Figure 4.14(b)** is after post-processing was performed, the overlaid plan view drawing illustrates the accuracy of the post-processing. The post-processed image was analysed and **Figure 4.14(c)** is how the results are displayed, with the non-moved rocks shown in grey. Accuracy for the experimental model was determined to be 97%, the slight reduction in accuracy was due to the thickness of the grid points used in the model and the boundary between the walls and the bed of the model.

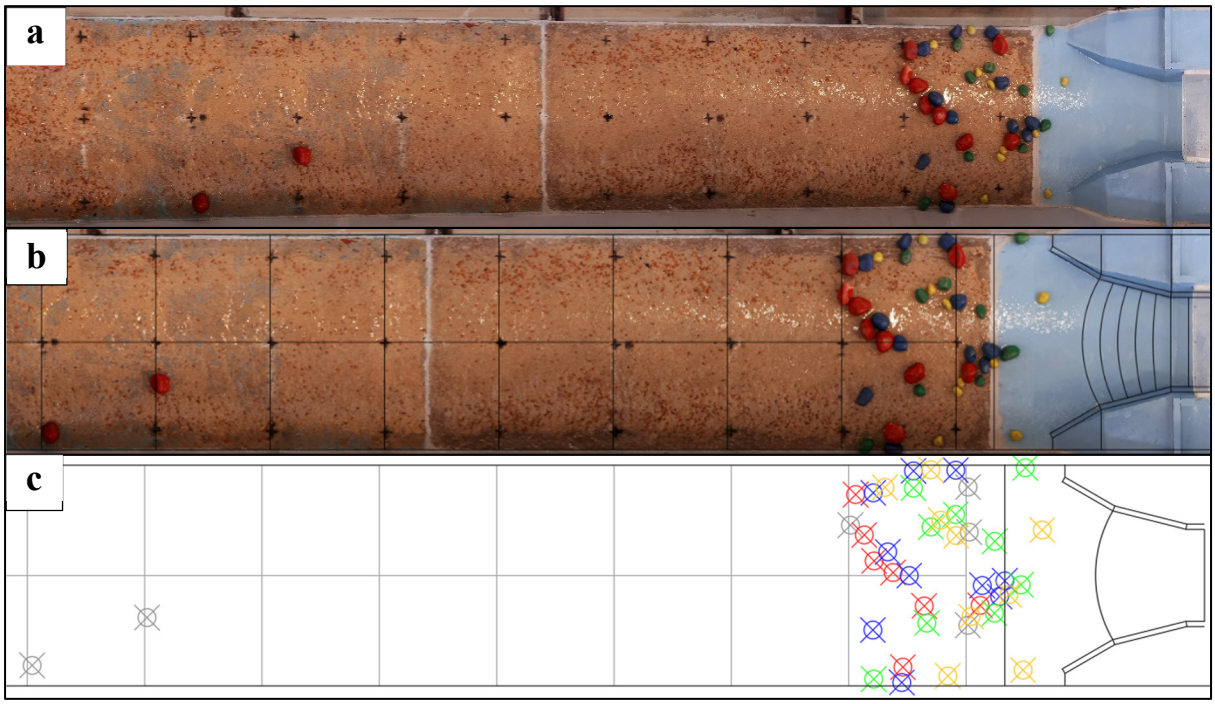

Figure 4.14: Example of post-processing of experimental models, Test: Compound Tapered Inlet Q = 28.53 m³/s.

4.8 Model Setup Summary

The setup, used for the experimental models, were described and illustrated in this Chapter, including all the apparatus used. The model size boulder properties and their accuracy relating to the prototype is explained and it was determined that scale effects would not influence the accuracy of the model. It was determined that the large scale of 1:16 was chosen to reduce the scale effects associated with hydraulic models. The experimental setup was scaled according to the Froude Scale similitude.

To ensure repeatability the need for an artificial bed was motivated and the development thereof was discussed. It was found that using a uniform particle size would not be suited as the boulders would behave as riprap, the criterion for incipient motion would, therefore, be inaccurate to the size of the culvert.

5. Preliminary Experimental Model

5.1 Introduction

Preliminary experimental tests comprise phase one of the experimental model as illustrated in **Figure 4.1**. This chapter deals with the calculations and experimental tests that were required to set-up an experimental model that could be used for tests in **Chapters 6** and **7**. Incipient motion of the bedload in the flume was used as the criteria to determine the bed slope of the flume.

Experimental tests were performed on two models, a flume with a rectangular cross-section with no culvert installed and a rectangular box culvert installed downstream of the test area. A single 5 x 2 m (B x D) rectangular box culvert was used to determine the design discharge of the flume.

Results from the preliminary tests are shown, analysed and the optimal bed slope selected. Water levels between the culvert and normal flow conditions are compared. From the flow depth measurements, the bed roughness (k_s) was calculated. Comparisons are drawn between water levels taken with and without the rock added for the culvert model. The Chapter concludes with a summary of the findings and observations made during the preliminary tests.

5.2 Preliminary Experimental Model Overview

The development of the proposed inlets in **Section 6**, was carried out by making use of the flow conditions of the flume. Developing a model based on flow conditions of the site allows the design to be adaptable to suit different streams with site-specific characteristics. A preliminary model was therefore required to determine the flow and channel parameters that were used in the development of the inlet models. The preliminary model consisted of two test scenarios, a no-culvert (NC) model and a culvert (C) model. The two scenarios were tested with the artificial bed developed in **Section 4.5**.

Incipient motion of the coarse bedload was achieved through adjusting the bed slope of the flume, all other parameters remained constant. The motivation behind using the bed slope as the only variable is discussed in **Section 0**. It was critical to determine a slope that would be capable of just transporting a boulder downstream, the minimum slope would encourage boulder deposition as the flow changes at the culvert.

5.3 Hydraulic Design of a Rectangular Culvert

The discharge capacity of the culvert determined the design flow for the experimental models in the flume. A 5 x 2 m (B x D) rectangular culvert was used for the experimental model calculations and tests. Using a large culvert for the experimental model ensures that the inlet is sized large enough to

prevent the boulder from depositing due to an undersized barrel. As a first estimate, it was assumed that the culvert would operate under inlet control, outlet control could not be calculated beforehand. Calculating H_1 for outlet control requires a bed slope (S_0) to calculate the elevation difference in **Equation 2-13.** Outlet control was checked once the desired slope has been achieved.

An H_1/D ratio of 1.2 was selected for the inlet control calculation, this is the optimal inlet damming height, providing the largest discharge for a given head (Rooseboom and Van Vuuren, 2013b). Free-surface exists at the inlet of the culvert operating under inlet control for an H_1/D ratio of 1.2 (Henderson, 1966). The inlets are considered to be square with a C_B value of 0.9 and using **Equation 2-6**, a design discharge (Q_d) of 28.53 m³/s was calculated. **Table 5.1** lists the properties as calculated for the culvert. As-built drawings for the model is found in **Appendix C**.

Table 5.1: Design summary for 5x2 m rectangular culvert.

Description	Prototype	Unit	Model	Unit
Design Discharge (Q_d) =	28,529	m³/s	27,86	L/s
Inside Width (B) =	5	m	312,5	mm
Inside Height (D) =	2	m	125	mm
Upstream Head (H_1) =	2,4	m	150	mm
Freeboard =	0,3	m	18,75	mm
Total culvert Height =	2,7	m	168,75	mm
Wing-wall Angle (α) =	30	°	30	°
Wing-Wall Length =	4,8	m	300	mm
Apron Length =	≈4	m	250	mm

5.4 Scenarios Tested

For the preliminary tests, two models were tested, an artificial bed with an array of boulders as illustrated in **Figure 4.6** and a culvert installed downstream of the test area as illustrated in **Figure 5.1**. Two scenarios were tested on the NC-model and three on the C-model, the scenarios tested were as follow:

No-Culvert Model (NC):

- Normal flow depth measurement.
- Incipient motion of boulders.

Culvert Model (C):

- Flow depth measurement upstream and downstream without boulders added.
- Flow depth measurement upstream and downstream with boulders added.
- Incipient motion of boulders and transport through the culvert.

The purpose of the scenarios was to determine a suitable flow rate at a suitable slope at which each boulder size would move as well as to determine the effect of the presence of boulders in the flume. A roughness coefficient (k_s) was calculated from the NC-model. Normal flow depths were required to check for outlet control of the model. The normal flow depths were required for the calculations of the inlet designs in **Chapters 6** and **7**.

The design discharge (Q_d) of the culvert was calculated to be 28.53 m³/s (27.86 L/s model discharge). Therefore the 1.01 m (prototype) boulder would need to become mobile at 28.53 m³/s, or at least before overtopping was reached. After each tested flow rate the test area would be reset before the flow rate is increased. Each test is considered to be independent of the previous test and boulder movement for the current tests cannot be influenced by the movement of the boulders in the smaller flow rate. The experimental tests were performed at incremental flow rates of 5.12 m³/s from 10.24 m³/s to 35.84 m³/s, including the design flow of 28.53 m³/s. The design flow rate was included to compare the hydraulic design to the measured results. Overtopping of the culvert was achieved at 35.84 m³/s.

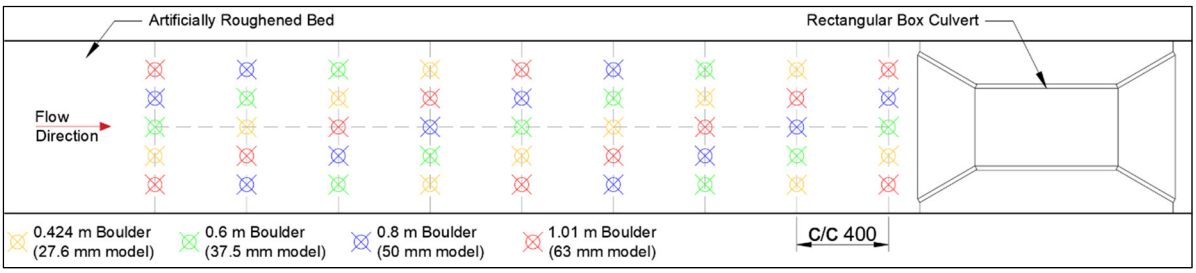

Figure 5.1: Boulder and culvert layout for experimental tests.

Table 5.2 lists a summary of the tests performed and measurements taken at three slopes, namely 1:40 (2.5%), 1:30 (3.3%), 1:25 (4%). The 1:30 slope was only tested for boulder movement as part of establishing a bed slope at which the boulders would deposit in proximity of the culvert inlet. Flow depths and no culvert tests were therefore not performed at the 1:30 bed slope. Results for the 1:40 test produced unfavourable results, as discussed in **Section 5.6**, for the tests with the culvert installed. As per the procedure in **Figure 4.1**, the slope was then adjusted until a suitable result was obtained after which the water levels and no culvert test were tested at a suitable slope.

Table 5.2: Schedule of preliminary tests performed.

Slope	Flow Depth	Boulder Movement	
	NC- & C - Model	NC – Model	C - Model
1:40 (2.5%)	✓	✓	✓
1:30 (3.3%)	×	×	✓
1:25 (4%)	✓	✓	✓

5.5 Test Procedure

The following steps outline the experimental test procedure followed during the preliminary testing of the scenarios mentioned:

1. For each test, the boulders were placed in the same order as depicted in **Figure 5.1** before the gate valves were opened.
2. The gate valves were opened to allow the upstream stilling basin to fill up before the flow was gradually increased to the required flow rate. The gradual increase in discharge was to prevent the effects of a "flood wave" influencing the results, ensuring consistency throughout the tests.
3. After the desired flow rate was achieved the timer was started, each test ran for 30 minutes. Observations showed that most boulders would initiate movement within the first 15 minutes of testing, adequate time was allowed to ensure equilibrium was reached.
4. Water level measurements with the point gauge and carriage were taken of the inlet after 15 minutes had passed.
5. After 30 minutes the gate valves were closed, once the water drained from the test area a plan view photograph was taken, the image was post-processed and used to measure boulder movement.
6. The remaining boulders were removed and the gate valves were opened to the same flow rate.
7. Once the flow was uniform for the given flow rate, upstream and downstream water levels were measured with the point gauge and carriage.
8. Steps 1-7 were repeated for each flow rate (10-, 15-, 20-, 25-, 27.86-, 30- and 35 L/s).
9. If the 1 m (prototype) boulders did not move sufficiently before overtopping was achieved the slope of the flume was increase incrementally and step 8 were repeated until sufficient movement was achieved.

Sufficient movement of the boulders was defined as the minimum slope at which the boulders would be transported downstream within reasonable bounds of the design flow rate of the selected culvert. If at least 50% movement of the 1.01 m boulder (63 mm model) were observed for the design discharge (28.53 m^3/s), sufficient movement of the boulders was achieved. The bed slope had to be as small as possible to provide optimal conditions for the boulders to settle out at the inlet.

Flow depths were recorded for each flow rate for the normal depth measurements (NC-model) and for the C-model. The depth measurements were recorded at three locations and the average of the measurements taken for each cross-section. The upstream inlet face is the datum (zero on the x-axis) for the longitudinal distance, downstream at 10 m prototype (625 mm) is the outlet face of the culvert. Upstream was defined as positive and downstream negative, the outlet, therefore, starts at minus 625 mm (model).

5.6 Preliminary Results

This section contains the results obtained from the preliminary experimental models. **Table 5.2** shows the tests performed for each model. The recorded results for each test performed is found in **Appendix D**, in this section, the results for each model are summarised.

The preliminary results focused on determining the following:

- A suitable roughness parameter for the artificial bed.
- Flow depth under uniform flow conditions.
- Flow depths upstream and downstream of a rectangular box culvert.
- Comparing flow depths between boulders added upstream and omitted near the inlet and outlet of the culvert.
- Establishing a baseline for comparison of boulder movement through a culvert.

Results are presented for three slopes that have been tested as part of the preliminary tests, a 1:40, 1:30 and 1:25 slope have been tested. The optimal slope for the experimental model was initially determined by a slope at which the largest boulders would be transported downstream at a flow rate within the bounds of the design discharge of 28.53 m^3/s. During testing, however, it was observed that the boulders settled out of the flow too far upstream of the culvert inlet to either influence the inlet or to be affected by any design changes. A steeper than required slope was therefore selected that would allow the boulders to settle out closer to the inlet of the culvert. The optimal slope was therefore selected to be 1:25 (4%).

5.6.1. Normal Flow depth

The normal flow depth levels without the boulders were used in the development of the model, due to the layout and a large number of boulders present. During testing it was discovered that the boulders would move during measurement, resulting in inconsistent depth measurements. Almost all boulders remained stationary during the lower flows, resulting in a large channel roughness (higher water levels). As the flow rate increased the boulders would become mobile and would be transported downstream, resulting in a smoother channel. Considering that a natural bed would not have such a large concentration of the largest boulders spanning the cross-section of the river, the smoother bed measurements would yield flow conditions that can be used for design purposes.

Normal flow depth measurements were recorded for the 1:40 slope and the 1:25 slope. From the recorded water depths, the roughness of the flume could be determined. **Table 5.3** illustrates the averaged normal flow depths of the recorded results of each flow rates along with the Reynolds number, Velocity, Froude number and the MN. The MN is based on a 1 m boulder with a C_D of 1.086 and a

density of 2640 kg/m³. The roughness (k) used in **Equation 2-27** was selected to be equal to the smallest test boulder present in the test, the smallest sized rock had a b-axis diameter of 424 mm (26.5 mm). The MN for the design is 0.115 which is close to the critical MN of 0.12. A different roughness value is used in **Equation 2-27** as opposed to the roughness coefficient (k_s) of the flume to account for the smoother bed when the boulders are not present.

Table 5.3: Uniform flow properties for NC-model, S_0 = 1:40.

Discharge (m³/s)	y_n (m)	V (m/s)	y_c (m)	Fr	Re	MN
10,24	0,344	2,481	0,420	1,35	7,08E+05	0,09
15,36	0,423	3,023	0,551	1,48	1,05E+06	0,10
20,48	0,500	3,414	0,667	1,54	1,38E+06	0,10
25,6	0,567	3,764	0,774	1,60	1,71E+06	0,11
28,53	0,603	3,945	0,832	1,62	1,90E+06	0,11
30,72	0,630	4,066	0,874	1,64	2,03E+06	0,12
35,84	0,693	4,308	0,969	1,65	2,35E+06	0,12

Figure 5.2 is a longitudinal section of measurements for the NC-model experimental tests of the 1:40 bed slope (S_0). The measurements were limited to the central area of the artificial bed to ensure uniform flow conditions. Indicated as dashed lines is the average flow depth for each flow rate listed in **Table 5.3**. The measured flow depths at 0 m and 64 m upstream have been excluded, the water was considered to not be uniform at that location.

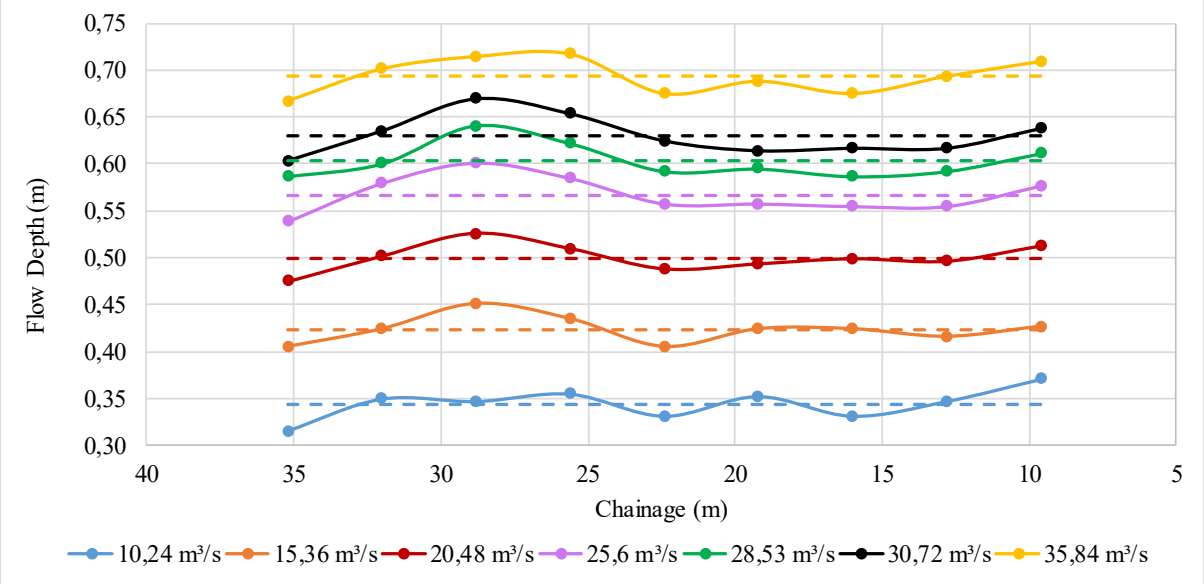

Figure 5.2: Longitudinal view of the recorded uniform flow depths, NC-model, S_0 = 1:40.

Normal flow depth experimental tests were carried out for an S_0 of 1:25. **Table 5.4** shows the averaged flow depth results from the NC-model for a slope of 1:25. The NM number has been determined by

using the same parameters as used to determine the MN of the results from the S_0 = 1:40 tests. An MN of 0.139 was calculated for the Q_d.

Table 5.4: Uniform flow properties for NC-model, S0 = 1:25.

Discharge (m³/s)	y_n (m)	V (m/s)	y_c (m)	Fr	Re	MN
10,24	0,306	2,785	0,420	1,61	7,12E+05	0,104
15,36	0,381	3,361	0,551	1,74	1,06E+06	0,116
20,48	0,445	3,837	0,667	1,84	1,39E+06	0,125
25,6	0,504	4,233	0,774	1,90	1,73E+06	0,133
28,53	0,553	4,301	0,832	1,85	1,91E+06	0,139
30,72	0,580	4,414	0,874	1,85	2,05E+06	0,143
35,84	0,650	4,598	0,969	1,82	2,36E+06	0,151

The recorded flow depths for the 1:25 bed slope is shown in **Figure 5.3**, the dashed lines indicate the averaged flow depths shown in **Table 5.4**. Flow depths at 0 m and 64 m have been excluded from the calculation, the flow at the two points was not considered to be uniform.

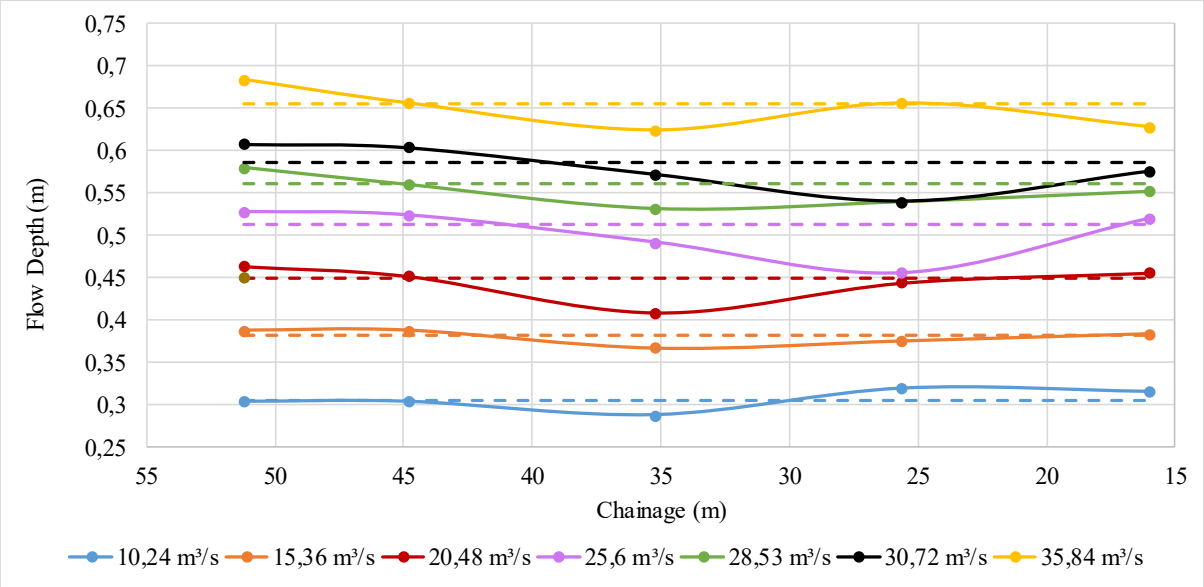

Figure 5.3: Longitudinal view of the recorded uniform flow depths, NC-model, S0 = 1:25.

Estimation of the Roughness Coefficient

Uniform flow conditions were assumed over the section of the experimental area, the roughness coefficient (k_s) could be calculated from the measured data and the known variables in the Chézy equation (**Equation 2-5**). The bed roughness was required to calculate the culvert capacity for outlet control and for the model development performed in **Chapter 6**.

$$Q = A18\text{Log}\left(\frac{12R}{k_s}\right)\sqrt{RS_0} \qquad \textbf{2-5}$$

The wetted perimeter (P) is defined as the length of the surface wetted by the flow perpendicular to the direction of flow (Chadwick *et al.*, 2013). For the experimental model, the sides of the flume were not included in determining P. Two arguments were made to exclude the sides of the flume. The sides of the flume are constructed from glass which is much smoother than the artificial bed. The flume width to flow depth ratio (**Table 5.5**) is relatively large with a minimum b/y_n ratio of 18.47, this relates to a P = 13.3 m. Considering that the sides of the flume are smooth glass and only contribute 1.3 m to the wetted perimeter, makes excluding the depth from the wetted perimeter an accurate assumption to make.

Table 5.5 contains the variables required in **Equation 2-5** and the calculated k_s roughness coefficient for S_0 = 1:25. An average k_s coefficient for the artificial bed was determined to be 0.156 m (prototype). The calculated k_s is lower than what is typically expected for a mountain stream. Boulder or cobble stream beds with a bed roughness between 0.3 m and 0.4 m are typically expected for Western Cape mountain streams (Rooseboom and Van Vuuren, 2013a). The lower calculated k_s of the experimental model is attributed to the removal of the mobile model boulders for flow depth measurements.

Table 5.5: Hydraulic roughness calculation.

Q (m^3/s)	y_n (m)	A (m^2)	R (m)	k_s (m)	b/y_n
10,240	0,306	3,677	0,306	0,147	39,164
15,360	0,381	4,570	0,381	0,140	31,513
20,480	0,445	5,338	0,445	0,135	26,978
25,600	0,504	6,048	0,504	0,133	23,810
28,529	0,553	6,634	0,553	0,164	21,708
30,720	0,580	6,960	0,580	0,171	20,690
35,840	0,650	7,795	0,650	0,203	18,473
			Average =	**0,156**	

C-Model Flow Depth Results

Water level measurements were recorded for the C-model with, and without, rock added into the flume upstream of the culvert. Measurements were taken to determine the effect the boulders would have on the flow depth upstream and downstream of a culvert compared to flow conditions with no boulders added. The recorded flow depths for each flow rate, with and without the model boulders added, is shown in **Appendix D**. Flow depth measurements for the C-model tests were recorded for a bed slope of 1:40 and 1:25.

Figure 5.4 illustrates the flow depths recorded just upstream of the culvert for an S_0 = 1:40. Flow depths are shown for the tests with and without the rock included in the tests. Normal flow depths (y_n) prior to the install of the culvert is also shown to illustrate the damming effect of the culvert on the flow depth. The flow direction is from left to right across the page and the culvert inlet is illustrated on the right-hand side of the figure.

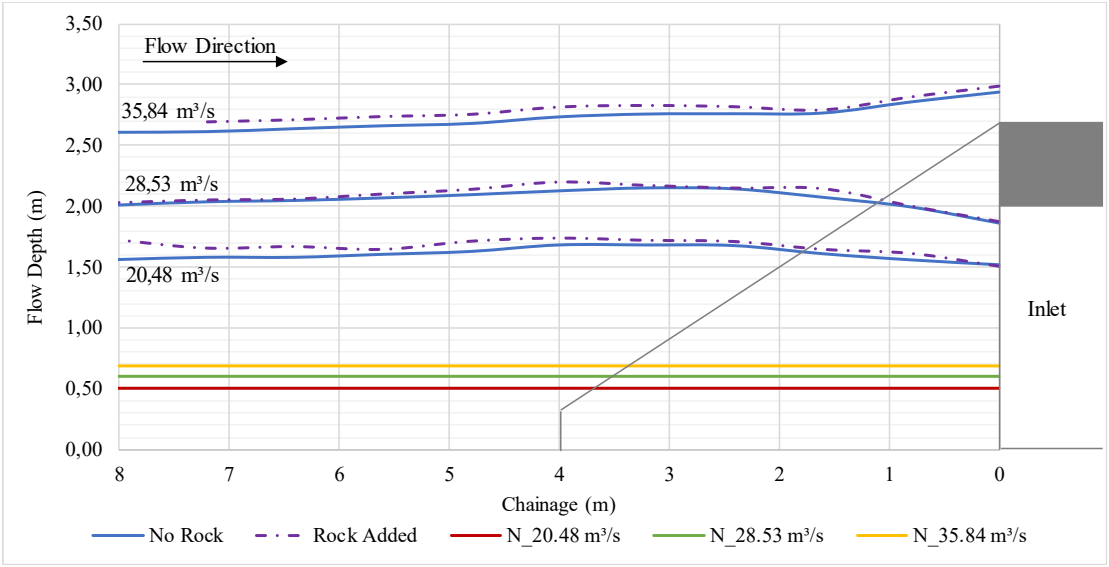

Figure 5.4: C-model flow depths upstream of the culvert inlet, S_0 = 1:40.

Three flow rates are illustrated, two of the flows (20.48 m³/s and 28.53 m³/s) being free-surface and the third flow (35.84 m³/s) causing overtopping. Only three of seven flow rates are shown to illustrate the similarity between the flow depths with and without the boulders added. All the flow rates show the same trend as illustrated in **Figure 5.4**, the other flow rates were omitted from the figure to simplify the comparison between the two tests.

A similar trend was seen for the S_0 = 1:25 tests on the C-model. The flow depths between the no-boulder and boulder-added tests shows that the boulders provided some form of energy dissipation just upstream of the culvert, as shown in **Figure 5.5**. A hydraulic jump formed upstream of the culvert due to the culvert constricting the supercritical flow and the hydraulic jump undulations propagated downstream. A plan view of the location of the hydraulic jump is shown in **Figure 5.14** and how the location relates to the location of the deposited boulders. **Figure 6.15** shows a longitudinal section where the location of the hydraulic jump is compared to the Compound-Tapered model described in **Chapter 6**. The presence of the boulders reduced the undulations resulting in a smoother free-surface profile.

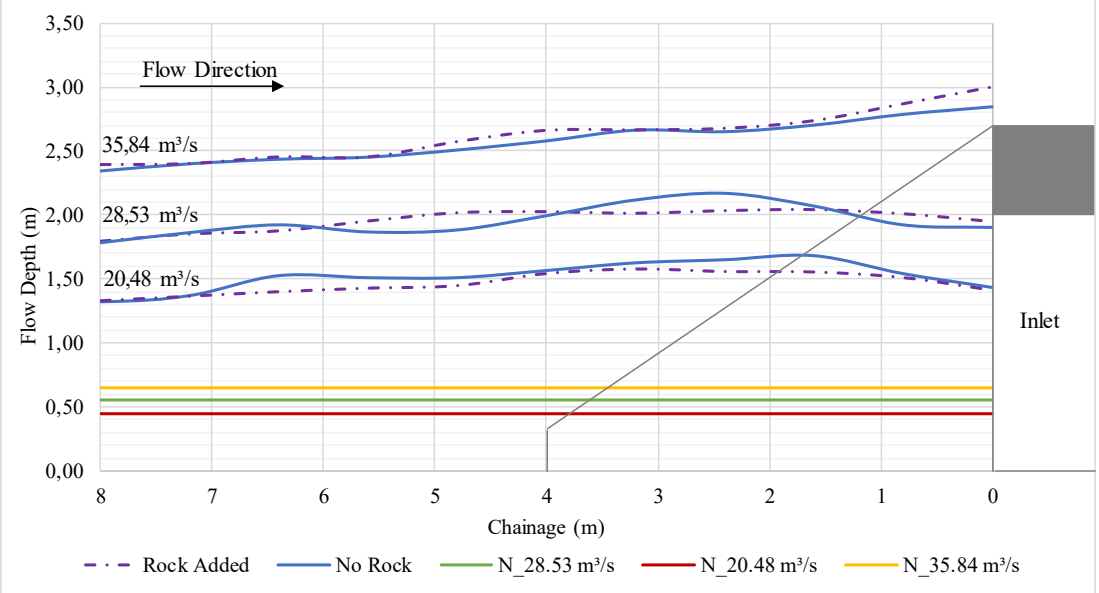

Figure 5.5: C-model flow depths upstream of the culvert inlet, S_0 = 1:25.

A culvert is an obstruction in the flow path and the results between the 1:40 and 1:25 C-model tests shows that the flow depth is controlled by the size of the culvert. **Table 5.6** shows the flow depths just upstream of the culvert for each slope tested at the maximum depth and the flow depth as the flow enters the culvert. The greatest difference in depth between the S_0 = 1:40 and the S_0 = 1:25 for the maximum flow depth is a 3% decrease in flow depth. At the inlet of the culvert (x = 0 m), the greatest difference is a 6% increase in flow depth. The comparison between the two slopes shows that the size of the inlet controls the flow depth for an inlet-controlled culvert.

Table 5.6: Inlet flow depth comparison for the C-model at different bed slopes.

Discharge (m^3/s)	S_0 = 1:40		S_0 = 1:25		1:25 as % difference of 1:40	
	y_{max} (m)	y_{inlet} (m)	y_{max} (m)	y_{inlet} (m)	y_{max} (m)	y_{inlet} (m)
10,24	1,024	0,925	1,004	0,888	2%	4%
15,36	1,387	1,211	1,368	1,2	1%	1%
20,48	1,685	1,523	1,680	1,432	0%	6%
25,6	1,952	1,752	1,928	1,744	1%	0%
28,53	2,152	1,861	2,172	1,904	-1%	-2%
30,72	2,256	1,989	2,252	2,112	0%	-6%
35,84	2,939	2,939	2,848	2,848	3%	3%

5.6.2. Downstream Flow Depth

Outlet flow depths for the C-model, with and without boulders, at a bed slope of 1:40, were compared. **Figure 5.6** shows the recorded flow depths for four flow rates. All seven flow rates showed the same trend in outlet flow depths, three results have been omitted to show a simplified longitudinal section for easy comparison.

Results from the experimental tests show that the upstream boulders in the stream do not influence the outlet flow. The inlet of the culvert acts as a control section, the flow passes from subcritical to supercritical at this point. Results from **Figure 5.4** and **Figure 5.5** showed that the presence of the boulders does not influence the upstream head, the flow at the outlet will, therefore, remain unchanged. If the barrel of the culvert remains free from boulders the outlet flow will remain unchanged. Further testing only measured the outlet flow depths for the case of no boulders added into the flume.

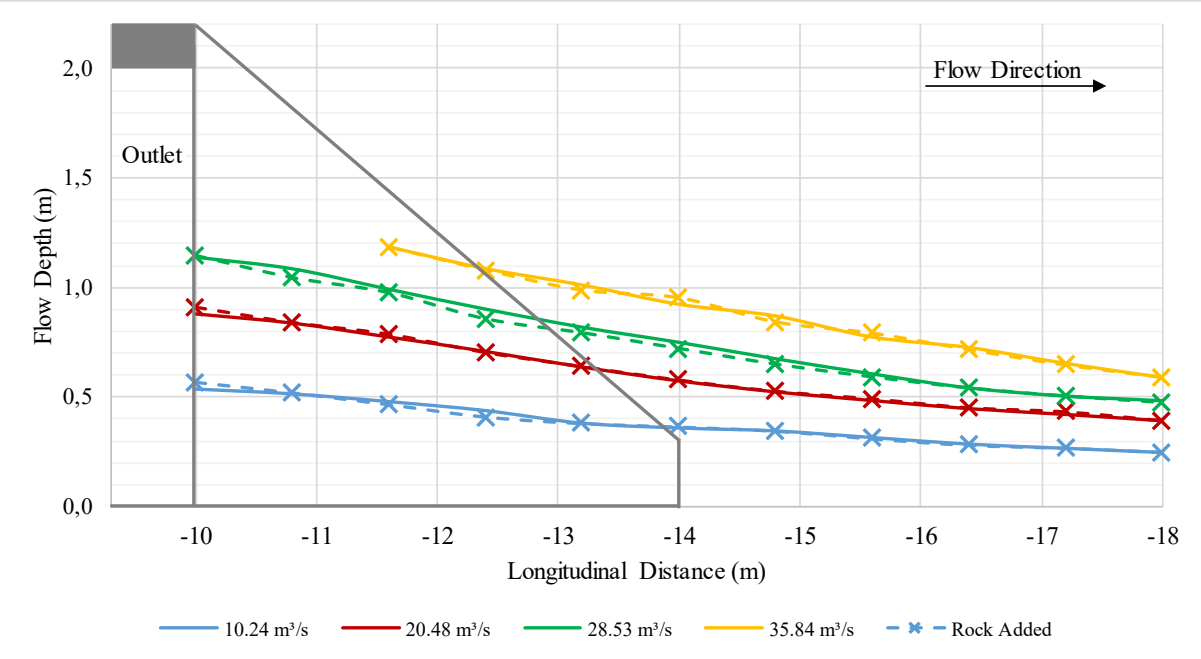

Figure 5.6: Outlet flow depth comparison for C-model, S0 = 1:40.

Table 5.7 lists the measured outlet flow properties, on the apron of the culvert, compared to the normal flow depth measurements taken without the culvert installed. The flow velocity and Froude number exiting the culvert is less than the normal flow conditions. Erosion protection measurements would not be required for the culvert installed at the S_0 = 1:25 if the outlet flow conditions are only compared to the normal flow conditions. If the maximum permissible velocity for coarse gravel is considered, each flow rate would require some form of erosion protection downstream of the apron to prevent erosion (Rooseboom and Van Vuuren, 2013c). In the case where erosion protection would be required, the guideline set out in HEC 14 (2005) provides a detailed guideline on erosion protection measures. **Section 2.11.3** describes the erosion protection methods that can be used where a high volume of boulders is expected.

Table 5.7: Outlet flow parameter on the apron for a normal culvert installed.

Flow Rate, Q (m^3/s)	Normal Flow Conditions				Culvert Installed			
	Normal Depth, y_n, (m)	Area, A (m^2)	Velocity, V (m/s)	Froude Number, Fr	Flow Depth, y (m)	Area, A (m^2)	Velocity (m/s)	Froude Number, Fr
10,240	0,306	3,677	2,785	1,606	0,384	3,694	2,772	1,428
15,360	0,381	4,570	3,361	1,739	0,472	4,540	3,383	1,572
20,480	0,445	5,338	3,837	1,837	0,624	6,002	3,412	1,379
25,600	0,504	6,048	4,233	1,904	0,744	7,156	3,577	1,324
28,529	0,553	6,634	4,301	1,847	0,760	7,310	3,903	1,429
30,720	0,580	6,960	4,414	1,850	0,848	8,157	3,766	1,306
35,840	0,650	7,795	4,598	1,821	0,880	8,465	4,234	1,441

5.6.3. Boulder Movement

The post-processed results of the boulder movement for the preliminary tests can be found in **Appendix D**. For each of the photographs of the results taken during testing a grid has been overlaid and the boulders that moved during the tests could be identified and highlighted. By scaling the photographs and making use of the referencing marks on the photo an accurate representation could be obtained for measurement and comparisons. The image post-processing is described in detail in **Section 4.7**.

Boulder movement experiments were performed on the NC- and C-models. For the NC-model, boulder movement was tested for an S_0 of 1:40 and 1:25. The C-model was tested at the same bed slopes as well and an additional slope of 1:30. The NC-model results are presented separately from the C-model results.

Results Presentation

Each experimental test for boulder movement have been captured and the post-processed image is shown in **Appendix D**. The boulder movement test results have been grouped for each boulder size and presented to illustrate the movement capability of an increasing flow rate. A boulder was recorded as "moved" (M) if it has moved from the position that it was placed prior to the start of the test. The boulder is described as "through" (T) if it moved downstream off the test area and through the culvert if present. The movement of the boulders is illustrated as a ratio between the moved boulder and all of the similar-sized boulders in the flume.

Each boulder size, except for the red (1.01 m prototype) boulder have 11 reference boulders placed in the flume. There were 12 red boulders for each test present in the flume. **Figure 5.7** is an example of the results for the 424 mm boulder size for the NC-model tests. The light-coloured bars represent the boulders that have been moved as a ratio of the same sized boulders in the flume. The dark coloured bars represent the ratio between the boulders that were transported downstream off the experimental area and the number of same-sized boulders in the flume. The columns are not stacked, if only the dark-coloured bar is shown, then it shows that all the moved boulders were transported downstream. All the

results are compared to the number of same reference size boulder in the flume, this means that the ratio of moved boulders will always be greater than the "through" boulders.

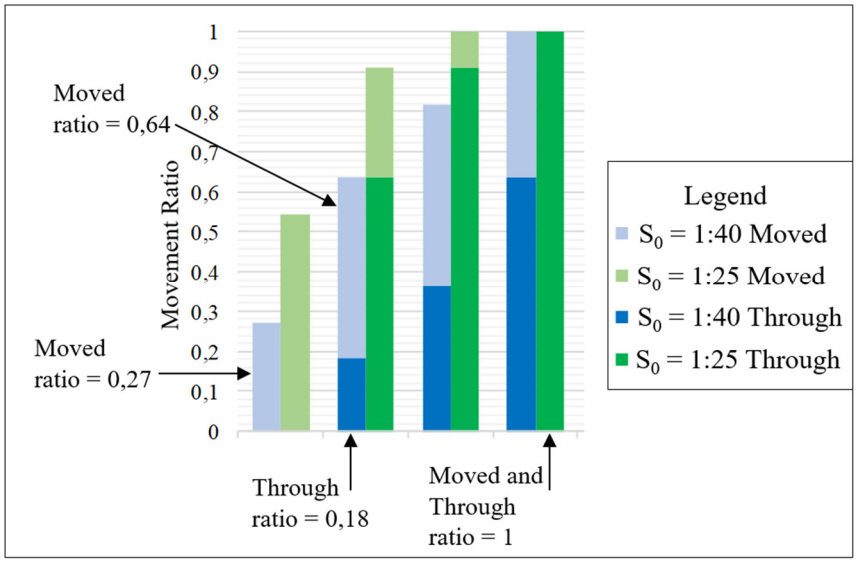

Figure 5.7: Example of experimental results.

NC-Model Boulder Movement Results

Boulder movement tests were performed on the NC-model to determine a baseline test to compare the results of the C-model and the Models tested in **Chapter 6**. **Figures 5.8** to **5.11** shows the results for the boulder movement tests on the NC-model for each boulder size (0.424 m, 0.6 m, 0.8 m, 1.01 m). The Figures shows the results for the two bed slopes tested (S_0 = 1:40 and S_0 = 1:25). The discussion in this section views **Figures 5.8** to **5.11** as a whole when referring to the results unless stated otherwise.

Figure 5.11 shows that for the design discharge of 28.53 m³/s the boulder movement and "through" movement of the 1.01 m boulder was 50%. Boulder movement of 50% was defined as the lower limit for sufficient boulder movement. The 1:40 slope was determined to provide the required movement for the experimental tests on the proposed culvert inlets.

Inadequate movement for the C-model resulted in further testing to determine a suitable slope. Results from the S_0= 1:25 tests show that the boulders are transported at lower flows as compared to the S_0 = 1:40 tests. At the design flow rate, the movement of the 1.01 m boulders was determined to be 70% with all the moved boulders being transported off the experimental area.

Figure 5.12 shows the experimental model results for the S_0 = 1:40 test plotted on the Modified Lui diagram. The plot on the Modified Lui diagram for the S_0 = 1:25 test is shown in **Figure 5.13**. Both Figures show the critical MN for incipient motion. Above the MN line movement is expected to take place. The MN is grouped and plotted according to the flow rate and colour coded to match the experimental boulder sizes. In **Equation 2-27** the MN is dependent on a roughness coefficient, k.

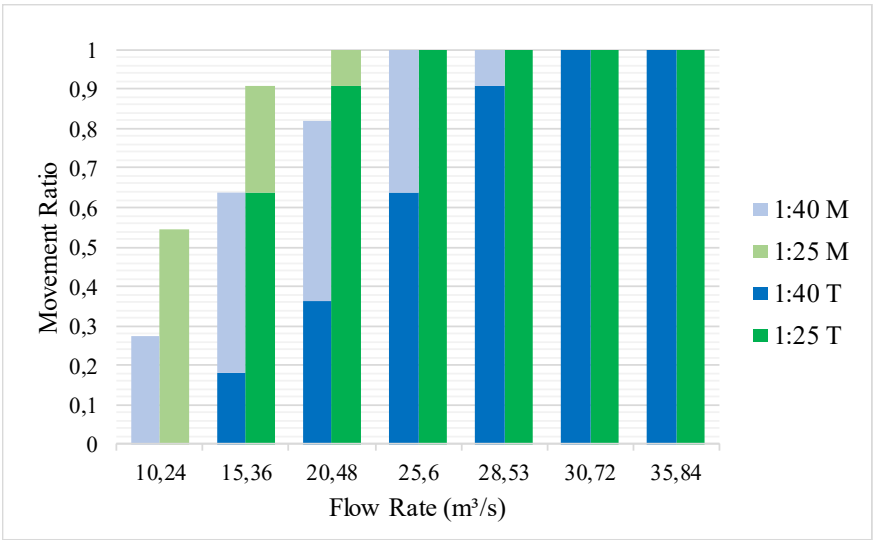

Figure 5.8: NC-Model - 0.424 m Boulder.

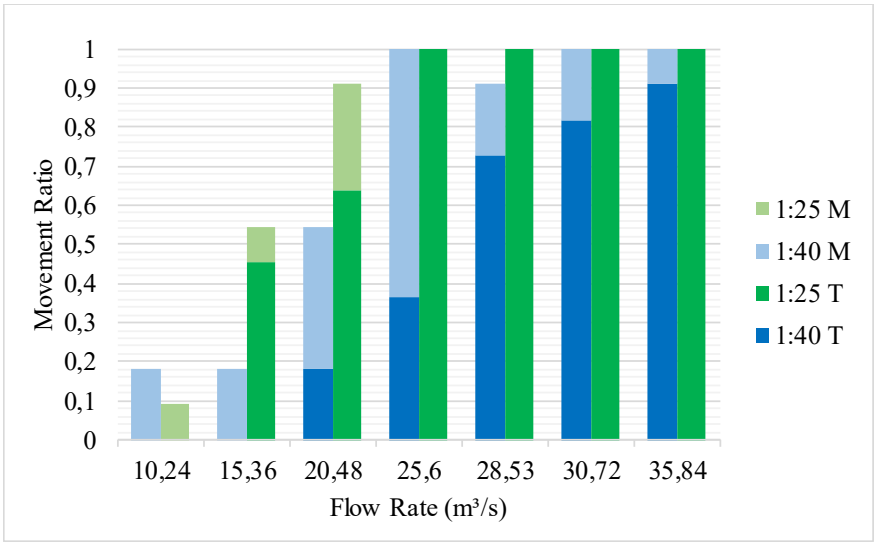

Figure 5.9: NC-Model - 0.6 m Boulder.

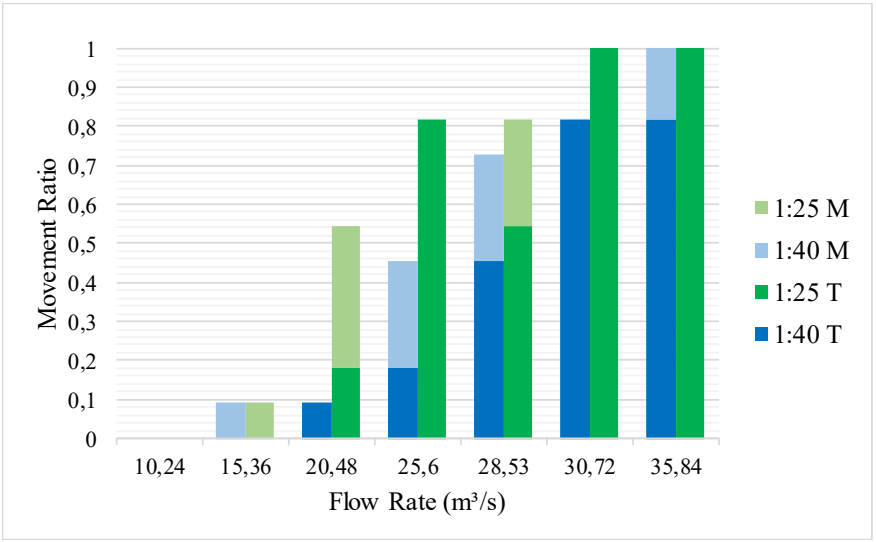

Figure 5.10: NC-Model - 0.8 m Boulder.

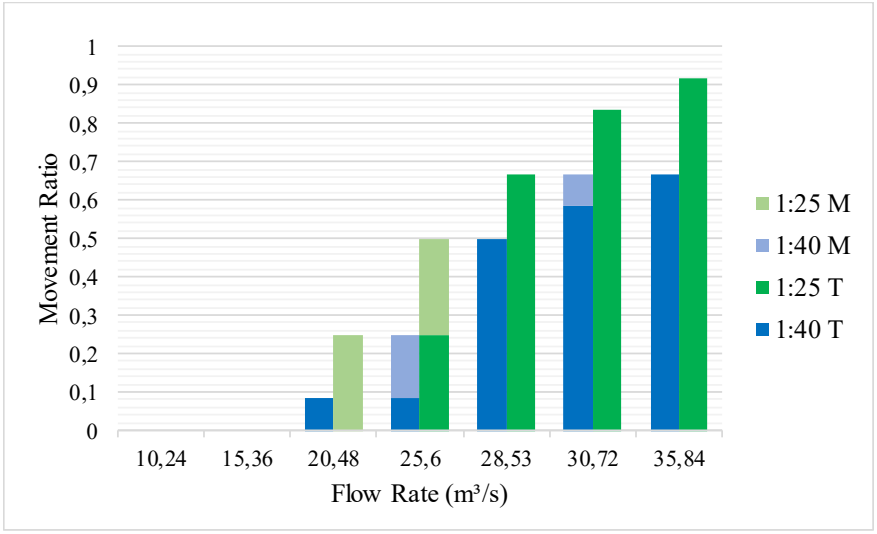

Figure 5.11: NC-Model - 1.01 m Boulder.

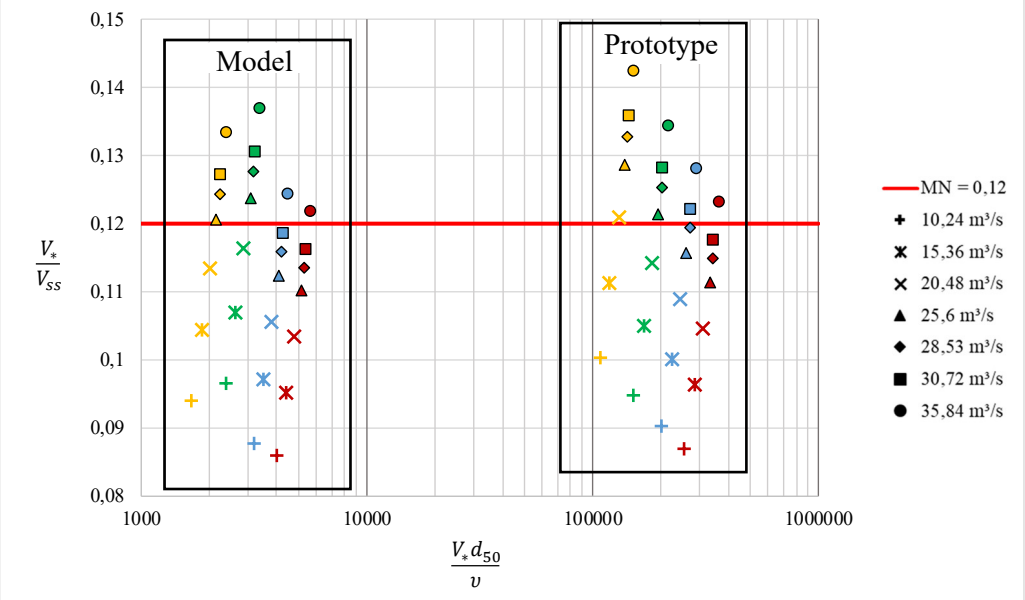

Figure 5.12: MN for model and prototype boulders plotted on the Modified Lui diagram S_0 = 1:40.

Literature suggests that the k-coefficient should be set equal to the d_{84} particle size in the channel (Cullis *et al.*, 2008). The experimental model is comprised of a fixed bed with unknown grading. The k-coefficient has been assumed to be equal to 0.424 m (26.5 mm model) the smallest size test boulder in the flume.

$$MN = \frac{\sqrt{gDS}}{V_{ss}} \cdot \left(\frac{d}{k}\right)^{1/3} \qquad \textbf{2-27}$$

Comparing the MN to the moved boulders shows that there is no defined separation between no movement and incipient motion of the boulders. Several factors were believed to have an influence on the accuracy of the MN for the experimental boulders. The value of the k-coefficient has a major influence of the accuracy of the MN, a small variation of the k-coefficient resulted in a substantial shift in the MN. The conclusion was that the largest boulders were considered for the experiment which increases the difference between the boulder diameter and the k-coefficient. For the experiment, the k-coefficient could not be accurately predicted. Considering that an artificially roughened bed was used for the model and that the boulders were placed in a pattern away from other particles, the MN could have been influenced.

For the experimental study, the MN does not produce an accurate estimate for boulder movement, inaccuracy of the MN is believed that is limited to the setup of the experimental model. The concern was that the largest boulders are considered as potential blocking hazards in this research. In the following Chapters, it was assumed that if the boulder is present in the stream prior to the installation of the culvert then the culvert should be designed to allow the boulder to flow through.

In **Figure 5.12** and **Figure 5.13** the MN was compared to calculated prototype sized boulders. The settling velocity for the prototype was required. Using a C_D of 1.086 and **Equation 2-21** the settling velocity could be calculated for the prototype. The MN for the model and prototype is within good agreement considering that the C_D was assumed to remain constant between the model and prototype. The C_D was also calculated using an SF of 0.7 which differs from the varying SF of each model boulder used for testing.

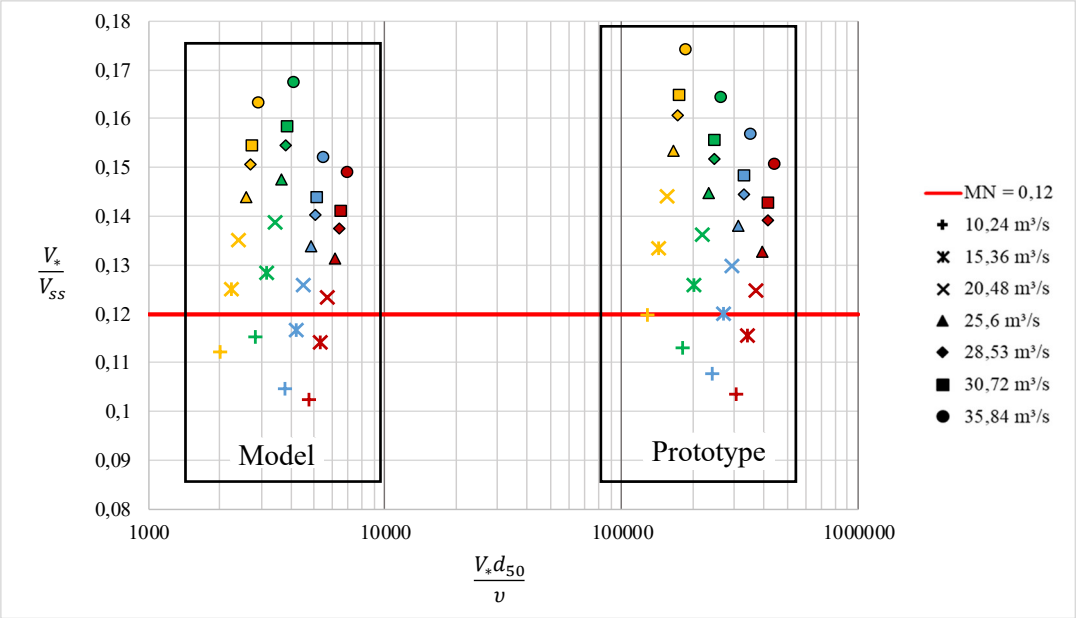

Figure 5.13: MN for model and prototype boulders plotted on the Modified Lui diagram S_0 = 1:25.

C-Model Boulder Movement Results

Bed slopes S_0 = 1:40, 1:30 and 1:25 were tested to determine a slope that would settle out the boulders just upstream of the inlet. The results for each test are found in **Appendix D**. The additional bed slopes apart from the S_0 = 1:40 slope was required to determine a slope that deposits the boulders in the near vicinity of the inlet. **Figure 5.14** illustrates the deposition location for the boulders for the design discharge of 28.53 m³/s. **Figure 5.14(a)** is for S_0 = 1:40, **Figure 5.14(b)** is for S_0 = 1:30 and **Figure 5.14(c)** is for S_0 = 1:25. Included in each figure is the location of the hydraulic jump that formed due to the constriction caused by the culvert. Comparing the location of the hydraulic jump with the location of the boulder deposition shows that the boulders settle out just after the hydraulic jump.

Deposition takes place just after the jump due to the negative energy slope caused by the increase in flow depth. Following on from **Equation 2-27** for the MN which is dependent on the friction slope in the shear velocity (V_*) term. A negative friction slope (S_f) cannot produce a positive V_* to produce an MN > 0.12. **Figure 5.14** shows how an increase in bed slope moves the hydraulic jump downstream towards the culvert inlet.

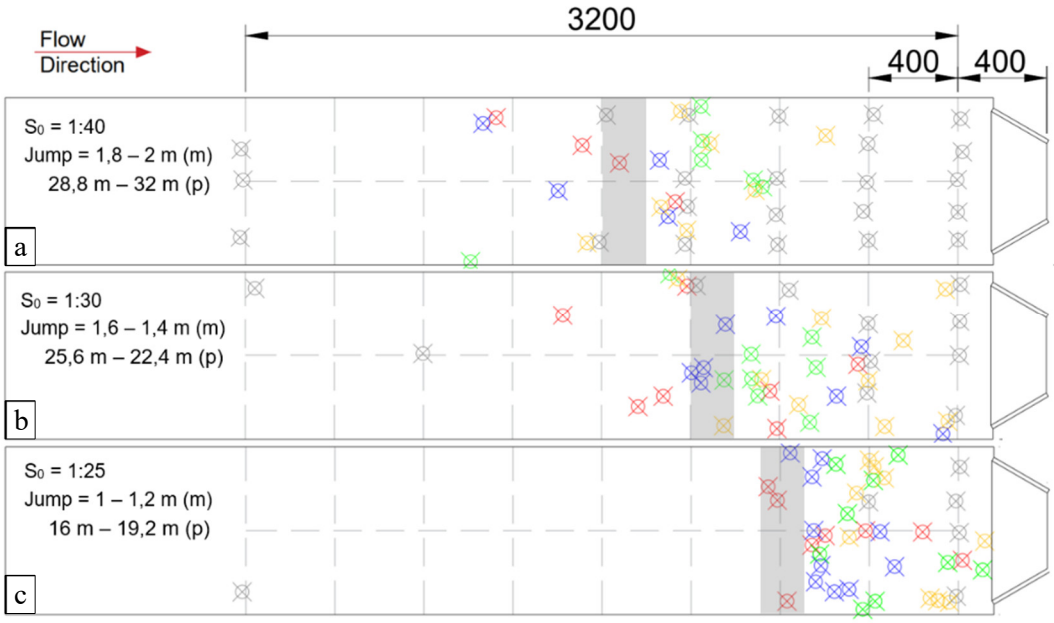

Figure 5.14: Boulder settle out location and location of the hydraulic jump, Q = 28.53 m³/s**.**

A bed slope of 1:25 was determined to provide a bed slope that is steep enough to cause deposition near the culvert inlet. An observation was made during testing that the lower flows tend to deposit the boulders further downstream, due to the reduced afflux caused by the culvert. As the flow increases the hydraulic jump moves upstream and the boulders deposits further upstream. **Figure D-1** in **Appendix D** clearly illustrates this phenomenon.

Boulder movement was recorded for each flow rate with the C-model culvert installed. **Figures 5.15** to **5.18** shows the recorded results for the different boulder sizes for the C-model tests. When referring to the results in this section, **Figures 5.15** to **5.18** should be in conjunction with each other. Tests from the NC-model revealed that an S_0 = 1:40 resulted in a sufficiently steep slope to induce incipient motion on the largest boulder at the design flow of the C-model culvert.

The boulder movement results showed that downstream of the hydraulic jump none of the boulders could be moved downstream through the culvert. Some of the boulders managed to be transported downstream through the culvert due to the momentum carried from upstream as observed during the experimental tests. When considering that all deposition of the boulders took place upstream of the inlet an assumption was made that the inlet should be modified to prevent deposition from taking place in the inlet, provided that the barrel is sufficiently steep. Deposition in the barrel of the culvert was not observed during the experimental tests.

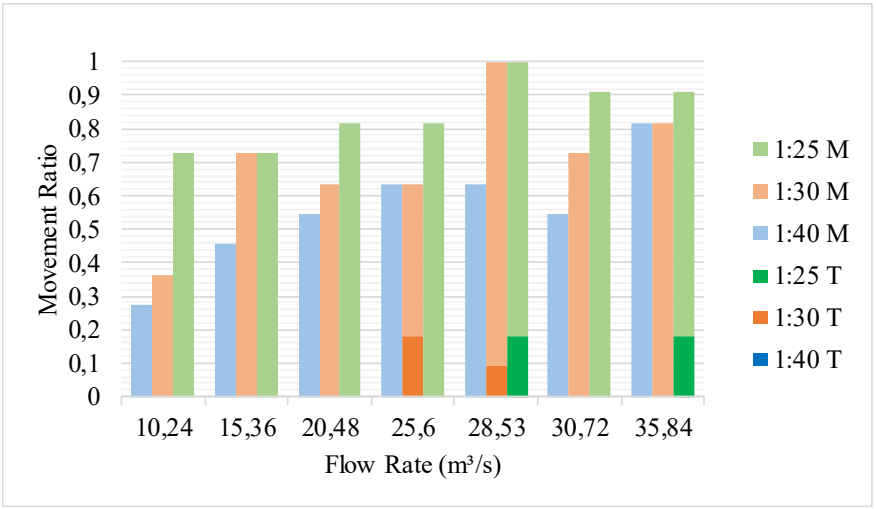

Figure 5.15: Culvert - 0.424 m Boulder.

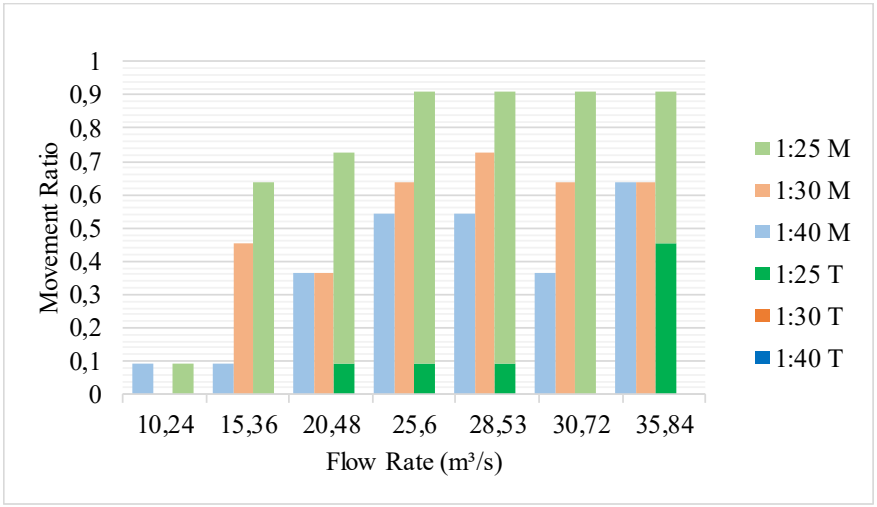

Figure 5.16: Culvert - 0.6 m Boulder.

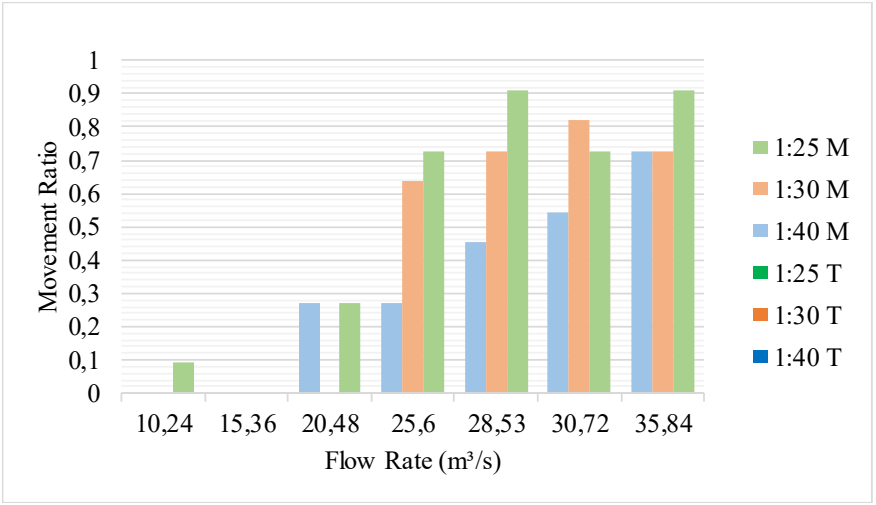

Figure 5.17: Culvert - 0.8 m Boulder.

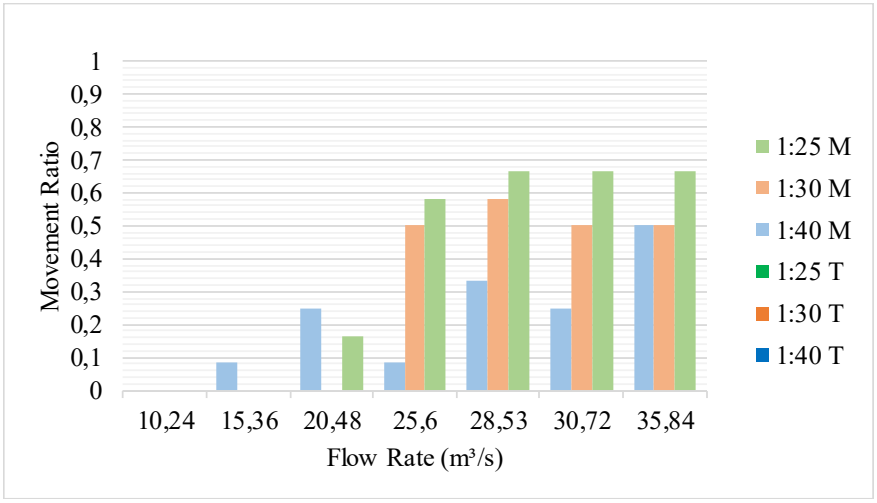

Figure 5.18: Culvert - 1.01 m Boulder.

5.7 Outlet Control

After the experimental model tests were carried out, outlet control was checked for the C-model to ensure that the assumption of inlet control was correct. The Q_d = 28.53 m³/s and S_0 = 1:25 (0.025) was used for the calculations. **Equation 2-13** was used to determine the required H_1 for outlet control. K_e and K_o were assumed to be 0.5 (blunt Inlet) and 1 (sudden outlet) respectively and a Manning's roughness coefficient of 0.016 was used for the barrel of the culvert (Rooseboom and Van Vuuren, 2013a).

Outlet control assumes full-flow conditions at the outlet of the culvert (Rooseboom and Van Vuuren, 2013b). An outlet depth of 2 m was used for the hydraulic calculation. The required upstream head (H_1) was calculated as 2.266 m, therefore the culvert operated as an inlet-controlled culvert. Observations in the flume showed that the culvert operated as an inlet-controlled culvert, the upstream headwater remained constant between the S_0 = 1:40 and S_0 = 1:25 flow depth measurements.

5.8 Conclusion to Preliminary Experimental Tests

The purpose of the preliminary tests was to determine a suitable slope at which boulder movement would take place in the flume and to determine the hydraulic properties of the flow at the selected slope. The experimental tests were performed on two models, namely, a no-culvert model (NC-model) and a culvert model (N-model). Hydraulic calculations for a 5 × 2 m (B x D) culvert was performed and a design discharge Q_d = 28.53 m³/s was determined. The culvert operated as an inlet-controlled culvert.

The experimental tests were divided into two sections, flow depth measurement and boulder movement for each of the two models mentioned. Flow depth tests were performed for two bed slopes, a 1:40 and a 1:25 bed slope. The boulder movement tests were performed for three slopes, a 1:40, 1:30 and 1:25 bed slope.

Flow depth calculations revealed that the flow in the flume was supercritical for the NC-model and that the constriction caused by the culvert in the C-model caused a hydraulic jump to form upstream of the culvert. Tests were performed on the inlet and outlet to determine if the presence of boulders had an effect on the flow depth. The results showed that the presence of boulders did not have an effect on the inlet or outlet flow depths. Boulders have an effect on culvert capacity, however, in the case of the hydraulic model, the number of boulders used for the tests were not sufficient to influence flow depth.

Boulder movement tests were performed to determine a suitable slope that produces movement of the boulders in the flume. Boulder movement thresholds in terms of discharge were determined with the post-processing of the photographs taken during the tests. Post-processed results allowed for a visual

representation of the cause and effect of the boulders settling out as well as the location of the problem area. The 1:40 slope showed sufficient boulder movement for the NC-model, however, the tests for the C-model showed that the boulders settled out too far upstream of the culvert for the C-model. The slope was increased and a bed slope of 1:25 was determined to be a suitable slope to allow for deposition of the boulder at the inlet of the culvert. During the boulder movement tests, the inlet was identified as the cause of boulder depositions if the culvert operated as an inlet-controlled culvert.

Results from the NC-model tests showed that the MN was not an accurate measure for estimating the movement of the boulders for this experimental setup. The MN was sensitive to the k_s-coefficient which could not be accurately determined for the model. An assumption was made that if the boulders are present in the stream, then the flow has the capacity to transport the boulders downstream. The opening of the culvert should, therefore, be able to accommodate the boulders to be able to pass through.

6. Development of Modified Inlet Models

6.1 Introduction

Chapter 6 comprise the first of two chapters of Phase II (**Figure 4.1**). A desktop study on the development of three culvert inlets has been performed. From the three developed prototypes, the two optimal prototypes were selected based on a selection criterion that included factors such as cost and practicality. Experimental tests were performed on the two selected models to determine the flow depths and boulder moving capability of each model. The results are presented for each of the models tested and an optimal design inlet was selected for further testing. Outlet flow depths on the apron were measured and evaluated to determine if the developed prototype requires downstream erosion protection.

6.2 Inlet Prototype Design Criteria

6.2.1. Design Considerations

Factors that influence the ability for a boulder to be transported downstream have been identified in the literature and observed during the preliminary tests presented in **Chapter 5**. An increase in water level upstream of the inlet was shown in the literature to cause particles to deposit just upstream of the inlet (Wellman *et al.*, 2000; Wargo and Weisman, 2007; Ho, 2010). The field investigation of Site B (**Section 3.4.2**) confirmed that the boulders settled at the inlet of the bridge structure.

Experimental results for the boulder movement of the C-model described in **Section 5.6.3** showed that the boulders settled just downstream of the hydraulic jump that forms upstream of the culvert for supercritical approach flow. A conclusion was drawn from the results that the boulders would settle downstream of the hydraulic jump, which was confirmed in the literature presented by Carling (1994). The finding by Carling (1994) makes inlet-controlled culverts with a hydraulic jump forming in the barrel undesirable as shown in **(b)** and **(c)**. Following the same reasoning, outlet control for a culvert is considered to be undesirable in situations where boulder transport is expected. The slower, subcritical flow is assumed to cause boulders to settle out in the barrel.

Estimating boulder movement through the MN was found to not be accurate for the experimental model in **Chapter 5**. The inaccuracy was concluded to be due to the focus around the largest boulders in the flume and the use of a fixed bed model. The accuracy of the MN for incipient motion of the largest boulders in a stream is unknown. Based on the MN results in **Chapter 5**, it was assumed that if the boulder is present in the stream at the location of the culvert site and upstream of the culvert, then the culvert should be designed to be able to pass the boulder through the culvert without flooding of the roadway.

Considering the results from the literature, fieldwork and the preliminary experimental model, the following assumptions and design considerations were made. The design of the model was based on the following assumptions:

- The focus of the study is on mountainous areas, it was assumed that the streams would have a steep slope, the steep slope would produce supercritical flow upstream of the culvert.
- Inlet-control is present at the culvert.
- To prevent boulder deposition in the barrel, a hydraulic jump must be avoided inside the barrel.
- Outlet control must be avoided to prevent deposition inside the barrel.
- Afflux caused by the culvert causes the boulders to settle out at the inlet of the culvert.
- The design flow and bed slope are capable of transporting the boulders downstream if the boulders are present in the stream.

Based on the design assumptions listed above, observations during fieldwork, observations from the experimental model and literature, the inlet of the culvert was identified to be modified to mitigate boulder deposition. The inlet was modified after the culvert has been sized using the method set out in **Section 2.6**, the motivation behind first using the prescribed design guidelines was to ensure that the barrel was capable of conveying the flow through the structure at a decreased flow depth.

6.2.2. Culvert inlet design I: Modified MEL Inlet

The modified MEL inlet was designed based on the design guidelines presented by Apelt (1983) and Chanson (2002) on the design of MEL structures. Only the design of the inlet was used for the design of the modified MEL inlet. Chanson (2002) advised that the Froude number through the structure should be between 0.6 and 0.8 to prevent the formation of undulating flow when designing at critical flow. The design of the modified inlet differs here from Apelt's (1983) design, at the inlet of the barrel, the design flow depth should be 90% of critical flow depth y_c, or $y_{inlet}/y_c = 0.9$. The MELS user guideline compiled by Keller and Winston (2005) defined the y/y_c ratio as the sub-criticality factor (λ).

By designing for a $\lambda = 0.9$ at the inlet, the assumption was made that the flow would be in the supercritical flow regime and not at critical depth where undulating flow could form. The focus of the design was not to design a MEL culvert inlet, the design merely uses the concept of streamlining the flow at the inlet. By not aiming to achieve minimum energy loss throughout the culvert, the design of the inlet fan could be adapted for supercritical flow.

Inlet Fan Geometry

Following Apelt's (1983) guidelines, the shape of the fan was determined before determining the bed profile of the inlet. To determine the geometry of the inlet fan, the width of the lip and the width of the inlet was required. The inlet width (y_{inlet}) was known from the hydraulic design of the culvert performed in **Section 5.3**. Normally critical flow at the lip would be assumed, to act as the control of the inlet, but from the results for the normal flow depth (y_n), it was determined that the approaching flow is supercritical. The design, therefore, assumed that $y_n = y_{lip}$ and $b = b_{lip}$, b_{lip} was taken as 12 m.

Three inlet fan angles (φ) were considered, φ = 120°, 90° and 60°, as shown in **Figure 6.1(a) to (c)**. The Trigonometric method used to determine the shape is shown in **Appendix E**. Keeping in mind that the barrel of the culvert is only 10 m long, the φ = 60° fan (**Figure 6.1(c)**) was considered to be very long. The contraction of the sidewalls for the φ = 120° (**Figure 6.1(a)**) is equal to 1:0.577 (H:V). The φ = 90° fan was selected (**Figure 6.1(b)**) based on the balance between length (L_{fan} = 10.2 m) and contraction ratio (1:1) of the side walls. Ideally, the contraction ratio should be 1:3Fr for supercritical conditions (USBR, 1987) which would be unpractical for the inlet fan of the culvert. Having a 1:3Fr contraction would result in a very long inlet when compared to the length of the barrel. A transition section was used between the fan and the inlet, with $L_t = D/2 = 1$ m, as recommended by the FHWA (2012) for inlet depressions.

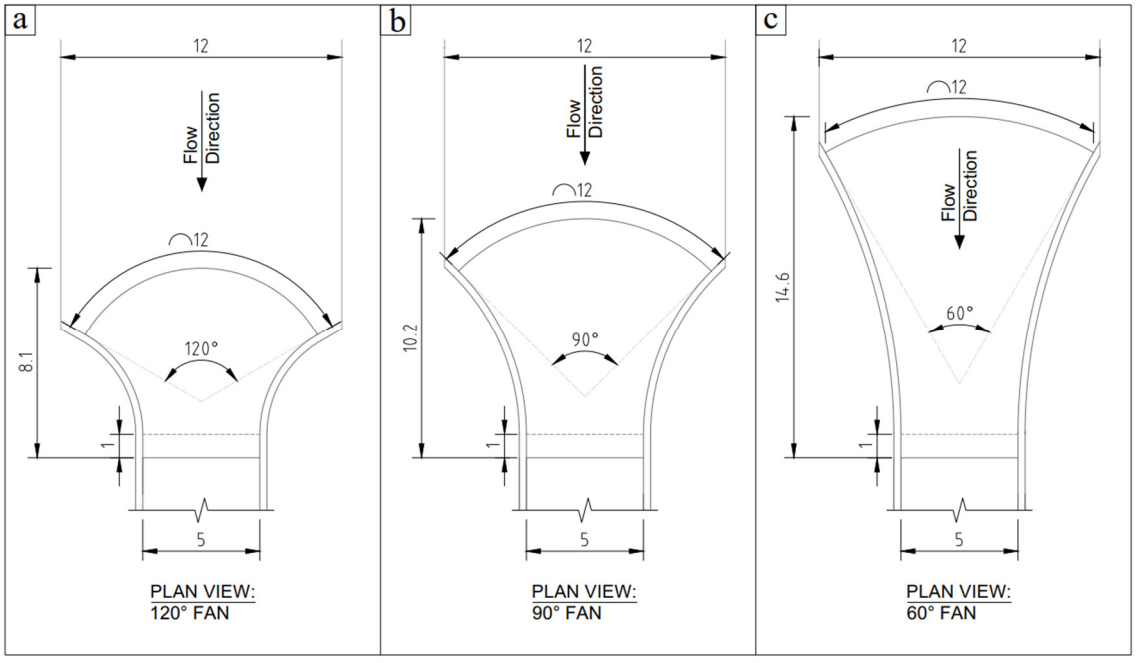

Figure 6.1: Inlet fan design of modified MEL culvert.

Inlet Bed Elevation

The elevation profile of the bed of the inlet fan was obtained through **Equation 6-1** and by assuming constant energy along the flow of the inlet (Apelt, 1983). Friction losses along the inlet fan were included in the calculation of the bed profile by means of the Manning's friction head loss equation (**Equation 2-9**), however local head losses at the inlet have been excluded from the calculation.

$$E = \Delta z + y_2 + \frac{V_2^2}{2g} + H_f \qquad \textbf{6-1}$$

Table 6.1 shows the elevation profile obtained along the centreline of the inlet fan, measurements are in prototype scale. The datum for the longitudinal length and elevation is at the bed of the culvert inlet. The transition section between the culvert and fan has been included in the calculation. **Figure 6.2** shows the plan view and sectional view of the inlet

Table 6.1: Inlet fan design for 90° inlet fan.

Transect Number	Measured Transect Length (m)	Longitudinal Upstream Length, x (m)	Flow Depth, y (m)	Calculated Bed Elevation, z (m)
9	12	10,179	0,553	0,832
8	10,393	9,031	0,712	0,831
7	8,991	7,884	0,908	0,780
6	7,796	6,737	0,998	0,631
5	6,809	5,589	1,093	0,471
4	6,033	4,442	1,184	0,316
3	5,474	3,295	1,264	0,182
2	5,126	2,147	1,320	0,086
1	5	1	1,332	0,040
0	5	0	1,256	0

The bed slope of the barrel has been kept at the same bed slope as that of the flume to ensure that the boulders would flush through the barrel when the boulders enter the barrel of the culvert. Due to the depression of the inlet and the bed slope of the barrel, the outlet invert is below the natural ground level (NGL), the adverse slope at the outlet of the culvert to the NGL was determined to be 1:12 (V:H). The effect of having the outlet below the NGL was tested in the experimental model.

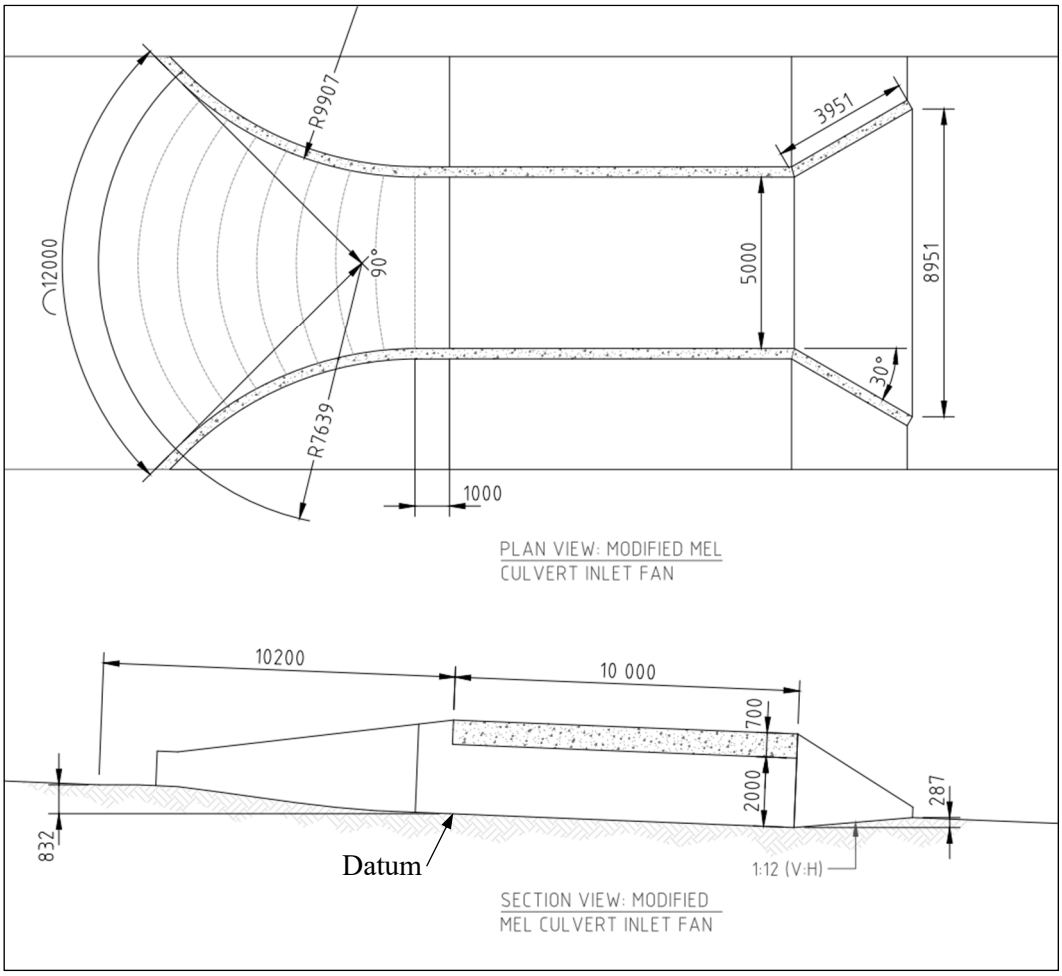

Figure 6.2: Modified MEL culvert design drawings, 90° inlet fan.

6.2.3. Culvert inlet design II: Tapered Inlet

The tapered inlet can be viewed as a simplified inlet compared to that of the MEL culvert. Since the objective of the study was not to have minimal energy losses through the structure, the inlet is not required to be streamlined with the flow. The tapered inlet was designed to contract the flow from the width of the flume to the width of the barrel while having a steep bed slope to promote boulder movement and to prevent a hydraulic jump from forming in the inlet.

Three proposed bed slopes were considered for the design of the tapered inlet, S_0 = 1:10, 1:6.67 and 1:5. The width of the inlet (B_{barrel}) and the width of the inlet at the lip of the taper (B_{lip}) have remained 5 m and 12 m respectively. Wing wall angles and the length of the taper were thereby controlled by the slope and required elevation to achieve the desired flow conditions at the inlet. A sub-criticality factor of 0.9 was used to determine the flow depth at the inlet.

Inlet Geometry Calculation

Three potential bed slopes were considered, with the flow conditions known at the lip and the required conditions calculated at the inlet of the barrel the required elevation (Δz) could be determined.

Figure 6.3 shows the three potential tapered inlets considered, (a) S_0 = 1:5, (b) S_0 = 1:6.67 and (c) S_0 = 1:10. The contraction ratio of the sidewalls for all three proposed inlets is greater than proposed by the USBR (1987) or the FHWA (2012). **Figure 6.3(a)** shows the S_0 = 1:5 taper, the resulting wing wall taper is close to a ratio of 1:1 (V:H). The S_0 = 1:6.67 design has a wing wall contraction ratio of 1:1.75 (V:H). Flow separation at the inlet transition is expected for the S_0 = 1:5 and 1:6.67 taper, especially considering supercritical flow.

The S_0 = 1:10 design has a contraction ratio of 1:2.88, the contraction ratio is considered to be too great and the only method to reduce the contraction is by reducing the bed slope or by adjusting the width of the tapered lip (B_{lip}). To accommodate a 1:4 (V:H) sidewall contraction ratio an inlet structure of approximately 14.5 m in length would be required, such an inlet would then be comparable to the inlet fan of **Figure 6.2(c)**.

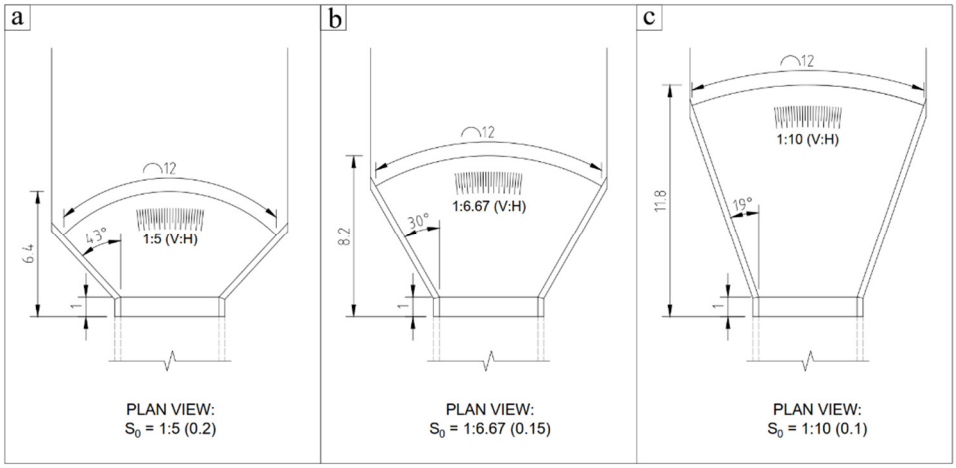

Figure 6.3: Inlet design for Tapered inlet model (T-model).

The S_0 = 1:10 taper was selected as the best option for the tapered inlets. **Figure 6.4** shows the proposed inlet prototype for the S_0 = 1:10 slope of the tapered inlet design.

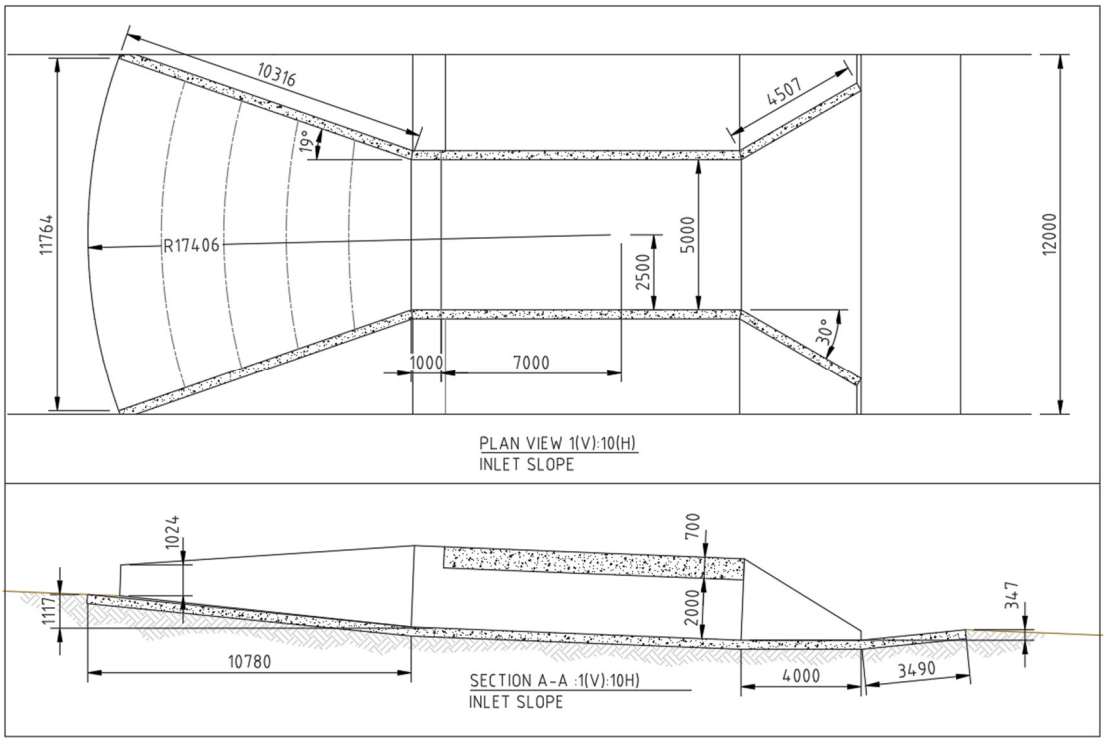

Figure 6.4: Tapered inlet design drawings, S_0 = 1:10.

The contraction ratio of the side walls is not at the recommended contraction ratio, but it becomes impractical to consider an inlet structure that would be larger than the culvert itself. The effect of the contraction ratio was studied in the experimental tests. **Table 6.2** shows the standard-step method performed on the inlet structure to determine the flow profile.

The flow depth results from the step-method is lower than that of the flow depth obtained by the energy equation (**Equation 6-1**). The discrepancy is due to the calculation of the head loss between the lip and the barrel, whereas the standard step method calculates this value more accurately between points. Local head loss (H_l) have not been included in the standard step method.

Table 6.2: Standard-step method performed on tapered inlet model (T-model), S_0 = 1:10.

Step Point Number	Longitudinal Upstream Length, x (m)	Flow Depth, y (m)	Measured Transect Length (m)	Froude Number, dimensionless	Velocity, m (m/s)
0	11,779	0,548	12	1,873	4,341
1	9,623	0,579	10,580	1,955	4,658
2	7,468	0,635	9,165	1,964	4,902
3	5,312	0,725	7,758	1,901	5,070
4	3,156	0,874	6,366	1,752	5,130
5	1	1,154	5	1,470	4,945
6	0,984	1,153	5	1,471	4,948
7	0	1,131	5	1,514	5,045

6.2.4. Culvert inlet design III: Compound Tapered Inlet

The compound tapered (CT) inlet aims to address the design limitations identified by the modified MEL design and the Tapered Inlet design. Both above-mentioned prototype models have an outlet that is situated below the NGL of the channel, the depression is due to the steep slope, or long taper section, required at the inlet to achieve the desired flow rates at the inlet. The contraction ratio of the tapered inlet prototypes falls outside the recommended contraction ratio. Both the proposed prototypes are also quite long when compared to the barrel length of the culvert.

Considering that it is not always practical to have the inlet span the entire width of the channel and that having the outlet below the NGL can cause additional deposition and requires drainage of the barrel, a third model was proposed. The objective of the compound taper inlet (CT-inlet) was to move the control point of the culvert upstream to a point away from the inlet of the barrel, as illustrated in **Figure 6.5**. Between the newly formed control and the barrel, a section was placed that would prevent boulders from settling out, upstream of the control point the boulders are able to settle out away from the inlet.

The newly formed section is not enclosed allowing the water to flow over a blockage through the culvert in the event of a blockage upstream. Boulder depositions are prevented in the section between the control section and the barrel (taper section) by means of an increased bed slope. The elevation required to install the taper section is obtained by placing the downstream apron level ($S_0 = 0$) and adding a level section (apron) upstream of the inlet lip. Scour of the apron was not considered in any of the experimental models or designs, the study deals with a fixed bed. Throughout the design, existing guidelines for the contraction and depression was adhered to as set out by The FHWA (2012).

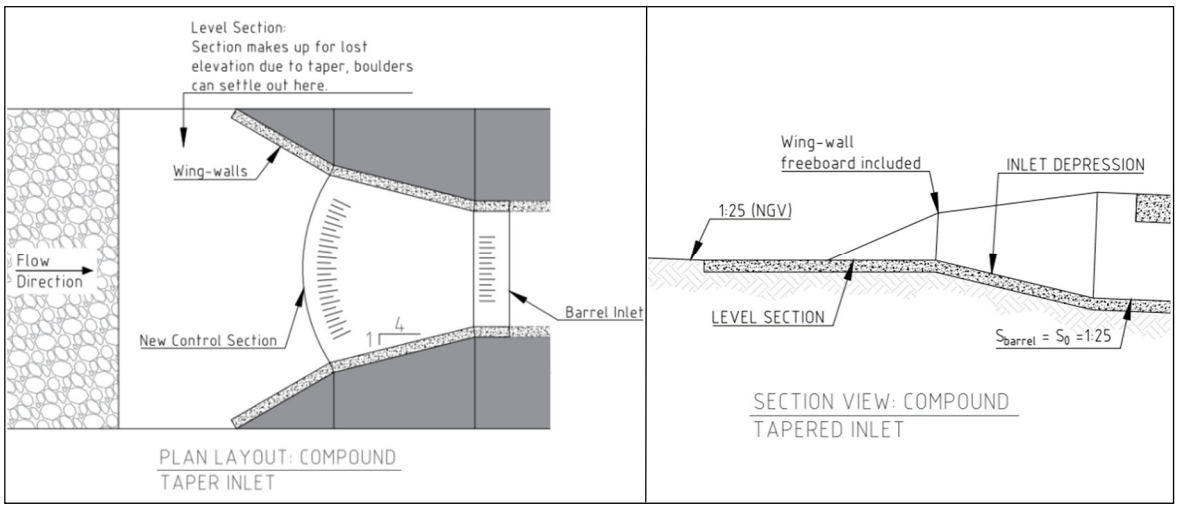

Figure 6.5: Compound taper (CT-model) inlet layout schematic.

Hydraulic Design of CT-Inlet

The method to design the CT-inlet is described in this section, **Table 6.3** shows the model scale parameters of the existing barrel and the flume setup in the laboratory as used in the design. The design is performed by calculating the desired flow depth at the inlet of the barrel, for the design flow a subcriticality factor (λ) of 0.9 was selected. The following steps outline the procedure followed to design the compound tapered inlet:

1. Determine inlet conditions at the inlet of the culvert barrel.
2. Select the contraction coefficient and length of the taper.
3. Select the wing-wall angle.
4. Determine the inlet lip geometry.
5. Determine flow conditions at the inlet lip and perform a check for hydraulic control.
6. Including friction losses, determine the elevation required between the inlet lip and the barrel to achieve flow conditions at the inlet of the barrel.
7. Include freeboard tot the inlet lip location and above the culvert barrel.

Table 6.3: Parameters used in the design of the CT-model.

Flume Properties				Culvert Barrel Properties			
Description	**Model**	**Prototype**	**Unit**	**Description**	**Model**	**Prototype**	**Unit**
Discharge, Q =	0,0279	28,529	m^3/s	**Barrel height, D =**	0,1250	2,000	m
Flume width, b =	0,7500	12,000	m	**Barrel width, B =**	0,3125	5,000	m
Roughness coefficient, k_s =	0,0098	0,156		**Mannings roughness, n =**	0,0120	0,012	
Bed slope, S_0 =	0,0400	0,040	m/m	**Barrel bed slope, S_b =**	0,0400	0,040	m/m
Uniform flow depth, yn =	0,0346	0,553	m	**Critical flow depth, y_c =**	0,0932	1,492	m
Froude number, Fr_n =	1,8468	1,847					
Specific energy, E =	0,0935	1,495	m				

Setting $\lambda = y_{inlet}/y_c = 0.9$ and calculating the critical flow depth with **Equation 2-14** at the inlet of the barrel a design flow depth of 1.342 m was obtained (Chadwick *et al.*, 2013).

$$y_c = \left(\frac{q^2}{2g}\right)^{1/3} \qquad \textbf{2-14}$$

Figure 6.6 shows a schematic of the inlet taper with the locations of the variables used in the design. The size and shape of the inlet taper determine the geometry of the inlet. A side-wall contraction of 1:4 was selected for the design, a 1:4 contraction provides the shortest section while remaining within the boundary set by the FHWA (2012). The length of the taper was set to 2D, there is no recommended length for the taper, setting the L_t = 2D provides a taper relative to the culvert it is designed for.

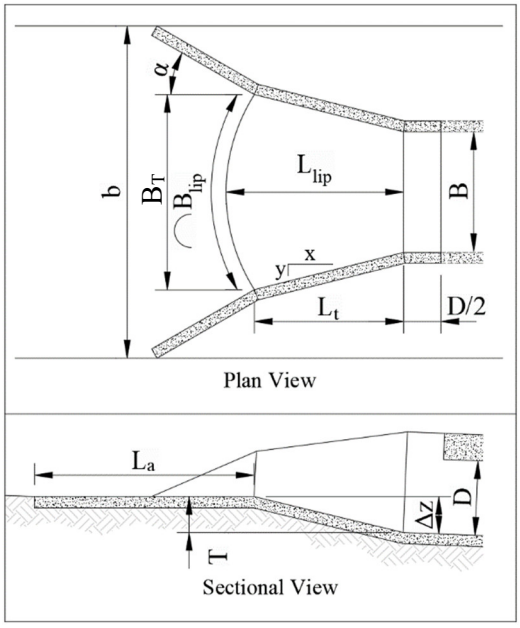

Figure 6.6: Compound taper design parameters.

The inlet fan geometry was calculated by the trigonometric method shown in **Appendix E**. Parameters required for the inlet lip geometry is the width of the culvert, the taper length, taper ratio and wing-wall angle. The inlet lip curve is set normal to the wing-wall angle and not the inlet taper to produce a longer effective inlet lip.

Critical flow was assumed at the lip of the inlet, the critical depth was determined by **Equation 2-14**. The specific energy for normal flow conditions and at the inlet lip was calculated and compared. If the Specific energy at the inlet lip is greater, a hydraulic control forms (Chow, 1959; Chadwick *et al.*, 2013), the upstream conjugate flow depth is calculated by **Equation 2-3**.

$$y_2 = \frac{y_1}{2}\left(\sqrt{1 + 8Fr_1^2} - 1\right) \qquad \textbf{2-3}$$

The elevation required (Δz) to achieve the desired flow depth at the inlet was calculated by including the friction losses of the inlet taper. **Equation 6-1** was used to determine Δz.

Design Summary of CT-Inlet

Table 6.4 shows the parameters for the developed CT-Inlet in model and prototype scale. The elevation loss due to the depression (taper in the vertical axis) is accounted for in the design by setting the outlet apron to a zero-bed slope, the remaining elevation is made up by adding a zero slope section just upstream of the inlet lip. Deposition is expected upstream of the lip and the formation of the hydraulic jump causes the boulders to settle out upstream of the inlet, the short horizontal section should therefore not have an adverse effect on sedimentation or boulder deposition.

Table 6.4: Design characteristics of the compound taper prototype.

Description	Design Characteristics		Unit	Description	Design Characteristics		Unit
	Model	Prototype			Model	Prototype	
Transition section, D/2 =	0,0625	1	m	Taper height, T =	0,0322	0,515	m
Wall contraction, 1 : x =	4	4	m/m	Total elevation change, Δz =	0,0347	0,555	m
Taper length, L_t =	0,2500	4	m	Bed slope of taper, S_{taper} =	0,1044	0,104	m
Wing-wall angle, α =	30	30	°	Barrel inlet flow depth, y_{inlet} =	0,0839	1,342	m
Taper width, B_t =	0,4375	7	m	Taper lip flow depth, y_{lip} =	0,0722	1,156	m
Taper lip length, B_{lip} =	0,4581	7,330	m	Specific energy at lip, E_c =	0,1084	1,734	m
Length of taper, L_{lip} =	0,3086	4,938	m	Wing-wall height at lip =	0,1015	1,624	m

6.2.5. Selection Criteria

Three inlet models were designed and compared to one another. Two of the models, namely the modified MEL and tapered inlet, were very similar in terms of size, shape and inlet depression profiles. The best-suited culvert inlet model between these two models had to be selected. A set of factors were considered, apart from the obvious hydraulic efficiency factor, other factors such as cost, design simplicity and practicality in terms of construction were considered.

Cost

The modified MEL inlet consists of curved sidewalls and a curved inlet invert profile. Curved sections in formwork require more preparation time to set up the formwork for the walls and to bend the reinforcing. A construction contractor specified the cost of casting concrete sections at R2800/m³ (De Jagers Civil Contractors, 2019) and a 30% increase in cost when working with curved sections as opposed to regular straight formwork.

Assuming the sidewalls and the apron of the inlet is curved, the cost breakdown for the construction of the inlet would be as set out in **Table 6.5**. The MEL structure is 1.73% more economical when compared to the inlet tapered model. The CT-prototype was the least costly model layout, with the apron floor included, and the taper section taken as a curved section.

Table 6.5: Cost analysis of prototype inlets.

Prototype	Form work Cost / m²	Wall Area (m²)	Floor Area (m²)	Wall Area asjusted for curve (m²)	Concrete Required (R)
Modified MEL	1,3	28,15	68,22	125,27	105230,58
1:10 Inlet Taper	1	38,08	89,40	127,48	107084,04
Compound Taper	1	22,44	83,16	105,59	88698,12
Wall Thickness =	0,3	m			
Concrete/m³	R2 800,00	/m³			

Design Simplicity

Culverts are widely used to drain streams under roadways, the proposed structure should be simple to design for a wide range of conditions. The modified MEL culvert is the most complex inlet to design between the three proposed models. Designing the CT-inlet requires a more detailed design than opposed to the tapered inlet.

Construction Practicality

Constructing a structure with straight walls and inverts is more practical as opposed to circular walls and inverts with a shaped profile. Considering that the study focusses on mountainous areas, it is safe to assume that the culvert would be constructed on bedrock. All three culverts require some form of excavation to accommodate the required slope at the inlets. The CT-inlet requires the least amount of excavation as a large portion of the elevation is gained by the level section just upstream of the inlet lip.

Conclusion to Selection Criteria

Based on the criterion discussed, the compound tapered inlet prototype is favoured above the two remaining prototypes. The CT-inlet is the most cost-effective inlet to construct and requires the least amount of excavation to construct the culvert. A drawback of the CT-inlet is the restriction created upstream by forcing a control section.

In terms of cost, the tapered prototype would be the least economical design, albeit only by 1.75% when compared to the modified MEL prototype. The modified MEL requires a more detailed design for an inlet shape and bed profile similar to that of the tapered inlet. Considering the practical aspects of constructing a curved inlet as opposed to a straight-walled section and apron floor, the tapered inlet was considered to be the more practical design of the two.

Experimental model tests were therefore performed on the compound tapered inlet and the tapered inlet prototypes.

6.3 Experimental Test Procedure

Steps 1 to 7 for the test procedure described in **Section 5.5** were followed to test the performance of the two models tested in this section. The experimental test procedure was carried out for each flow rate mentioned in the test schedule.

Table 6.6 shows the flow rates at which each model was tested, special test scenarios that were tested is included in the table. To ensure that the results of the boulder movement were consistent, critical tests

or tests showing the most movement were repeated two to three times. A further 10% of tests were repeated to ensure repeatability of the experimental tests.

Table 6.6: Test schedule for Chapter 6 experimental tests.

Model	Code	Additional tests	Flow Rate (m³/s)				
Tapered Inlet Model	T-model	Flow depth & boulder movement	15,36	20,48	28,53	30,72	35,84
Compound Taper Model	CT-model	Flow depth & boulder movement	10,24	15,36	20,48	25,60	28,53
			30,72	35,84	40,96		
		Outlet Submergence	28,53				
		1 m Inlet blockage	28,53				

6.4 Tapered Experimental Model Results

Experimental test results for the T-model is presented and discussed in this section, boulder movement and water level measurements are discussed separately. Observations were made that contributed to the analysis or understanding of the results.

6.4.1. Observations

Observations made during testing served to mention notable visual occurrences during testing. Most notably for the T-model test was the formation of a standing shock wave forming from the contraction downstream into the inlet. The shock wave forms in supercritical flow at the location of a linear contraction (Defina and Viero, 2010). Formation of the shock wave was present at every flow rate tested, **Figure 6.7** illustrates the shock wave for (a) 15.36 m³/s, (b), 20.48 m³/s and (c) 35.84 m³/s.

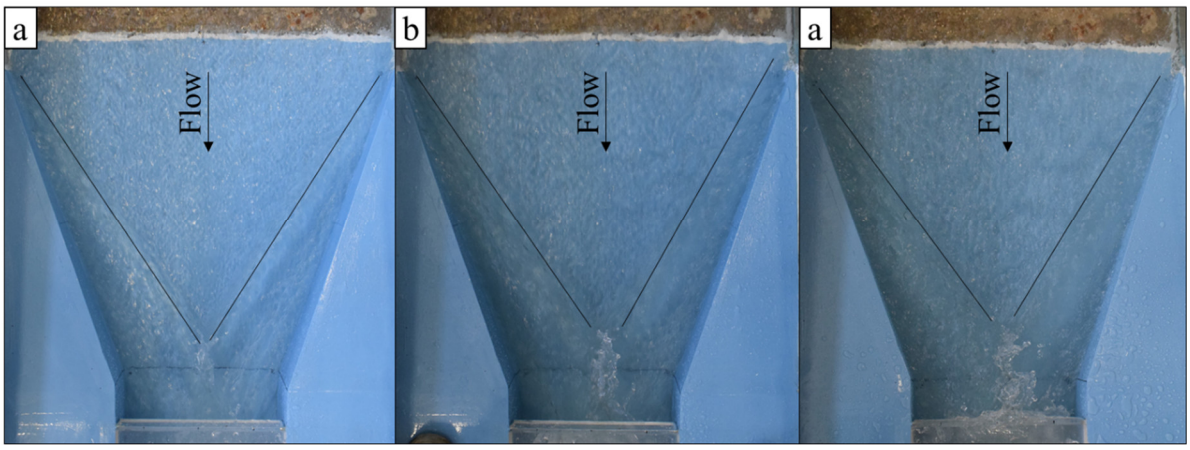

Figure 6.7: Shock wave experienced at T-model inlet.

Figure 6.8 illustrates the location of the shock wave as measured for the design flow rate of 28.53 m³/s. The pair of shock waves are nearly symmetrical in form, the flume has flow straighteners upstream of the test area and the culvert model is symmetrical, Symmetry of the shock wave was to be expected. A

linear trend line was drawn for each wavefront, the slope parameter of the trendline function was found to be similar, 0.703 (left wave) compared to 0.711 (right wave).

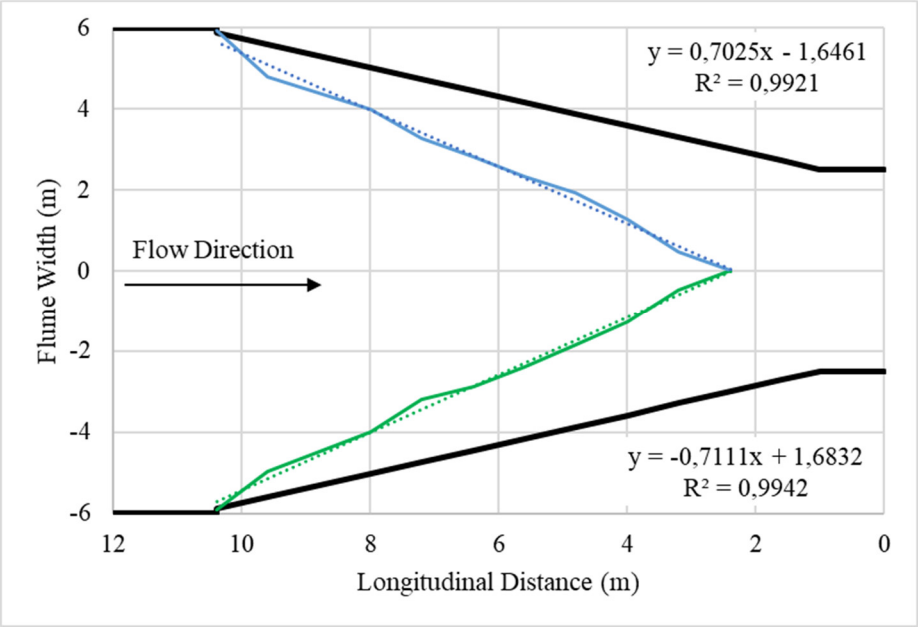

Figure 6.8: Measured location of the shock wave, Q = 28.53 m³/s.

The confluence of the two shock waves is approximately 2.5 m upstream of the barrel of the culvert, at this point superposition of the waves took place and a standing jump formed. **Figure 6.9** illustrates the resulting jump from the confluence, the jump touches the headwall of the barrel, occasionally spilling onto the roadway.

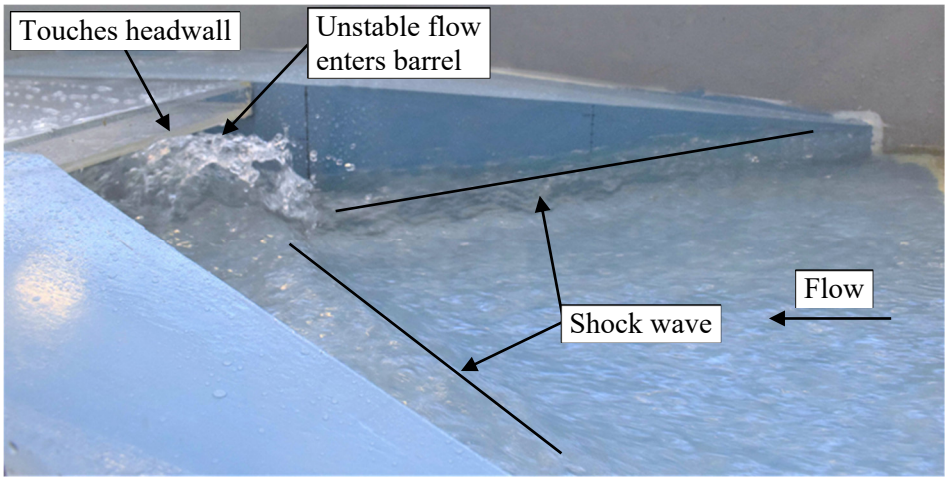

Figure 6.9: Standing wave formed at the inlet of T-model, Q = 28.53m³/s.

The T-model design that was tested was declared to be unsuitable for a feasible solution to boulder blockages based on the formation of the shock wave. The consequence of the formation of the shock wave was the jump that formed just upstream of the inlet and the unstable flow through the culvert.

Further investigation and experimental testing into the optimal taper shape and bed slope would be required before a taper type inlet can be considered as a feasible solution.

6.4.2. Flow Depth

Water levels were recorded for the flow rates mentioned in **Section 6.3** and converted to flow depth, the recorded flow depths are listed in **Appendix F** for each model tested. Only the flow depths, shown in **Table 6.7**, for the design flow rate (Q = 28.53 m³/s) are discussed in this section for comparison to the calculated design. The formation of the shock wave resulted in an unfavourable design; the flow depths of the other flow rates tested were therefore not discussed.

Table 6.7: Measured flow depths upstream of the culvert, Q = 28.53 m³/s.

Chainage (m)	Flow Depth, y (m)	Shock Wave	
		Offset from Centerline (m)	Flow Depth (m)
16	0,496	–	–
11,2	0,472	–	–
9,6	0,456	4,880	0,872
8	0,416	4,000	0,952
6,4	0,412	2,840	0,936
5,6	0,432	2,360	0,912
4,8	0,413	1,880	0,885
4	0,448	1,280	0,848
3,2	0,544	0,480	0,824
2,4	–	0,000	0,843

Flow depths were recorded in the shallow, fast-flowing water upstream of the inlet and above the location of the shock wave. The recorded flow depths for the design flow rate including the shockwave are shown in **Figure 6.10**. Due to the formation of the jump at approximately 2.5 m, measurements between 2.5 m and the inlet could not be recorded.

A difference in flow depth was observed between the calculated flow depth and measured flow depth in the inlet of the model. The difference in flow depth between the calculated prototype and experimental model was attributed to the variation in flow depth normal to the direction of flow. The design calculations assumed a uniform flow depth and velocity distribution across the cross-section of the inlet. however, the shock wave voids this assumption leading to the variation in flow depth experienced across the cross-section of the flow. As the width of the shock wave grew, the flow depth in the main section remained low at an average depth of 1.102 m.

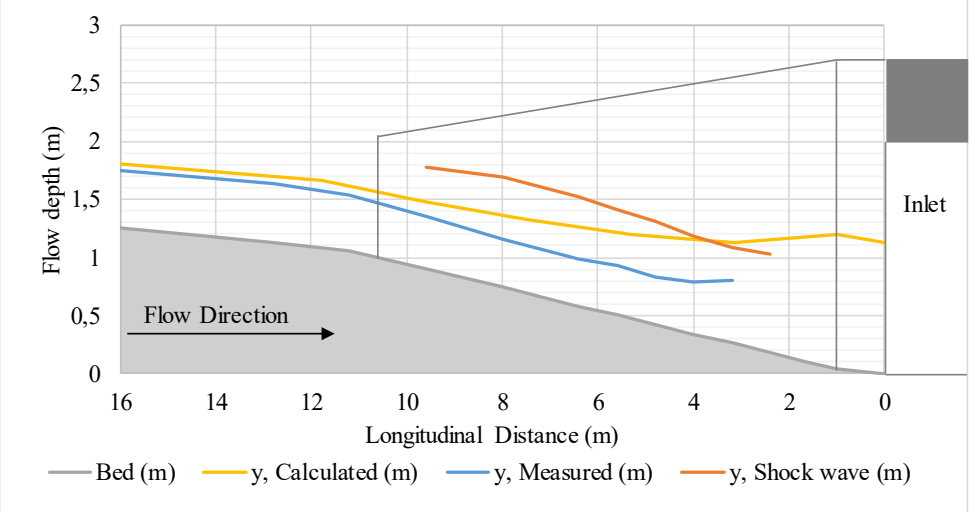

Figure 6.10: Recorded flow depths at the inlet of the T-model, Q = 28.53 m³/s.

6.4.3. Boulder Movement

Boulder movement results were recorded for the flow rates mentioned in **Section 6.3** and the results for each test performed is shown in **Appendix F**. The recorded boulder movement results for boulders that moved in the flume and boulders that were transported through the culvert are shown in **Table 6.8**.

Table 6.8: Recorded boulder movement for T-model.

		Moved in Flume				Transported Through Culvert			
	Boulder Size (mm):	**424**	**600**	**800**	**1008**	**424**	**600**	**800**	**1008**
	Total:	**11**	**11**	**11**	**12**	**11**	**11**	**11**	**12**
Flow Rate (Test Number) [m³/s]	15,36	11	9	5	0	8	4	0	0
	20,48	11	11	8	8	6	8	5	3
	28,53	11	11	11	8	11	11	9	7
	30,72	11	11	11	11	11	11	11	8
	35,84	11	11	11	11	11	11	11	10
	15,36 (2)	11	7	1	0	9	4	1	0
	15,36 (Repeat)	11	9	3	2	8	6	2	0
	28,53 (2)	11	11	11	11	11	10	10	9

Figure 6.11 shows a bar chart representing a summary of the boulder movement tests performed for each flow rate on the T-model. The results are displayed as the boulders that were transported through the culvert as a percentage of the number of boulders that moved for a given boulder size. Boulder size did not influence the performance of the inlet, as seen in **Figure 6.11** the movement of the boulders through the culvert was only influenced by the flow rate. The lower flow rates were not capable of transporting the boulders to the inlet of the culvert, therefore the variation in boulder transport through the culvert was dependent on flow rate and not the performance of the inlet. The results in **Appendix F** illustrates how the boulders deposited upstream away from the inlet.

Figure 6.11 and show that the T-model operated effectively as an inlet to prevent blockages. Not a single boulder settled out in the vicinity of the inlet. The success of the model was attributed to the zero-afflux provided by the model, meaning that a boulder that became mobile due to the flow would not be able to settle out at the inlet as previously observed due to the increase in flow depth.

The adverse slope downstream of the outlet to return to the NGL did not have an influence on the boulder movement for any of the tests performed. The effect of the adverse slope on the potential for deposition in the outlet has not been tested for low flows or repeated long-term flows, and therefore conclusions cannot be drawn on the use of the adverse slope.

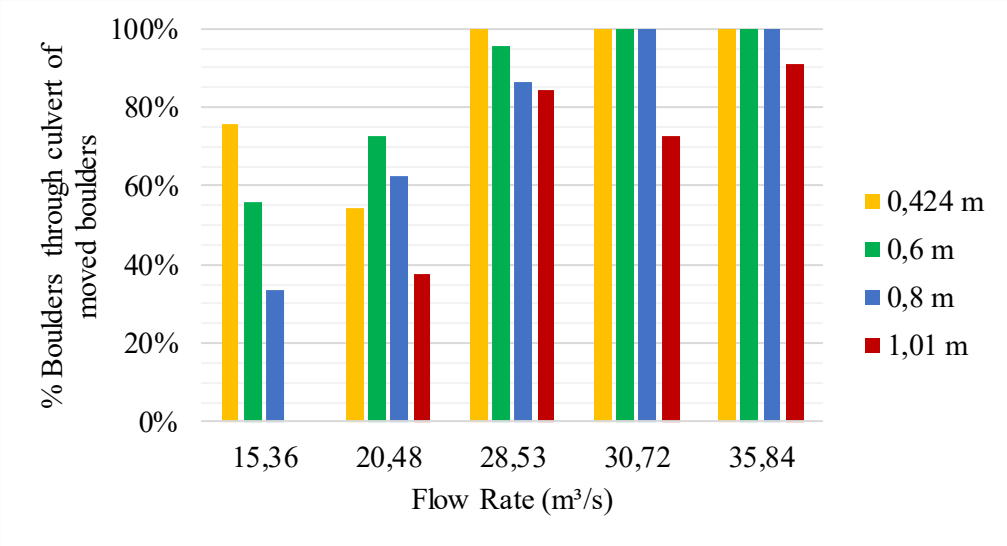

Figure 6.11: Recorded boulder transport through culvert of T-model.

6.5 Compound Tapered Inlet Experimental Model Results

Results for the experimental CT-model tests are shown and discussed in this section. Observations made during testing are made and discussed, the observations that were made aims to aid in the development of a working prototype and to identify problem areas not shown by measured data. Flow depths were recorded for the flow rates mentioned in **Section 6.3**, the recorded depths are shown in **Appendix F**. The recorded flow data was compared to the C-model test results to evaluate the performance of the CT-model. Boulder movement was recorded, and stored in **Appendix F**, the effectiveness of the CT-model evaluated against the C-model.

6.5.1. Observations

During testing, valuable observations have been made that contributes to the performance assessment of the CT-model. Each observation is discussed in detail in this section and the impact the observation had on the performance of the model is discussed.

The introduction of a tapered section following a defined control resulted in the reduction of contraction effects and mitigated the formation of extreme shock waves as experienced by the T-model, discussed in **Section 6.4**. Illustrated by **Figure 6.12**, slight cross-waves can be seen on the surface of the flow, the flow, however, is aligned well with the barrel of the culvert. The taper section has a side wall contraction ratio of 1:4 as recommended by the FHWA (2012) for inlet tapered culverts.

Flow through the barrel of the culvert is much more stable as compared to the T-model, the stable flow was attributed to the reduced contraction caused by the side walls. The flow profile normal to the direction of flow was uniform, resulting in more stable flow passing through the culvert.

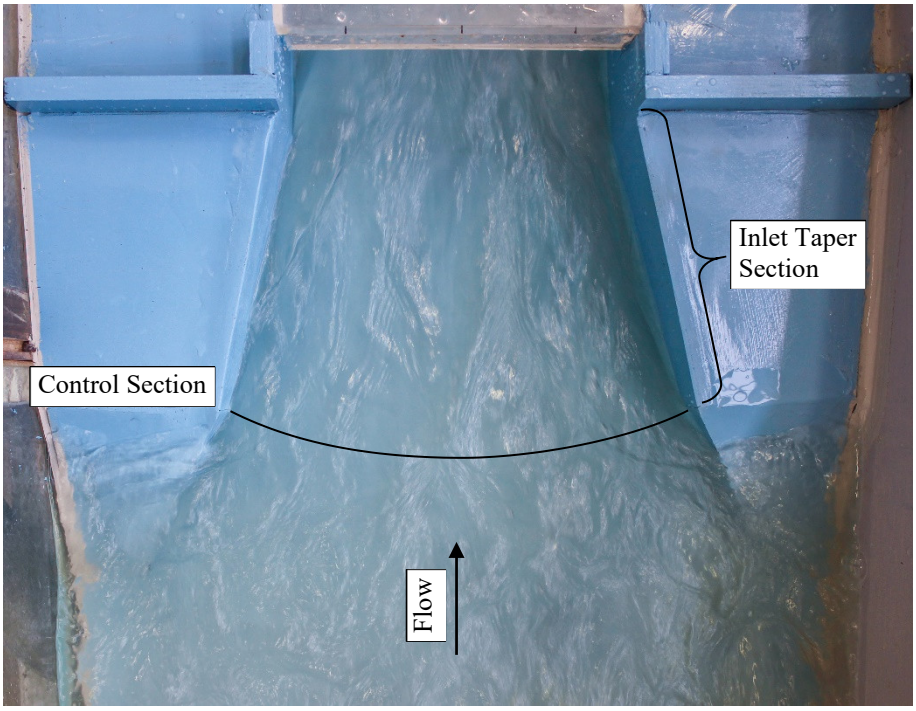

Figure 6.12: Compound taper inlet, experimental model.

A curved inlet lip seemed to have no bearing on the performance of the inlet. A possible explanation was that the size of the drop from the lip is relatively small. There is, therefore, no defined lip that can act as a crest. Flow depth measurements provide further insight into the effectiveness of defining the lip width as the curved section instead of a section normal to the direction of flow.

The embankment of the side walls was designed to slope upwards from the control section towards the roadway. At the control section, the sidewall height was equal to the upstream damming height caused by the contraction. The purpose of the upwards sloping embankment was to allow water to flow onto the embankment and into the taper section in the event of blockages at the control section. The effectiveness of the CT-model was tested under a blockage of 1 m (50% of the barrel height) at the control section. At the design flow rate of Q_d = 28.53 m³/s, the barrel could accept the design flow

without spilling onto the roadway as illustrated in **Figure 6.13**. The embankments on either side and the blockage create weir-flow condition into the culvert.

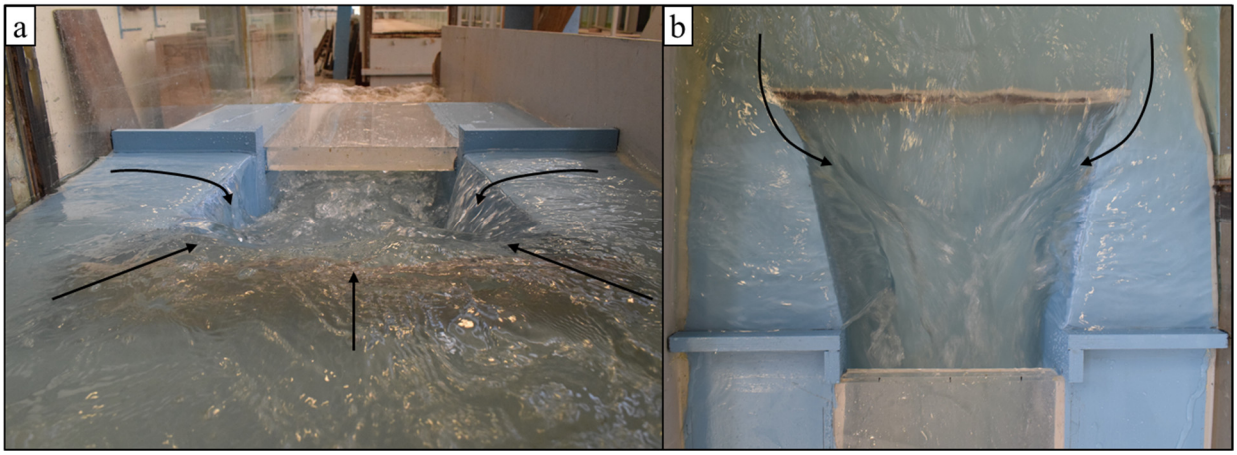

Figure 6.13: CT-model, inlet blocked 50% of culvert height.

The inclusion of sloped embankments resulted in the water running up the embankment and spilling onto the roadway. Balustrade walls were installed on the edge of the roadway on the embankments, a 0.4 m high wall was sufficient to prevent water from spilling onto the roadway. The balustrade walls are visible in **Figure 6.13(a)** and **(b)**, with the section above the culvert open to prevent additional damming in the case of an overtopping.

6.5.2. Water Levels

Water levels were recorded for each flow rate mentioned in **Section 6.3**. The water levels were converted to flow depths to compare the measured results with the C-model results, the measured flow depths for each flow rate tested are shown in **Table 6.9**. Water levels were recorded for each flow rate with the boulders included in the flume, only the upstream water levels were recorded, and the recorded results are shown in **Appendix F**.

Figure 6.14 shows a longitudinal section of the inlet of CT-model where the water levels for tests with and without boulders are shown to compare the effect of the presence of the boulders in the flume. Only the water levels for four of the eight flow rates are shown in the figure to simplify the figure, all eight flow rates display the same trend. There is a slight increase in flow depth between the 13 m and 16 m mark for the lower flow rates, this location coincides with the deposition location of the boulders during the experimental models. The presence of the boulders increased the channel roughness in the deposition location resulting in slightly increased flow depths. As the flow rate increased the presence of the boulders had a negligible effect on the flow depth.

Table 6.9: Recorded flow depth results for the CT-model inlet.

Discharge (m^3/s)	10,24	15,36	20,48	25,60	28,53	30,72	35,84	40,96
Distance Upstream (m)	Flow Depth - Prototype (m)							
Upstream								
64	0,296	0,360	0,448	0,536	0,580	0,620	0,684	0,736
57,6	0,296	0,360	0,432	0,504	0,552	0,592	0,644	0,700
38,4	0,272	0,360	0,428	0,496	0,532	0,576	0,608	0,664
32	0,272	0,360	0,432	0,480	0,512	0,544	0,608	0,632
25,6	0,276	0,364	0,440	0,484	0,524	0,568	0,600	1,528
22,4	0,256	0,324	0,412	0,468	0,492	0,524	0,564	1,636
19,2	0,288	0,332	0,400	0,468	0,532	0,652	1,188	2,036
16	0,296	0,392	0,640	1,328	1,488	1,672	1,792	2,088
12,8	0,696	0,872	1,056	1,392	1,512	1,616	1,960	2,304
11,2	0,800	1,032	1,248	1,568	1,640	1,824	1,976	2,400
9,6	0,752	1,056	1,264	1,496	1,560	1,736	1,952	2,408
8	0,776	1,024	1,208	1,464	1,576	1,752	1,896	2,472
7,2	0,740	1,020	1,268	1,516	1,588	1,764	1,996	2,468
6,4	0,684	0,940	1,252	1,508	1,612	1,745	1,996	2,452
5,6	0,603	0,864	1,232	1,435	1,573	1,717	1,872	2,368
4,8	0,605	0,843	1,152	1,387	1,589	1,717	1,867	2,432
4	0,576	0,779	1,083	1,355	1,488	1,659	1,915	2,597
3,2	0,587	0,773	1,008	1,237	1,443	1,467	1,952	2,581
2,4	0,555	0,755	0,952	1,224	1,416	1,549	1,864	2,797
1,6	0,541	0,744	0,968	1,221	1,416	1,512	1,912	2,829
1	0,560	0,771	0,995	1,235	1,389	1,560	1,869	2,835
0	0,531	0,787	1,043	1,203	1,400	1,501	1,843	3,229
Overtopping	–	–	–	–	–	–	–	0,112
Downstream								
-10	0,459	0,715	0,880	1,024	1,104	1,179	1,339	2,629
-10,8	0,461	0,664	0,835	0,989	1,064	1,101	1,277	3,725
-11,6	0,488	0,608	0,843	0,955	1,005	1,061	1,189	1,184
-12,4	0,467	0,613	0,693	0,885	0,931	0,987	1,109	1,083
-13,2	0,432	0,581	0,693	0,827	0,885	0,904	1,019	1,019
-14	0,445	0,568	0,659	0,781	0,808	0,845	0,936	0,952

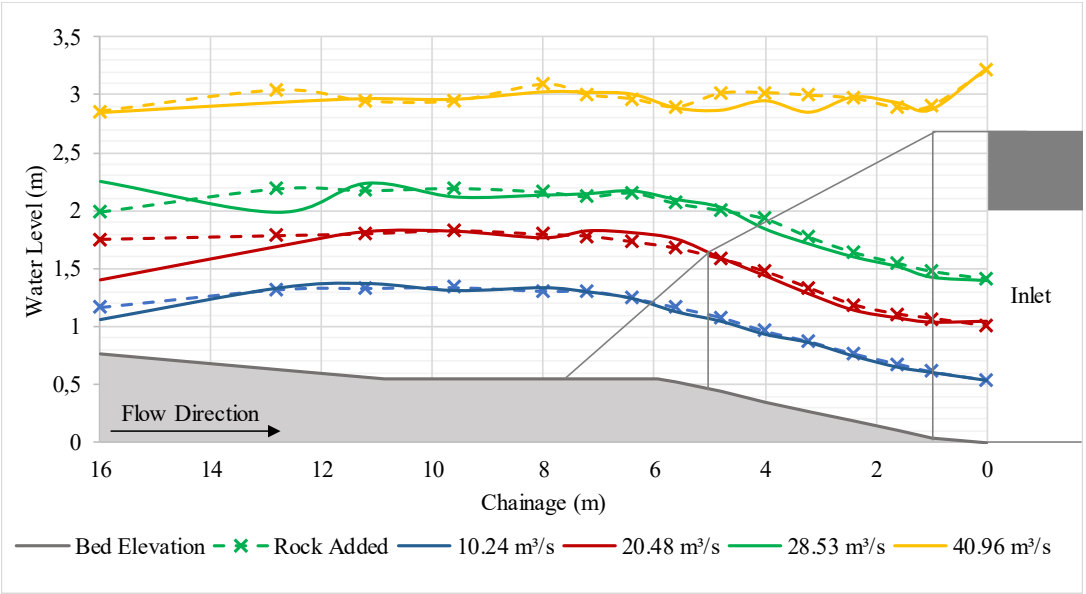

Figure 6.14: CT-model, inlet water level comparison between boulders and no boulders added.

The effectiveness of the tested models was negatively influenced by the formation of the hydraulic jump which caused the boulders to settle out just downstream of the jump. A comparison was therefore made between the recorded flow depths between the C-model and CT-model to establish if the CT-model promoted boulder transport through the culvert. Flow depths were compared between the two models to account for the variation in bed profiles between the two models, as illustrated in **Figure 6.15**.

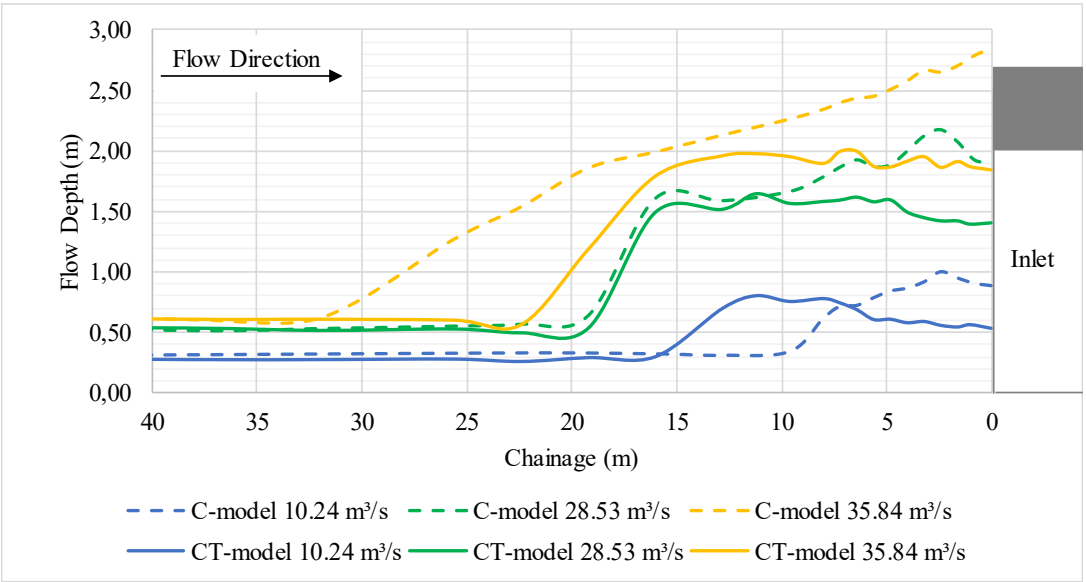

Figure 6.15: CT-model, inlet flow depth comparison.

At the lower flows (Q = 10.24 m³/s) the hydraulic jump moved slightly upstream (12 m). The design flow rate (Q = 28.53 m³/s) showed that the jump formed in the same location for the C- and CT-models. At a Q = 35.84 m³/s, the CT-model is unsubmerged, and the jump moves downstream towards the control section. The flow depth at the inlet for each flow rate was reduced for the CT-model when

compared to the C-model. For the Q = 10.24 m³/s, 28.53 m³/s and 35.84 m³/s, flow depth reductions of 40.4%, 26.3% and 35.1% were achieved when compared to the C-model, the reduced flow depths, in turn, increased the velocity at the inlet of the culvert.

Comparing the Calculated flow depths with the measured flow depths revealed a discrepancy between the control section flow depth. **Table 6.10** shows the calculated versus measured flow depths at points along the test area. At the control the calculated flow depth differed by 0.434 m to the measured flow depth, the significant discrepancy points to the critical depth being downstream between the inlet lip and culvert barrel. The flow depth at the barrel and the afflux upstream of the inlet lip produced an accurate comparison.

Table 6.10: Comparison between calculated and measured flow depths.

Location	Calculated Depth (m)	Measured Depth (m)	Δ	% Difference of Calculated
Afflux	1,624	1,580	0,044	3%
Inlet Lip	1,156	1,589	-0,434	-38%
Barrel Inlet	1,342	1,400	-0,058	-4%
Barrel Outlet =	1,055	1,104	-0,049	-5%

Hydraulic performance of the inlet was evaluated for the case of high tailwater. The tailgate was raised until the water touched the soffit of the outlet, a hydraulic jump formed in the barrel of the culvert, just downstream from the inlet. Flow depth measurements were taken at the design discharge to determine if the culvert continued to operate as an inlet-controlled culvert. As shown in **Table 6.11** the difference between the normal flow depth and submerged outlet condition is not adversely negative. High negative Δ/y values indicate an increased headwater, the variation in flow depth was most probably due to undulations in the water surface. The hydraulic jump formed just inside the inlet; the upstream depth would not be affected by the downstream conditions.

Table 6.11: Inlet measurements for submerged outlet conditions.

Chainage (m)	Normal Flow Depth, y (m)	Submerged Flow Depth (m)	Δ	Δ/y (%)
16	1,488	1,264	0,224	15%
12,8	1,512	1,372	0,140	9%
11,2	1,640	1,548	0,092	6%
9,6	1,560	1,500	0,060	4%
8	1,576	1,488	0,088	6%
7,2	1,588	1,468	0,120	8%
6,4	1,612	1,468	0,144	9%
5,6	1,573	1,461	0,112	7%
4,8	1,589	1,525	0,064	4%
4	1,488	1,568	-0,080	-5%
3,2	1,443	1,581	-0,139	-10%
2,4	1,416	1,565	-0,149	-11%
1,6	1,416	1,544	-0,128	-9%
1	1,389	1,555	-0,165	-12%
0	1,400	1,451	-0,051	-4%

Finally, the conditions at the outlet were compared on the apron to determine there was a need for erosion protection downstream, the comparison between normal flow conditions and measured flow conditions are shown in **Table 6.12**. The velocity and Froude number parameters were less than the compared normal flow parameters, erosion protection was therefore not required. The outlet for the CT-model compared to the C-model showed an increase in flow depth and flow area, subsequently, lower velocities and Froude numbers were recorded for the CT-model. The apron of the outlet for the CT-model has a zero slope to return the culvert to the NGL which offers some increase in flow depth.

Table 6.12: Outlet flow comparison between CT-inlet and normal, uniform conditions.

Flow Rate, Q (m^3/s)	Normal Flow Conditions				Culvert Installed			
	Normal Depth, y_n, (m)	Area, A (m^2)	Velocity, V (m/s)	Froude Number, Fr	Flow Depth, y (m)	Area, A (m^2)	Velocity (m/s)	Froude Number, Fr
10,240	0,306	3,677	2,785	1,606	0,445	4,284	2,391	1,144
15,360	0,381	4,570	3,361	1,739	0,568	5,463	2,811	1,191
20,480	0,445	5,338	3,837	1,837	0,659	6,336	3,233	1,272
25,600	0,504	6,048	4,233	1,904	0,781	7,515	3,406	1,230
28,529	0,553	6,634	4,301	1,847	0,808	7,772	3,671	1,304
30,720	0,580	6,960	4,414	1,850	0,845	8,131	3,778	1,312
35,840	0,650	7,795	4,598	1,821	0,936	9,003	3,981	1,314

6.5.3. Boulder Movement

Boulder movement for the flow rates mentioned in **Section 6.3** was recorded, **Table 6.13** illustrates the recorded movement of each test. The post-processed images of the boulder movement are found in **Appendix F**.

Table 6.13: Recored boulder movement results, CT-model.

		Moved in Flume				Transported Through Culvert			
	Boulder Size (mm):	**0,424**	**0,6**	**0,8**	**1,01**	**0,424**	**0,6**	**0,8**	**1008**
	Total:	**11**	**11**	**11**	**12**	**11**	**11**	**11**	**12**
Flow Rate (Test Number) [m³/s]	10,24	6	2	0	0	0	0	0	0
	15,36	8	8	1	1	0	0	0	0
	20,48	10	10	5	3	0	0	0	0
	25,6	11	11	10	9	2	5	1	2
	28,53	11	11	9	10	1	2	0	0
	30,72	11	10	10	9	4	1	0	0
	35,84	11	10	10	10	1	2	0	1
	40,96	11	10	9	9	2	2	1	0
	20,48 (2)	11	11	9	5	2	0	1	1
	20,48 (3)	11	11	10	10	3	2	0	0
	25,6 (2)	11	11	8	5	1	1	1	1
	25,6 (3)	11	11	10	9	2	3	0	0
	28,53 (2)	11	11	11	9	2	3	0	0
	28,53 (3)	11	10	10	6	1	1	1	0
	30,72 (2)	11	10	10	8	1	1	0	0
	30,72 (3)	11	11	10	9	2	2	0	0
	35,84 (2)	10	10	10	9	3	3	0	1
	35,84 (3)	11	11	8	10	4	1	0	1
	40,96 (2)	11	11	11	9	2	4	3	2
	25,6 (Repeat)	11	10	9	9	1	1	0	1
	28,53 (Repeat)	11	11	10	8	2	2	0	1
	28,53 (Repeat - 2)	11	10	8	7	3	2	0	2
	30,72 (Repeat)	11	10	9	8	1	1	0	0
	35,84 (Repeat)	11	11	9	9	4	5	1	0

The results from the boulder movement tests shown in **Table 6.13**, was used to determine the boulders that flowed through the culvert shown as a percentage of the boulders that moved in the flume.

Figure 6.16 shows the results of the boulders that flowed through the culvert. The CT-model is capable of consistently transport the smaller faction of boulder through the culvert. Results for the transport of boulders through the culvert varied greatly in quantity, during testing in the laboratory. During testing an observation was made that the transport quantity is based on whether a boulder is deposited near the inlet of the culvert during testing. The experimental results do however show and increase in boulder movement for the CT-model, which is discussed in **Section 6.6**.

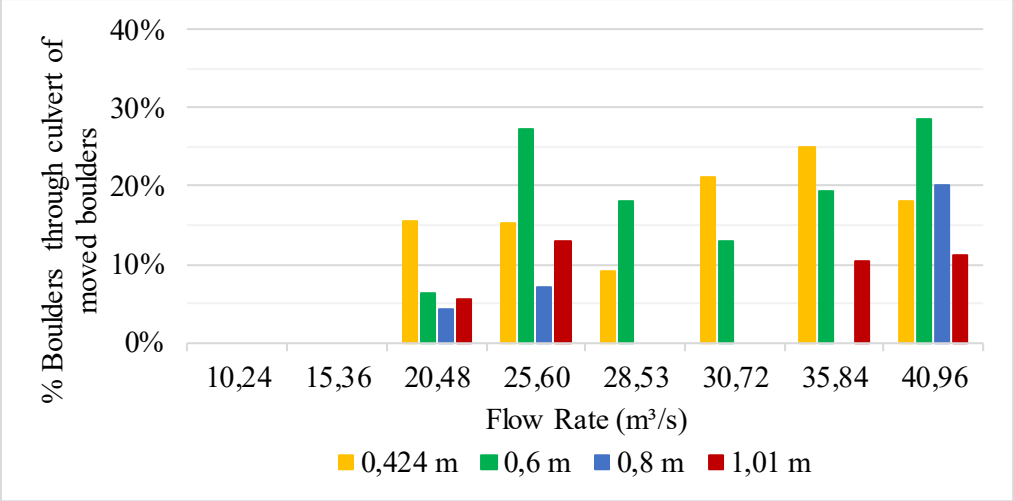

Figure 6.16: Boulder movement results CT-model.

6.6 Experimental Model Results Summary

The discussion surrounding the boulder movement of the CT- and T-model will mainly refer to **Figures 6.17** to **6.20**. Results from the normal culvert test at an S_0 = 1:25 was used as the baseline test, the results of which have been included in the figures.

The tapered model outperformed each model in the boulder movement tests, but the hydraulic performance of the tapered model disqualified the model as a feasible solution. **Figures 6.17** to **6.20** indicate that the T-model transported close to all the boulders moved by the flow for each boulder size. Further investigation into a similar type of inlet is recommended, the structure is clearly capable of preventing boulder deposition at the inlet of the culvert.

Comparing the C-model to the CT-model indicate that the CT-model is capable of transporting boulders through the culvert. The CT-model outperformed the C-model at each test, except for one test where the C-model managed to transport nearly 50% of the 0.6 m sized boulder through the culvert. Based on the experimental results presented, the smaller sized boulders were more active in being transported downstream, compared to the larger boulders. The large boulders presented a reduction in movement around the design discharge and increase again as the flow rate increased. Boulder movement could be influenced by the location of the hydraulic jump, which would explain the reduction in boulder movement at the flow rate increases.

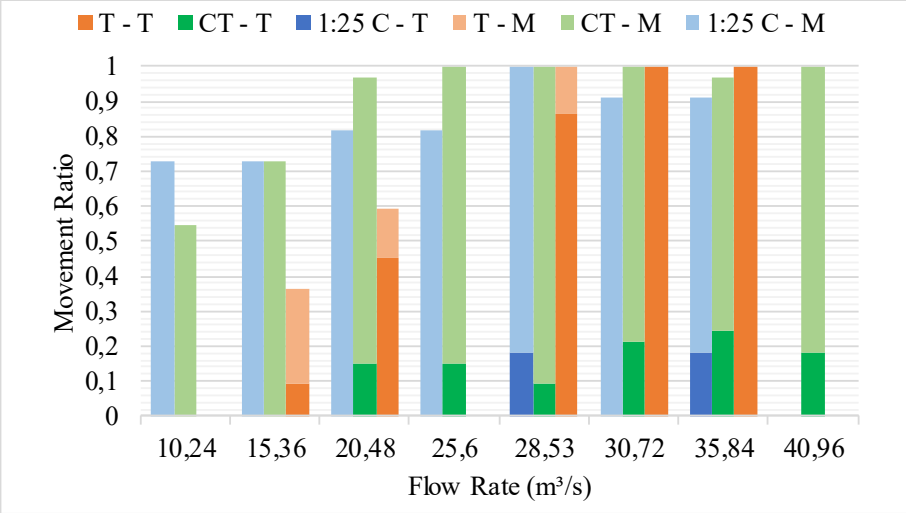

Figure 6.17: 0.424 m Results.

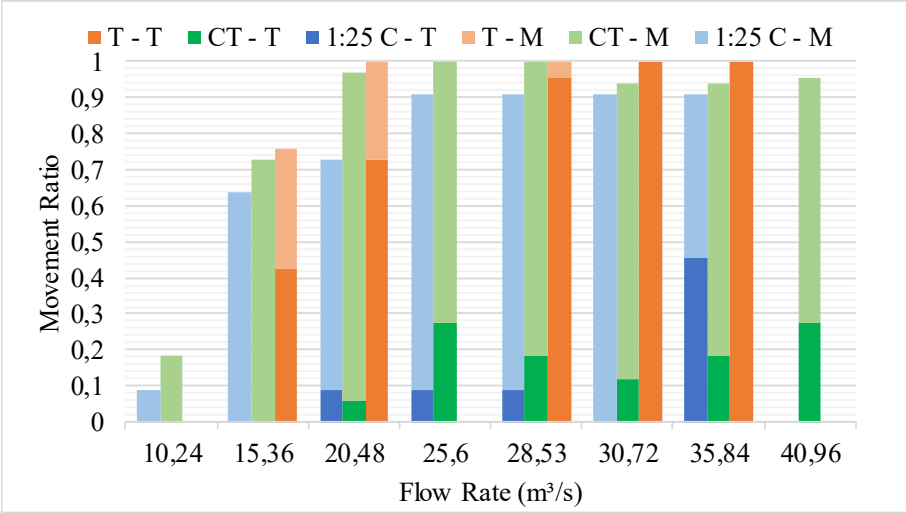

Figure 6.18: 0.6 m Results.

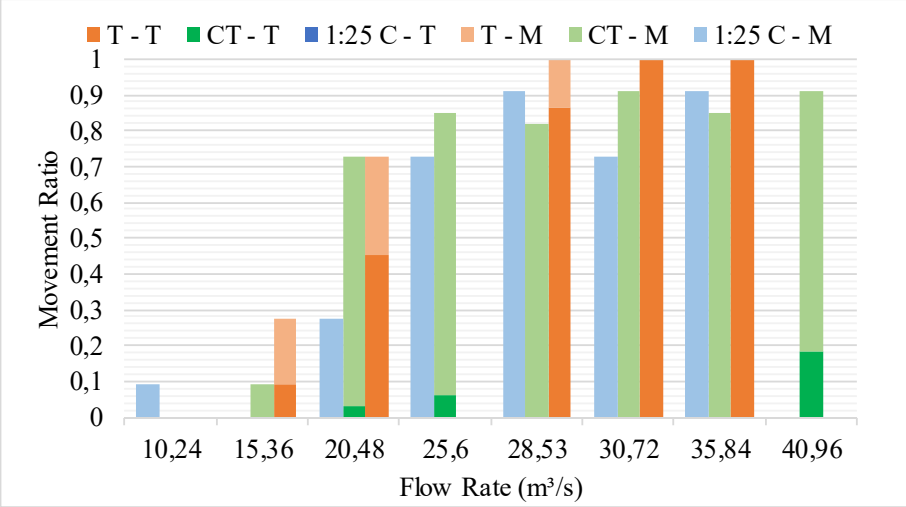

Figure 6.19: 0.8 m Results.

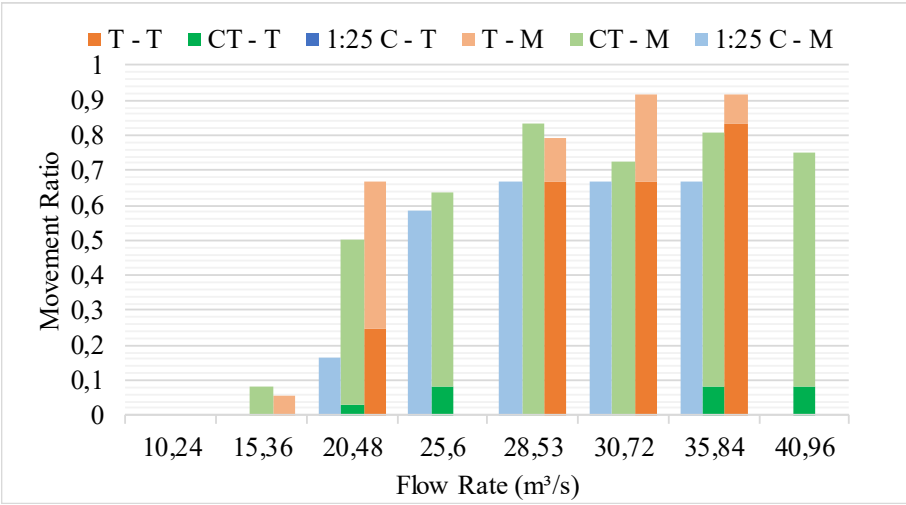

Figure 6.20: 1.01 m Results.

Figure 6.21 shows the location of the hydraulic jump for the CT- and C- model at 20.48 m³/s, 28.53 m³/s and 35.84 m³. The hydraulic jump is indicated as a grey box, the location of the jump for the C-model has not moved for the CT-model, the CT-model has noticeably fewer boulders between the inlet and the location of the hydraulic jump. The comparison between the distance of the first boulder and the inlet can clearly be seen between the C and CT-models.

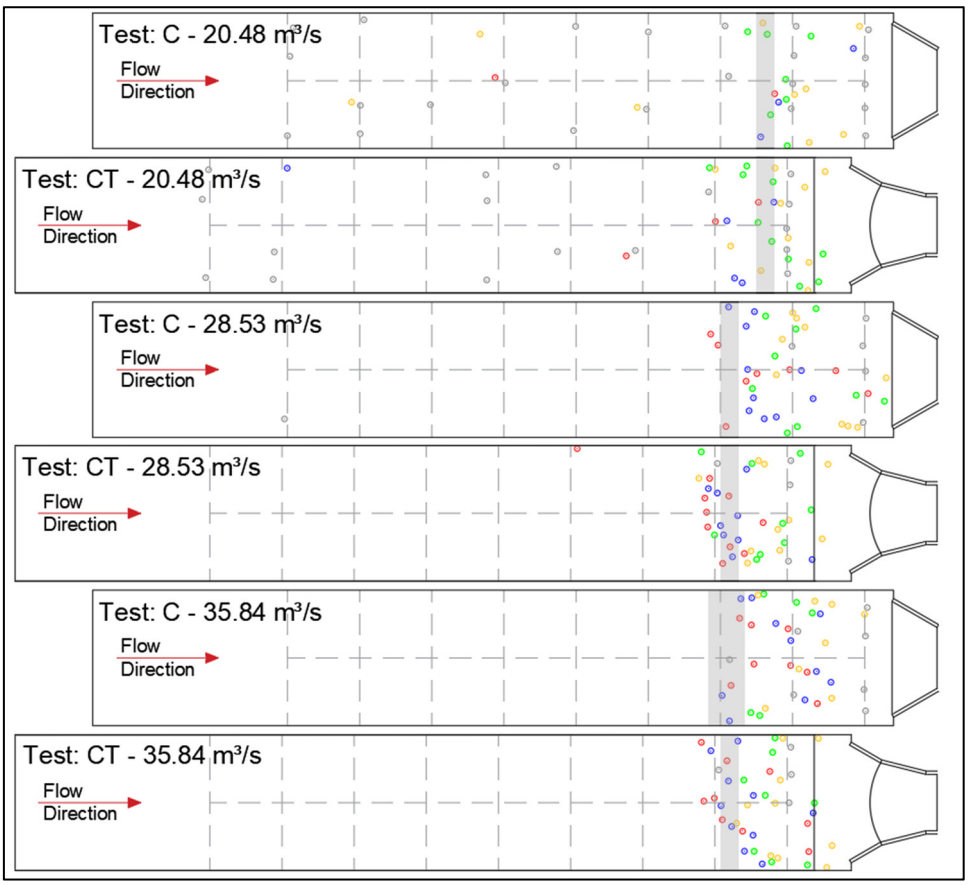

Figure 6.21: Hydraulic jump locations for the C and CT experimental models.

6.7 Conclusion on Modified Inlet Model Designs

A desktop study was conducted to develop three possible inlet prototypes that would increase boulder transport through the culvert whilst reducing the potential for blockages by the boulders. A modified MEL inlet was developed based on the design of a minimum energy culvert. The tapered (T) inlet consisted of a selected bed slope of 1:10. A compound tapered (CT) inlet was developed from existing guidelines with the objective of developing a design that could easily be adapted to different stream characteristics.

The T-inlet and the CT-inlet were selected as optimal designs based on cost, design complexity and construction complexity. Experimental tests were performed on each of the two models, and water

levels and boulder movement were recorded. The data from the recorded results were used to determine the optimal design between the two models tested.

Experimental tests for measuring water levels revealed the formation of a shock wavefront in the contraction of the inlet for the T-model. The shock wavefronts from each contracting wall formed a standing jump at the confluence just upstream of the barrel inlet. Based on the poor hydraulic performance, the T-model could not be selected as the optimal design.

The CT-model produced a streamlined inlet into the barrel of the culvert with a control section a distance upstream from the inlet. Upstream of the control section, the boulders could be deposited, downstream of the control the boulders were unable to settle out and had to flow straight through the culvert. Not a singular boulder settled out in the tapered section, of the CT-model, past the control section. As a result, the boulders were transported through the culvert.

The outlet flow velocity of the CT-model was compared to the normal flow conditions of the flume to check for erosion control measures. Flow exiting the culvert was slower than the normal flow conditions, therefore no erosion protection would be required if only flow velocity was considered as a criterion for erosion protection. The permissible flow velocity for coarse gravel varies between 1.6 m/s and 1.8 m/s (0.4 m – 1 m flow depth), some form of outlet scour protection would be required to prevent undermining of the outlet.

Boulder transport ratio in the CT-model was consistently higher when compared to the C-model results. Deposition distance of boulders upstream of the inlet could also be considered greater for the CT-model than for the C-model as no boulders settled out past the control section on the CT-model. The CT-model was selected as the optimal inlet from the models tested. Considering that the CT-model improved flow conditions and boulder the transport ratio compared to the normal C-model and that the T-model produced unfavourable results.

7. Optimal Inlet Multi-Cell Detail Design

7.1 Introduction

Experimental tests in Chapter 6 revealed that the compound taper (CT) inlet model was found to be the optimal inlet model that has been tested. The CT-model were tested for multiple inlets to study the effects of a pier separating the flow in the inlet. Experimental tests were performed on a two-cell culvert and a three-cell culvert. The design of the multi-cell culverts was performed in the same manner as for the single-span culvert. Water levels and boulder movement were recorded for the experimental tests in this section. To account for floating debris, two debris fins were incorporated into the design.

7.2 Objective of Testing Multi-Cell Culverts

Culvert walls in multi-span culverts create an obstruction in the flow path for debris or even boulders to become stuck around the wall, reducing the flow capacity of the culvert. The objective of the experimental tests on the multiple inlets was to determine if the culvert walls could influence the movement of the boulders. As part of the design, a debris fin was incorporated into the design to reduce the blockage potential of the culvert due to floating debris.

7.3 Experimental Test Schedule

Experimental tests were performed on a two-cell and three cell culvert model with a compound taper inlet. **Table 7.1** lists the test schedule for each model tested, the two-cell (2C) model were tested with two pier configurations, namely a notched type pier and a solid fin pier,

Table 7.1: Test schedule for Chapter 7.

# Cells	Pier Type	Flow Rate (m³/s)				
Two	Notched Fin	28,53				
	Solid Fin	15,36	20,48	25,6	28,53	35,84
Three	Solid Fin	30,72	61,44	85,575		

7.1 Experimental Procedure

The experimental procedure for Chapter 6 and 7 remained exactly the same, the test schedule differed between the two chapters. **Section 7.3** describes the procedure followed in this section in combination with the experimental test procedure described in **Section 5.5**. Steps 1 to 7 were followed for each experimental model and flow rate. For each model, the boulder movement test was repeated three times and a further 10% repeated to show the repeatability of the experimental procedure.

7.2 Debris Fin and Pier Width

Literature showed that a 900 mm wide pier was effective in reducing floating debris accumulation around the pier (Hydraulics Department, 2014), 900 mm wide piers were therefore used in the multi-cell culverts.

Debris mitigation methods were considered at the inlet to reduce the blockage potential of the inlet. Debris fins were used as a measure against debris accumulation. The CT-inlet extends away from the inlet upstream which effectively moves the inlet upstream creating a rectangular channel section leading up to the barrel of the culvert. The objective of the CT-inlet was to move the control and deposition location upstream away from the inlet. A debris fin could be used to extend the pier upstream to the location of the inlet lip of the CT-inlet, isolating the two barrels from each other. The debris fin extension also served the purpose of preventing boulders from depositing against the culvert wall at the inlet as observed in **Figure 2.9**

Two debris fin configurations were developed and tested as part of the experimental models. A solid debris fin consisting of a 30° fin extending from the inlet up to the height of the afflux depth of the upstream flow (1.62 m), as shown by **Figure 7.1(a)** was selected. The fin is then connected to the culvert at the height of the roadway (2.7 m). The function of the fin is to allow debris to ride up the fin as the flow depth increases, effectively reducing the effective blockage of the debris. A second debris fin was developed from the design proposed by Tooley (2017). The second debris fin consisted of a debris wall constructed upstream at the inlet lip, the debris wall was connected to the barrel of the culvert with a connecting wall to separate the barrels. **Figure 7.1(b)** illustrated the notched debris fin proposed as the second debris fin that was tested as part of the experimental models. The notched design was aimed at reducing the volume of concrete required to construct the debris fin. Design drawings for the prototype debris fins are found in **Appendix C**.

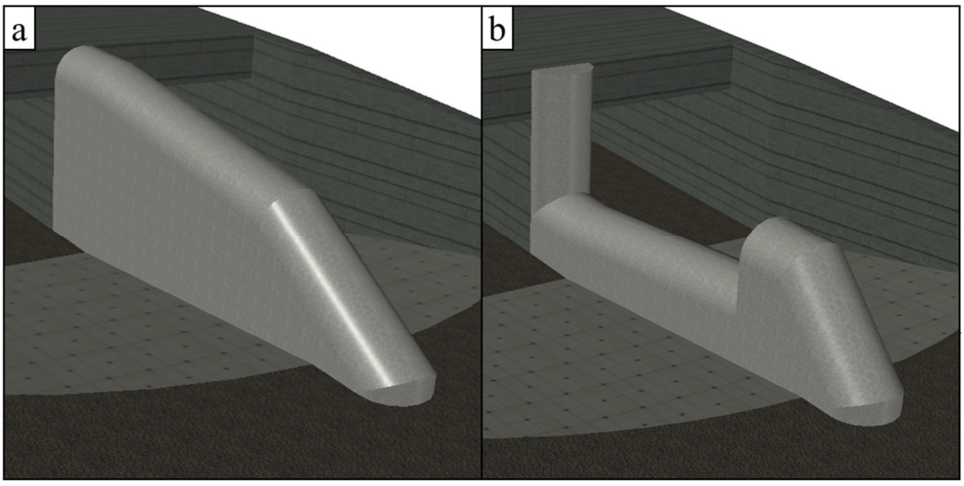

Figure 7.1: Prototype debris fin configurations.

7.3 Hydraulic Design of Multiple Inlets

The hydraulic design of the multiple inlet models followed the same basic procedure followed in **Section 5.3** to determine the design discharge of the culvert barrel. One barrel was considered to calculate the design discharge and multiplied by the number of cells to determine the design discharge used in the experimental model. A check for outlet control was performed for each barrel size.

The same procedure used in **Section 6.2.4** for the design of the inlet shape was used to design the multiple inlet structures. Pier width needed to be taken into account when determining the size of the inlet taper and inlet lip. While pier width had to be included for the geometric layout of the inlet shape, the effective lip width subtracted the width of the piers. Critical depth at the inlet lip was assumed and calculated, for all the cells included, at the total design discharge. The y_c was the same for each barrel and the elevation change required was calculated for a single cell.

7.3.1. Two-Cell Culvert

The barrel size was adjusted for the two-cell culvert to allow the model to be tested in the same 750 mm wide flume in the laboratory. Two 2.5 x 2 m (B x D) barrels were selected for the design, each with a design discharge of 14.26 m³/s. **Table 7.2** lists the design parameters obtained for the design of the CT-inlet and culvert barrel. The design drawings are shown in **Appendix C**.

Table 7.2: Two cell compound taper design parameters.

Description	Design Characteristics		Unit	Description	Design Characteristics		Unit
	Model	Prototype			Model	Prototype	
Transition section, D/2 =	0,0625	1	m	Taper height, T =	0,0324	0,518	m
Wall contraction, 1 : x =	4	4	m/m	Total elevation change, Δz =	0,0349	0,558	m
Taper length, Lt =	0,2500	4	m	Bed slope of taper, Staper =	0,1024	1,798	m
Wing-wall angle, α =	30	30	°	Barrel inlet flow depth, yinlet =	0,0839	1,342	m
Taper width, Bt =	0,4938	7,9	m	Taper lip flow depth, ylip =	0,0720	1,151	m
Taper lip length, Blip =	0,4938	7,900	m	Specific energy at lip, Ec =	0,1079	1,727	m
Length of taper, Llip =	0,3161	5,058	m	Wing-wall height at lip =	0,1010	1,617	m

7.3.2. Three-Cell Culvert

A three-cell culvert was designed to be tested as part of the experimental procedure. The width (B) of each individual barrel could not be reduced enough to fit into the flume. Flow patterns in the flume and the setup of the model in the flume allowed for symmetry of the flow to be accepted. Meaning the three-cell culvert that was designed was tested by installing one half of the culvert into the flume as shown in **Figure 7.2**.

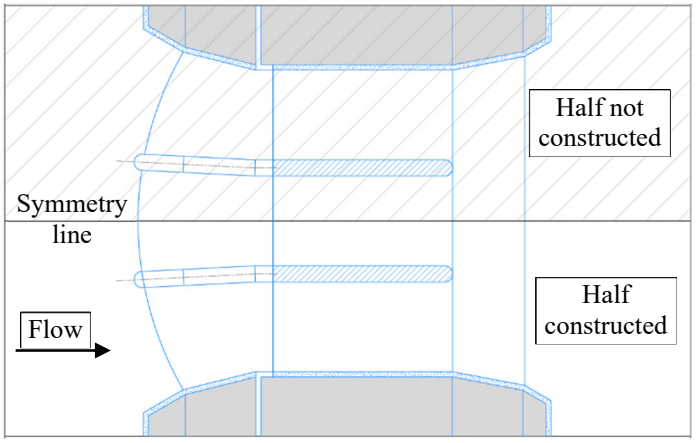

Figure 7.2: Symmetry illustration of three-barrel culvert install in the flume.

A single cell consisted of a 5 x 2 m (B x D) sized barrel, a design discharge of 28.53 m³/s was obtained for a single barrel. The total design discharge of the culvert was therefore 85.575 m³/s and the flow rate for the experimental models was halved to account for using symmetry in the model. **Table 7.3** list the design parameters for the three-cell culvert in prototype and model scale. Design drawings are shown in **Appendix C**.

Table 7.3: Three-cell CT inlet design parameters.

Description	Design Characteristics		Unit	Description	Design Characteristics		Unit
	Model	Prototype			Model	Prototype	
Transition section, D/2 =	0,0625	1	m	Taper height, T =	1,0186	16,297	m
Wall contraction, 1 : x =	4	4	m/m	Total elevation change, Δz =	1,1748	18,797	m
Taper length, Lt =	0,2500	4	m	Bed slope of taper, Staper =	0,0400	0,040	m
Wing-wall angle, α =	30	30	°	Barrel inlet flow depth, yinlet =	0,0829	1,326	m
Taper width, Bt =	1,1750	18,8	m	Taper lip flow depth, ylip =	0,0720	1,151	m
Taper lip length, Blip =	1,1750	18,800	m	Specific energy at lip, Ec =	0,1079	1,727	m
Length of taper, Llip =	0,4074	6,519	m	Wing-wall height at lip =	0,1010	1,617	m

7.4 Multi-Cell Experimental Results

This section contains the results obtained from the experimental tests performed on the two- and three-cell culvert. Results were recorded for the flow rates mentioned in **Section 7.3**. and were separated into observations, water levels and boulder movement. Additional measured data not shown in this section can be viewed in **Appendix G**, including the post-processed experimental results on boulder movement.

7.4.1. Two-Cell Compound Taper Experimental Model Results

Observations

Observations made during the experimental model test provided insight into the flow of the water around the structure which was not picked up through measurements. One of the two debris fins tested was the notched type debris fin (**Figure 7.3**). Two factors were identified that made the notched fin not a suitable debris control structure for the flow conditions experienced in the model setup. Water ran up and over the nose of the fin, as illustrated by **Figure 7.3**, at the design discharge (Q = 28.53 m^3/s), the implication was that debris could potentially flow over the nose and get caught on the culvert wall or at any point along the dividing wall. The second factor was the increase in flow depth at the barrel face caused by the culvert dividing wall, the flow depth at the face of the round wall reached depths equal to the soffit of the barrel. An increased flow depth at the barrel was an unfavourable condition that the CT inlet prototype sought to solve.

From the observations made the notched-pier was not a suitable design for the specific design, however, the upstream debris wall has been successfully used to mitigate debris blockages at culverts (Tooley, 2017). The high-velocity flow and the need for reduced flow depths at the inlet made the structure not suitable.

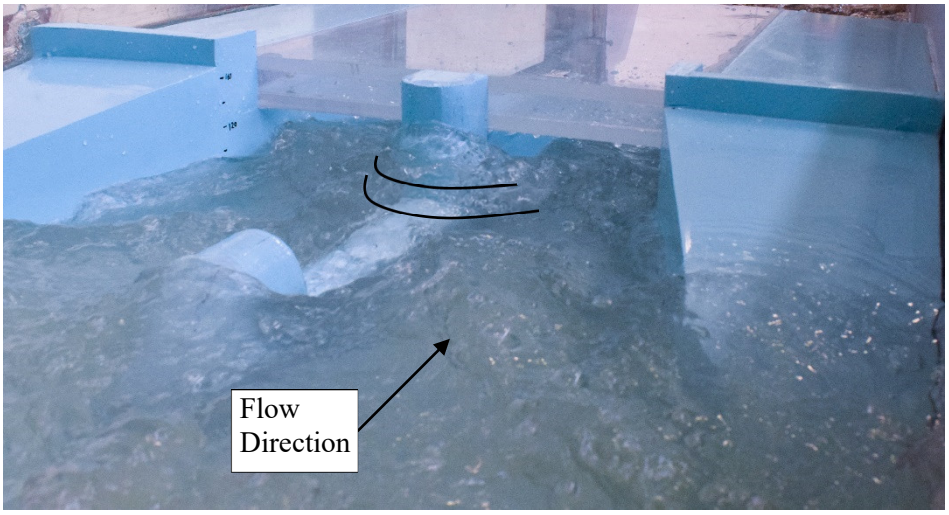

Figure 7.3: Notched debris fin experimental test.

A second debris fin was tested, the solid debris fin. The flow was completely separated by the debris wall from the inlet lip of the taper section. As a result of the flow isolation, the flow was more uniform in depth into the barrel, as opposed to the notched fin. **Figure 7.4** shows the solid debris fin for the two cell-culvert, the uniform flow depth and afflux caused by the fin is visible. The debris fin edge meets at the roadway, resulting in no blockage potential at the inlet where the debris fin meets the culvert wall or pier.

A boulder that has been deposited against the fin is visible in **Figure 7.4**, the location of the fin is just upstream of the inlet lip. Boulders depositing at this location was not considered to be of any concern as the location is upstream of the inlet lip. The boulder would not have any influence of the flow at the nose of the debris fin.

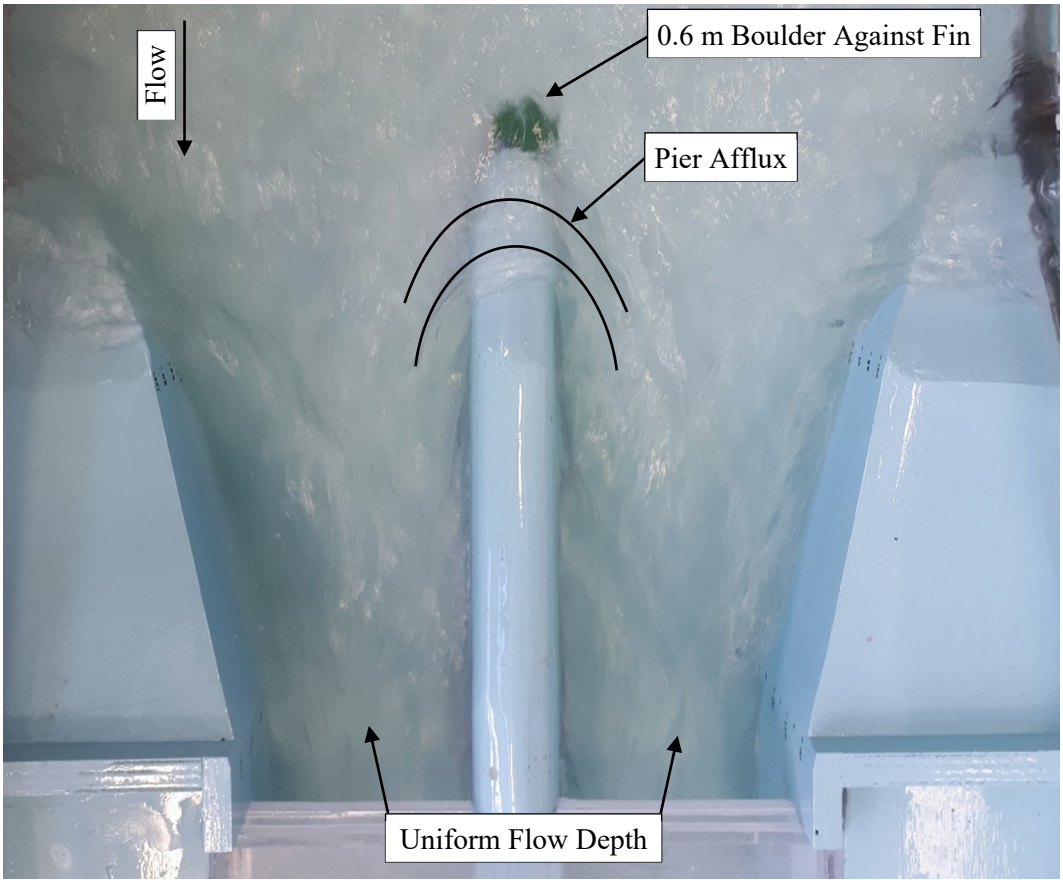

Figure 7.4: Solid debris fin experimental test.

Flow Depths

Flow depths were recorded for the two-cell culvert (2C-model) for the notched (2CN-model) and solid fin (2CS-model). The notched fin was only tested at the design discharge of 25.83 m^3/s and the solid fin was tested at the flow rates mentioned in **Section 7.3**. Two flow depth measurements were taken in the left and right cell and averaged to compare the flow depths in each barrel. The average depth between the two depths was used in further discussions. Averaged flow depths for the 2C-model with the solid fin is shown in **Table 7.4**, the measurements for the left and right cell measurements is shown in **Appendix G**. The measured flow depths for the notched fin is also shown in **Appendix G**.

Table 7.4: Recorded flow depths for the two-cell, solid fin culvert.

Discharge, Q (m³/s)	15,36 m³/s	20,48 m³/s	25,6 m³/s	28,53 m³/s	35,84 m³/s
Chainage (m)	Flow Depth (m)				
64	0,42	0,468	0,56	0,592	0,688
57,6	0,416	0,48	0,544	0,592	0,664
38,4	0,34	0,392	0,444	0,488	0,568
32	0,316	0,392	0,424	0,472	0,544
25,6	0,324	0,4	0,456	0,496	0,576
22,4	0,324	0,368	0,448	0,492	0,568
19,2	0,32	0,392	0,44	0,496	1,056
16	0,336	0,608	0,96	1,244	1,576
12,8	0,944	1,152	1,248	1,344	1,776
11,2	0,928	1,184	1,392	1,512	1,848
9,6	1,016	1,248	1,48	1,656	1,872
8	1,02	1,188	1,396	1,514	1,824
7,2	1,038	1,186	1,376	1,52	1,88
6,4	0,956	1,196	1,356	1,568	1,932
5,6	0,85	1,156	1,404	1,576	1,88
4,8	0,812	1,102	1,392	1,54	1,89
4	0,828	1,036	1,428	1,54	1,938
3,2	0,708	0,902	1,242	1,398	1,8
2,4	0,712	0,904	1,164	1,308	1,736
1,6	0,776	1	1,232	1,348	1,688
1	0,818	1,052	1,336	1,42	1,714
0	0,75	0,948	1,256	1,362	1,684

Flow depth measurements for the 2C-model were compared to that of the CT-model. Two of the five flow rates have been omitted for clarity, the flow rates follow the same trend as observed in **Figure 7.5**. Recorded flow depths between the single-cell and multi-cell culvert show similar flow depths, the same design methodology was followed for each of the two models (CT- and 2C-models). The 2C-model with the solid debris fin installed produced accurate flow depth results when compared to that of the CT-model. Considering the comparable accuracy between the CT- and 2C model, it was assumed that the same discrepancy between the calculated and measured flow depth, at the inlet lip, existed for the 2C-model.

Figure 7.5 includes the measured flow depths for the 2CN- and 2CS-models. Comparing the results for the two debris fin configurations illustrates the observation made that the notch in the debris fin causes an increase flow depth at the face of the barrel. The sudden flow depth increase is caused by the culvert wall as discussed in the observations section.

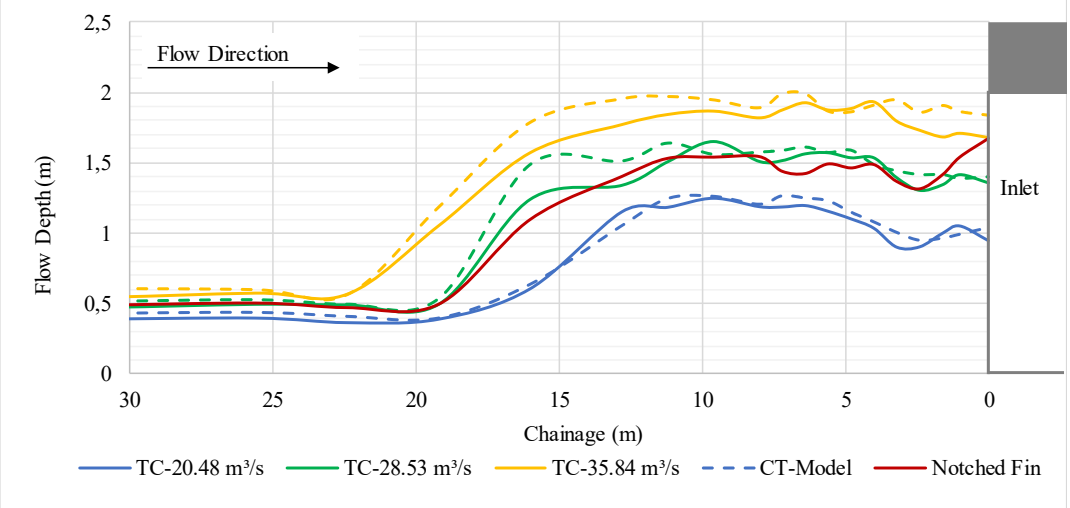

Figure 7.5: Flow depth comparison between single and multi-cell culvert.

Boulder Movement

The results from the boulder movement tests for the 2CS-model are shown in **Table 7.5**. The tests were performed for the flow rates mentioned in **Section 7.3**. **Appendix G** shows the post-processed test results for each boulder movement test.

Table 7.5: Boulder movement results for the two-cell, solid fin culvert.

		Moved				Through			
	Boulder Size (mm):	**424**	**600**	**800**	**1008**	**416**	**600**	**800**	**1008**
	Total:	**11**	**11**	**11**	**12**	**11**	**11**	**11**	**12**
Flow Rate (Test Number) [m³/s]	15,36	11	6	1	0	0	0	0	0
	15,36 (2)	9	6	0	0	2	1	0	0
	15,36 (3)	11	5	0	0	0	1	0	0
	20,46	11	9	8	3	1	2	0	1
	20,46 (2)	10	10	4	1	0	2	0	0
	20,46 (3)	11	10	1	1	2	0	0	0
	25,6	11	11	8	8	2	5	0	0
	25,60 (2)	11	11	9	8	5	1	3	3
	25,60 (3)	11	10	9	8	1	3	1	0
	28,53	11	11	9	10	3	2	1	1
	28,53 (2)	11	10	8	8	4	3	0	1
	28,53 (3)	11	11	9	9	1	2	0	0
	35,84	11	10	10	10	6	1	0	1
	35,84 (2)	11	11	11	12	4	2	0	1
	35,84 (3)	11	11	11	9	2	2	1	0
	20,48 (Repeat)	11	10	5	6	2	4	0	0
	28,53 (Repeat)	11	10	10	8	3	1	1	1

The boulder movement results for the ‘moved’ and ‘through’ boulders were combined to produce the bar chart illustrated in **Figure 7.6**. The graph shows the number of boulders transported through the

culvert barrel as a percentage of the total number of moved boulders for the given reference boulder size. **Figure 7.6** illustrates the trend where the boulders would be more likely to be transported through the culvert barrel at lower flows than compared to the peak flow of 35.84 m³/s. Based on the results presented by **Figure 7.6** it was concluded that at the lower flow rates, the upstream damming depth and hydraulic jump location allows the boulders to be deposited in closer vicinity of the culvert inlet. As the flow rate increases, the damming depth increases, causing the hydraulic jump to move upstream, away from the inlet. **Figure 6.21** confirms that the hydraulic jump moves upstream as the flow rate increases.

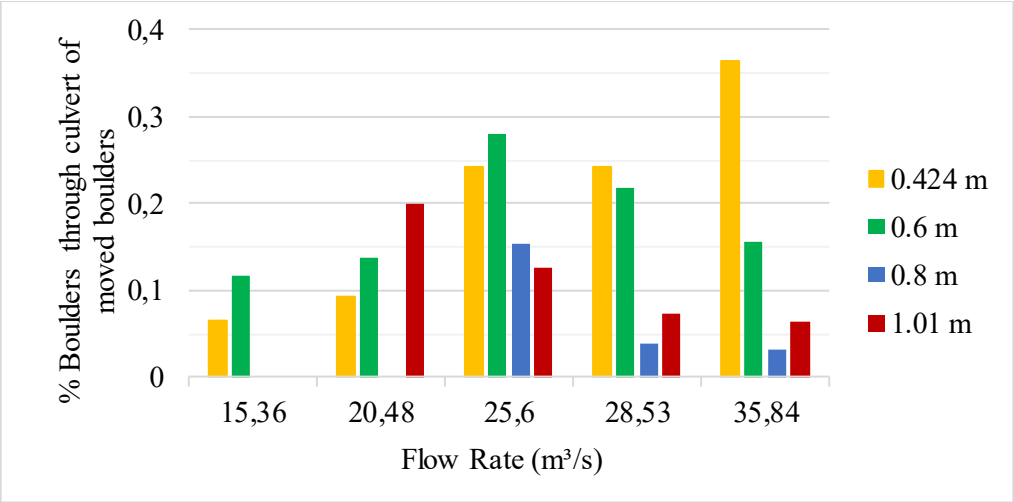

Figure 7.6: Boulder transport as a percentage of boulder movement.

Figure 7.7 to **Figure 7.10** compares the boulder movement ratios between the 2CS- and CT models for the boulders that have been transported through the culvert. The four figures should be viewed in conjunction with each other to better compare the results between the 2CS and CT models. Overall, the 2CS model performed marginally better than the CT model. Where the 2CS and CT model have "through" ratios the 2CS shows a better 'through' ratio for all but three tests. However, the results for each boulder size and flow rate are very consistent between the two models. Movement ratios compare well across the tests and the test results are in most cases within 10% of each other, which equates to about one boulder per size per test.

The two models are almost identical in the sense that their flow characteristics are identical. Obtaining comparable results between the two models should have been expected. The 2C model does have the disadvantage of a pier wall obstructing flow. The debris fin has dealt with the effect of the obstruction well and the advantage of the debris fin is that the disturbance in the flow is situated further upstream, away from the inlet.

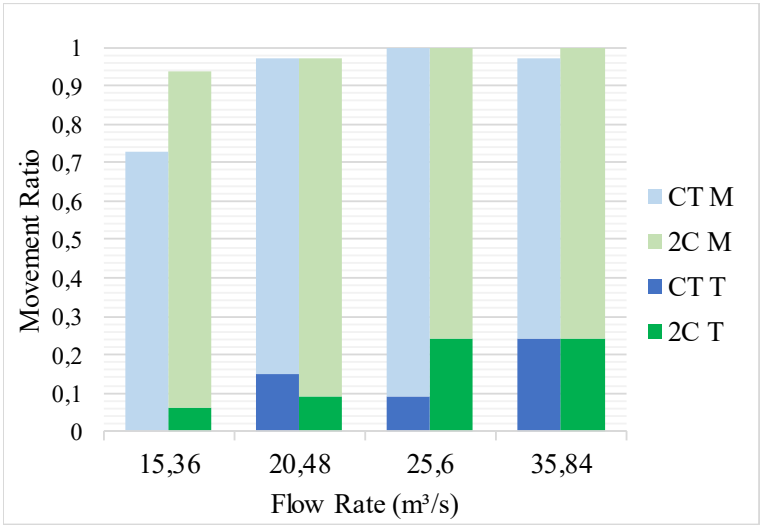

Figure 7.7: 0.424 m Results.

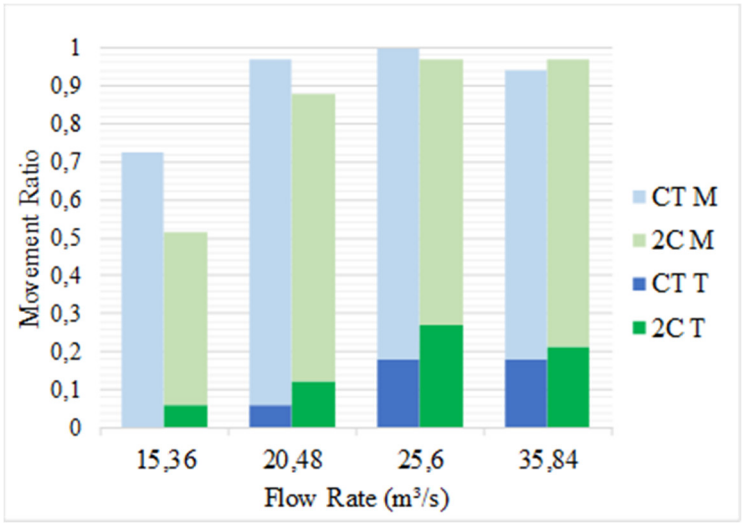

Figure 7.8: 0.6 m Results.

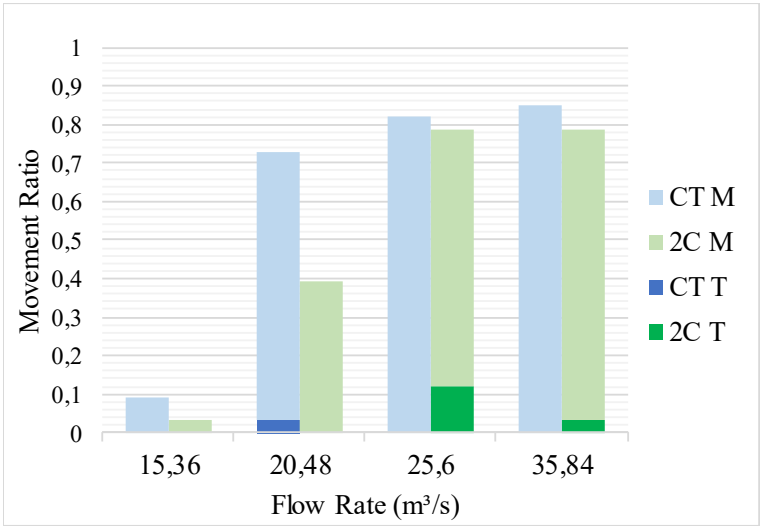

Figure 7.9: 0.8 m Results.

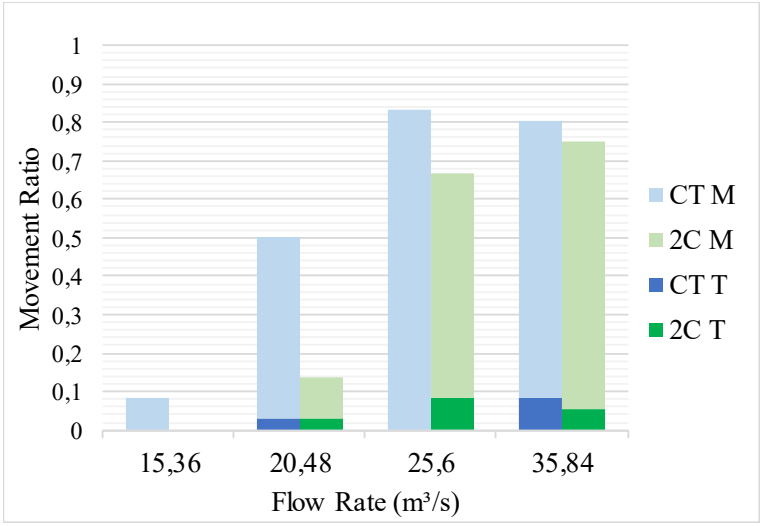

Figure 7.10: 1.01 m Results.

7.4.2. Three-Cell Compound Taper Experimental Model Results

Observations

The three-cell compound taper (3C-model) model did not perform as well as the CT and 2CT models. Boulders settled out multiple times during the design flow (Q_d = 85.575 m³/s) tests. **Figure 7.11** illustrates two observations made during the experimental tests. The first was the hydraulic jump that formed in the right-hand barrel, depicted by the S-curve shown and the second observation identified locations of secondary currents.

The design assumption stated that the control would form at the inlet lip (B_{lip}) of the taper and any particle that flows past the control will flow through the barrel. In this case for the 3C model, the design calculation showed that the control section was not of sufficient width to act as a control and it was assumed that the inlet would operate as anticipated. The assumption made was clearly incorrect and the design, therefore, calls for a control section upstream for the successful operation of the inlet.

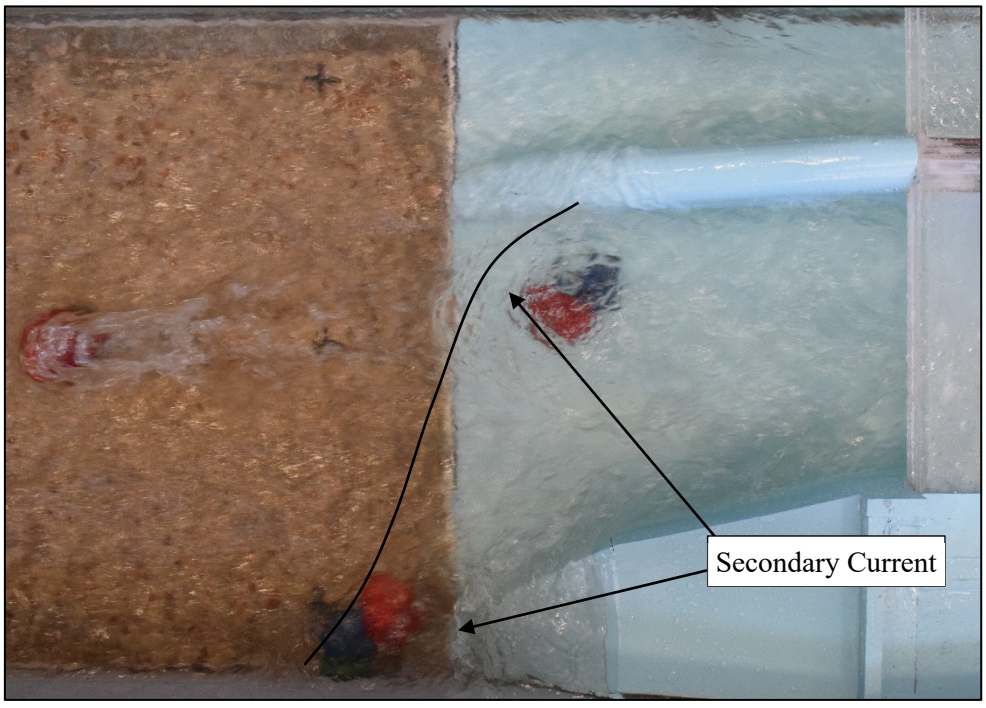

Figure 7.11: Three-cell CT culvert inlet observations.

The location of the hydraulic jump was such that continuous secondary currents formed, the secondary current flowed in an oscillating pattern across between an upstream and downstream location. The oscillation was visualised through the use of a dye to see the currents, illustrated in **Figure 7.12**. The effect of the current was that the boulders would become stationary in the current through the duration of the test run.

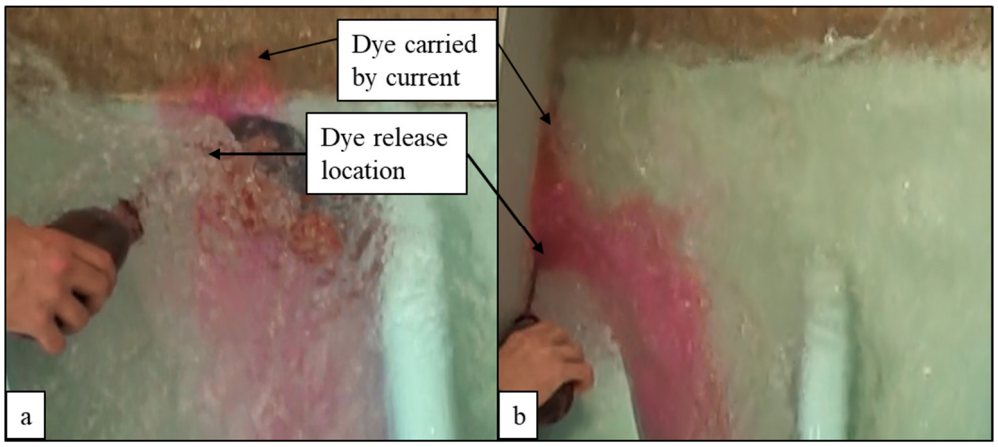

Figure 7.12: Movement of current capture by slow-motion camera and dye.

As the experimental model was unsuccessful due to the incorrect design assumptions the flow depths were not recorded.

Boulder Movement

Boulder movement test was performed for the 3C model with a solid debris fin. The flow rates tested were based on the design of the 3C inlet since the culvert had a design discharge of 85.575 m³/s, three times that of the tests performed thus far. **Table 7.6** shows the recorded results for the boulder movement. The post-processed results for each test of the 3C model are found in **Appendix G**.

Table 7.6: Boulder movement results for three cell culvert.

		Moved				Through			
	Boulder Size (mm):	**424**	**600**	**800**	**1008**	**424**	**600**	**800**	**1008**
	Total:	**26**	**37,5**	**50**	**63**	**26**	**37,5**	**50**	**63**
Flow Rate (Test Number) [m³/s]	30,72	10	8	0	0	9	60	0	0
	30,72 (2)	9	9	0	0	8	7	0	0
	30,72 (3)	9	8	0	0	8	3	0	0
	61,44	11	11	11	10	11	11	9	8
	61,44 (2)	11	11	10	10	11	11	9	7
	61,44 (3)	11	11	11	11	11	11	8	9
	85,575	11	11	11	12	11	11	10	11
	85,575 (2)	11	11	11	12	11	10	7	10
	85,575 (3)	11	11	11	12	11	11	10	11
	30,72 (Repeat)	11	7	0	1	9	4	0	0

Due to the design of the 3C model, the results obtained for the boulder movement tests were comparable to that of the tapered inlet discussed in **Section 6.4.3**. The lack of a hydraulic jump upstream of the inlet to cause damming resulted in most boulders that moved in the flume would be transported downstream. **Figure 7.13** illustrates that nearly 80% of all boulders that moved were transported downstream, as a similar trend seen by the results of the tapered inlet model. Interestingly, for each of the design flow

tests, at least one boulder settled out in the inlet or against the wing wall where the secondary currents were identified.

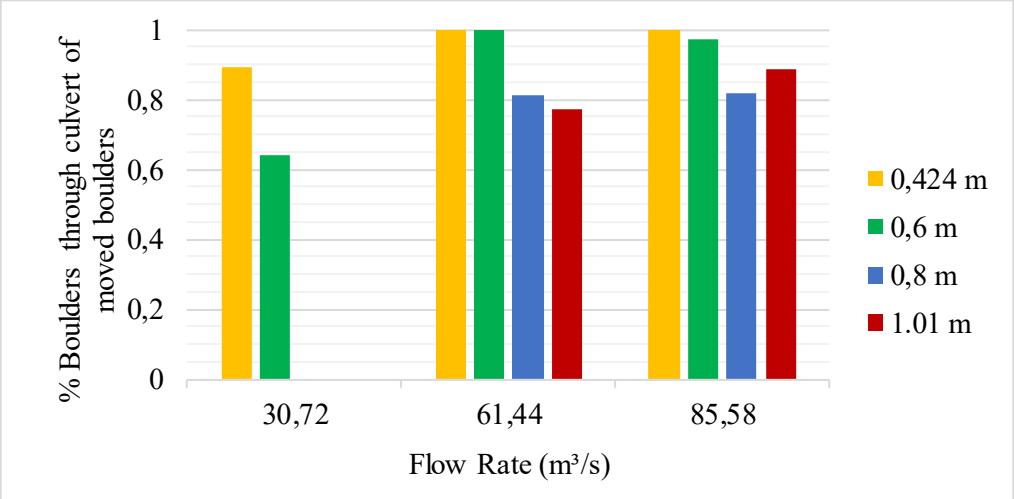

Figure 7.13: Boulder transport as a percentage of moved boulders.

7.5 Multi-Cell Experimental Tests Conclusion

Chapter 7 comprised the latter part of Phase II of the experimental tests. Multi-cell setups were designed for the optimal inlet identified in Chapter 6. A two- and three- cell culvert inlet was designed with the inclusion of two proposed debris fins. A notched fin and solid debris fin were considered for floating debris mitigation measures.

The two-cell culvert with the solid fin (2CS-model) performed similarly to the compound tapered (CT) model which the 2CS-model was based on. Since the 2CS-model was based on the CT-model the results were expected. The experimental tests revealed that lower flows that are competent to transport boulders would have a greater chance of transporting the boulders through the inlet.

Flow depth at the inlet and the hydraulic jump location determined whether a boulder would be deposited near the inlet. Higher flow rates deposited the boulders further upstream due to the upstream location of the hydraulic jump. As the flow increased further the force of the water was able to move the boulders into the vicinity of the inlet which led to an increase in boulder transport through the culvert.

Experimental tests on the notched debris fin on the 2C-model revealed that the notch resulted in an increase in flow depth due to the afflux around the culvert wall. The notched fin was considered not suitable for the high-velocity characteristics of the experimental model.

The solid debris fin performed well to align the flow with the barrel entrance. The performance under floating debris was not tested during the experimental procedure. However, floating debris has been

identified as a flooding risk hence their inclusion in the design. The fins also act as guides for the boulders to prevent deposition against the culvert wall. Some boulder deposits were noted at the nose of the fin, the fin is upstream of the control point, therefore boulders at that location were considered t acceptable.

The multi-cell setup proved that a control section is required at the taper lip to produce a culvert with boulder flushing capabilities. Deposition in the inlet taper took place at the design flow due to the formation of a hydraulic jump in the taper. While the multi-cell test was unsuccessful, an important condition was identified that needs to be met for the CT model to operate as designed.

8. Conclusion

A method had to be determined to mitigate blockages caused by boulders at culverts in mountainous streams. The study was limited to the Western Cape area to limit the type and the size boulder that was considered for the design. Streams in mountain areas are typically regarded as hydraulically steep and the maximum boulder size that had to be accommodated was a 1 m diameter boulder. Boulders sized between 0.424 m and 1.01 m was used in the study which typically represents the largest boulders found in the rivers, say the largest 15% of boulders found in the river.

The greatest challenge with the study was the lack of research surrounding boulder movement around culverts. Two field visits were carried out to two sites with known boulder problems. Data obtained from the field visits aided in the development of the experimental model layout and prototypes.

A model scaled, according to the Froude law similitude, to 1:16 was used for all the experimental models in the Hydraulics Laboratory of Stellenbosch University. The large scale and resulting Reynolds number allowed the use of linearly scaled rock to represent the boulder movement. A set of preliminary experimental tests were performed with a single 5 × 2 m (B × D) rectangular box culvert. To better simulate boulder movement an artificially roughened bed was developed to mimic the bed roughness of Site A. The aim of the preliminary tests was to be able to develop a model specific to a site, instead of having a fixed set of design parameters. A bed slope of 1:40 was determined to be sufficient to transport the boulders downstream at a discharge rate of 28.53 m^3/s with no culvert installed. However, the boulders settled upstream at the location of the hydraulic jump, the bed slope was adjusted until the boulders would deposit in close proximity to the culvert. A bed slops of 1:25 was determined. The remaining experimental procedures were tested at a bed slope of 1:25.

Experimental test results were recorded, and the MN was compared to the boundary of particle movement on the modified Lui diagram, equal to 0.012. Boulder movement results showed variability in accurately predicting the MN for the different boulder sizes. The absolute roughness parameter had a large influence on the MN of the boulders. A method to accurately estimate the movement of the largest boulders in a stream could not be found. Considering that the largest boulders present in the flow would need to be able to pass through the culvert, it was assumed that if the boulder is present in the stream then the flow has the competence to transport the boulder downstream.

Literature, field investigations and the preliminary experimental model identified the inlet as the location for potential boulder deposition. The study was focussed on mountain streams where approach flow would be supercritical and predominantly inlet controlled at the culvert. A desktop study was carried out to develop three inlet layouts. The two optimal inlet designs were selected based on practical and economic considerations and were constructed to be tested in the experimental model. The two inlet

designs tested were a tapered model (T-model) with a bed slope of 1:10 and contracting side walls of 1:2.88, and a compound tapered model (CT-model) with a short, steep sloping bed combined with a moderate sidewall taper of 1:4 as recommended by the literature.

Experimental tests revealed that the T-model was not suited for the steep flume with supercritical flow conditions since a shockwave formed that extended to the inlet of the barrel. At the confluence of the two shock waves, a standing wave formed which touched the soffit of the headwall at the design discharge. The boulder flushing capability of the T-model far exceeded that of the N- and CT-models. However, poor hydraulic performance made the model an unfeasible solution.

The CT-model produced an inlet that allowed boulders to settle out, either far enough upstream of the inlet or to be transported through the barrel of the culvert. The controlling inlet was effectively moved upstream to prevent boulders from settling out in entrance of the barrel. Between the new control section and barrel, the water was open to the air to allow the water to flow over the control in the event of a blockage. A discrepancy was identified between the measured and theoretical flow depths at the control section of the inlet. The measured flow depth at the control section differed by 38% with the theoretical depths, while the upstream and downstream flow depths measured within 5% of the calculated depths. A possible explanation for the discrepancy is that critical flow does not form at a fixed, known point but rather in the near vicinity of the theoretical control section. Critical depth could, therefore, occur slightly downstream of the control section.

The CT-model was selected as the optimal inlet of the models tested, further tests for a multi-cell application were carried out. A 2C- and 3C-model were developed each with a solid debris fin. A notched fin was tested with the 2C-culvert, however, the notch resulted in the flowing water hitting the round face of the culvert wall, resulting in a sudden flow depth increase at the barrel inlet.

Results from the 2C-model test were comparable to that of the CT-model for flow depth and boulder transport capability. The effect of the dividing wall was moved upstream to the control point, the inlet flow depth was therefore unaffected by the presence of a debris fin.

The three-cell model was tested by assuming symmetry in the flume, the model was tested without a control section forming upstream of the inlet. The test albeit unsuccessful highlighted the importance of establishing the control section upstream of the inlet. The contraction ratio between the upstream flow and the control point was not sufficient to control the flow. A hydraulic jump formed in the taper section which resulted in boulder deposition inside one of the inlet sections.

9. Guidelines to Mitigate Boulder Blockages at Culverts

The guidelines provided in this section are meant to be used as an extension of the existing guidelines on culvert design. Recommendations are only made based on the design of the inlet section of the culvert to mitigate boulder blockage. The barrel of the culvert should be sized according to the methods set out in Chapter 7 (Design of Lesser Culverts by Rooseboom and van Vuuren (2013b)) of the SANRAL Drainage Manual.

It is important to ensure that the barrel is large enough to accommodate the boulders present in the stream. The design size of the boulders would be the boulders found at the specific site.

The following design guidelines should be followed to design a compound tapered inlet (CT) to mitigate the potential for culvert blockages caused by boulders in steep streams:

- The barrel should be designed as an inlet-controlled structure with $H_1/D = 1.2$, once the barrel has been sized for the design discharge, the barrel size may not be changed to allow it to flow full.
- The barrel slope should be steeper than 1:50, ideally, the barrel slope should be the same slope as the stream where possible.
- A short transition of D/2 in length is added between the barrel and the inlet taper.
- L_T is equal to $2 \times D$.
- Sidewall taper from the barrel face to the control section should be between 1:4 and 1:6 (Schall *et al.*, 2012).
- The width of the control section is determined by the selected sidewall taper, the length of the taper section (recommended 2D) and the width of the barrel, $B_t = (2 \times \text{taper ratio} \times L_T) + B$.
- B_{lip} is determined graphically, the centre point of the arc can be found by extending the wing-wall to the centre of the barrel. The centre point from to the wing walls is the radius of the arc, the arc is drawn in between the two walls.
- The subcritically factor, λ, should not be larger than 1, the design aims for a λ of around 0.9, meaning the flow depth at the culvert barrel inlet will be $0.9y_c$.
- Assume critical flow on the taper lip, determine the critical flow depth.
- Check if the taper controls the flow by comparing the specific energy, E, of the normal upstream depth with the specific energy at the taper, E_c. The taper will control the flow if the upstream E is smaller than E_c.
- The elevation change, Δz, between the taper lip and the culvert barrel is obtained through the use of the energy equation (**Equation 2-1)** friction loss should be accounted for.

- The wall height at the taper is equal to the flow depth with freeboard included or the upstream damming depth without freeboard added, the highest wall is selected for the side walls.
- Freeboard must be included at the culvert barrel.
- If water run-up onto the roadway is expected provide sufficient balustrade walls. The balustrade should only be placed on the sidewall sections and not overt the culvert barrels.
- The downstream taper is equal to 1:3Fr, with the Froude number taken at the outlet.
- The wall height at the apron is equal to the flow depth with the required freeboard included.

For the multi-cell setup, the following adjustments are required:

- The debris fin width of 900 mm is included in the width of the culvert when determining the lip width, B_{lip}, for the hydraulic calculations, an effective B_{lip} width is used by subtracting the debris fin width.
- A typical debris fin angle for the face is 30° up to the height of y_d, and then joining the culvert wall at the freeboard height.
- The recommended debris fin shape is a round nose shape, as depicted in **Figure 9.1**.

Once the design has been completed the outlet apron is set to a zero slope, the remaining elevation is gained by setting the slope of the inlet apron upstream of the control level to zero. Discretion should be used not to specify an excessively long apron upstream. Check the outlet velocity for erosion protection.

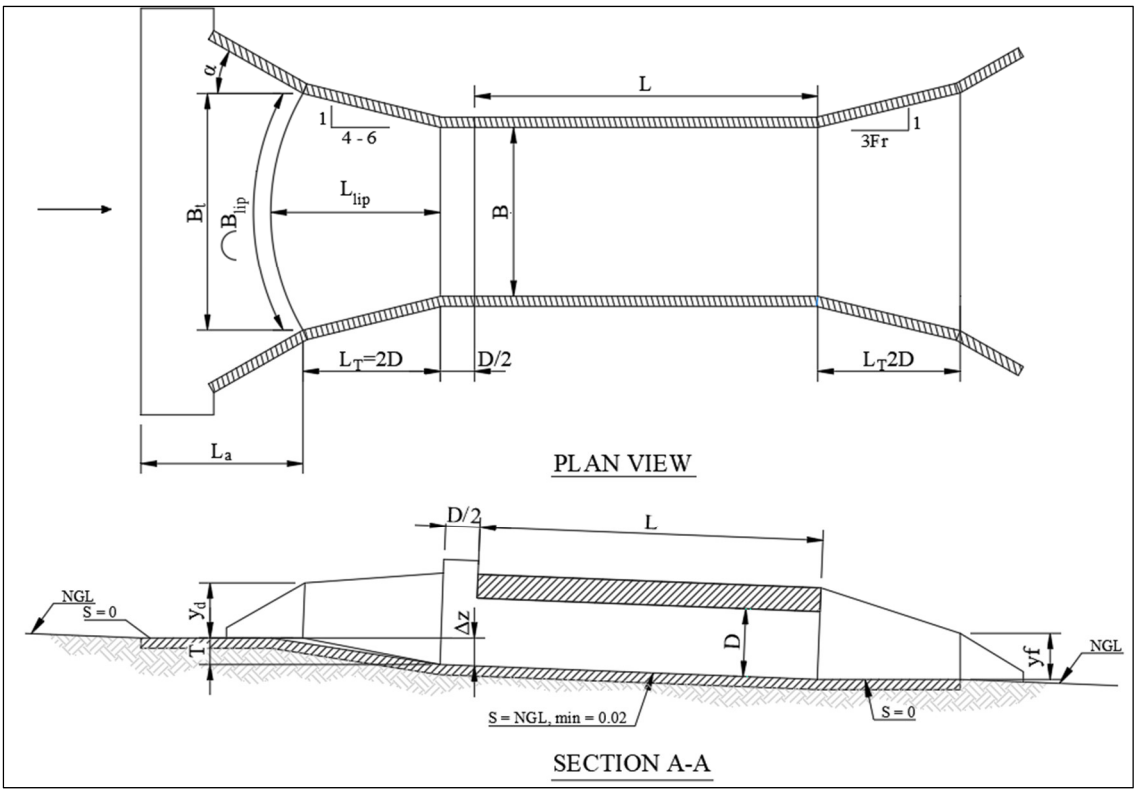

Figure 9.1: Schematic layout of the compound tapered inlet.

10. Future Research Recommendations

This study served as an introduction to boulder blockages at culverts. Only two inlets were tested under specific laboratory conditions. The following recommendations were made based on the challenges experienced during research or the breakthroughs achieved:

- A study is proposed into boulder blockages at culverts to study site-specific locations to determine what contributes to boulder blockages at culverts.
- The proposed CT-model should be redesigned according to a site-specific location where boulder blockages are considered a problem, the experimental model should consist of a movable bed to determine the scour potential upstream and downstream of the prototype. The effect of the level aprons should be tested under low flows for sedimentation concerns.
- Erosion protection measures at the outlet must be evaluated and the deposition patterns of boulders downstream of the structure investigated to determine if the boulder deposition just downstream of an outlet can influence the probability of upstream deposition.
- An investigation into the accuracy of a scaled boulder bed river in a lab environment would be beneficial for experimental models where non-uniform sediment or the coarse fraction of a movable bed is investigated.
- The proposed CT-inlet should be modelled by CFD software to determine the optimal shape of the inlet, the current design was derived and adapted from existing guidelines that serve a different purpose.
- Determining the optimal barrel slope to transport a given sized boulder would produce a design were the inlet can consist of a steeper section to prevent deposition at the inlet. At the same time, the design would reduce the risk of having culvert outlets below the natural ground level.

References

Apelt, C. J. (1983) Minimum Energy Culverts and Bridge Waterways, *Transactions of the Institution of Engineers*. Australia, CE 25(2), pp. 89–95

Armitage, N. (2002) *A unit stream power model for the prediction of local scour*. Stellenbosch University. Available at: http://scholar.sun.ac.za/handle/10019.1/52716.

Baker, V. R. and Ritter, D. F. (1975) Competence of rivers to transport coarse bedload material, *Geological Society of America Bullein*, 86(7), pp. 975–978. doi: 10.1130/0016-7606(1975)86<975:CORTTC>2.0.CO;2.

Balkham, M., Fosbeary, C., Kitchen, A. and Rickard, C. (2010) *Culvert Design and Operation Guide*. CIRIA

Basson, G. R. (2005) *Considerations for the design of river abstraction works in South Africa*. Available at: http://www.wrc.org.za/wp-content/uploads/mdocs/TT 260-06.pdf.

Bathurst, J. C. (1987) Critical Conditions for Bed Material Movement in Steep, Boulder-bed Streams, in *Erosion and Sedimentation in the Pacific Rim*. Wallingford: International Association of Hydrologgical Sciences, pp. 309–318

Blom, A., Ribberink, J. S. and De Vriend, H. J. (2003) Vertical sorting in bed forms: Flume experiments with a natural and a trimodal sediment mixture, *Water Resources Research*, 39(2), pp. 1–13. doi: 10.1029/2001WR001088.

Bradley, W. C. and Mears, A. I. (1980) Calculations of flows needed to transport coarse fraction of Boulder Creek alluvium at Boulder, Colorado, *Geological Society of America Bulletin*, 91(3 Part II), pp. 1057–1090

Breusers, H. N. C. (1974) Lecture notes on Sediment transport 1, in *International Course In Hydraulic Engineering*. Delft, p. 75

Buffington, J. . and Montgomery, D. . (2013) Geomorphic Classification of Rivers, in Shroder, J. and Wohl, E. (eds) *Treatise on Geomorphology*. San Diego: Academic Press, pp. 730–767. Available at: http://dx.doi.org/10.1016/B978-0-12-374739-6.00263-3.

Bunte, K., Abt, S. R., Swingle, K. W., Cenderelli, D. A. and Schneider, J. M. (2013) Critical Shields values in coarse-bedded steep streams, *Water Resources Research*, 49(11), pp. 7427–7447. doi: 10.1002/2012WR012672.

Carling, P. A. (1995) Flow-seperation berms downstream of a hydraulic jump in a bedrock channel, *Geomorphology*, II, pp. 245–253

Carling, P. A., Hoffmann, M. and Blatter, A. S. (2002) Initial Motion of Boulders in Bedrock Channels, *Water Science and Application*, 5, pp. 147–160. doi: 10.1029/ws005p0147.

Chadwick, A., Morfett, J. and Borthwick, M. (2013) *Hydraulics in Civil and Environmental Engineering*. 5th edn. Boca Raton: CRC Press

Chanson, H. (2003) History of minimum energy loss weirs and culverts 1960-2002, in *Proc. 30th IAHR Congress, Thessaloniki*. Thessaloniki, pp. 65–73

Chanson, H. (2004) *The Hydraulics of Open Channel Flow: An Introduction*. 2nd edn, *Elsevier Butterworth-Heinemann*. 2nd edn. Oxford: Elsevier Butterworth-Heinemann

Chow, V. Te (1959) *Open Channel Hydraulics*. 1st edn. New York: McGraw-Hill

Concha, F. (2009) Settling velocities of particulate systems, *KONA Powder and Particle Journal*. Concepción, Chile, 27, pp. 18–37. doi: 10.1016/s0301-7516(99)00017-4.

CPAA (2012) *Hydraulics of Precast Concrete Conduits Hydraulics of Precast Concrete Conduits*. 5th edn

Cullis, J., Gazendam, M., Rooseboom, A. and Ractliffe, G. (2008) *The development of a hydraulic model for determining bed disturbance due to floods in cobble and boulder bed rivers*. Pretoria

Defina, A. and Viero, D. Pietro (2010) Open channel flow through a linear contraction, *Physics of Fluids*, 22(3), pp. 2–13. doi: 10.1063/1.3370334.

Gazendam, M. (2005) Incipient motion in cobble/boulder bed rivers, (December), p. 148

Gill, T. W. and Pugh, C. A. (2009) Sediment transport similitude for scaled physical hydraulic modeling, in *33rd IAHR Congress: Water Engineering for a Sustainable Environment*. Vancouver, BC

Gross, A., Molinas, A. and Mertes, P. (2019) Chapter 11 ENERGY DISSIPATORS, in Gross, A. and Molinas, A. (eds) *Drainage Design Manual*. Colorado Department of Transportation, pp. 1–30

Hee, M. (1969) Hydraulics of culvert design including constant energy concept, in *Proceedings of the 20th Conference of Local Authority Engineers*. Queensland, Australia: Department of Local Government, pp. 1–27

Henderson, F. M. (1966) *Open Channel Flow*. 1st edn. Edited by G. Nordy. New York: Macmillan Publishing Co.,Inc.

Ho, H. (2010) *Investigation of unsteady and non-uniform flow and sediment transport characteristics at culvert sites*. University of Iowa. doi: https://doi.org/10.17077/etd.zp388rmo.

Hydraulics Department, S. U. (2014) Experimental study on Pier Width for Debris Mitigation

Jansen Van Vuuren, A. ., Rooseboom, A. and Kruger, E. J. (2013) Bridges and Culverts, in Kruger, E., Van Vuuren, N., Gomes, N., and van Dijk, M. (eds) *Drainage Manual*. 6th edn. Pretoria: South African National Roads Agency SOC Ltd., pp. 8-1:8-51

Jones, J., Kerenyi, K. and Stein, S. (2006) *Effects of inlet geometry on hydraulic performance of box culverts*. Georgetown. Available at: http://trid.trb.org/view.aspx?id=807194.

Keller, R. J. and Winston, F. B. (2005) MELS User Guide. Catchment Hydrology, p. 42

King, H. (2007) *Investigation into runoff from the Horlosiekloof, De Doorns*

Langmaak, K. R. (2013) *Incipient Motion of Riprap on Steep Slopes*. Stellenbosch University. Available at: http://scholar.sun.ac.za/handle/10019.1/85816.

Macdonald, R. G. (2012) *Flow and sediment transport at hydraulic jumps*, *School of Environmental Sciences*

Metzler, D. E. and Rouse, H. (1959) *Hydraulics of Box Culverts*

Mizuyama, T. (2008) Sediment hazards and SABO works in Japan, *International Journal of Erosion Control Engineering*, 1, pp. 1–4. doi: 10.13101/ijece.1.1.

Munson, B. R., Young, D. F., Okiishi, T. H. and Huebsch, W. W. (2009) *Fundamentals of fluid mechanics*. 6th edn. Edited by M. Owens, J. Welter, L. Sapira, and S. Dumas. Hoboken: John Wiley & Sons, Inc.

National Geospatial Institute (2019a) *CDNGI Geospatial Portal*. Available at: http://www.cdngiportal.co.za/cdngiportal/ (Accessed: 23 September 2019).

National Geospatial Institute (2019b) *Trignet Sensor Map*. Available at: http://www.trignet.co.za/Map/SensorMap.aspx (Accessed: 23 September 2019).

Peakall, J. and Warburton, J. (1996) Surface tension in small hydraulic river models - the significance of the Weber number, *Journal of Hydrology (New Zealand)*, 35(2), pp. 199–212. Available at: http://www.jstor.org/stable/43944772.

Raudkivi, A. J. (1998) *Loose Boundary Hydraulics*. Balkema, A. A.

Robertson, J. M. and Rouse, H. (1941) On the four regimes of open-channel flow, *Civil Engineering*, 11(3), pp. 169–171

Rooseboom, A. and Van Vuuren, S. . (2013a) Hydraulic Calculations, in Kruger, E., Gomes, N., Van Vuuren, F., and van Dijk, M. (eds) *Drainage Manual*. 6th edn. Pretoria: South African National Roads Agency SOC Ltd., pp. 4-1:4-36

Rooseboom, A. and Van Vuuren, S. . (2013b) Lesser Culverts (and Stormwater Conduits), in Kruger, E., Van Vuuren, F., Gomes, N., and van Dijk, M. (eds) *Drainage Manual*. 6th edn. Pretoria: South African National Roads Agency SOC Ltd., pp. 7-1:7-18

Rooseboom, A. and Van Vuuren, S. . (2013c) Surface Drainage, in Kruger, E., Gomes, N., Van Vuuren, F., and van Dijk, M. (eds) *Drainage Manual*. 6th edn. Pretoria: South African National Roads Agency SOC Ltd., pp. 5–1:5:50

Schall, J. D., Thompson, P. L., Zerges, S. M., Kilgore, R. T. and Morris, J. L. (2012) *Hydraulic design of highway culverts*, *Hydraulic Design Series N° 5*. Fort Collins, Colorado

Shields, A. (1936) *Application of similarity principles and turbulence research to bed-load movement*. Berlin

Simões, F. J. M. (2014) Shear velocity criterion for incipient motion of sediment, *Water Science and Engineering*. Hohai University. Production and hosting by Elsevier B.V., 7(2), pp. 183–193. doi: 10.3882/j.issn.1674-2370.2014.02.006.

Simons, D. B. and Senturk, F. (1992) *Sediment Transport Technology*. Littleton, Colorado, USA: Water Resource Publications

Stockstill, R. L. (2006) *Hydraulic Design of Channels Conveying Supercritical Flow*, *Urban Flood Damage Reduction and Channel Restoration Demonstration Program for Arid and Semi-Arid Regions*. Vicksburg. Available at: http://www.dtic.mil/dtic/tr/fulltext/u2/a454871.pdf.

Stoffberg, F. (2005) *Evaluation of the incipient motion criteria for rock in reno mattress and rip rap*. Stellenbosch University. Available at: http://scholar.sun.ac.za/handle/10019.1/3004.

Thompson, P. L. and Kilgore, R. T. (2006) *Hydraulic design of energy dissipators for culverts and channels.*, *Hydraulic Engineering Circular No. 14*. Arlington: Federal Highway Administration

Tooley, G. A. (2017) Catchment Co-ordinated Interventions Related to Stormwater Managemnet, in. Stellenbosch, pp. 1–30

Trimble (2013) Trimble R4 GNSS System Datasheet

Tulsi, K. R. and Schoonees, P. J. S. (2016) *Three dimensional method for monitoring damage to dolos breakwaters*. Stellenbosch University. Available at: http://scholar.sun.ac.za/handle/10019.1/100122.

USBR (1987) *Design of Small Dams*. 3rd edn. Water Resource Technical Publication

Wargo, R. S. and Weisman, R. N. (2007) A comparison of single-cell and multicell culverts for stream crossings, *Journal of the American Water Resource Association*, 04126, pp. 989–995

Webber, N. B. (1971) *Fluid Mechanics for Civil Engineers*. 1st edn. London: Chapman and Hall

Weisstein, E. . (2019a) *Circular Sector*, *Mathworld*. Available at: http://mathworld.wolfram.com/CircularSector.html (Accessed: 14 May 2019).

Weisstein, E. . (2019b) *Kite*. Available at: http://mathworld.wolfram.com/Kite.html (Accessed: 14 May 2019).

Wellman, J. C., Combs, D. L. and Cook, S. B. (2000) Long-term impacts of bridge and culvert construction or replacement on fish communities and sediment characteristics of streams, *Journal of Freshwater Ecology*, 15(3), pp. 317–328. doi: 10.1080/02705060.2000.9663750.

Appendix A: Field Research Photographs

Site A

Individual boulder laying above rest of bed material, diameter of approximately 500mm.

Distribution of large mobile boulders in bed in the upper reaches of the stream.

Downstream view of stream showing the wide grading of bed material ranging from large boulders to sand.

Upstream view of excavated channel just upstream of road crossing. Steep side slopes has potential to introduce boulders into stream before incipient motion on the bed can take place.

Large floating debris in excess of 2 m on bed the of the stream. Increases potential for additional blockages.

Overgrown culverts (450 mm diameter concrete pipe) and filled with fine sediment reduces flow capacity.

Site B

Overgrown riverbanks provide large quantities of floating debris to the stream. Dead plant material flows downstream and accumulates around the piers.

Severe debris accumulation experienced at bridge pier. Accumulation reduces available flow capacity and reduces flow velocity just downstream of the accumulation increasing the potential for sediment deposition.

Scour experienced against each wing wall, the whole wing wall up to the wall foundation is exposed.

Floating debris deposited inside the centre span, additional deposition took place due to the accumulation around the pier. The accumulation extends approximately 12 m into the span.

Abrasion caused by the high volume of coarse sediment transported through the bridge.

Sand deposition inside the centre span caused by the accumulation around the pier. The presence of the fine sediment indicates the reduced flow velocity caused by the debris accumulation. The Accumulation could contribute to boulder deposition due to the reduced flow velocity.

Diverging ratio of the point bar away from the left span is approximately 1:3. The ratio of the point bar could indicate the spread of the water out of the left span.

Visual comparison between a partially blocked span and an open span. The left span is blocked by a combination of boulders and debris reducing the available flow area by approximately 50%.

Appendix B: Rock Properties and Settling Test Results

Table B - 1: Site A - Rock density results.

Sample No	Weight (g)	H 0 (mm)	H 1 (mm)	Δ H (mm)	Density (kg/m³)	Sample No	Weight (g)	H 0 (mm)	H 1 (mm)	Δ H (mm)	Density (kg/m³)
1	7,185	131	194	63	2585,23	16	2,64	126,5	149	22,5	2659,71
2	4,684	131	171	40	2654,42	17	2,656	126,5	149,5	23	2617,66
3	3,948	131	165	34	2632,16	18	2,556	126	148	22	2633,61
4	3,388	130	160	30	2559,97	19	1,752	126	141	15	2647,62
5	1,786	130	146	16	2530,32	20	4,032	126	160,5	34,5	2649,20
6	3,676	122	154	32	2603,99	21	4,942	125	167	42	2667,27
7	2,37	130	153	23	2335,79	22	1,762	125	139	14	2852,93
8	2,756	129	152	23	2716,22	23	2,266	124,5	144	19,5	2634,14
9	4,098	129	165	36	2580,38	24	3,142	124,5	151,5	27	2637,88
10	2,264	128,5	148	19,5	2631,81	25	1,596	124	138	14	2584,15
11	4,394	128	165,5	37,5	2656,09	26	2,602	124	146	22	2681,01
12	6,455	128	183	55	2660,40	27	1,664	123	138	15	2514,64
13	3,688	127,5	160	32,5	2572,30	28	2,848	122,5	148	25,5	2531,71
14	3,802	127	160	33	2611,63	29	2,196	122,5	142	19,5	2552,77
15	2,842	127	151	24	2684,27	30	4,026	122	157	35	2607,47

Table B - 2: Settling Test Results - 26.5 mm Rock.

No.	Triaxial Dimensions			SF	ΔT (s)	V_{ss} (s)	Cd	Re
	a	b	c					
1	31	28	27	0,92	5,89	0,866	0,80	21 267
2	35	27,5	22	0,71	6,94	0,735	1,10	17 727
3	36	29	24	0,74	–	–	–	–
4	34	33	20	0,60	6,21	0,821	1,05	23 773
5	33	28,5	19	0,62	7,65	0,667	1,38	16 667
6	31	29	21	0,70	6,36	0,802	0,97	20 399
7	44	30,5	19	0,52	8,05	0,634	1,64	16 950
8	32	30	24,6	0,79	–	–	–	–
9	34	31	24,5	0,75	6,07	0,840	0,95	22 847
10	36,5	32	23	0,67	6,54	0,780	1,13	21 890
11	34,8	29	21	0,66	6,49	0,786	1,01	19 990
12	30	28	27	0,93	6,09	0,837	0,86	20 569
13	38	33	22	0,62	6,3	0,810	1,08	23 434
14	38	31	18,5	0,54	7,98	0,639	1,63	17 379
15	41	28	27	0,80	6,48	0,787	0,97	19 331
16	42	32	24	0,65	6,29	0,811	1,05	22 760
17	37	31,5	19	0,56	6,43	0,793	1,08	21 916
18	38,5	35	20,5	0,56	6,43	0,793	1,20	24 351
19	37	32	19,5	0,57	7,15	0,713	1,35	20 022
20	34	30	20	0,63	–	–	–	–
21	43	27	22	0,65	6,81	0,749	1,04	17 737
22	34	32	24,5	0,74	6,1	0,836	0,99	23 469
23	36	28	27	0,85	5,76	0,885	0,77	21 747
24	44	32,2	22	0,58	7,18	0,710	1,37	20 063
25	34	26,5	25	0,83	6,15	0,829	0,83	19 277
26	39	31	22	0,63	6,8	0,750	1,19	20 395
27	36	34	24	0,69	6,75	0,756	1,28	22 534
28	39	31	21	0,60	7	0,729	1,26	19 812
29	37	26	22	0,71	5,83	0,875	0,73	19 951
30	42	27	22	0,65	7,9	0,646	1,39	15 290
		Average =		0,68	6,65	0,77	1,11	20 428

Table B - 3: Settling Test Results - 37.5 mm Rock.

No.	Triaxial Dimensions			SF	ΔT (s)	V_{ss} (s)	Cd	Re
	a	b	c					
1	40	37,5	19	0,49	–	–	–	–
2	39	35	19,5	0,53	7,98	0,639	1,84	19 621
3	51	39	32	0,72	6,53	0,781	1,38	26 719
4	41	34	25	0,67	–	–	–	–
5	48	35	32	0,78	–	–	–	–
6	44	34,9	31	0,79	5,9	0,864	1,01	26 463
7	41	34	30,2	0,81	6,27	0,813	1,11	24 259
8	48,5	31	31	0,80	6,33	0,806	1,03	21 909
9	48	37,5	24	0,57	7,53	0,677	1,76	22 279
10	48	37	29,5	0,70	6,84	0,746	1,43	24 200
11	52,5	35	26	0,61	–	–	–	–
12	48	39,5	36	0,83	5,3	0,962	0,92	33 342
13	45	41	37	0,86	5,11	0,998	0,89	35 895
14	43	38,8	34,5	0,84	–	–	–	–
15	49	38	26,5	0,61	5,25	0,971	0,87	32 381
16	40,5	31	28	0,79	–	–	–	–
17	43	37	20,5	0,51	7,43	0,686	1,69	22 278
18	42	33	24	0,64	6,92	0,737	1,31	21 334
19	45,5	41	23	0,53	6,83	0,747	1,58	26 855
20	47	46	35	0,75	–	–	–	–
21	41	41	29	0,71	5,38	0,948	0,98	34 093
22	57	40	37	0,77	5,32	0,959	0,94	33 637
23	53,8	37,5	27	0,60	6,21	0,821	1,20	27 015
24	46,5	40,8	35	0,80	–	–	–	–
25	55	41	30	0,63	5,51	0,926	1,03	33 289
26	52	43	27	0,57	5,65	0,903	1,14	34 048
27	55	44	28	0,57	5,82	0,876	1,23	33 822
28	58	44	32,6	0,65	6,12	0,833	1,36	32 164
29	51	36	29	0,68	6,02	0,847	1,08	26 753
30	57	45	34,5	0,68	5,44	0,938	1,10	37 007
		Average =		0,68	6,17	0,84	1,22	28 607

Table B - 4: Settling Test Results - 50 mm Rock.

No.	Triaxial Dimensions			SF	ΔT (s)	V_{ss} (s)	Cd	Re
	a	b	c					
1	62	54	32	0,55	5,5	0,927	1,35	43 923
2	56	48,6	45,8		–	–	–	–
3	66	55	43	0,71	6,5	0,785	1,92	37 854
4	68	59	39,5	0,62	7,5	0,680	2,75	35 193
5	62	56	30		–	–	–	–
6	67	54	39	0,65	8,5	0,600	3,23	28 421
7	67	45	38	0,69	9,5	0,537	3,36	21 191
8	64	48	30	0,54	10,5	0,486	4,38	20 451
9	56	47	30	0,58	11,5	0,443	5,14	18 284
10	65	43	42	0,79	12,5	0,408	5,56	15 389
11	61	54	40,5	0,71	–	–	–	–
12	75	59	43	0,65	13,5	0,378	8,90	19 552
13	68	54,5	53	0,87	14,5	0,352	9,48	16 815
14	62,5	49	40	0,72	15,5	0,329	9,74	14 143
15	80	55	47	0,71	–	–	–	–
16	66	64	39	0,60	16,5	0,309	14,42	17 352
17	67	55	47	0,77	–	–	–	–
18	69	61	39,5	0,61	–	–	–	–
19	68	49,5	39	0,67	24,5	0,208	24,58	9 039
20	65	56	48	0,80	–	–	–	–
21	71	59	46	0,71	17,5	0,291	14,95	15 083
22	66	58	44,8	0,72	18,5	0,276	16,42	14 026
23	71	53	49,5	0,81	–	–	–	–
24	67	61	37	0,58	19,5	0,262	19,19	13 995
25	55,2	52	32	0,60	–	–	–	–
26	71	55	50	0,80	20,5	0,249	19,12	12 003
27	77	52	37	0,58	–	–	–	–
28	57	49	42	0,79	23,5	0,217	22,39	9 328
29	73	59	37	0,56	21,5	0,237	22,57	12 277
30	63,5	57	46	0,76	22,5	0,227	23,88	11 333
		Average =		0,69	15,00	0,41	11,67	19 283

Table B - 5: Settling Test Results - 63 mm Rock.

No.	Triaxial Dimensions			SF	ΔT (s)	V_{ss} (s)	Cd	Re
	a	b	c					
1	84	58,6	37	0,53	6,34	0,804	1,95	41 350
2	82	64	49	0,68	26,34	0,194	36,74	10 870
3	77,5	60	51	0,75	–	–	–	–
4	68	59	39,5	0,62	–	–	–	–
5	76	70	44	0,60	–	–	–	–
6	72	55	54	0,86	7,34	0,695	2,45	33 522
7	84	71	40	0,52	–	–	–	–
8	72	64	58	0,85	–	–	–	–
9	85	62	45	0,62	8,34	0,612	3,57	33 258
10	83	70	56	0,73	9,34	0,546	5,05	33 529
11	93	69	57	0,71	10,34	0,493	6,10	29 853
12	90	68	55	0,70	–	–	–	–
13	81	64	43	0,60	11,34	0,450	6,81	25 248
14	69	65	44	0,66	12,34	0,413	8,19	23 565
15	70	65	56	0,83	13,34	0,382	9,57	21 798
16	73	59	56	0,85	25,34	0,201	31,35	10 416
17	87	67	60	0,79	–	–	–	–
18	82	61	52	0,74	14,34	0,356	10,38	19 030
19	75	64	55	0,79	–	–	–	–
20	95	65	56	0,71	15,34	0,332	12,66	18 956
21	88	70,5	58	0,74	–	–	–	–
22	104	59	59	0,75	16,34	0,312	13,03	16 153
23	74	68	62	0,87	17,34	0,294	16,92	17 544
24	71	66	56	0,82	18,34	0,278	18,37	16 099
25	71	62	43	0,65	19,34	0,264	19,19	14 342
26	82	69	49	0,65	20,34	0,251	23,62	15 176
27	99	64,5	55	0,69	21,34	0,239	24,30	13 522
28	96	63	50	0,64	22,34	0,228	26,01	12 616
29	75	64	46	0,66	23,34	0,219	28,85	12 267
30	95	61	61	0,80	24,34	0,210	29,90	11 212
		Average =		0,71	16,34	0,37	15,95	20 492

Appendix C: Design Drawings

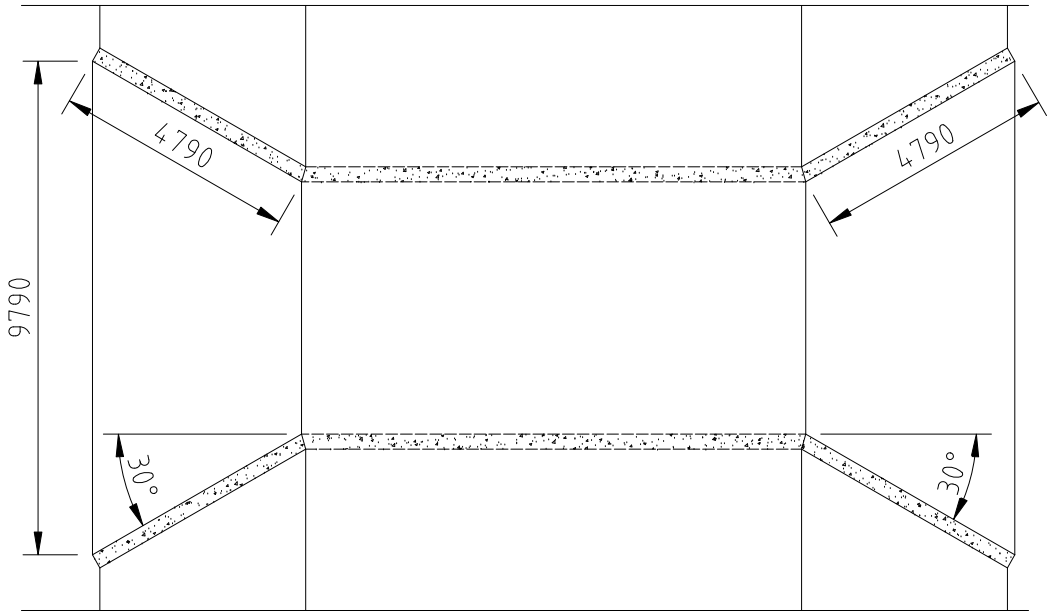

PLAN VIEW

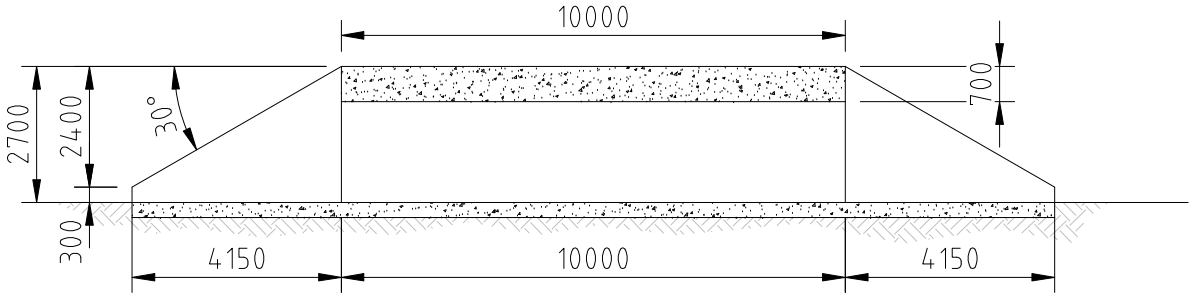

SECTION VIEW

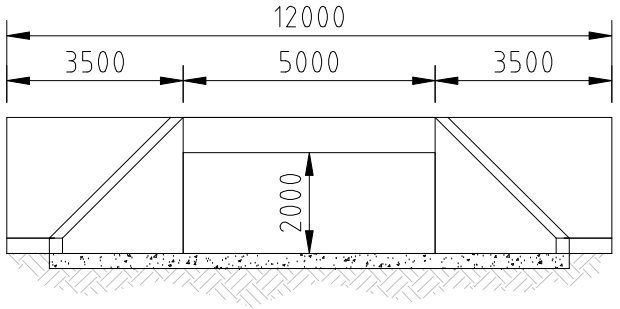

FRONT VIEW

5x2m RECTANGULAR CULVERT - PROTOTYPE	
	SCALE: 1:150
	12/07/2019

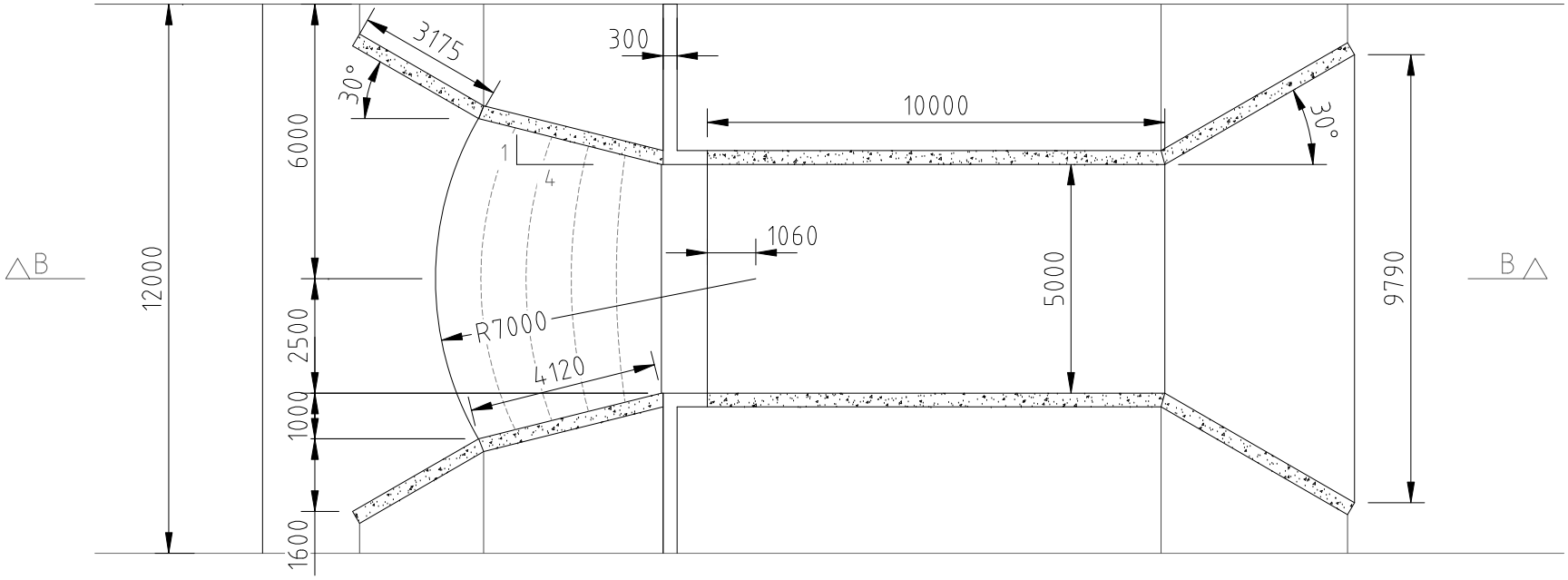

PLAN VIEW

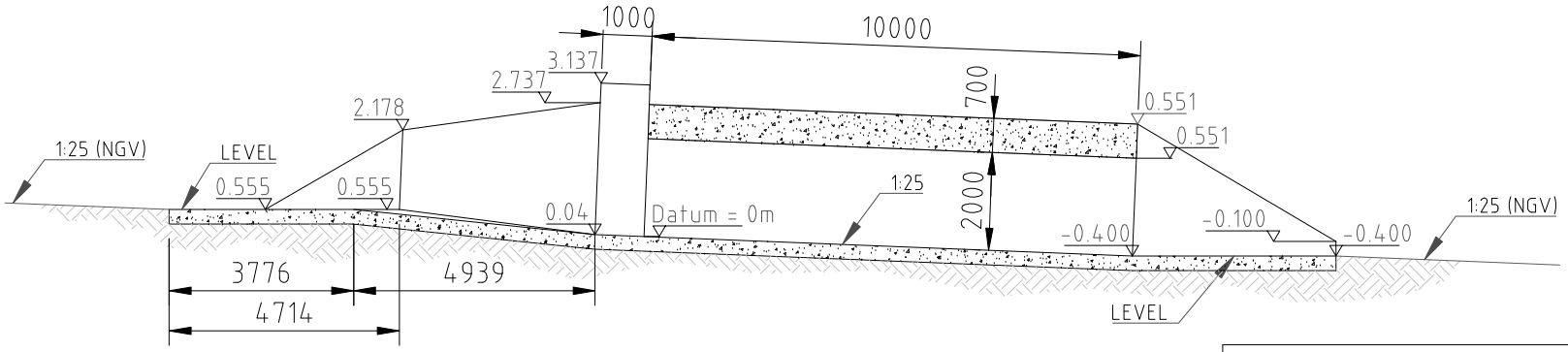

SECTION A-A

NOTE: Elevations shown in meter above the datum
Dimensions shown in millimeter (mm).

COMPOUND TAPER INLET - PROTOTYPE

SCALE: 1:150

09/06/2019

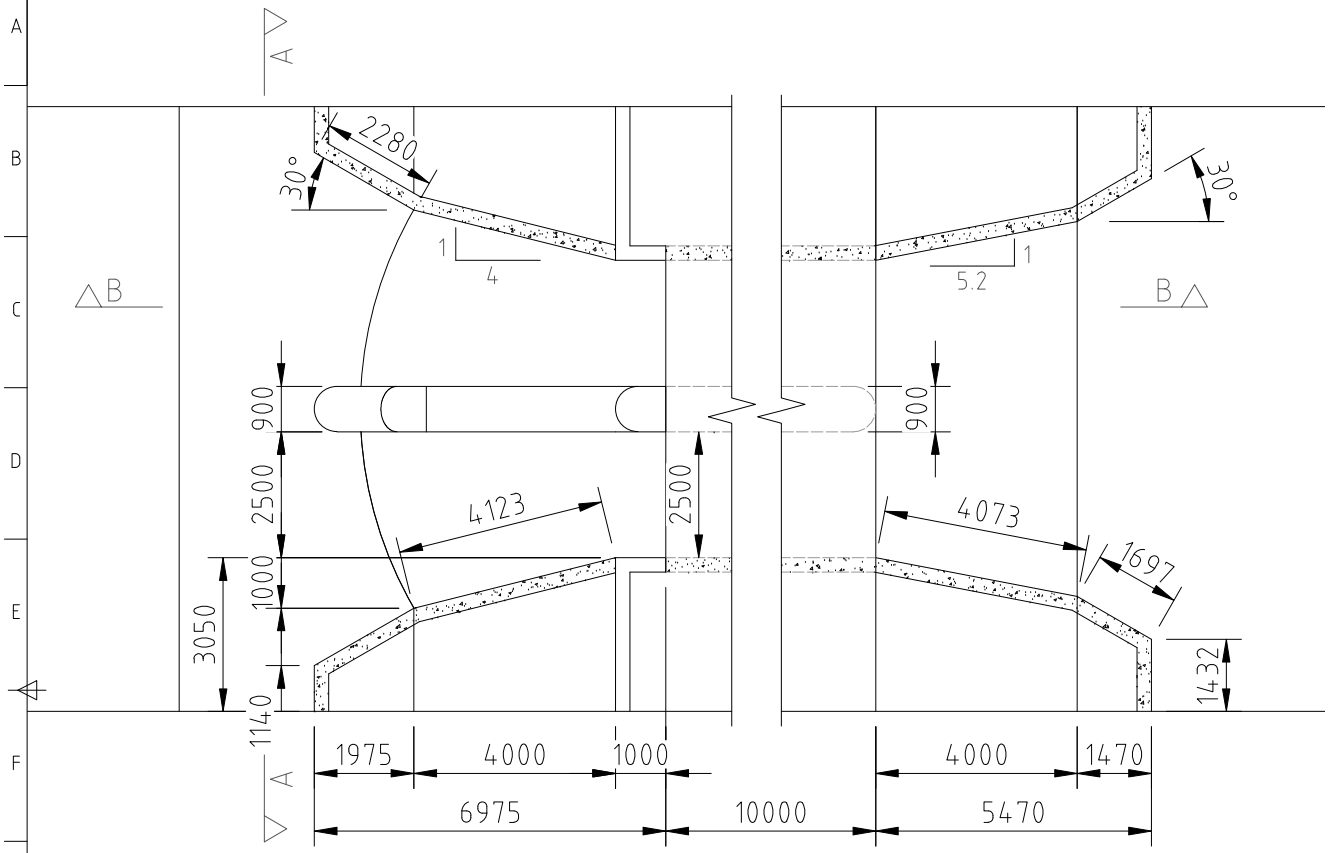

PLAN VIEW

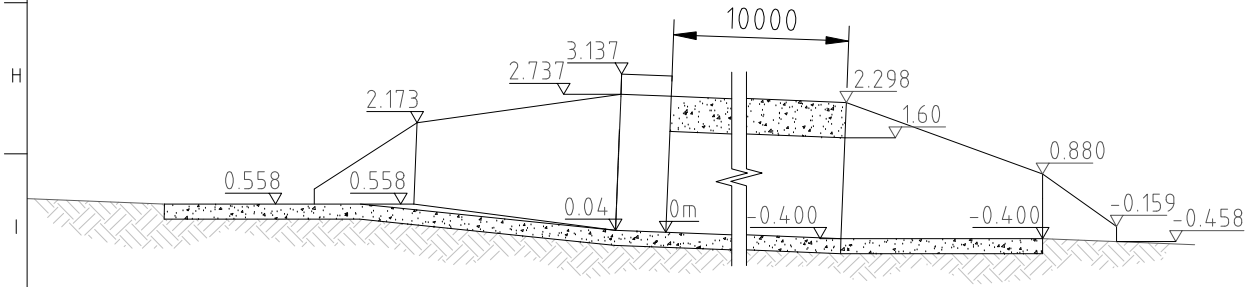

SECTION A-A

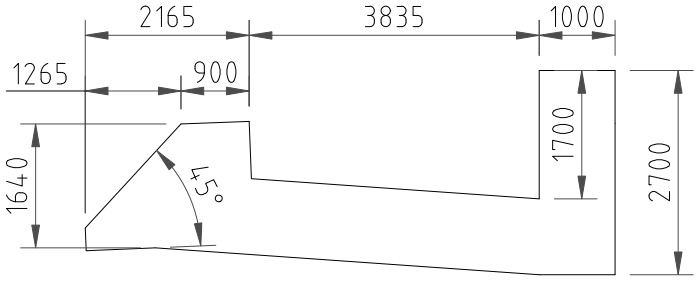

NOTCHED DEBRIS FIN 45° NOSE

Scale: 1:100

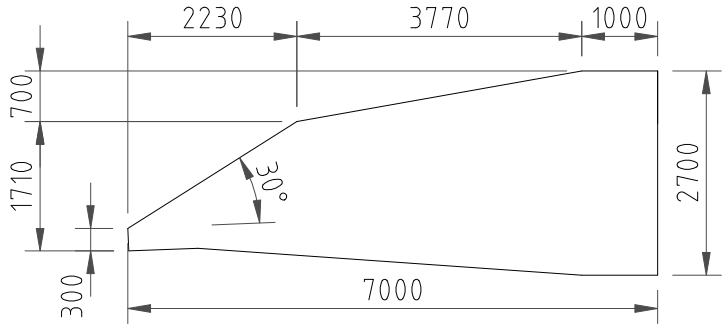

SOLID DEBRIS FIN 30° NOSE

Scale: 1:100

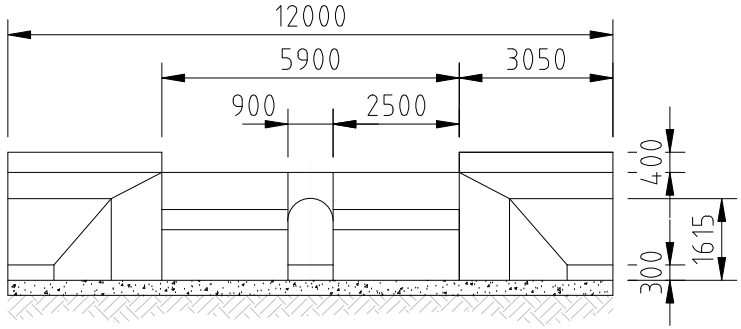

FRONT VIEW: SECTION B-B

NOTE: Elevations shown in meter above the datum
Dimensions shown in millimeter (mm).

TWO BARREL SETUP - PROTOTYPE

SCALE: 1:150

12/07/2019

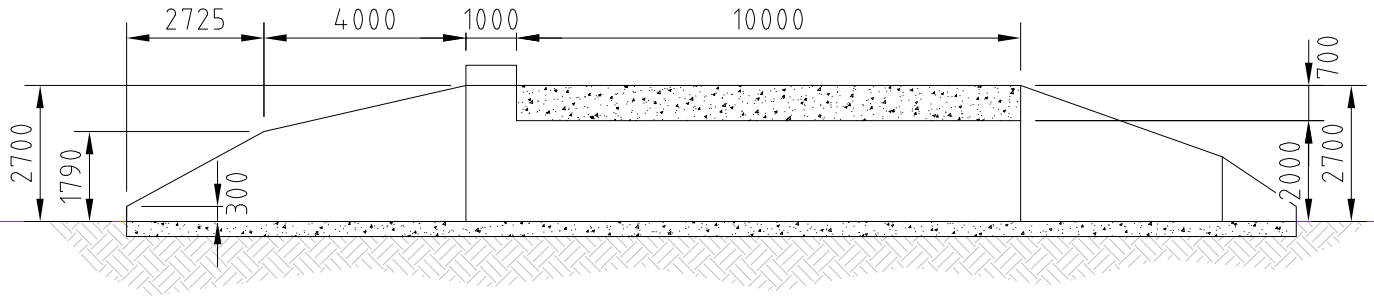

SECTION A-A: SOLID
DEBRIS FIN

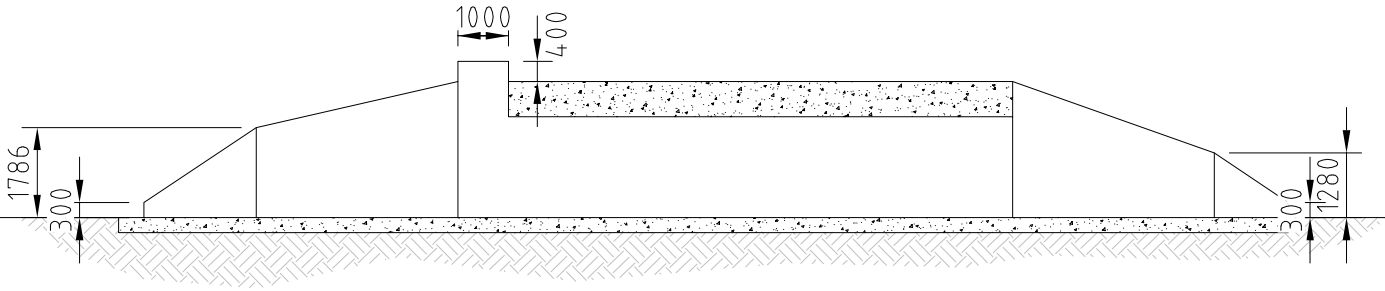

SECTION B-B

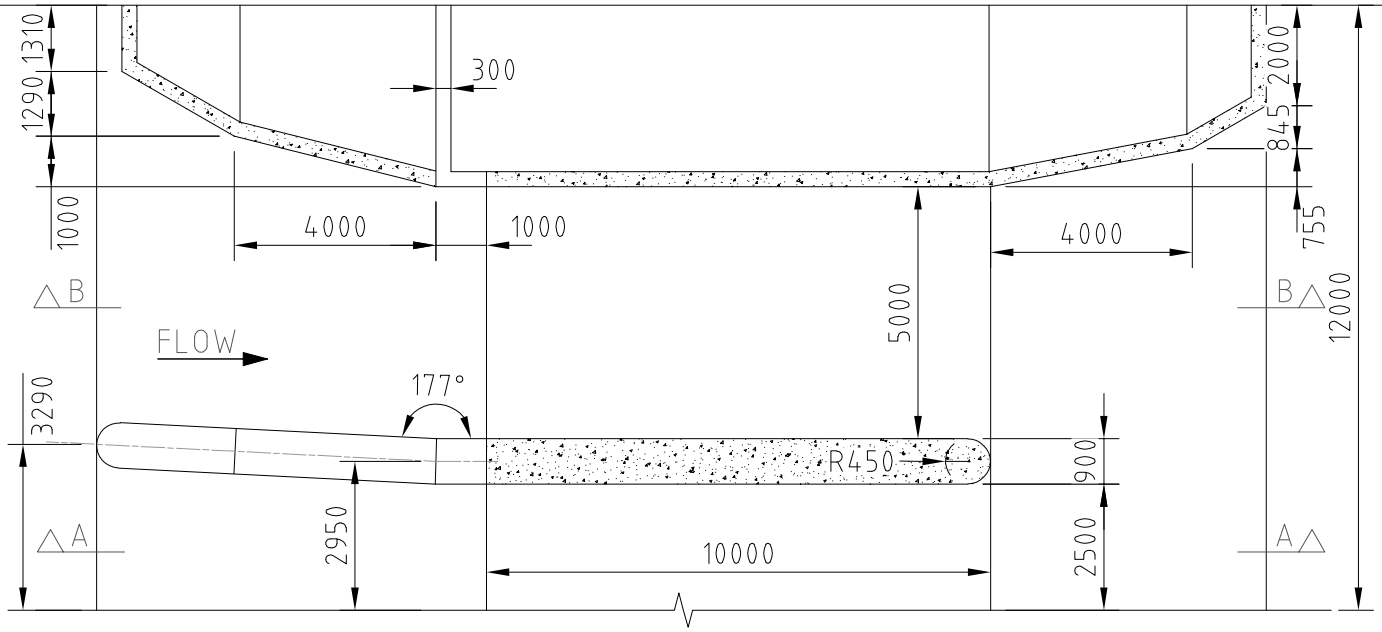

PLAN VIEW

THREE BARREL SETUP- PROTOTYPE	
SYMMETRY INCLUDED	SCALE: 1:150
	12/07/2019

Appendix D: Preliminary Experimental Test Results

Table D - 1: Normal flow depth measurements, S_0 = 1:40.

Discharge (m^3/s)	**10,24**	**15,36**	**20,48**	**25,60**	**28,53**	**30,72**	**35,84**
Distance Upstream (m)	**Flow Depth - Prototype (m)**						
9,6	0,371	0,427	0,512	0,576	0,611	0,637	0,709
12,8	0,347	0,416	0,496	0,555	0,592	0,616	0,693
16	0,331	0,424	0,499	0,555	0,587	0,616	0,675
19,2	0,352	0,424	0,493	0,557	0,595	0,613	0,688
22,4	0,331	0,405	0,488	0,557	0,592	0,624	0,675
25,6	0,355	0,435	0,509	0,584	0,621	0,653	0,717
28,8	0,347	0,451	0,525	0,600	0,640	0,669	0,715
32	0,349	0,424	0,501	0,579	0,600	0,635	0,701
35,2	0,315	0,405	0,475	0,539	0,587	0,603	0,667
Average =	0,344	0,423	0,500	0,567	0,603	0,630	0,693

Table D - 2: Recorded flow depths, normal culvert installed, S_0 = 1:40.

Discharge (m^3/s)	**10,24**	**15,36**	**20,48**	**25,6**	**28,53**	**30,72**	**35,84**
Distance Upstream (m)	**Flow Depth - Prototype (m)**						
Upstream							
0	0,93	1,21	1,52	1,75	1,86	1,99	2,94
0,8	1,00	1,29	1,56	1,83	1,99	2,15	2,86
1,6	1,01	1,32	1,61	1,89	2,07	2,21	2,77
2,4	1,02	1,37	1,68	1,95	2,14	2,24	2,76
3,2	1,02	1,39	1,69	1,94	2,15	2,25	2,76
4	1,00	1,37	1,69	1,94	2,13	2,26	2,74
4,8	0,96	1,32	1,63	1,90	2,10	2,26	2,68
5,6	0,93	1,30	1,61	1,89	2,07	2,24	2,66
6,4	0,90	1,27	1,58	1,84	2,05	2,19	2,64
7,2	0,86	1,25	1,58	1,84	2,04	2,18	2,62
8	0,85	1,21	1,57	1,82	2,01	2,18	2,61
Downstream							
-10	0,53	0,71	0,88	1,04	1,14	1,21	–
-10,8	0,51	0,68	0,84	0,97	1,09	1,14	–
-11,6	0,48	0,64	0,78	0,91	0,99	1,05	1,19
-12,4	0,44	0,57	0,71	0,83	0,90	0,97	1,09
-13,2	0,38	0,51	0,64	0,76	0,82	0,89	1,01
-14	0,36	0,47	0,57	0,70	0,75	0,79	0,93
-14,8	0,35	0,43	0,52	0,61	0,67	0,70	0,87
-15,6	0,32	0,41	0,48	0,56	0,61	0,63	0,78
-16,4	0,29	0,38	0,45	0,51	0,54	0,58	0,73
-17,2	0,27	0,35	0,42	0,48	0,50	0,53	0,66
-18	0,25	0,32	0,39	0,44	0,48	0,50	0,59
Overtopping							0,16

Table D - 3: Recorded flow depths, normal culvert installed and rock added, S_0 = 1:40.

Discharge (m^3/s)	**10,24**	**15,36**	**20,48**	**25,6**	**28,53**	**30,72**	**35,84**
Distance Upstream (m)	**Flow Depth - Prototype (m)**						
Upstream							
0	0,93	1,23	1,50	1,72	1,88	1,97	2,99
0,8	0,98	1,29	1,61	1,81	2,01	2,15	2,90
1,6	1,02	1,34	1,65	1,92	2,14	2,25	2,79
2,4	1,04	1,37	1,71	2,03	2,15	2,24	2,82
3,2	1,03	1,39	1,73	2,02	2,17	2,27	2,83
4	1,02	1,38	1,74	2,03	2,20	2,29	2,81
4,8	0,97	1,31	1,72	1,98	2,14	2,25	2,75
5,6	0,96	1,30	1,65	1,92	2,10	2,24	2,73
6,4	0,93	1,28	1,67	1,88	2,06	2,19	2,71
7,2	0,97	1,27	1,66	1,89	2,05	2,18	2,69
8	0,96	1,25	1,73	1,88	2,03	2,16	–
Downstream							
0	0,57	0,72	0,91	1,06	1,15	1,21	–
-0,8	0,52	0,69	0,84	0,99	1,05	1,10	–
-1,6	0,47	0,64	0,79	0,91	0,98	1,01	1,18
-2,4	0,41	0,57	0,70	0,81	0,86	0,91	1,08
-3,2	0,38	0,50	0,64	0,75	0,79	0,84	0,99
-4	0,37	0,47	0,58	0,69	0,72	0,74	0,95
-4,8	0,35	0,43	0,53	0,60	0,65	0,68	0,84
-5,6	0,31	0,41	0,49	0,56	0,59	0,62	0,79
-6,4	0,28	0,37	0,45	0,51	0,54	0,57	0,72
-7,2	0,27	0,35	0,43	0,48	0,50	0,53	0,65
-8	0,25	0,32	0,39	0,44	0,47	0,50	0,59
Overtopping							0,16

Table D - 4: Normal flow depth measurements, S_0 = 1:25.

Discharge (m³/s)	**10,24**	**15,36**	**20,48**	**25,6**	**28,53**	**30,72**	**35,84**
Distance Upstream (m)	**Flow Depth - Prototype (m)**						
Upstream							
57,6	0,33	0,41	0,50	0,57	0,61	0,64	0,72
51,2	0,30	0,39	0,46	0,53	0,58	0,61	0,68
44,8	0,30	0,39	0,45	0,52	0,56	0,60	0,66
35,2	0,29	0,37	0,41	0,49	0,53	0,57	0,62
25,6	0,32	0,38	0,44	0,46	0,54	0,54	0,66
16	0,32	0,38	0,46	0,52	0,55	0,58	0,63
8	0,28	0,36	0,42	0,50	0,55	0,57	0,61
Average =	0,31	0,38	0,45	0,51	0,56	0,59	0,65

Table D - 5: Recorded flow depths, normal culvert installed, S0 = 1:25.

Discharge (m³/s)	**10,24**	**15,36**	**20,48**	**25,6**	**28,53**	**30,72**	**35,84**
Distance Upstream (m)	**Flow Depth - Prototype (m)**						
Upstream							
64	0,28	0,40	0,46	0,58	0,60	0,64	0,71
57,6	–	0,42	0,50	0,58	0,60	0,65	0,72
38,4	–	0,37	0,42	0,50	0,52	–	0,61
32	–	0,36	0,45	–	0,54	–	0,62
25,6	–	–	0,46	0,52	0,56	0,60	1,27
22,4	0,33	0,40	0,46	0,54	0,57	0,60	1,54
19,2	–	0,41	0,47	0,54	0,64	1,01	1,86
16	0,32	0,39	0,47	1,06	1,61	1,43	1,99
12,8	0,31	0,42	1,25	1,31	1,59	1,69	2,13
9,6	0,34	0,96	1,33	1,51	1,66	1,82	2,26
8	0,62	1,05	1,32	1,62	1,78	1,88	2,34
7,2	0,72	1,07	1,37	1,60	1,86	1,90	2,40
6,4	0,72	1,09	1,52	1,81	1,92	2,00	2,44

5,6	0,79	1,12	1,51	1,72	1,87	2,06	2,45
4,8	0,84	1,28	1,51	1,77	1,88	2,06	2,51
4	0,87	1,26	1,56	1,88	2,00	2,17	2,58
3,2	0,92	1,24	1,62	1,93	2,12	2,20	2,66
2,4	1,00	1,31	1,65	1,92	2,17	2,25	2,65
1,6	0,95	1,37	1,68	1,90	2,07	2,17	2,70
0,8	0,91	1,28	1,54	1,81	1,92	2,16	2,79
0	0,89	1,20	1,43	1,74	1,90	2,11	2,85
Downstream							
-10	0,57	0,71	0,86	0,95	1,10	1,11	0,00
-10,8	0,54	0,72	0,87	1,00	1,10	1,06	0,00
-11,6	0,50	0,71	0,84	0,94	1,06	1,01	1,01
-12,4	0,41	0,63	0,78	0,89	0,96	0,98	0,92
-13,2	0,39	0,57	0,66	0,82	0,90	0,95	0,98
-14	0,38	0,47	0,62	0,74	0,76	0,85	0,88
Overtopping							0,14

Table D - 6: Recorded upstream flow depths, normal culvert added and rock added, S_0 = 1:25.

Discharge (m³/s)	**10,24**	**15,36**	**20,48**	**25,6**	**28,53**	**30,72**	**35,84**
Distance Upstream (m)	**Flow Depth - Prototype (m)**						
Upstream							
8	0,67	1,01	1,32	1,55	1,79	1,83	2,39
7,2	0,71	1,06	1,36	1,62	1,85	1,90	2,40
6,4	0,74	1,10	1,40	1,65	1,87	1,90	2,45
5,6	0,78	1,14	1,42	1,68	1,95	1,96	2,45
4,8	0,84	1,20	1,44	1,58	2,01	1,92	2,57
4	0,90	1,24	1,54	1,82	2,02	1,97	2,66
3,2	0,92	1,28	1,58	1,85	2,01	2,11	2,66
2,4	0,95	1,29	1,56	1,86	2,03	2,22	2,68
1,6	0,94	1,24	1,55	1,78	2,04	2,37	2,74
0,8	0,93	1,23	1,51	1,73	2,00	2,30	2,87
0	0,88	1,22	1,41	1,66	1,94	2,65	3,00
Overtopping							0,14

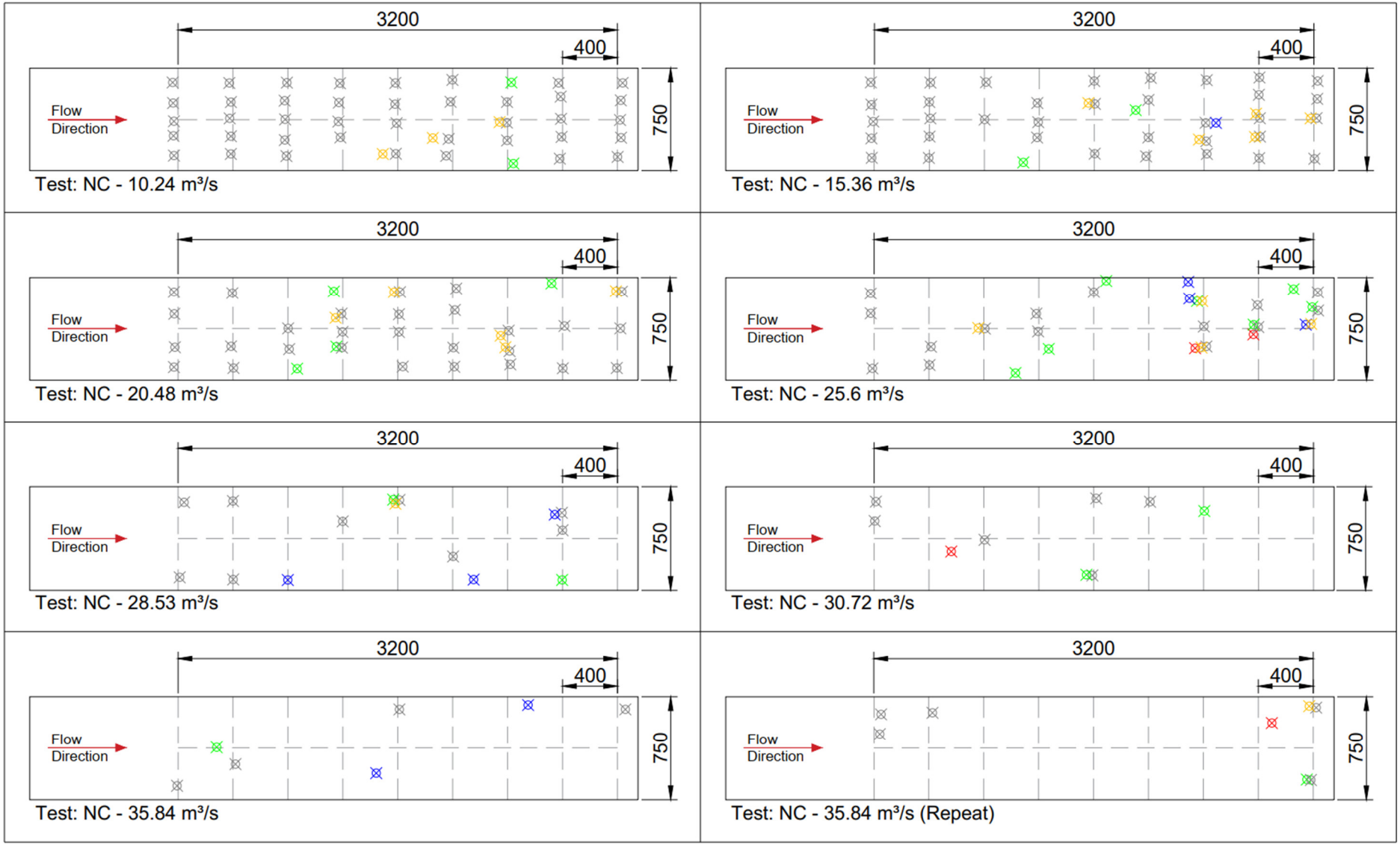

Figure D - 1: No culvert boulder movement results, S_0 = 1:40.

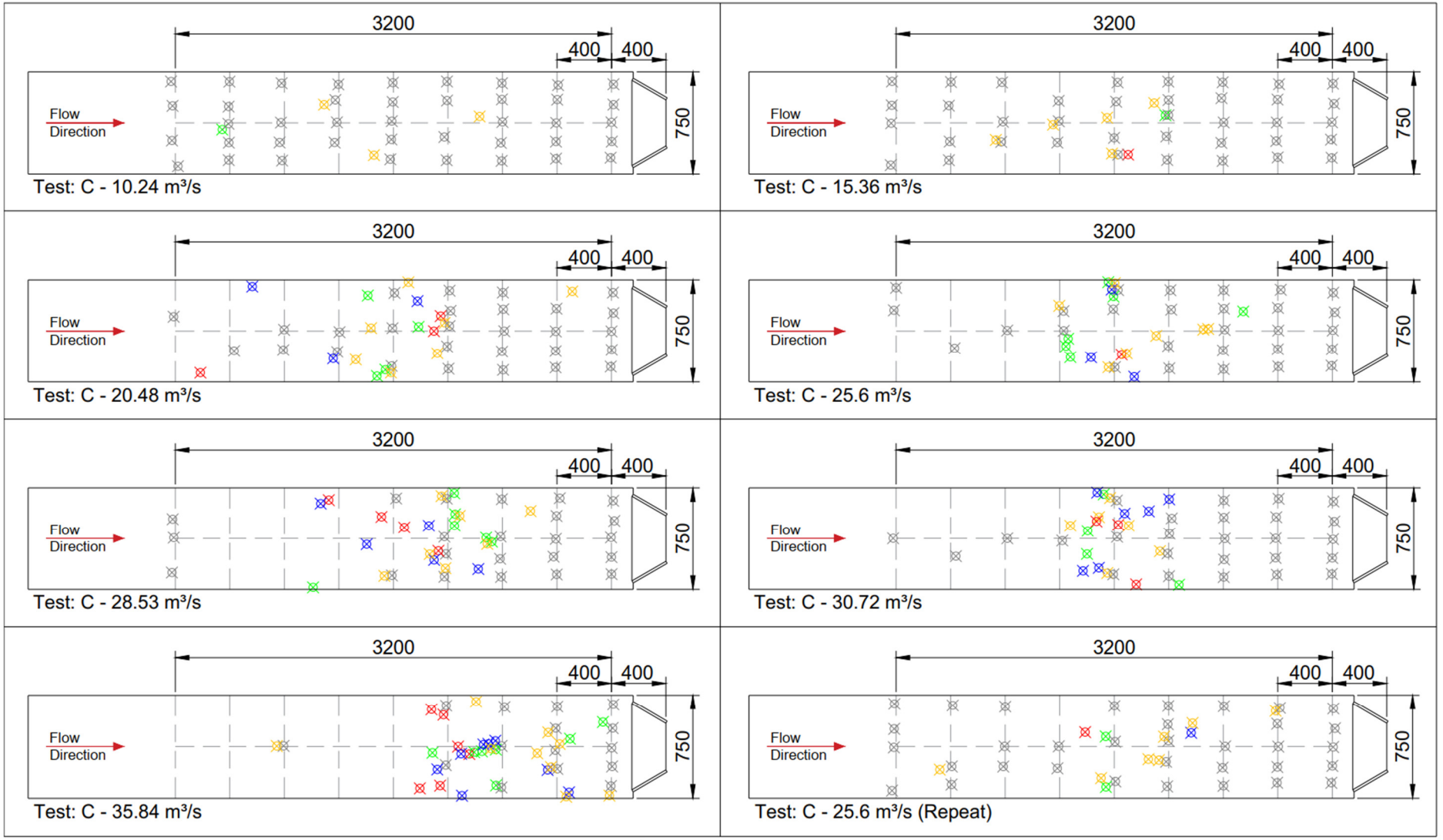

Figure D - 2: Normal culvert boulder movement results, S_0 = 1:40.

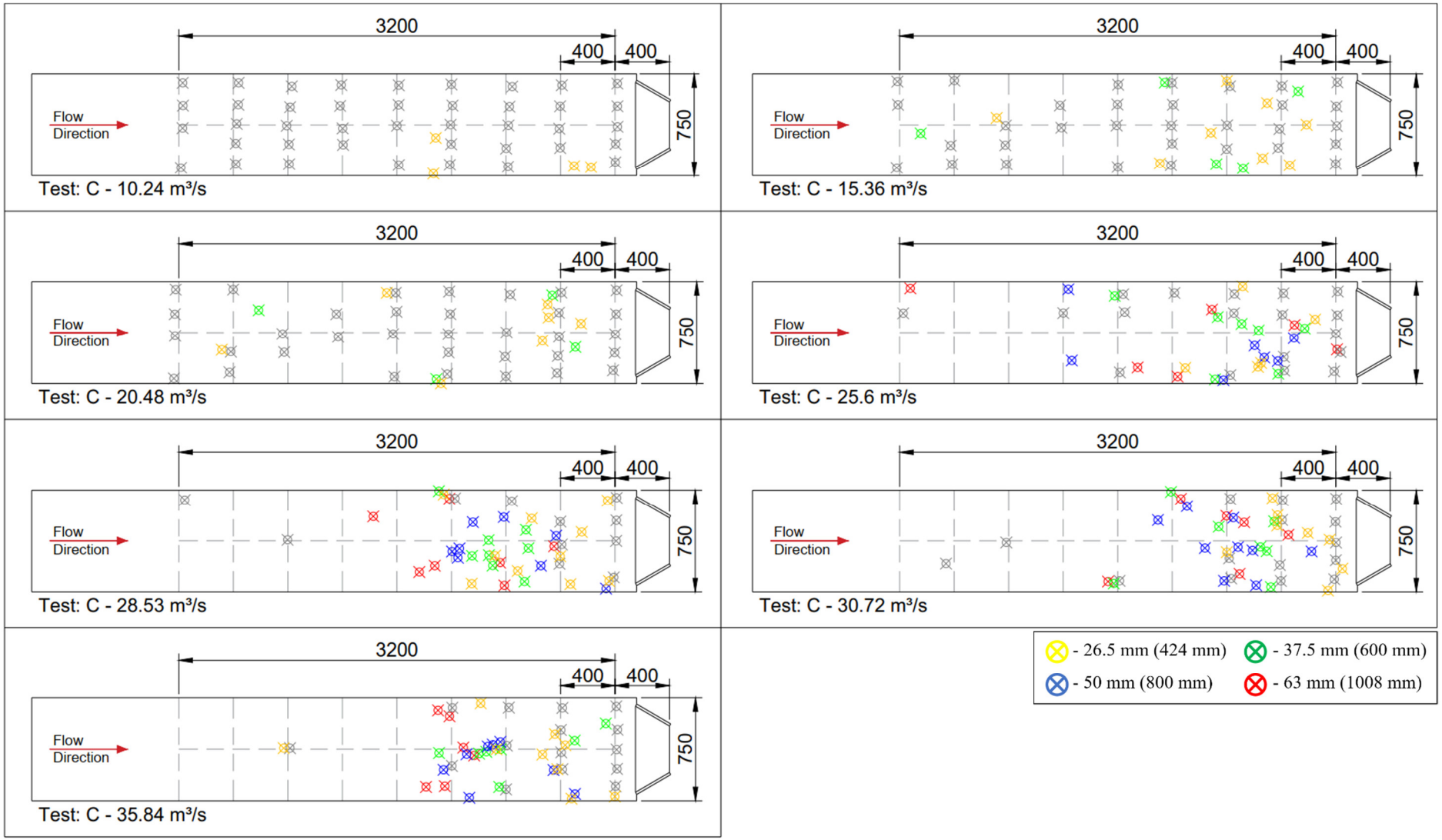

Figure D - 3: C-Model boulder movement results, S_0 = 1:30.

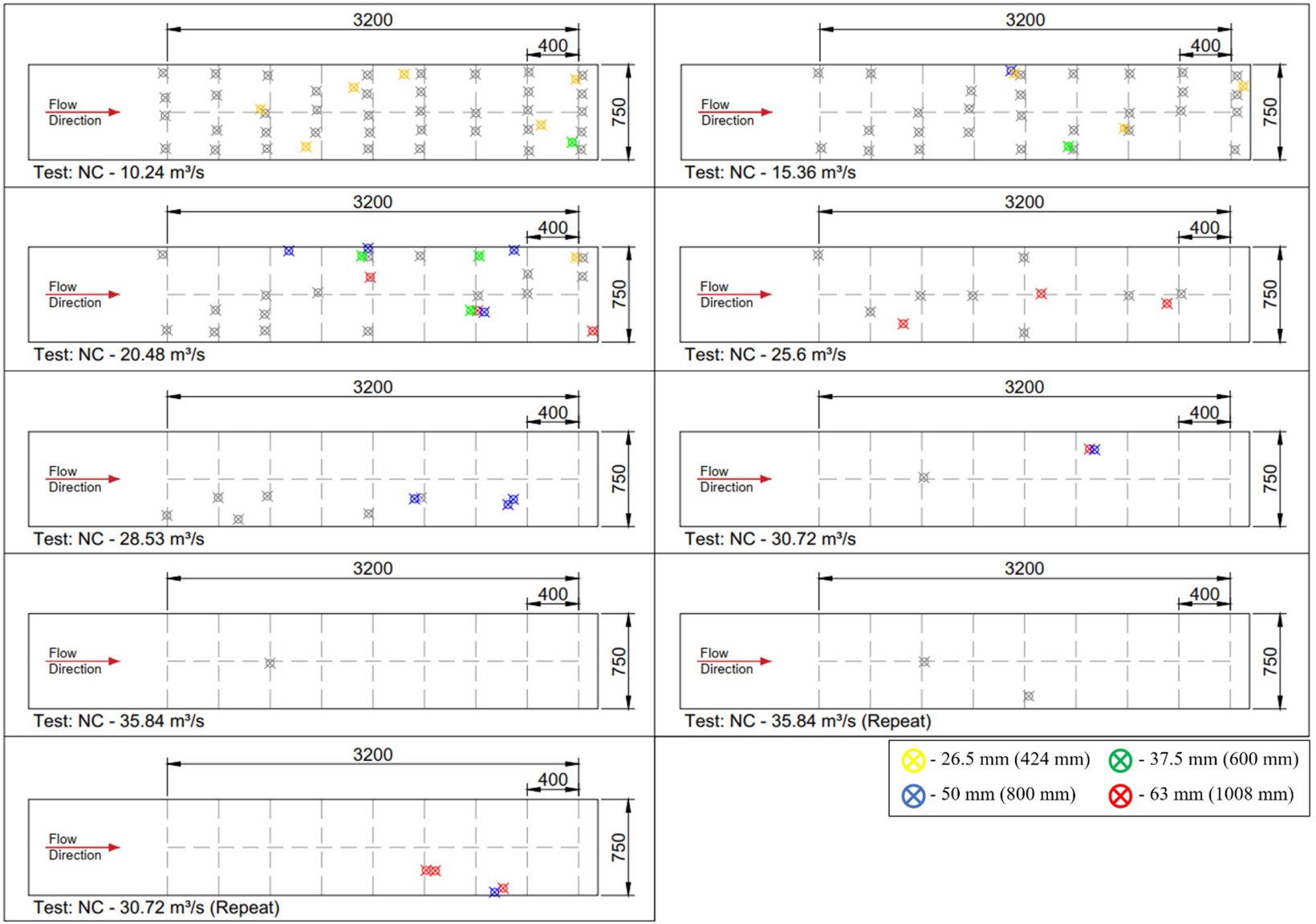

Figure D - 4: No culvert added, boulder movement results, S0 = 1:25.

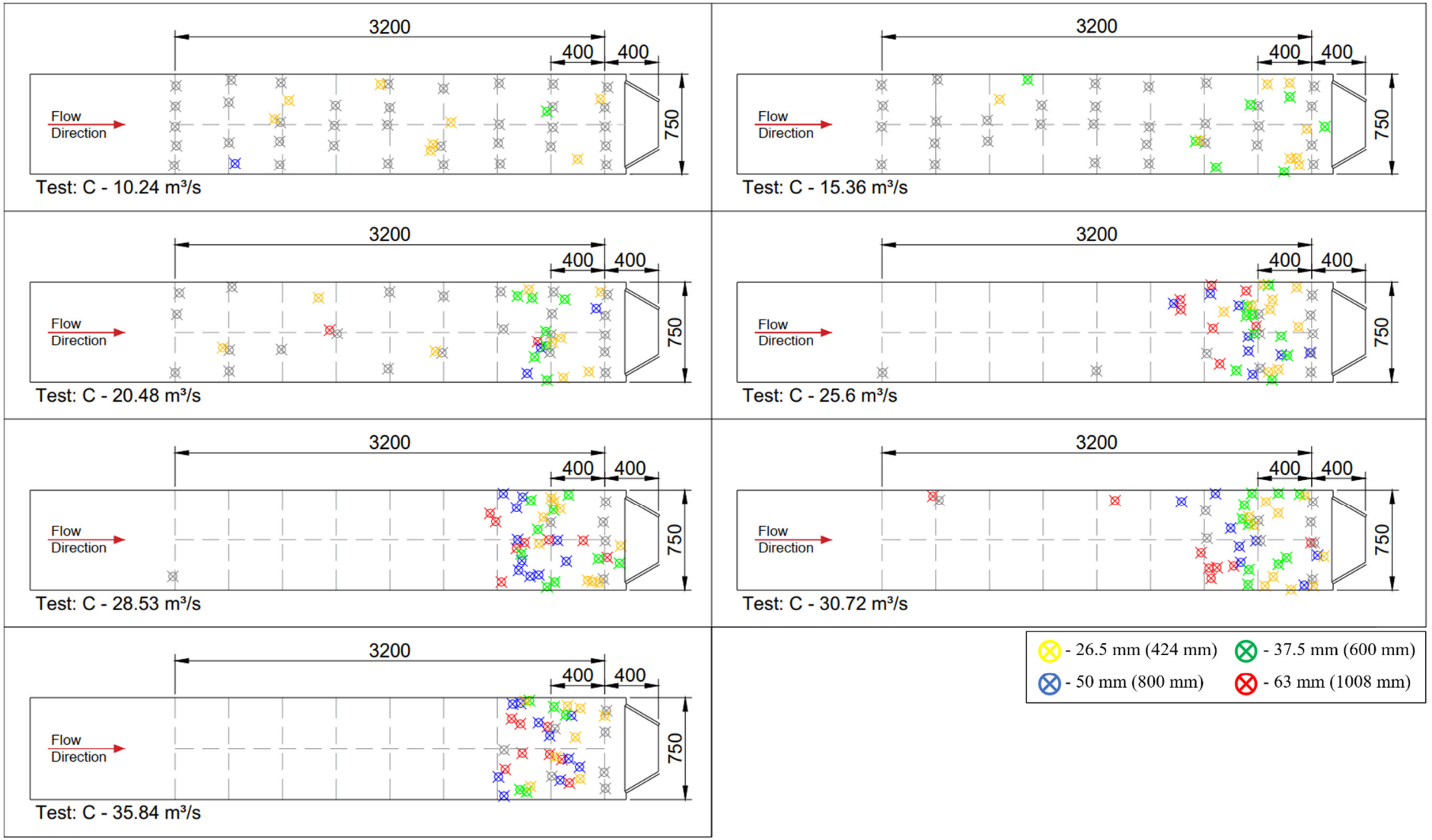

Figure D - 5: Normal culvert boulder movement results, S_0 = 1:25.

Appendix E: Trigonometric Functions

The fan profile and lip for the modified MEL and Compound taper models can be determined through the following basic trigonometric functions. If the barrel width (B), fan lip width (B_{lip}) and fan angle (ϕ) are known the shape of the fan can be determined to connect perpendicular to the wing-walls and the connecting profile drawn in. The equations listed below have all been sourced from Weisstein (2019b & 2019a).

- $r = \frac{B_{lip}}{2\pi\phi} \cdot 360$
- Solve the radius to find B_t:

  $$r = \sqrt{\left[0.5B_t \cdot \tan\left(90 - \frac{\phi}{2}\right]^2 + [0.5B_t]^2}$$
- $L_{ab} = 0.5B_t - 0.5B$
- $L_{bc} = L_{ce} = \frac{L_{ab}}{\sin\left(\frac{\phi}{2}\right)}$
- $L_{cd} = \frac{L_{bc}}{\sin\left(\frac{\phi}{4}\right)}$
- $L_{bd} = L_{de} = \sqrt{L_{cd}^2 - L_{bc}^2}$

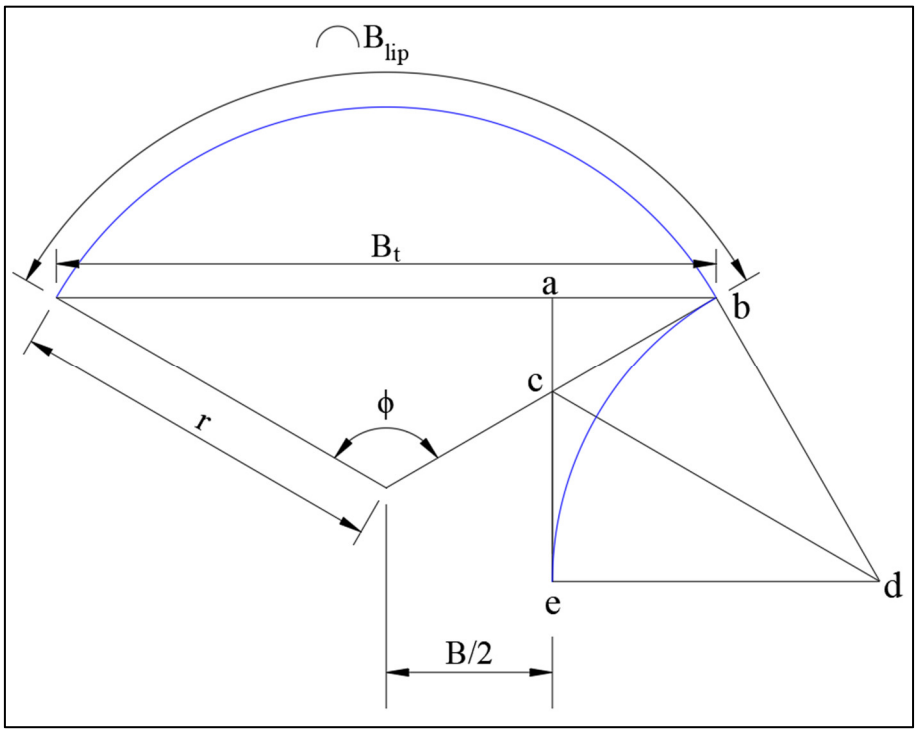

Figure E-10.1: Inlet fan geometric layout.

Appendix F: Experimental Results for Chapter 6

Table F - 1: Recorded flow depths for inlet tapered model.

15,36 m³/s				20,48 m³/s			
Chainage (m)	Flow Depth, y (m)	Shock Wave		Chainage (m)	Flow Depth, y (m)	Shock Wave	
		Offset from Centerline (m)	Flow Depth (m)			Offset from Centerline (m)	Flow Depth (m)
16	0,348	–	–	16	0,400	–	–
11,2	0,324	–	–	11,2	0,400	–	–
9,6	0,272	5,440	0,632	9,6	0,352	5,440	0,816
8	0,280	4,320	0,584	8	0,328	3,920	0,768
6,4	0,264	2,880	0,608	6,4	0,320	3,040	0,744
5,6	0,280	2,240	0,608	5,6	0,320	2,480	0,712
4,8	0,253	1,920	0,549	4,8	0,309	1,920	0,693
4	0,240	1,280	0,536	4	0,304	1,280	0,688
3,2	0,256	0,640	0,520	3,2	0,352	0,880	0,688
2,4	0,467	0,000	0,555	2,4	0,707	0,000	0,651

28,53 m³/s				30 m³/s			
Chainage (m)	Flow Depth, y (m)	Shock Wave		Chainage (m)	Flow Depth, y (m)	Shock Wave	
		Offset from Centerline (m)	Flow Depth (m)			Offset from Centerline (m)	Flow Depth (m)
16	0,496	–	–	16	0,544	–	–
11,2	0,472	–	–	11,2	0,664	–	–
9,6	0,456	4,880	0,872	9,6	0,496	4,800	1,032
8	0,416	4,000	0,952	8	0,456	4,160	1,080
6,4	0,412	2,840	0,936	6,4	0,456	2,832	0,984
5,6	0,432	2,360	0,912	5,6	0,448	2,240	0,952
4,8	0,413	1,880	0,885	4,8	0,453	1,920	0,933
4	0,448	1,280	0,848	4	0,496	1,440	0,904
3,2	0,544	0,480	0,824	3,2	0,656	0,960	0,856
2,4	–	0,000	0,843	2,4	1,283	0,000	0,867

35 m³/s			
Chainage (m)	Flow Depth, y (m)	Shock Wave	
		Offset from Centerline (m)	Flow Depth (m)
16	0,576	–	–
11,2	0,504	–	–
9,6	0,544	4,800	1,128
8	0,512	4,320	1,144
6,4	0,512	2,880	1,104
5,6	0,536	2,400	1,096
4,8	0,517	1,920	1,069
4	0,576	1,280	1,064
3,2	0,752	0,800	1,072
2,4	1,443	0,000	1,059

Table F - 2: Recorded outlet flow depths for inlet tapered model.

Distance from Outlet (m)	Flow Rate, Q (m³/s)	15,36	20,48	28,53	30,72	35,84
	Chainage (m)	Prototype Flow Depth, y (m)				
0	-10	0,112	0,912	1,083	1,227	1,461
0,8	-10,8	1,721	0,873	1,129	1,193	1,284
1,6	-11,6	0,284	0,791	1,039	1,169	1,233
3,2	-13,2	0,387	0,789	0,936	1,016	1,112
4,8	-14,8	0,552	0,680	0,777	0,864	0,912
7,04	-17,04	0,332	0,456	0,529	0,540	0,616
8,64	-18,64	0,300	0,384	0,429	0,440	0,512

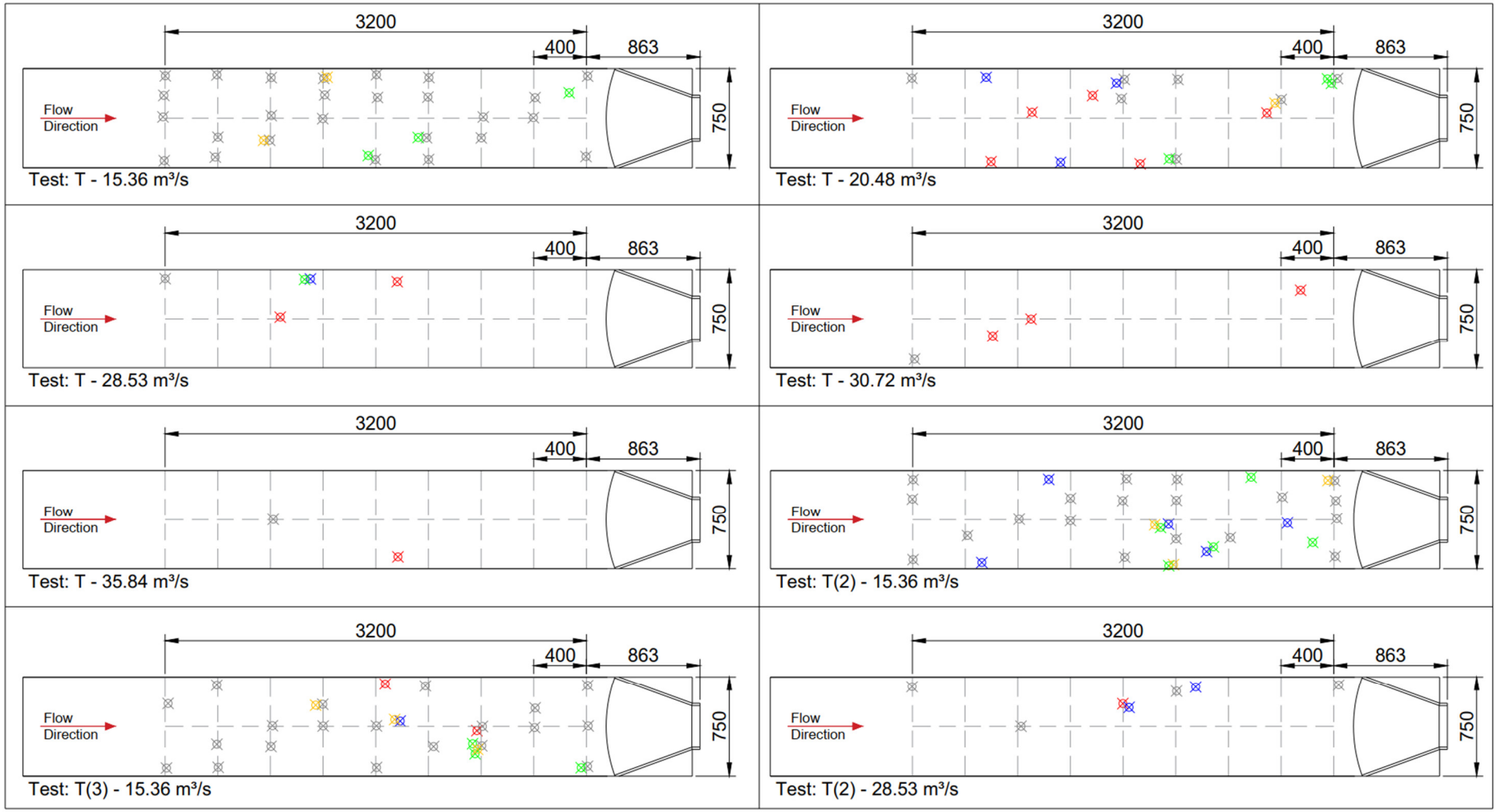

Figure F - 1: Tapered inlet model boulder movement results.

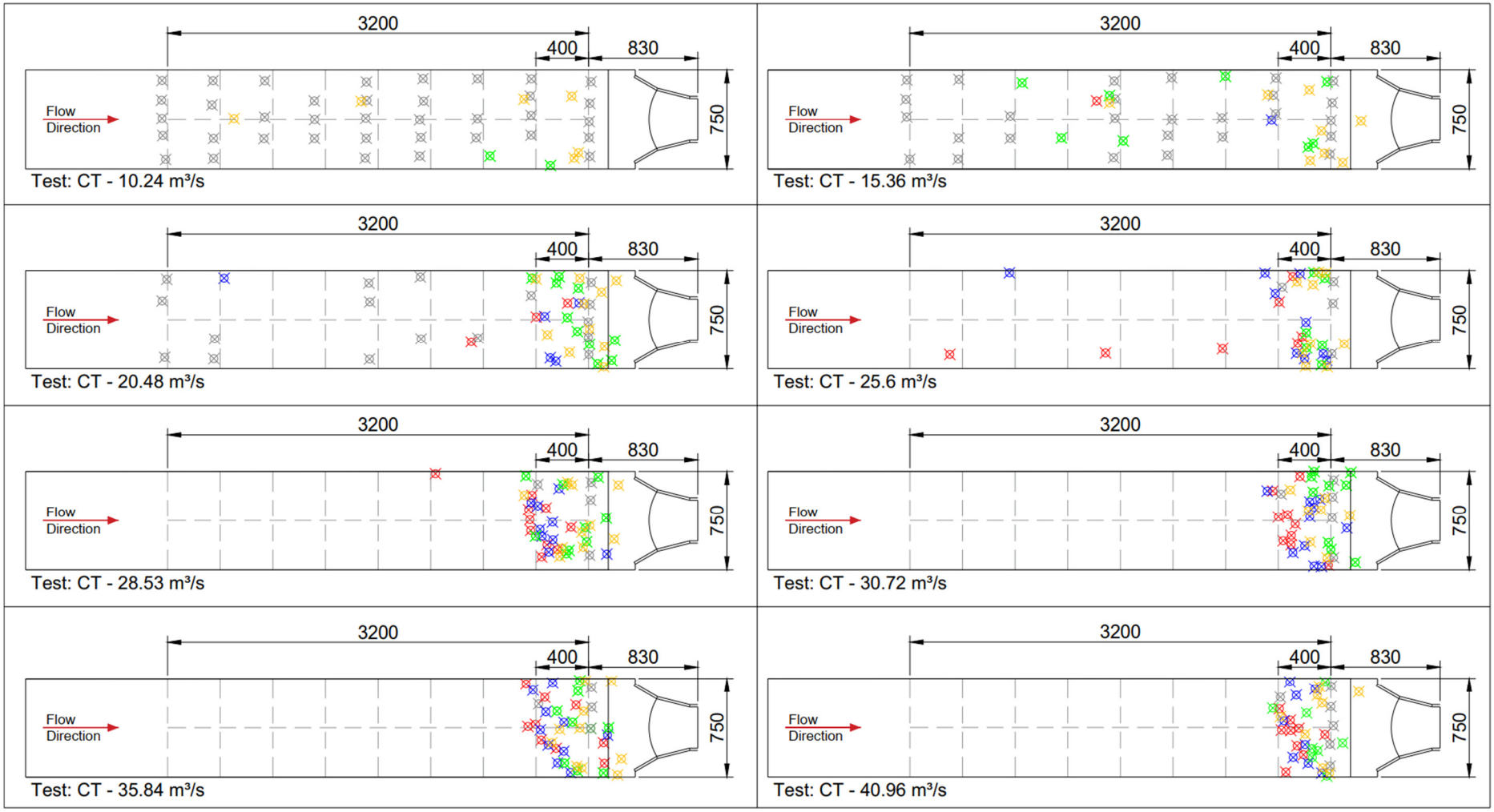

Figure F - 2: Compound taper inlet boulder movement results 1 of 3.

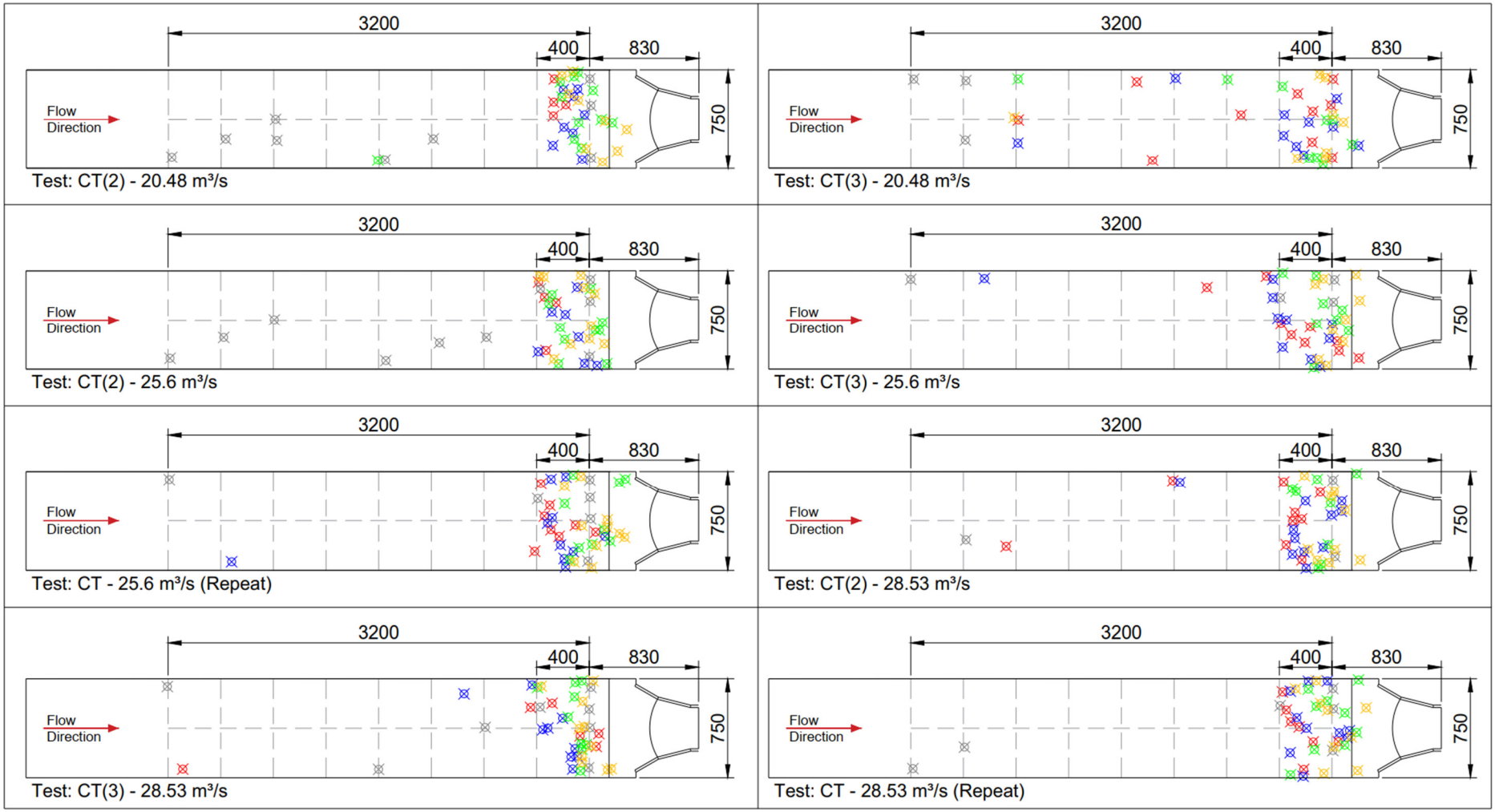

Figure F - 3: Compound taper inlet model boulder movement results, 2 of 3.

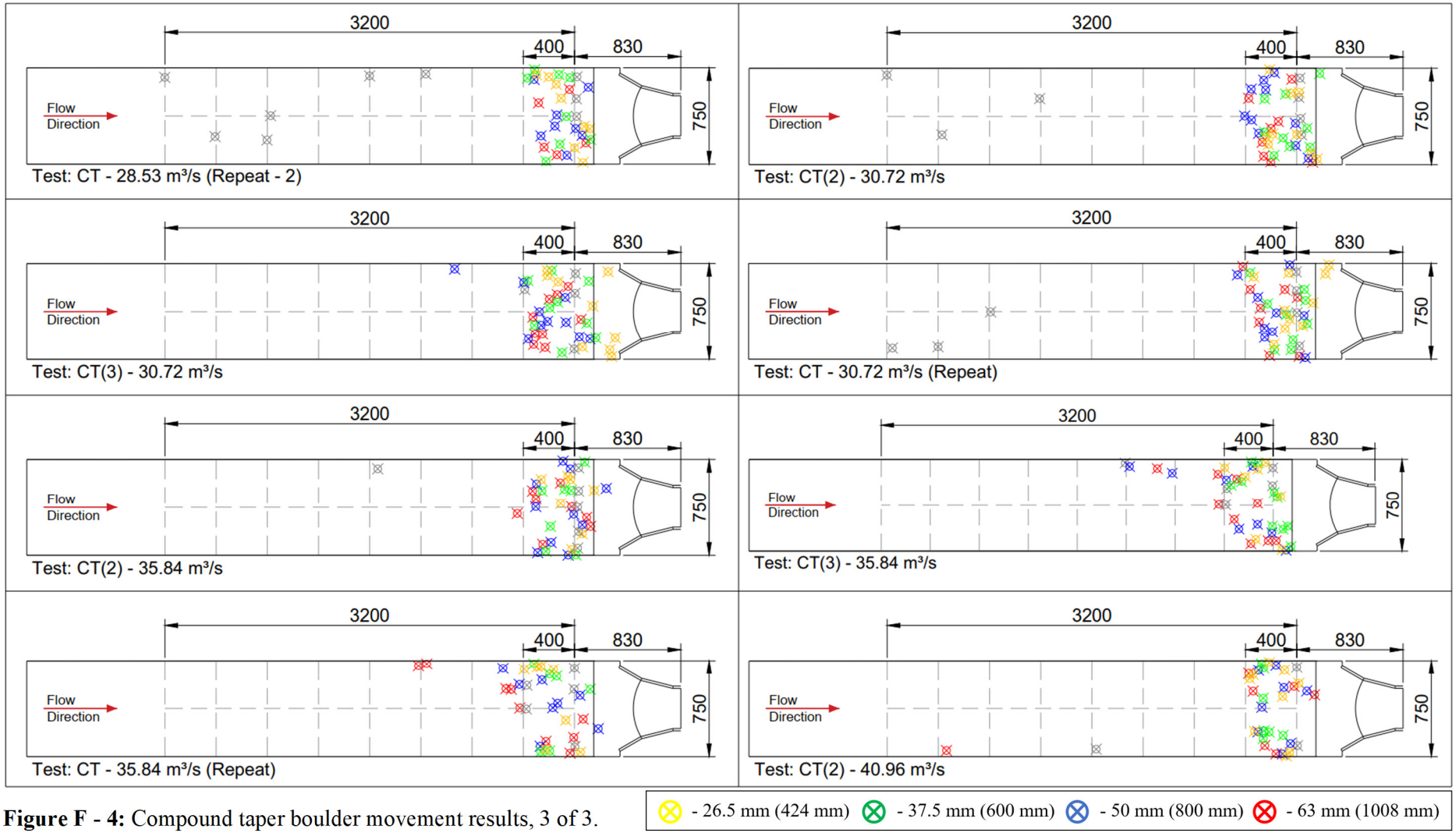

Figure F - 4: Compound taper boulder movement results, 3 of 3.

Appendix G: Experimental Results for Chapter 7

Table G - 1: Two-cell CT model notched flow depth measurements.

Discharge	28,53 m³/s		
Chainage (m)	Left	Right	Average
	Upstream Flow Depth (m)		
64,000	0,600	0,584	0,592
57,600	0,576	0,584	0,580
38,400	0,512	0,480	0,496
32,000	0,512	0,464	0,488
25,600	0,496	0,512	0,504
22,400	0,464	0,480	0,472
19,200	0,448	0,544	0,496
16,000	1,296	0,896	1,096
12,800	1,376	1,424	1,400
11,200	1,560	1,496	1,528
9,600	1,520	1,552	1,536
8,000	1,536	1,544	1,540
7,200	1,420	1,452	1,436
6,400	1,392	1,448	1,420
5,600	1,488	1,488	1,488
4,800	1,416	1,504	1,460
4,000	1,448	1,520	1,484
3,200	1,320	1,408	1,364
2,400	1,344	1,280	1,312
1,600	1,412	1,412	1,412
1,000	1,544	1,528	1,536
0,000	1,668	1,668	1,668
Downstream Flow depth (m)			
-10,000	1,008	1,000	1,004
-10,800	0,916	0,892	0,904
-11,600	0,828	0,812	0,820
-12,400	0,756	0,716	0,736
-13,200	0,684	0,636	0,660
-14,000	0,692	0,620	0,656

Table G - 2: Two-cell CT model solid fin flow depth measurements, 1 of 2.

Discharge	15,36 m³/s			20,48 m³/s			25,6 m³/s		
Chainage (m)	Left	Right	Average	Left	Right	Average	Left	Right	Average
	Upstream Flow Depth (m)								
64	0,440	0,400	0,420	0,480	0,456	0,468	0,568	0,552	0,560
57,6	0,400	0,432	0,416	0,464	0,496	0,480	0,544	0,544	0,544
38,4	0,328	0,352	0,340	0,400	0,384	0,392	0,464	0,424	0,444
32	0,328	0,304	0,316	0,416	0,368	0,392	0,448	0,400	0,424
25,6	0,312	0,336	0,324	0,400	0,400	0,400	0,464	0,448	0,456
22,4	0,304	0,344	0,324	0,336	0,400	0,368	0,408	0,488	0,448
19,2	0,320	0,320	0,320	0,400	0,384	0,392	0,448	0,432	0,440
16	0,384	0,288	0,336	0,784	0,432	0,608	1,184	0,736	0,960
12,8	0,944	0,944	0,944	1,184	1,120	1,152	1,328	1,168	1,248
11,2	0,968	0,888	0,928	1,208	1,160	1,184	1,400	1,384	1,392
9,6	1,040	0,992	1,016	1,264	1,232	1,248	1,520	1,440	1,480
8	1,040	1,000	1,020	1,248	1,128	1,188	1,456	1,336	1,396
7,2	1,024	1,052	1,038	1,200	1,172	1,186	1,404	1,348	1,376
6,4	0,976	0,936	0,956	1,176	1,216	1,196	1,352	1,360	1,356
5,6	0,892	0,808	0,850	1,128	1,184	1,156	1,360	1,448	1,404
4,8	0,800	0,824	0,812	1,080	1,124	1,102	1,336	1,448	1,392
4	0,832	0,824	0,828	1,000	1,072	1,036	1,368	1,488	1,428
3,2	0,696	0,720	0,708	0,872	0,932	0,902	1,172	1,312	1,242
2,4	0,696	0,728	0,712	0,888	0,920	0,904	1,096	1,232	1,164
1,6	0,756	0,796	0,776	0,988	1,012	1,000	1,196	1,268	1,232
1	0,792	0,844	0,818	1,024	1,080	1,052	1,320	1,352	1,336
0	0,760	0,740	0,750	0,980	0,916	0,948	1,248	1,264	1,256
Downstream Flow Depth (m)									
-10	0,592	0,564	0,578	0,728	0,720	0,724	0,864	0,872	0,868
-10,8	0,540	0,556	0,548	0,704	0,676	0,690	0,812	0,780	0,796
-11,6	0,484	0,516	0,500	0,616	0,648	0,632	0,716	0,728	0,722
-12,4	0,444	0,464	0,454	0,568	0,580	0,574	0,672	0,676	0,674
-13,2	0,408	0,420	0,414	0,532	0,512	0,522	0,628	0,584	0,606
-14	0,420	0,428	0,424	0,548	0,484	0,516	0,628	0,604	0,616

Table G - 3: Two-cell CT model solid fin flow depth measurements, 2 of 2.

Discharge	28,53 m³/s			35,84 m³/s		
Chainage (m)	Left	Right	Average	Left	Right	Average
	Upstream Flow Depth (m)					
64,000	0,600	0,584	0,592	0,712	0,664	0,688
57,600	0,592	0,592	0,592	0,656	0,672	0,664
38,400	0,496	0,480	0,488	0,592	0,544	0,568
32,000	0,496	0,448	0,472	0,560	0,528	0,544
25,600	0,480	0,512	0,496	0,560	0,592	0,576
22,400	0,456	0,528	0,492	0,544	0,592	0,568
19,200	0,496	0,496	0,496	1,248	0,864	1,056
16,000	1,368	1,120	1,244	1,440	1,712	1,576
12,800	1,456	1,232	1,344	1,792	1,760	1,776
11,200	1,560	1,464	1,512	1,816	1,880	1,848
9,600	1,648	1,664	1,656	1,936	1,808	1,872
8,000	1,564	1,464	1,514	1,888	1,760	1,824
7,200	1,532	1,508	1,520	1,868	1,892	1,880
6,400	1,520	1,616	1,568	1,904	1,960	1,932
5,600	1,552	1,600	1,576	1,840	1,920	1,880
4,800	1,472	1,608	1,540	1,872	1,908	1,890
4,000	1,488	1,592	1,540	1,924	1,952	1,938
3,200	1,328	1,468	1,398	1,752	1,848	1,800
2,400	1,272	1,344	1,308	1,704	1,768	1,736
1,600	1,300	1,396	1,348	1,676	1,700	1,688
1,000	1,400	1,440	1,420	1,676	1,752	1,714
0,000	1,376	1,348	1,362	1,708	1,660	1,684
Downstream Flow Depth (m)						
-10,000	0,936	0,976	0,956	1,116	1,152	1,134
-10,800	0,844	0,828	0,836	1,052	1,044	1,048
-11,600	0,780	0,808	0,794	1,016	0,992	1,004
-12,400	0,732	0,732	0,732	0,844	0,868	0,856
-13,200	0,680	0,652	0,666	0,788	0,788	0,788
-14,000	0,692	0,636	0,664	0,764	0,764	0,764

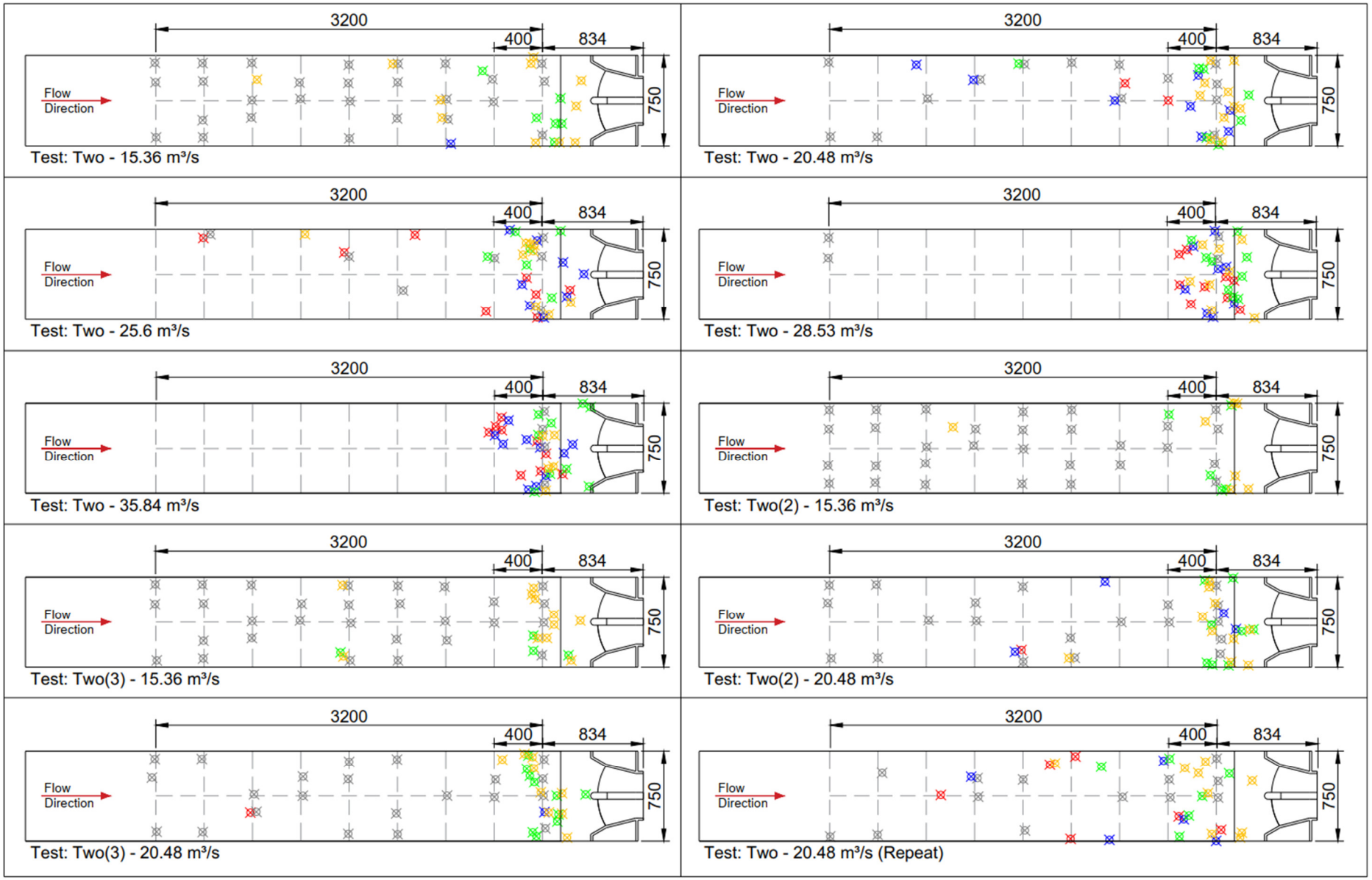

Figure G - 1: Two-cell CT model boulder movement results.

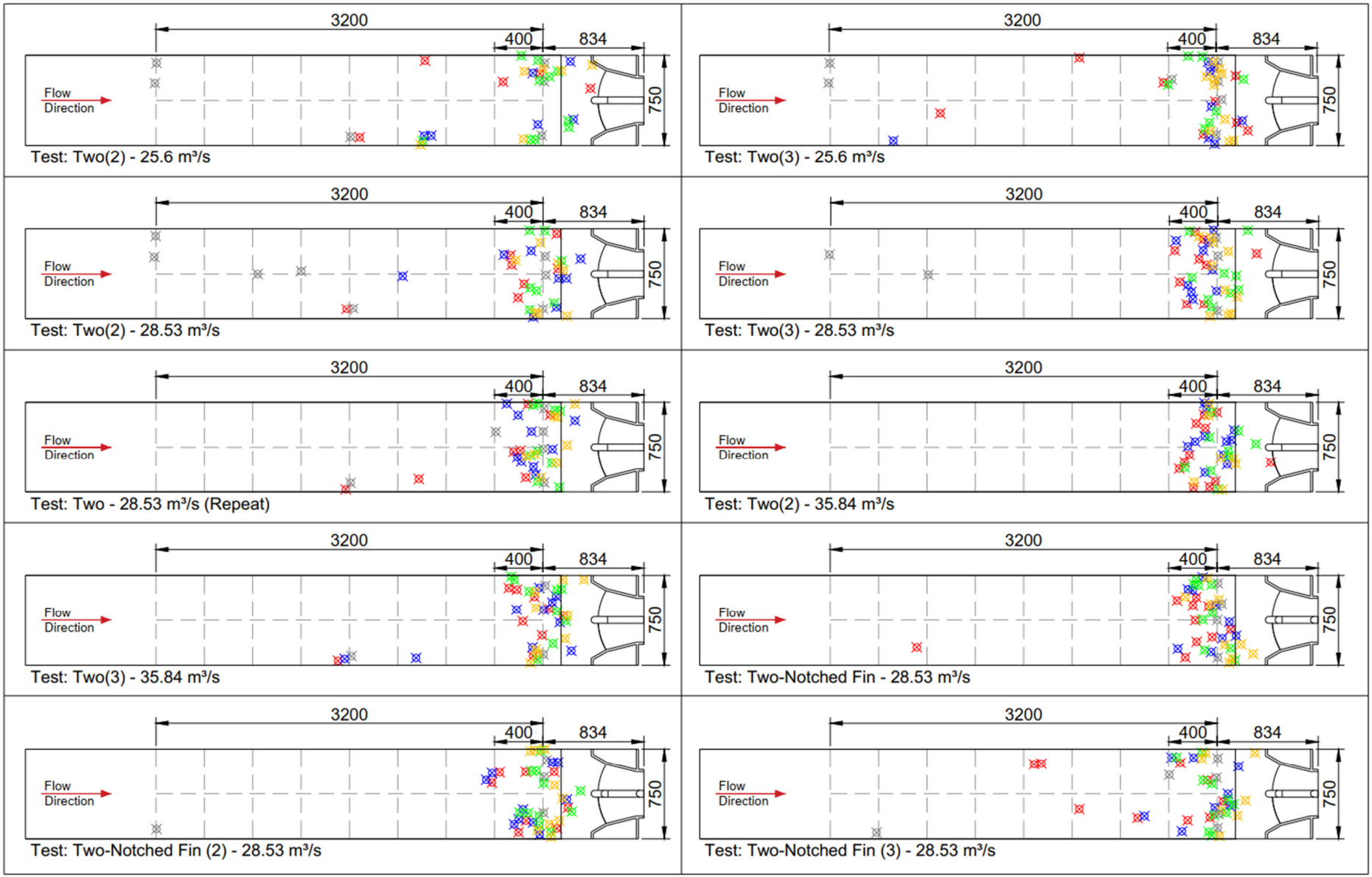

Figure G - 2: Two-cell CT model boulder movement results.

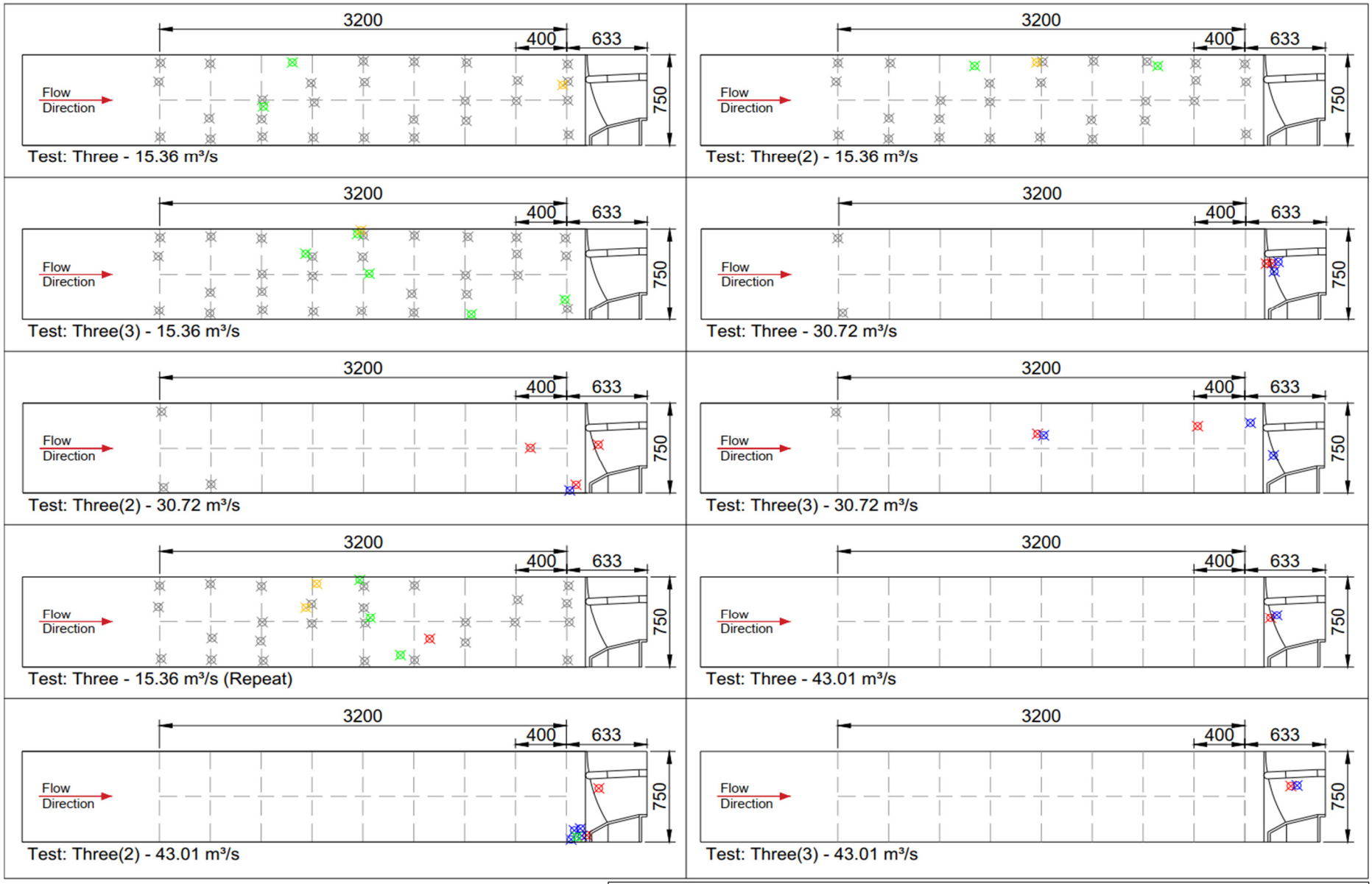

Figure G - 3: Three-cell CT model boulder movement results.